

ISSN 1997-1397 (Print)
ISSN 2313-6022 (Online)

**Журнал Сибирского
федерального университета
Математика и физика**

**Journal of Siberian
Federal University
Mathematics & Physics**

2024 17 (2)

ISSN 1997-1397
(Print)

ISSN 2313-6022
(Online)

2024 17 (2)

ЖУРНАЛ
СИБИРСКОГО
ФЕДЕРАЛЬНОГО
УНИВЕРСИТЕТА
Математика и Физика

JOURNAL
OF SIBERIAN
FEDERAL
UNIVERSITY
Mathematics & Physics

Издание индексируется Scopus (Elsevier), Emerging Sources Citation Index (WoS, Clarivate Analytics), Российским индексом научного цитирования (ИИН), представлено в международных и российских информационных базах: Ulrich's periodicals directory, ProQuest, EBSCO (США), Google Scholar, MathNet.ru, КиберЛенинка.

Включено в список Высшей аттестационной комиссии «Рецензируемые научные издания, входящие в международные реферативные базы данных и системы цитирования».

Все статьи представлены в открытом доступе http://journal.sfu-kras.ru/en/series/mathematics_physics.

**Журнал Сибирского федерального университета.
Математика и физика.**

Journal of Siberian Federal University. Mathematics & Physics.

Учредитель: Федеральное государственное автономное образовательное учреждение высшего образования "Сибирский федеральный университет" (СФУ)

Главный редактор: А.М. Кытманов. Редакторы: В.Е. Зализняк, А.В. Щуплев.
Компьютерная верстка: Г.В. Хрусталева

№ 2. 29.04.2024. Индекс: 42327. Тираж: 1000 экз. Свободная цена
Адрес редакции и издателя: 660041 г. Красноярск, пр. Свободный, 79,
оф. 32-03.

Отпечатано в типографии Издательства БИК СФУ
660041 г. Красноярск, пр. Свободный, 82а.

*Свидетельство о регистрации СМИ ПИ № ФС 77-28724 от 29.06.2007 г.,
выданное Федеральной службой по надзору в сфере массовых
коммуникаций, связи и охраны культурного наследия
<http://journal.sfu-kras.ru>*

Подписано в печать 15.04.24. Формат 84×108/16. Усл.печ. л. 12,0.

Уч.-изд. л. 11,8. Бумага тип. Печать офсетная.

Тираж 1000 экз. Заказ 20398

Возрастная маркировка в соответствии с Федеральным законом № 436-ФЗ:16+

Editorial Board:

Editor-in-Chief: Prof. Alexander M. Kytmanov
(Siberian Federal University, Krasnoyarsk, Russia)

Consulting Editors Mathematics & Physics:

Prof. Viktor K. Andreev (Institute Computing Modelling SB RUS, Krasnoyarsk, Russia)
Prof. Dmitry A. Balaev (Institute of Physics SB RUS, Krasnoyarsk, Russia)
Prof. Silvio Ghilardi (University of Milano, Milano, Italy)
Prof. Sergey S. Goncharov, Academician,
(Institute of Mathematics SB RUS, Novosibirsk, Russia)
Prof. Ari Laptev (KTH Royal Institute of Technology, Stockholm, Sweden)
Prof. Yury Yu. Loginov
(Reshetnev Siberian State University of Science and Technology, Krasnoyarsk, Russia)
Prof. Mikhail V. Noskov (Siberian Federal University, Krasnoyarsk, Russia)
Prof. Sergey G. Ovchinnikov (Institute of Physics SB RUS, Krasnoyarsk, Russia)
Prof. Gennady S. Patrin (Institute of Physics SB RUS, Krasnoyarsk, Russia)
Prof. Vladimir M. Sadovsky (Institute Computing Modelling SB RUS, Krasnoyarsk, Russia)
Prof. Azimbay Sadullaev, Academician
(Nathional University of Uzbekistan, Tashkent, Uzbekistan)
Prof. Vasily F. Shabanov, Academician, (Siberian Federal University, Krasnoyarsk, Russia)
Prof. Vladimir V. Shaidurov (Institute Computing Modelling SB RUS, Krasnoyarsk, Russia)
Prof. Avgust K. Tsikh (Siberian Federal University, Krasnoyarsk, Russia)
Prof. Eugene A. Vaganov, Academician, (Siberian Federal University, Krasnoyarsk, Russia)
Prof. Valery V. Val'kov (Institute of Physics SB RUS, Krasnoyarsk, Russia)
Prof. Alecos Vidras (Cyprus University, Nicosia, Cyprus)

CONTENTS

A. Benraouda Optimal Control for an Elastic Frictional Contact Problem	151
A. O. Afonin, A. A. Alexandrovsky, I. V. Govorun, A. A. Leksikov, A. V. Ugryumov, D. K. Ogorodnikov Dual Band HTSC Power Limiter	162
E. D. Leinartas, E. K. Leinartas Difference Equations and Hadamard Composition of Power Series	169
V. K. Beloshapka On Hypergeometric Functions of Two Variables of Complexity One	175
A. V. Eikhler, V. V. Prudnikov, P. V. Prudnikov Hysteresis Effects in the Critical Behavior of Heisenberg Thin Films in an External Oscillating Field	189
V. K. Andreev Thermocapillary Convection of Immiscible Liquid in a Three-dimensional Layer at Low Marangoni Numbers	195
V. B. Bekezhanova, O. N. Goncharova On One Exact Solution of an Evaporative Convection Problem with the Dirichlet Boundary Conditions	207
A. A. Imomov, S. B. Iskandarov Further Remarks on the Explicit Generating Function Expression of the Invariant Measure of Critical Galton-Watson Branching Systems	220
A. V. Shmidt Approximate Solution to a Model of the far Momentumless Axisymmetric Turbulent Wake	229
A. A. Chubarova, M. V. Mamonova, P. V. Prudnikov A Study of the Scaling Behavior of the Two-dimensional Ising Model by Methods of Machine Learning	238
A. A. Levitskiy, P. S. Marinushkin, V. A. Bakhtina Analysis of the Electric Current Distribution in a Three-Layer Conductive Structure	246
M. Krishna, S. B. Kappala, R. Santhikumar Cylindrically Symmetric Generalized Ghost Pilgrim Dark Energy Cosmological Univers	257
A. Kilicman, S. K. Kumari, A. K. Rathie On a New Class of Integrals Involving Generalized Hypergeometric Functions	266
I. V. Smolekho Analysis of the Unstable State of a Nematic Liquid Crystal Based on a Simplified Dynamic Model	272
T. Hamaizia, S. Radenović, A. H. Ansari Coincidence and Common Fixed Point Theorems for Hybrid Mappings Via C-class Function	282

СОДЕРЖАНИЕ

А. Бенрауда Оптимальное управление для задачи упругого фрикционного контакта	151
А. О. Афонин, А. А. Александровский, И. В. Говорун, А. А. Лексиков, А. В. Угрюмов, Д. К. Огородников ВТСП ограничитель мощности с двумя рабочими полосами	162
Е. Д. Лейнартас,, Е. К. Лейнартас Разностные уравнения и композиция Адамара кратных степенных рядов	169
В. К. Белошапка О гипергеометрических функциях двух переменных сложности один	175
А. В. Ейхлер, В. В. Прудников, П. В. Прудников Эффекты гистерезиса в критическом поведении тонких гейзенберговских пленок во внешнем осциллирующем поле	189
В. К. Андреев Термокапиллярная конвекция несмешивающихся жидкостей в трехмерном слое при малых числах Марангони	195
В. Б. Бекежанова, О. Н. Гончарова Об одном точном решении задачи испарительной конвекции с граничными условиями Дирихле	207
А. А. Имомов, С. Б. Искандаров Дальнейшие замечания о явном выражении производящей функции инвариантной меры критических ветвящихся систем Гальтона-Ватсона	220
А. В. Шмидт Приближенное решение модели дальнего безымпульсного осесимметричного турбулентного следа	229
А. А. Чубарова, М. В. Мамонова, П. В. Прудников Исследование скейлингового поведения двумерной модели Изинга методами машинного обучения	238
А. А. Левицкий, П. С. Маринушкин, В. А. Бахтина Анализ распределения электрического тока в трехслойной проводящей структуре	246
М. Кришна, С. Капала, Р. Сантикумар Цилиндрически-симметричный обобщенный призрачный странник, темная энергия космологических вселенных	257
А. Киликман, Ш. К. Курумуджи, А. К. Рати О новом классе интегралов, включающем обобщенные гипергеометрические функции	266
И. В. Смолехо Анализ неустойчивого состояния нематического жидкого кристалла на основе упрощенной динамической модели	272
Т. Хамайзия, С. Раденович, А. Х. Ансари Теоремы о совпадении и общих неподвижных точках для гибридных отображений с помощью функции C -класса	282

EDN: AAVCFR

УДК 539

Optimal Control for an Elastic Frictional Contact Problem

Ahlem Benraouda*

Department of mathematics
University of Science and Technology Houari Boumediene
Bab-Ezzouar, Algeria

Received 10.03.2023, received in revised form 15.06.2023, accepted 04.10.2023

Abstract. We consider a mathematical model which describes a frictional contact between an elastic body and a foundation. We prove the existence of a unique weak solution to the problem. Then, we study the continuous dependence of the solution with respect to the data. Finally, we address an optimal control problem for which we prove the existence of at least one solution.

Keywords: weak solution, Coulomb's friction, continuous dependence, lower semicontinuity, optimal control.

Citation: A. Benraouda, Optimal Control for an Elastic Frictional Contact Problem, J. Sib. Fed. Univ. Math. Phys., 2024, 17(2), 151–161. EDN: AAVCFR.



Introduction

Contact problems abound in industry and everyday life. For this reason, the modelling, numerical analysis and computer simulations of such problems has been extensively studied in engineering and mathematical literature. See for instance [6, 9, 12–14].

Variational inequalities are a powerful mathematical tool to represent various nonlinear boundary value problems and mathematical models arising in Contact Mechanics. Their theory was developed based on arguments of monotonicity and convexity, including properties of the subdifferential of a convex function. References in the field are [1, 3, 4, 7, 8, 10], for instance.

The optimal control theory in the study of mathematical models of contact is quite limited. The difficulties are generated by the strong nonlinearities which arise in the boundary conditions included in such models, also by some features like non-convexity and non-differentiability. Results on optimal control for various contact problems could be found in [2, 5, 11, 16].

In this paper, we consider a mathematical model which describes the contact between an elastic body and a foundation. We assume that the foundation is made of a rigid-plastic material of yield limit ξ . The body is acted upon by body forces of density φ_0 and by tractions of density φ_2 , which act on a part of its boundary. The variational formulation of the model is in a form of an elliptic variational inequality in which the unknown is the displacement field and the data are the densities of applied forces (φ_0, φ_2), the yield limit ξ and the friction bound F_b .

The paper is structured as follows. In Section 1 we introduce some notation and preliminaries. In Section 2 we state the contact model, then we list the assumptions on the data and derive its variational formulation. Also, we state and prove the unique weak solvability of the problem, Theorem 2.1. Section 3 is dedicated to a convergence result, Theorem 3.1, which establishes the continuous dependence of the solution with respect to the densities of applied forces, the yield limit of the foundation and the friction bound. In Section 4 we state an optimal control problem and we prove its solvability, Theorem 4.2.

*abenraouda@usthb.dz

© Siberian Federal University. All rights reserved

1. Preliminaries

In this section, we introduce the notation and some preliminaries materials we shall use. We use the notation \mathbb{R}_+ for the set of non-negative real numbers, \mathbb{S}^d for the space of second order symmetric tensors on \mathbb{R}^d ($d = 1, 2, 3$) and the zero element of the spaces \mathbb{R}^d and \mathbb{S}^d will be denoted by $\mathbf{0}$. The inner products and the corresponding norms on these spaces are defined by

$$\begin{aligned} \mathbf{u} \cdot \mathbf{v} &= u_i v_i, & \|\mathbf{v}\| &= (\mathbf{v} \cdot \mathbf{v})^{\frac{1}{2}} & \forall \mathbf{u}, \mathbf{v} \in \mathbb{R}^d, \\ \boldsymbol{\sigma} \cdot \boldsymbol{\tau} &= \sigma_{ij} \tau_{ij}, & \|\boldsymbol{\tau}\| &= (\boldsymbol{\tau} \cdot \boldsymbol{\tau})^{\frac{1}{2}} & \forall \boldsymbol{\sigma}, \boldsymbol{\tau} \in \mathbb{S}^d, \end{aligned}$$

where the indices i and j run between 1 and d and, unless stated otherwise, the summation convention over repeated indices is adopted.

Let $\Omega \subset \mathbb{R}^d$ be a bounded domain with a smooth boundary $\partial\Omega = \Gamma$ and let Γ_1, Γ_2 and Γ_3 be a partition of Γ into three measurable disjoint parts such that $meas(\Gamma_1) > 0$. We use the notation $\mathbf{x} = (x_i)$ for the generic point in $\Omega \cup \Gamma$ and note that, in order to simplify the notation, we usually do not indicate explicitly the dependence of various functions on the spatial variable \mathbf{x} . Moreover, an index that follows a comma represents the partial derivative with respect to the corresponding component of the spatial variable \mathbf{x} . Also, we denote by $\boldsymbol{\nu} = (\nu_i)$ the outward unit normal at Γ .

Everywhere in this paper, we use the standard notation for Sobolev and Lebesgue spaces of real-valued functions defined on Ω and Γ . In particular, we use the spaces

$$H = L^2(\Omega)^d, \quad H_2 = L^2(\Gamma_2)^d, \quad L^2(\Gamma_3)^d, \quad L^2(\Gamma)^d \quad \text{and} \quad H^1(\Omega)^d,$$

endowed with their canonical inner products and associated norms. Moreover, we recall that for a function $\mathbf{v} \in H^1(\Omega)^d$ we still write \mathbf{v} for the trace $\gamma\mathbf{v} \in L^2(\Gamma)^d$ of \mathbf{v} on the boundary Γ . Let

$$\begin{aligned} V &= \{ \mathbf{v} \in H^1(\Omega)^d : \mathbf{v} = \mathbf{0} \text{ a.e. on } \Gamma_1 \}, \\ Q &= \{ \boldsymbol{\sigma} = (\sigma_{ij}) : \sigma_{ij} = \sigma_{ji} \in L^2(\Omega), 1 \leq i, j \leq d \}, \end{aligned}$$

which are real Hilbert spaces endowed with the canonical inner products given by

$$(\mathbf{u}, \mathbf{v})_V = \int_{\Omega} \boldsymbol{\varepsilon}(\mathbf{u}) \cdot \boldsymbol{\varepsilon}(\mathbf{v}) \, dx, \quad (\boldsymbol{\sigma}, \boldsymbol{\tau})_Q = \int_{\Omega} \boldsymbol{\sigma} \cdot \boldsymbol{\tau} \, dx.$$

The associated norms on these spaces are denoted by $\|\cdot\|_V$ and $\|\cdot\|_Q$, respectively. Here and below, $\boldsymbol{\varepsilon}$ and Div will represent the deformation and the divergence operators, respectively, i.e.,

$$\boldsymbol{\varepsilon}(\mathbf{u}) = (\varepsilon_{ij}(\mathbf{u})), \quad \varepsilon_{ij}(\mathbf{v}) = \frac{1}{2}(u_{i,j} + u_{j,i}), \quad \text{Div } \boldsymbol{\sigma} = (\sigma_{ij,j}),$$

where the quantity $\boldsymbol{\varepsilon}(\mathbf{u})$ represents the linearised strain tensor associated with the displacement \mathbf{u} .

Let $\mathbf{0}_{H_2}$ denote the zero element of H_2 and $\mathbf{0}_V$ the zero element of V . For any element $\mathbf{v} \in V$ we denote by v_ν and \mathbf{v}_τ its normal and tangential components on Γ given by $v_\nu = \mathbf{v} \cdot \boldsymbol{\nu}$ and $\mathbf{v}_\tau = \mathbf{v} - v_\nu \boldsymbol{\nu}$. Moreover, for a regular function $\boldsymbol{\sigma} : \Omega \rightarrow \mathbb{S}^d$ we denote by σ_ν and $\boldsymbol{\sigma}_\tau$ its normal and tangential components on Γ , that is $\sigma_\nu = (\boldsymbol{\sigma}\boldsymbol{\nu}) \cdot \boldsymbol{\nu}$ and $\boldsymbol{\sigma}_\tau = \boldsymbol{\sigma}\boldsymbol{\nu} - \sigma_\nu \boldsymbol{\nu}$ and, we recall that the following Green's formula holds:

$$\int_{\Omega} \boldsymbol{\sigma} \cdot \boldsymbol{\varepsilon}(\mathbf{v}) \, dx + \int_{\Omega} \text{Div } \boldsymbol{\sigma} \cdot \mathbf{v} \, dx = \int_{\Gamma} \boldsymbol{\sigma}\boldsymbol{\nu} \cdot \mathbf{v} \, da \quad \forall \mathbf{v} \in H^1(\Omega)^d. \quad (1.1)$$

Also, recall that there exists a positive constant c_{tr} , depending on Ω and Γ_1 , such that

$$\|\mathbf{v}\|_{L^2(\Gamma)^d} \leq c_{tr} \|\mathbf{v}\|_V \quad \forall \mathbf{v} \in V. \quad (1.2)$$

Inequality (1.2) represents a consequence of the Sobolev trace theorem.

We end this section with the following result.

Theorem 1.1. *Let X be a real Hilbert space and assume that K is a nonempty closed convex subset of X , $A : X \rightarrow X$ is a strongly monotone Lipschitz continuous operator and $j : X \rightarrow \mathbb{R}$ is a convex lower semicontinuous function. Then, for each $f \in X$ there exists a unique solution to the variational inequality*

$$u \in K, \quad (Au, v - u)_X + j(v) - j(u) \geq (f, v - u)_X \quad \forall v \in K. \quad (1.3)$$

Theorem 1.1 will be used in Section 2 to prove the unique weak solvability of our mathematical model of contact. Its proof could be found in [14].

2. Problem statement and variational formulation

The physical setting of the problem is the following. We consider a body made of an elastic material which occupies a bounded domain $\Omega \subset \mathbb{R}^d$ with a smooth boundary $\partial\Omega = \Gamma$, divided into three measurable disjoint parts Γ_1, Γ_2 and Γ_3 such that $meas(\Gamma_1) > 0$. The body is fixed on Γ_1 , it is acted by given body forces of density φ_0 . Also, we assume that surface tractions of density φ_2 act on Γ_2 , and the body is in contact with an obstacle on Γ_3 .

The classical formulation of the contact problem is as follows.

Problem \mathcal{P} . *Find a displacement field $\mathbf{u} : \Omega \rightarrow \mathbb{R}^d$ and a stress field $\boldsymbol{\sigma} : \Omega \rightarrow \mathbb{S}^d$ such that*

$$\boldsymbol{\sigma} = \mathcal{E}\boldsymbol{\varepsilon}(\mathbf{u}) \quad \text{in } \Omega, \quad (2.1)$$

$$\text{Div } \boldsymbol{\sigma} + \varphi_0 = \mathbf{0} \quad \text{in } \Omega, \quad (2.2)$$

$$\mathbf{u} = \mathbf{0} \quad \text{on } \Gamma_1, \quad (2.3)$$

$$\boldsymbol{\sigma}\boldsymbol{\nu} = \varphi_2 \quad \text{on } \Gamma_2, \quad (2.4)$$

$$-\xi \leq \sigma_\nu \leq 0, \quad -\sigma_\nu = \begin{cases} 0 & \text{if } u_\nu < 0 \\ \xi & \text{if } u_\nu > 0 \end{cases} \quad \text{on } \Gamma_3, \quad (2.5)$$

$$\|\boldsymbol{\sigma}_\tau\| \leq F_b, \quad -\boldsymbol{\sigma}_\tau = F_b \frac{\mathbf{u}_\tau}{\|\mathbf{u}_\tau\|} \quad \text{if } \mathbf{u}_\tau \neq \mathbf{0} \quad \text{on } \Gamma_3. \quad (2.6)$$

We now provide a description of the equations and boundary conditions in Problem \mathcal{P} . First, equation (2.1) represents the elastic constitutive law of the material. We assume that the non-linear elasticity operator \mathcal{E} satisfies the following conditions

$$\left\{ \begin{array}{l} \text{(a) } \mathcal{E} : \Omega \times \mathbb{S}^d \rightarrow \mathbb{S}^d. \\ \text{(b) There exists } L_\mathcal{E} > 0 \text{ such that} \\ \quad \|\mathcal{E}(\mathbf{x}, \boldsymbol{\varepsilon}_1) - \mathcal{E}(\mathbf{x}, \boldsymbol{\varepsilon}_2)\| \leq L_\mathcal{E} \|\boldsymbol{\varepsilon}_1 - \boldsymbol{\varepsilon}_2\| \\ \quad \forall \boldsymbol{\varepsilon}_1, \boldsymbol{\varepsilon}_2 \in \mathbb{S}^d, \text{ a.e. } \mathbf{x} \in \Omega. \\ \text{(c) There exists } m_\mathcal{E} > 0 \text{ such that} \\ \quad (\mathcal{E}(\mathbf{x}, \boldsymbol{\varepsilon}_1) - \mathcal{E}(\mathbf{x}, \boldsymbol{\varepsilon}_2)) \cdot (\boldsymbol{\varepsilon}_1 - \boldsymbol{\varepsilon}_2) \geq m_\mathcal{E} \|\boldsymbol{\varepsilon}_1 - \boldsymbol{\varepsilon}_2\|^2 \\ \quad \forall \boldsymbol{\varepsilon}_1, \boldsymbol{\varepsilon}_2 \in \mathbb{S}^d, \text{ a.e. } \mathbf{x} \in \Omega. \\ \text{(d) The mapping } \mathbf{x} \mapsto \mathcal{E}(\mathbf{x}, \boldsymbol{\varepsilon}) \text{ is measurable on } \Omega, \\ \quad \text{for any } \boldsymbol{\varepsilon} \in \mathbb{S}^d. \\ \text{(e) The mapping } \mathbf{x} \mapsto \mathcal{E}(\mathbf{x}, \mathbf{0}) \text{ belongs to } Q. \end{array} \right. \quad (2.7)$$

Concrete examples of operators \mathcal{E} which satisfy condition (2.7) can be found, for example, in [14, 17].

Equation (2.2) is the equation of equilibrium. Conditions (2.3), (2.4) represent the displacement and traction boundary conditions, respectively. We assume that the densities of body forces and tractions are such that

$$\varphi_0 \in H, \quad (2.8)$$

$$\varphi_2 \in H_2. \quad (2.9)$$

Next, (2.5) represent the contact condition in which σ_ν denotes the normal stress and u_ν is the normal displacement. Moreover, the function ξ satisfies

$$\xi \in L^2(\Gamma_3), \quad \xi(\mathbf{x}) \geq 0 \quad \text{a.e. } \mathbf{x} \in \Gamma_3. \quad (2.10)$$

We now provide some comments on this condition. It is described by the multivalued relation between the normal displacement and the opposite of the normal stress. This condition was already used in [15], where a detailed description was provided, together with some mechanical interpretation. It models the contact with a foundation made of a rigid-plastic material. Indeed, this condition shows that the foundation behaves like a rigid body as far as the inequality $|\sigma_\nu| < \xi$ holds, where the function ξ could be interpreted as the yield limit of the the foundation. It could allow penetration only when the equality $|\sigma_\nu| = \xi$ holds. In this case, the yield limit ξ is reached and the foundation offers no additional resistance to penetration.

Finally, (2.6) represents the contact with Coulomb's friction law where F_b is a given friction bound. We assume that

$$F_b \in L^2(\Gamma_3), \quad F_b(\mathbf{x}) \geq 0 \quad \text{a.e. } \mathbf{x} \in \Gamma_3. \quad (2.11)$$

In this section, we derive the variational formulation of Problem \mathcal{P} and, to this end, we assume in what follows that $(\mathbf{u}, \boldsymbol{\sigma})$ are sufficiently regular functions which satisfy (2.1)–(2.6). Let $\mathbf{v} \in V$. We use Green's formula (1.1), then we split the surface integral over Γ_1 , Γ_2 and Γ_3 and use equalities (2.2), (2.4) to obtain that

$$(\boldsymbol{\sigma}, \boldsymbol{\varepsilon}(\mathbf{v}) - \boldsymbol{\varepsilon}(\mathbf{u}))_Q = (\varphi_0, \mathbf{v} - \mathbf{u})_H + (\varphi_2, \mathbf{v} - \mathbf{u})_{H_2} + \int_{\Gamma_1} \boldsymbol{\sigma}_\nu \cdot (\mathbf{v} - \mathbf{u}) \, da + \int_{\Gamma_3} \boldsymbol{\sigma}_\nu \cdot (\mathbf{v} - \mathbf{u}) \, da.$$

Moreover, using this equality

$$\boldsymbol{\sigma}_\nu \cdot (\mathbf{v} - \mathbf{u}) = \sigma_\nu(v_\nu - u_\nu) + \boldsymbol{\sigma}_\tau \cdot (\mathbf{v}_\tau - \mathbf{u}_\tau) \quad \text{a.e. on } \Gamma,$$

and the condition (2.3), we obtain that

$$\begin{aligned} (\boldsymbol{\sigma}, \boldsymbol{\varepsilon}(\mathbf{v}) - \boldsymbol{\varepsilon}(\mathbf{u}))_Q &= (\varphi_0, \mathbf{v} - \mathbf{u})_H + (\varphi_2, \mathbf{v} - \mathbf{u})_{H_2} + \\ &+ \int_{\Gamma_3} \sigma_\nu(v_\nu - u_\nu) \, da + \int_{\Gamma_3} \boldsymbol{\sigma}_\tau \cdot (\mathbf{v}_\tau - \mathbf{u}_\tau) \, da. \end{aligned} \quad (2.12)$$

We use standard arguments and the hypothesis (2.10) to see that the contact condition (2.5) implies that

$$\int_{\Gamma_3} \sigma_\nu(v_\nu - u_\nu) \, da \geq \int_{\Gamma_3} \xi(u_\nu^+ - v_\nu^+) \, da, \quad (2.13)$$

where r^+ denotes the positive part of r , i.e., $r^+ = \max\{r, 0\}$. In addition, it is easy to see that the condition (2.6) yields

$$\int_{\Gamma_3} \boldsymbol{\sigma}_\tau \cdot (\mathbf{v}_\tau - \mathbf{u}_\tau) \, da \geq \int_{\Gamma_3} F_b(\|\mathbf{u}_\tau\| - \|\mathbf{v}_\tau\|) \, da. \quad (2.14)$$

Next, we combine (2.12)–(2.14), then we use the constitutive law (2.1) to see that

$$\begin{aligned} (\mathcal{E}\varepsilon(\mathbf{u}), \varepsilon(\mathbf{v}) - \varepsilon(\mathbf{u}))_Q + \int_{\Gamma_3} \xi(v_\nu^+ - u_\nu^+) da + \int_{\Gamma_3} F_b(\|\mathbf{v}_\tau\| - \|\mathbf{u}_\tau\|) da &\geq \\ &\geq (\varphi_0, \mathbf{v} - \mathbf{u})_H + (\varphi_2, \mathbf{v} - \mathbf{u})_{H_2}. \end{aligned} \quad (2.15)$$

Now, we introduce the operator $A : V \rightarrow V$ and the function $j : V \rightarrow \mathbb{R}$ defined by

$$(A\mathbf{u}, \mathbf{v})_V = \int_{\Omega} \mathcal{E}\varepsilon(\mathbf{u}) \cdot \varepsilon(\mathbf{v}) dx \quad \forall \mathbf{u}, \mathbf{v} \in V, \quad (2.16)$$

$$j(\mathbf{v}) = \int_{\Gamma_3} \xi v_\nu^+ da + \int_{\Gamma_3} F_b \|\mathbf{v}_\tau\| da \quad \forall \mathbf{v} \in V. \quad (2.17)$$

Using these definitions and inequality (2.15), we find the following variational formulation of Problem \mathcal{P} .

Problem \mathcal{P}_V . Find a displacement field $\mathbf{u} \in V$ such that

$$\begin{aligned} (A\mathbf{u}, \mathbf{v} - \mathbf{u})_V + j(\mathbf{v}) - j(\mathbf{u}) &\geq \\ &\geq (\varphi_0, \mathbf{v} - \mathbf{u})_H + (\varphi_2, \mathbf{v} - \mathbf{u})_{H_2} \quad \forall \mathbf{v} \in V. \end{aligned} \quad (2.18)$$

We have the following existence and uniqueness result.

Theorem 2.1. Assume that (2.7)–(2.11) hold. Then, Problem \mathcal{P}_V has a unique solution $\mathbf{u} \in V$.

Proof. We apply Theorem 1.1 with $K = X = V$. To this end, we use the definition (2.16) and assumption (2.7)(c) to see that

$$(A\mathbf{u} - A\mathbf{v}, \mathbf{u} - \mathbf{v})_V \geq m_\mathcal{E} \|\mathbf{u} - \mathbf{v}\|_V^2 \quad \forall \mathbf{u}, \mathbf{v} \in V. \quad (2.19)$$

On the other hand, using assumption (2.7)(b), we obtain that

$$\|A\mathbf{u} - A\mathbf{v}\|_V \leq L_\mathcal{E} \|\mathbf{u} - \mathbf{v}\|_V \quad \forall \mathbf{u}, \mathbf{v} \in V. \quad (2.20)$$

We conclude from (2.19) and (2.20) that A is a strongly monotone Lipschitz continuous operator on the space V .

Moreover, using (2.10)–(2.11) and (1.2), we see that the functional j defined by (2.17) is a seminorm on V and, in addition, it satisfies

$$j(\mathbf{v}) \leq c_{tr}(\|\xi\|_{L^2(\Gamma_3)} + \|F_b\|_{L^2(\Gamma_3)}) \|\mathbf{v}\|_V \quad \forall \mathbf{v} \in V.$$

It follows that j is a continuous seminorm and, therefore, it is a convex and lower semicontinuous function on V . Finally, using the Riesz representation theorem, we define $\mathbf{f} \in V$ as follows

$$(\mathbf{f}, \mathbf{v})_V = (\varphi_0, \mathbf{v})_H + (\varphi_2, \mathbf{v})_{H_2} \quad \forall \mathbf{v} \in V.$$

Theorem 2.1 now is a direct consequence of Theorem 1.1. \square

3. A continuous dependence result

In this section, we study the dependence of the solution \mathbf{u} of Problem \mathcal{P}_V with respect to the data φ_0 , φ_2 , ξ and F_b . To this end, we assume in what follows that (2.7)–(2.11) hold, and

we consider a perturbation $\varphi_{0\eta}$, $\varphi_{2\eta}$, ξ_η and $F_{b\eta}$ of φ_0 , φ_2 , ξ and F_b , respectively, which satisfy (2.8)–(2.11). For each $\eta > 0$, we introduce the functional $j_\eta : V \rightarrow \mathbb{R}$ defined by

$$j_\eta(\mathbf{v}) = \int_{\Gamma_3} \xi_\eta v_\nu^+ da + \int_{\Gamma_3} F_{b\eta} \|\mathbf{v}_\tau\| da \quad \forall \mathbf{v} \in V, \quad (3.1)$$

and, we consider the following variational problem.

Problem \mathcal{P}_V^η . Find a displacement field $\mathbf{u}_\eta \in V$ such that

$$(A\mathbf{u}_\eta, \mathbf{v} - \mathbf{u}_\eta)_V + j_\eta(\mathbf{v}) - j_\eta(\mathbf{u}_\eta) \geq (\varphi_{0\eta}, \mathbf{v} - \mathbf{u}_\eta)_H + (\varphi_{2\eta}, \mathbf{v} - \mathbf{u}_\eta)_{H_2} \quad \forall \mathbf{v} \in V. \quad (3.2)$$

It follows from Theorem 2.1 that, for each $\eta > 0$, Problem \mathcal{P}_V^η has a unique solution $\mathbf{u}_\eta \in V$. The behaviour of the solution \mathbf{u}_η as $\eta \rightarrow 0$ is given in the following result.

Theorem 3.1. Assume that (2.7)–(2.11) hold and, moreover, assume

$$\varphi_{0\eta} \rightharpoonup \varphi_0 \quad \text{in } H \quad \text{as } \eta \rightarrow 0, \quad (3.3)$$

$$\varphi_{2\eta} \rightharpoonup \varphi_2 \quad \text{in } H_2 \quad \text{as } \eta \rightarrow 0, \quad (3.4)$$

$$\xi_\eta \rightarrow \xi \quad \text{in } L^2(\Gamma_3) \quad \text{as } \eta \rightarrow 0. \quad (3.5)$$

$$F_{b\eta} \rightarrow F_b \quad \text{in } L^2(\Gamma_3) \quad \text{as } \eta \rightarrow 0. \quad (3.6)$$

Then, the following convergence holds

$$\mathbf{u}_\eta \rightarrow \mathbf{u} \quad \text{in } V \quad \text{as } \eta \rightarrow 0. \quad (3.7)$$

The proof of Theorem 3.1 will be carried out in two steps. First, we provide the following weak convergence result.

Lemma 3.2. The sequence $\{\mathbf{u}_\eta\}$ converges weakly in V to \mathbf{u} , i.e.,

$$\mathbf{u}_\eta \rightharpoonup \mathbf{u} \quad \text{in } V \quad \text{as } \eta \rightarrow 0. \quad (3.8)$$

Proof. Let $\eta > 0$. We take $\mathbf{v} = \mathbf{0}_V$ in (3.2) to obtain

$$(A\mathbf{u}_\eta - A\mathbf{0}_V, \mathbf{u}_\eta)_V + j_\eta(\mathbf{u}_\eta) \leq (\varphi_{0\eta}, \mathbf{u}_\eta)_H + (\varphi_{2\eta}, \mathbf{u}_\eta)_{H_2} - (A\mathbf{0}_V, \mathbf{u}_\eta)_V.$$

Next, using assumption (2.19), the positivity of the functional j and the inequality (1.2), we deduce that

$$\begin{aligned} \|\mathbf{u}_\eta\|_V &\leq \frac{1}{m_\mathcal{E}} (\|\varphi_{0\eta}\|_H + c_{tr} \|\varphi_{2\eta}\|_{H_2} + \|A\mathbf{0}_V\|_V) \leq \\ &\leq \frac{\max(1, c_{tr})}{m_\mathcal{E}} (\|\varphi_{0\eta}\|_H + \|\varphi_{2\eta}\|_{H_2} + \|A\mathbf{0}_V\|_V). \end{aligned}$$

The convergences (3.3) and (3.4) imply that the sequences $\{\varphi_{0\eta}\}$ and $\{\varphi_{2\eta}\}$ are bounded in H and H_2 , respectively. Therefore, we deduce that there exists $M > 0$, which does not depend on η , such that

$$\|\mathbf{u}_\eta\|_V \leq M. \quad (3.9)$$

Now, we combine (3.9) with a standard compactness argument to see that there exists $\tilde{\mathbf{u}} \in V$ such that, passing to a subsequence, still denoted $\{\mathbf{u}_\eta\}$, we have

$$\mathbf{u}_\eta \rightharpoonup \tilde{\mathbf{u}} \quad \text{in } V \quad \text{as } \eta \rightarrow 0. \quad (3.10)$$

We establish the equality

$$\tilde{\mathbf{u}} = \mathbf{u}. \quad (3.11)$$

Let $\eta > 0$. We take $\mathbf{v} = \tilde{\mathbf{u}} \in V$ in (3.2) to obtain that

$$(A\mathbf{u}_\eta, \mathbf{u}_\eta - \tilde{\mathbf{u}})_V \leq (\varphi_{0\eta}, \mathbf{u}_\eta - \tilde{\mathbf{u}})_H + (\varphi_{2\eta}, \mathbf{u}_\eta - \tilde{\mathbf{u}})_{H_2} + j_\eta(\tilde{\mathbf{u}}) - j_\eta(\mathbf{u}_\eta).$$

Next, we pass to the upper limit as $\eta \rightarrow 0$ in this inequality and taking into account the convergences (3.3)–(3.6), (3.10) and the compactness of the trace operator, we deduce that

$$\limsup_{\eta \rightarrow 0} (A\mathbf{u}_\eta, \mathbf{u}_\eta - \tilde{\mathbf{u}})_V \leq 0.$$

Therefore, assumptions (2.19)–(2.20) and the convergence (3.10) yield

$$\liminf_{\eta \rightarrow 0} (A\mathbf{u}_\eta, \mathbf{u}_\eta - \mathbf{v})_V \geq (A\tilde{\mathbf{u}}, \tilde{\mathbf{u}} - \mathbf{v})_V \quad \forall \mathbf{v} \in V. \quad (3.12)$$

On the other hand, we pass to the upper limit in (3.2) and we use again the convergences (3.3)–(3.6), (3.10) and the compactness of the trace operator to obtain that

$$\limsup_{\eta \rightarrow 0} (A\mathbf{u}_\eta, \mathbf{u}_\eta - \mathbf{v})_V \leq (\varphi_0, \tilde{\mathbf{u}} - \mathbf{v})_H + (\varphi_2, \tilde{\mathbf{u}} - \mathbf{v})_{H_2} + j(\mathbf{v}) - j(\tilde{\mathbf{u}}) \quad \forall \mathbf{v} \in V.$$

We combine now this inequality and (3.12) to see that

$$(A\tilde{\mathbf{u}}, \mathbf{v} - \tilde{\mathbf{u}})_V + j(\mathbf{v}) - j(\tilde{\mathbf{u}}) \geq (\varphi_0, \mathbf{v} - \tilde{\mathbf{u}})_H + (\varphi_2, \mathbf{v} - \tilde{\mathbf{u}})_{H_2} \quad \forall \mathbf{v} \in V. \quad (3.13)$$

Next, we take $\mathbf{v} = \mathbf{u}$ in (3.13) and $\mathbf{v} = \tilde{\mathbf{u}}$ in (2.18), then, adding the resulting inequalities and using assumption (2.19), we obtain that the equality (3.11) holds.

A carefully examination of the proof of Lemma 3.2 shows that any weakly convergent subsequence of the sequence $\{\mathbf{u}_\eta\} \subset V$ converges weakly to $\mathbf{u} \in V$, where, \mathbf{u} is the unique solution of (2.18). Moreover, the bound (3.9) shows that the sequence $\{\mathbf{u}_\eta\}$ is bounded in V and, therefore, Lemma 3.2 is a consequence of a standard compactness argument. \square

We proceed with the following strong convergence result.

Lemma 3.3. *The sequence $\{\mathbf{u}_\eta\}$ converges strongly in V to \mathbf{u} , i.e.,*

$$\mathbf{u}_\eta \rightarrow \mathbf{u} \quad \text{in } V \quad \text{as } \eta \rightarrow 0. \quad (3.14)$$

Proof. Let $\eta > 0$. We take $\mathbf{v} = \mathbf{u}$ in (3.2) to obtain that

$$(A\mathbf{u}_\eta, \mathbf{u}_\eta - \mathbf{u})_V \leq (\varphi_{0\eta}, \mathbf{u}_\eta - \mathbf{u})_H + (\varphi_{2\eta}, \mathbf{u}_\eta - \mathbf{u})_{H_2} + j_\eta(\mathbf{u}) - j_\eta(\mathbf{u}_\eta).$$

Next, we use this inequality and assumption (2.19) to see that

$$\begin{aligned} m_{\mathcal{E}} \|\mathbf{u}_\eta - \mathbf{u}\|_V^2 &\leq (A\mathbf{u}_\eta - A\mathbf{u}, \mathbf{u}_\eta - \mathbf{u})_V = \\ &= (A\mathbf{u}_\eta, \mathbf{u}_\eta - \mathbf{u})_V - (A\mathbf{u}, \mathbf{u}_\eta - \mathbf{u})_V \leq \\ &\leq (\varphi_{0\eta}, \mathbf{u}_\eta - \mathbf{u})_H + (\varphi_{2\eta}, \mathbf{u}_\eta - \mathbf{u})_{H_2} + j_\eta(\mathbf{u}) - j_\eta(\mathbf{u}_\eta) - (A\mathbf{u}, \mathbf{u}_\eta - \mathbf{u})_V. \end{aligned}$$

We now pass to the limit as $\eta \rightarrow 0$ and we use (3.3)–(3.6), (3.8) and the compactness of the trace operator. As a result we deduce that

$$\|\mathbf{u}_\eta - \mathbf{u}\|_V \rightarrow 0 \quad \text{as } \eta \rightarrow 0,$$

which concludes the proof. \square

We are now in position to present the proof of Theorem 3.1.

Proof. The convergence (3.7) is a consequence of Lemma 3.2. \square

The convergence result (3.7) is important from mechanical point of view, since it shows that the weak solution of the elastic contact problem (2.1)–(2.6) depends continuously on the densities of applied forces, the yield limit and the friction bound.

4. The optimal control problem

In this section, we formulate an optimal control problem associate to Problem \mathcal{P}_V . To this end, we assume that conditions (2.7)–(2.11) hold and, in order to control the solution of Problem \mathcal{P}_V by the density of surface tractions φ_2 , we assume that φ_0 , ξ and F_b are given and satisfy (2.8), (2.10), (2.11), respectively. Let $\phi \in V$ and $\delta, \gamma > 0$ be two positive constants and let us define the cost functional $\mathcal{L} : H_2 \times V \rightarrow \mathbb{R}$ by

$$\mathcal{L}(\varphi_2, \mathbf{u}) = \delta \|\mathbf{u} - \phi\|_V + \gamma \|\varphi_2\|_{H_2} \quad \forall (\varphi_2, \mathbf{u}) \in H_2 \times V. \quad (4.1)$$

Using standard arguments it is easy to see that \mathcal{L} is a convex lower semicontinuous functional on $H_2 \times V$ and, therefore, it is weakly lower semicontinuous. Also, we define the following admissible set

$$\mathcal{V}_{ad} = \{ (\varphi_2, \mathbf{u}) \in H_2 \times V, \text{ such that (2.18) holds } \}. \quad (4.2)$$

We formulate now the following optimal control problem.

Problem \mathcal{O} . Find $(\varphi_2^*, \mathbf{u}^*) \in \mathcal{V}_{ad}$ such that

$$\mathcal{L}(\varphi_2^*, \mathbf{u}^*) = \min_{(\varphi_2, \mathbf{u}) \in \mathcal{V}_{ad}} \mathcal{L}(\varphi_2, \mathbf{u}).$$

An element $(\varphi_2^*, \mathbf{u}^*)$ is called an *optimal pair* and the corresponding surface traction force φ_2^* is called an *optimal control*. The mechanical interpretation of Problem \mathcal{O} is the following : we are looking for a given surface traction force $\varphi_2 \in H_2$ such that the displacement $\mathbf{u} \in V$ given by (2.18) is as close as possible to the “desired displacement” ϕ . Furthermore, this choice has to fulfil a minimum expenditure condition which is taken into account by the second term in the definition (4.1).

Our result in this section is the following.

Theorem 4.1. *Assume that (2.7)–(2.8) and (2.10)–(2.11) hold. Then, there exists at least one solution $(\varphi_2^*, \mathbf{u}^*) \in \mathcal{V}_{ad}$ of Problem \mathcal{O} .*

The proof of Theorem 4.1 will be carried out in two steps, that we present in what follows. We start by considering the following functional $J : H_2 \rightarrow \mathbb{R}$ defined by

$$J(\varphi_2) = \delta \|\mathbf{u}(\varphi_2) - \phi\|_V + \gamma \|\varphi_2\|_{H_2} \quad \forall \varphi_2 \in H_2, \quad (4.3)$$

where $\mathbf{u} = \mathbf{u}(\varphi_2)$ is the solution of (2.18). Next, we consider the following optimization problem.

Problem \mathcal{O}_1 . Find $\varphi_2^* \in H_2$ such that

$$J(\varphi_2^*) = \min_{\varphi_2 \in H_2} J(\varphi_2). \quad (4.4)$$

We have the following existence result.

Lemma 4.2. *There exists at least one solution $\varphi_2^* \in H_2$ of Problem \mathcal{O}_1 .*

Proof. Let

$$\theta = \inf_{\varphi_2 \in H_2} J(\varphi_2) \in \mathbb{R}, \quad (4.5)$$

and let $\{\varphi_{2n}\} \subset H_2$ such that

$$\lim_{n \rightarrow \infty} J(\varphi_{2n}) = \theta. \quad (4.6)$$

We prove that the sequence $\{\varphi_{2n}\}$ is bounded in H_2 . Arguing by contradiction, assume that $\{\varphi_{2n}\}$ is not bounded in H_2 . Then, we pass to a subsequence, still denoted $\{\varphi_{2n}\}$, to see that

$$\|\varphi_{2n}\|_{H_2} \rightarrow +\infty \quad \text{in } H_2 \quad \text{as } n \rightarrow +\infty. \quad (4.7)$$

Using the definition (4.3) and the positivity of the parameters δ and γ to see that

$$J(\varphi_{2n}) = \delta \|\mathbf{u}(\varphi_{2n}) - \phi\|_V + \gamma \|\varphi_{2n}\|_{H_2} \geq \gamma \|\varphi_{2n}\|_{H_2},$$

then, passing to the limit as $n \rightarrow +\infty$ and using (4.7) we deduce that

$$\lim_{n \rightarrow +\infty} J(\varphi_{2n}) = +\infty.$$

We combine this equality with (4.6) to see that $\theta = +\infty$ which is a contradiction with (4.5) and, therefore, we conclude that the sequence $\{\varphi_{2n}\}$ is bounded in H_2 . Thus, a standard compactness argument implies that there exists $\varphi_2^* \in H_2$ such that, passing to a subsequence, still denoted $\{\varphi_{2n}\}$, we have

$$\varphi_{2n} \rightharpoonup \varphi_2^* \quad \text{in } H_2 \quad \text{as } n \rightarrow +\infty. \quad (4.8)$$

In addition, using the convergence (4.8) and the continuous dependence result given by Theorem 3.1, we have that

$$\mathbf{u}(\varphi_{2n}) \rightarrow \mathbf{u}(\varphi_2^*) \quad \text{in } V \quad \text{as } n \rightarrow +\infty. \quad (4.9)$$

We now use (4.8) and (4.9) to see that

$$\begin{aligned} \lim_{n \rightarrow +\infty} \|\mathbf{u}(\varphi_{2n}) - \phi\|_V &= \|\mathbf{u}(\varphi_2^*) - \phi\|_V, \\ \liminf_{n \rightarrow +\infty} \|\varphi_{2n}\|_{H_2} &\geq \|\varphi_2^*\|_{H_2}, \end{aligned}$$

which imply that

$$\liminf_{n \rightarrow +\infty} J(\varphi_{2n}) \geq J(\varphi_2^*). \quad (4.10)$$

It follows from (4.6) and (4.10) that

$$\theta \geq J(\varphi_2^*). \quad (4.11)$$

On the other hand, (4.5) implies that

$$\theta \leq J(\varphi_2^*). \quad (4.12)$$

Finally, we combine (4.11) and (4.12) to see that (4.4) holds, which concludes the proof. \square

We proceed with the following existence result.

Lemma 4.3. *There exists at least one solution $(\varphi_2^*, \mathbf{u}^*) \in \mathcal{V}_{ad}$ of Problem \mathcal{O} .*

Proof. We note that

$$(\varphi_2, \mathbf{u}) \in \mathcal{V}_{ad} \iff \varphi_2 \in H_2 \text{ and } \mathbf{u} = \mathbf{u}(\varphi_2) \text{ is the solution of (2.18)}. \quad (4.13)$$

The definitions (4.1) and (4.3) imply that

$$J(\varphi_2) = \mathcal{L}(\varphi_2, \mathbf{u}(\varphi_2)) \quad \forall \varphi_2 \in H_2.$$

Let $\varphi_2^* \in H_2$ be a solution of Problem \mathcal{O}_1 and $\mathbf{u}^* = \mathbf{u}(\varphi_2^*)$ be the solution of (2.18) with the data $\varphi_2 = \varphi_2^*$. Then, by using (4.13) we deduce that

$$(\varphi_2^*, \mathbf{u}^*) \in \mathcal{V}_{ad}. \quad (4.14)$$

Moreover, we have that

$$\mathcal{L}(\varphi_2^*, \mathbf{u}^*) = J(\varphi_2^*) \leq J(\varphi_2) = \mathcal{L}(\varphi_2, \mathbf{u})$$

for all $(\varphi_2, \mathbf{u}) \in \mathcal{V}_{ad}$. Combining this inequality with (4.14), we deduce that $(\varphi_2^*, \mathbf{u}^*)$ is a solution of Problem \mathcal{O} , which concludes the proof. \square

We are now in position to present the proof of Theorem 4.1.

Proof. Theorem 4.1 is a direct consequence of Lemma 4.3. \square

References

- [1] C.Baiocchi, A.Capelo, Variational and Quasivariational Inequalities: Applications to Free-Boundary Problems, John Wiley, Chichester, 1984.
- [2] V.Barbu, Optimal Control of Variational Inequalities, Pitman Advanced Publishing, Boston, 1984.
- [3] H.Brézis, Equations et inéquations non linéaires dans les espaces vectoriels en dualité, *Ann. Inst. Fourier (Grenoble)*, **18**(1968), 115–175.
- [4] A.Capatina, Variational Inequalities and Frictional Contact Problems, *Advances in Mechanics and Mathematics*, Vol. 31, Springer, New York, 2014.
- [5] A.Friedman, Optimal control for variational inequalities, *SIAM J. Control Optim.* **24**(1986), no. 3, 439–451.
- [6] W.Han, M.Sofonea, Quasistatic Contact Problems in Viscoelasticity and Viscoplasticity, *Studies in Advanced Mathematics*, Vol. 30, American Mathematical Society, Providence, RI–International Press, Somerville, MA, 2002.
- [7] I.Hlaváček, J.Haslinger, J.Nečas, J.Lovíšek, Solution of Variational Inequalities in Mechanics, Springer-Verlag, New York, 1988.
- [8] N.Kikuchi, J.T.Oden, Theory of variational inequalities with applications to problems of flow through porous media, *Int. J. Engng. Sci.*, **18**(1980), 1173–1284.
- [9] T.A.Laursen, Computational Contact and Impact Mechanics, Springer, Berlin, 2002.
- [10] J.-L.Lions, Quelques méthodes de résolution des problèmes aux limites non linéaires, Gauthiers-Villars, Paris, 1969.
- [11] R.Mignot, J.P.Puel, Optimal control in some variational inequalities, *SIAM J. Control Optim.*, **22**(1984), 466–476.
- [12] S.Migórski, A.Ochal, M.Sofonea, Nonlinear Inclusions and Hemivariational Inequalities. Models and Analysis of Contact Problems, *Advances in Mechanics and Mathematics*, Vol. 26, Springer, New York, 2013.
- [13] M.Shillor, M.Sofonea, J.J.Telega, Models and Analysis of Quasistatic Contact, *Lect. Notes Phys.*, Vol. 655, Springer, Berlin, 2004.
- [14] M.Sofonea, A.Matei, Mathematical Models in Contact Mechanics, London Mathematical Society Lecture Note Series **398**, Cambridge University Press, 2012.

- [15] M.Sofonea, S.Migórski, Variational Hemivariational Inequalities with Applications, Chapman and Hall/CRC, New York, 2017.
- [16] A.Touzaline, Optimal control of a frictional contact problem, *Acta Mathematicae Applicatae Sinica, English Series* **31**(2015), 991–1000. DOI: 10.1007/s10255-015-0519-8
- [17] E.Zeidler, Nonlinear Functional Analysis and its Applications. IV: Applications to Mathematical Physics, New York, Springer-Verlag,

Оптимальное управление для задачи упругого фрикционного контакта

Ахлем Бенрауда

Университет науки и технологий Хуари Бумедьена
Баб-Эззуар, Алжир

Аннотация. Рассматривается математическая модель, описывающая фрикционный контакт упругого тела с фундаментом. Доказано существование единственного слабого решения задачи. Изучается непрерывная зависимость решения от данных. Наконец, мы рассматриваем задачу оптимального управления, для которой доказываем существование хотя бы одного решения.

Ключевые слова: слабое решение, кулоновское трение, непрерывная зависимость, полунепрерывность снизу, оптимальное управление.

EDN: BKJSCW

УДК 537.621

Dual Band HTSC Power Limiter

Aleksey O. Afonin*

Alexander A. Alexandrovsky†

Kirensky Institute of Physics SB RAS
Krasnoyarsk, Russian Federation

Ilya V. Govorun‡

Kirensky Institute of Physics SB RAS
Krasnoyarsk, Russian Federation

Reshetnev Siberian State University of Science and Technology
Krasnoyarsk, Russian Federation

Alexander A. Leksikov§

Andrey V. Ugryumov¶

Kirensky Institute of Physics SB RAS
Krasnoyarsk, Russian Federation

Dmitriy K. Ogorodnikov||

Siberian Federal University
Krasnoyarsk, Russian Federation

Received 10.03.2023, received in revised form 15.06.2023, accepted 04.10.2023

Abstract. A new construction of dual band HTSC power limiter is proposed. The device consists of two microstrip bandpass filters. Each filter consists of two quarter-wave resonators which couple through a composite half-wave resonator with HTSC-element. The prototype of the device in the open mode has operation passband of about 10% and 11% with central frequency being equal to 1.48 GHz and 2.03 GHz, the minimum loss in the passband is equal 1.9 dB and 1.7 dB for LF-channel and HF-channel correspondingly. The transfer characteristics of the device were investigated in the case of microwave power level up to 3.15 W.

Keywords: power limiter, microwave, HTSC, microstrip structure.

Citation: A.O. Afonin, A.A. Alexandrovsky, I.V. Govorun, A.A. Leksikov, A.V. Ugryumov, D.K. Ogorodnikov, Dual Band HTSC Power Limiter, J. Sib. Fed. Univ. Math. Phys., 2024, 17(2), 162–168. EDN: BKJSCW.



Each receiving radio system must contain a device to protect against powerful radio pulses (power limiter). This device protects the active element of the radio receiver (transistor or amplifier) from an external radio pulse, whose power is critical for the active element. Power limiter has two operating modes. When the input signal has low power device works in open mode. In this mode, the device has low loss and a signal passes through it with small loss. The second mode is the closed one. In this mode, the high-power signal is limited to a safe level. Semiconductor protection devices are the most widespread [1]. However, they have some disadvantages. For example, their switching speed is not high enough. Devices based on cyclotron resonance have excellent characteristics [2]. But they require a magnetic field to operate, resulting

*afoninao@iph.krasn.ru

†a.a.aleksandrovskiy@gmail.com

‡govorun-ilya@mail.ru

§leksikov@iph.krasn.ru

¶ugrumovav@iph.krasn.ru

||vagabondclash@gmail.com

© Siberian Federal University. All rights reserved

in significant dimensions and weight. In a scientific literature there are described protection devices based on an ability of a high-temperature superconductor (HTSC) to transit from a superconducting state to a normal state when microwave current passes through HTSC. The time of this transition does not exceed ($< 10^{-12}$ s) [3]. Usually HTSC power limiter contains transmission line matched to the tract [3,4]. The operating principle of this type of limiter is to absorb input power in close mode. This can lead to evaporation of a thin layer of HTSC material. In [5–8] the new class of power limiters based on HTSC, in which power limitation occurs due to reflection is presented. Such a device contains three microstrip resonators. The configuration of the outer resonators and the distance between them are chosen in such a way that there is no electromagnetic coupling between the resonators. It occurs due to mutual compensation of inductive and capacitive interactions between outer resonators at the resonant frequencies. The center resonator provides coupling between the outer resonators. This resonator is composite. It contains an insert made of a HTSC-element. In the open mode, the device is a three pole bandpass filter that has low insertion loss. In the closed state, the HTSC-element switches to the normal state and the quality factor of the center resonator drops. As a result, limitation of input power is observed due to strong reflection.

Currently, receivers operating in two operating frequency bands are widespread. They are included in navigation satellite systems, for example, GLONASS, GPS, BeiDou and others. It is obvious that the use of broadband (non-selective) power limiter located at the input of such two-band receiving systems leads to their incorrect operation. When a powerful radio signal falls to an input of such a system at the frequency of one of the operating bands, the power limiter switches to closed mode in both frequency ranges. Of course, for a correct operation such two-band systems, the power limiter must be selective and operates in two working frequency bands that coincide with the operating bands of the entire receiving system.

The two-band HTSC power limiters are known [9]. Such a device consists of two bandpass microstrip filters and two circulators. The resonators in the filters are entirely made from HTSC material. These types of devices are complex because of they consist of two different devices. Circulators lead to an increase in size of the total device. In addition, as studies have shown, the threshold of power limitation (the input power level at which the device switches to limiting mode) is very high.

Our paper presents a design of dual-band HTSC power limiter. The device has two operating frequency bands: a low-frequency channel (LF-channel) and a high-frequency channel (HF-channel). I.e., in open mode the device operates as a dual-band filter and each channel filter has three resonators. The outer resonators are quarter-wave, and the center resonator is composite. A HTSC-element is located in the middle part of the center resonator.

The device under consideration (Fig. 1) consists of two feeding microstrip line 3, between which there are two bandpass filters (LF-channel filter and a HF-channel filter). Constructions of each channel are identical. The resonators forming the LF-channel have the larger sizes, than the resonators forming the HF-channel. Each channel filter consists of three resonators. The resonators forming the channel filter have the same resonant frequencies. The outer resonators 4 are quarter-wave and short-circuited to the ground. Conductors of these resonators are made of copper. The center resonator is half-wave, it consists of microstrip conductors 5, 6, 7 and HTSC-element 8, which is placed in middle part of the center resonator. The HTSC-element has the dumbbell form. The copper foils 9 are used to provide galvanic contact between conductors 7 and wide parts of HTSC-element on which a thin silver layers ($0.15 \mu\text{m}$) were deposited. HTSC-element is fulfilled on a separate substrate 10.

The overall dimensions of the additional strip conductor 11 and gap between them and the outer resonators, are chosen in such a way, that in the absence of the HTSC-element the outer resonators are tuned so that the inductive and capacitive couplings are mutually compensated. As a result, total coupling coefficient is equal to zero and the outer resonators do not interact with each other, and damping pole is observed at passband frequencies. In this case, the incident

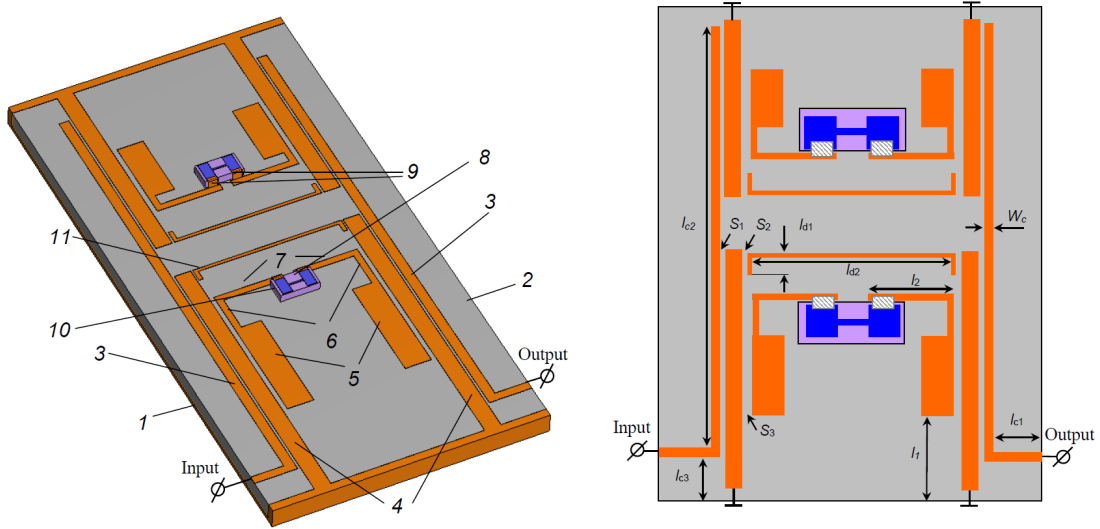


Fig. 1. Left: design of the dual band HTSC power limiter. Right: conductor's pattern and structure parameters of the designed and fabricated device

power is reflected from the input of device. As is known, for a pair of such resonators at any gaps, for a pair of such resonators at any gaps, the inductive interaction always prevails the capacitive one. At the same time these interactions have the opposite sign. Moreover, with increase the spacing between such resonators, capacitive interaction decreases faster than inductive one. In order to the damping pole appears at passband frequencies, it is necessary that the capacitive and inductive interactions are equal modulo. This requires to increase the capacitive interaction of the outer resonators, therefore an element 11 is inset. This additional capacitive interaction is very weak and does not affect the characteristics of the power limiter in the open mode. In the case, when the device is in the closed mode, and the HTSC-element has low conductivity, an additional capacitive interaction compensates the inductive one provided by the middle resonator. As a result, the device limits microwave power.

Using the topology of the dual band HTSC power limiter shown in Fig. 1, a prototype device was manufactured. The following design parameters for LF-channel were obtained: $l_1 = 5.8$ mm, $S_1 = 0.21$ mm, $S_2 = 0.28$ mm, $S_3 = 0.45$ mm, $l_{d1} = 8.6$ mm, $l_{d2} = 1.7$ mm the conductor 5 have next sizes 6.8×1.6 mm², the conductor 6 – 2.2×0.4 mm², the conductor 7 – 3.9×0.4 mm², the dimension of outer resonators is 17.6×1.0 mm². The following design parameters for HF-channel were obtained: $l_1 = 4.91$ mm, $S_1 = 0.21$ mm, $S_2 = 0.32$ mm, $S_3 = 0.31$ mm, $l_{d1} = 2.1$ mm, $l_{d2} = 8.52$ mm the conductor 5 have next sizes 4.0×1.6 mm², the conductor 6 – 0.7×0.4 mm², the conductor 7 – 4.0×0.4 mm², the conductor 7 – 3.9×0.4 mm², the dimension of outer resonators is 12.8×1.0 mm². The sizes of the feeding microstrip line 3 were $l_{c1} = 1.7$ mm, $l_{c2} = 28$ mm, $w_c = 0.5$ mm. Wide and narrow parts of the HTSC-element were 1.0×0.6 mm² and 0.9×0.2 mm², respectively. The YBaCuO HTSC film having thickness 150 nm was deposited on the NdGaO₃ 0.5 mm substrate. The surface resistance of the film in the normal state was $10 \Omega/\square$. The HTSC films were produced by technology described elsewhere [10]. The device was cooled with liquid nitrogen. The alumina substrate with a thickness of 0.5 mm ($\varepsilon = 10.8$). Note that the inner dimensions of the device housing are $16.7 \times 32.0 \times 6.0$ mm³.

Bandwidth passband of each channels of the power limiter is defined by electromagnetic coupling between central and outer resonators. This coupling depends on the gap S_3 between the outer resonators, and the inner composite resonator. To increase bandwidth of device the gap S_3 must be reduced. Value of gap S_1 were chosen from the condition of the maximum return

losses in the passband to be 15 dB.

In Fig. 2 left the frequency response of the simulated and developed prototype of the device are shown for both cases: superconducting state of the HTSC-element at liquid nitrogen temperature – 1; and normal state of the HTSC-element at room temperature – 2. The blue curves are the results of 3D electromagnetic simulation, and the red curves show the measured results. The experimental data were obtained with vector network analyzer R&S ZVA 40.

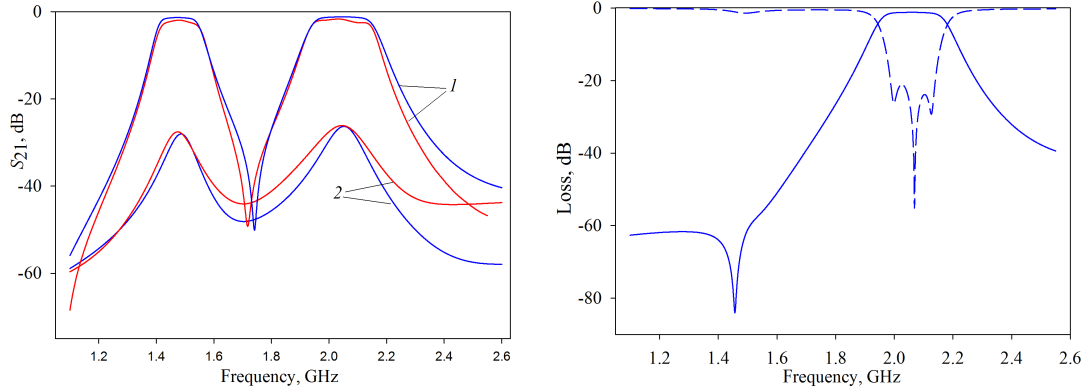


Fig. 2. Left: frequency response of the dual band HTSC power limiter in cases when the HTSC-element is in the superconducting (1) and normal state (2). The blue curves present for results of electromagnetic simulation; the red curves are experimental data. Right: frequency response of the electromagnetic simulation dual band HTSC power limiter for a case when HTSC-element is absent in the LP-channel. The solid curve is insertion loss; the dashed curve is return loss

It can be seen (Fig. 2) that when the HTSC-element is in the superconducting state, power limiter’s fractional width of passbands is about 10% and 11% with central frequency being equal to 1.48 GHz and 2.03 GHz, the minimum loss in the passbands is equal 1.9 dB and 1.7 dB for LF-channel and HF-channel correspondingly. The return loss inside the pass band in this case is less than -15 dB. In the close mode when HTSC-elements pass into the normal state the transmission coefficient decreases by about 28 dB and 26 dB at the operating frequencies, return loss is equal $|S_{11}| = 1$ dB in this case. It means that power of a signal in working bands will be attenuated approximately in four hundred times. At the same time this power limiting is caused by reflection of power. Comparison of the frequency responses obtained by means of 3D electromagnetic simulation and the measured results shows quite good agreement.

Fig. 2 right shows the frequency response of the 3D electromagnetic simulation of dual band HTSC power limiter for a case when HTSC-element is absent in the LP-channel and the HF-channel is in open mode. As we can see damping pole is located at working frequency band of LP-channel. Meanwhile at frequencies HF-channel the passband exists. This means that in the operating frequency band of the LF-channel, the input power is limited, and a significant part of this power is reflected from the input of the device. At the operating frequencies of the HF-channel, the signal passes through device with minimal attenuation.

In Fig. 3 a distribution of microwave current in HTSC power limiter at a central frequency of the HF-channel (2.03 GHz) is shown for two cases: HTSC-element is in superconducting state (left) and in is normal state (right). As we can see, the antinode of microwave current and therefore H-field is located in central part of HTSC-element for open mode. When device is in the closed mode microwave current in an element is practically absent and as a result signal doesn’t pass through the device. This is due to the conductivity of HTSC-element in this state is too small and quality factor of the central resonator is very small. As a result, coupling between

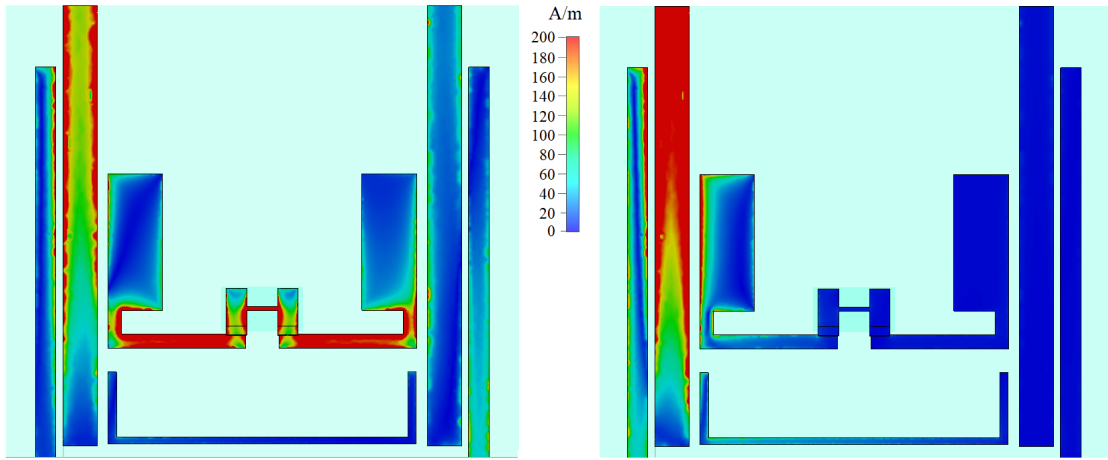


Fig. 3. Distribution of microwave current in HTSC power limiter at a central frequency of the HF-channel (2.03 GHz) for two cases: device in open mode (left) and device in close mode (right)

outer resonators through the center resonator is broken. In this situation the microwave power limitation occurs. The similar situation is observed for LF-channel too.

To determine the value of microwave power switching limiter into the closed mode, it is necessary to carry out measurements its transfer characteristic (Fig. 4). For this purpose, microwave generator R&S SMA100B, power amplifier R&S BBA150 and spectrum analyzer R&S FSW were used. The measurements were carried out at the temperature of liquid nitrogen, at the central frequency of LH-channel (1.48 GHz) and HF-channel (2.03 GHz). In the linear regime the device demonstrates around 1.8 dB insertion loss in both channel. When the input power reaches a critical level $P_{in}=13.5$ dBm (22.4 mW) drop in P_{out} occurs. The leakage power found to be 7.15 dBm (5.18 mW) and 9.4 dBm (8.7 mW) at the input power about 35 dBm (3.16 W) for LF-channel and HF-channel correspondingly. It means that limitation equals 26 dB in this case. These data are in good agreement with results of the measured device frequency response (see Fig. 2 left).

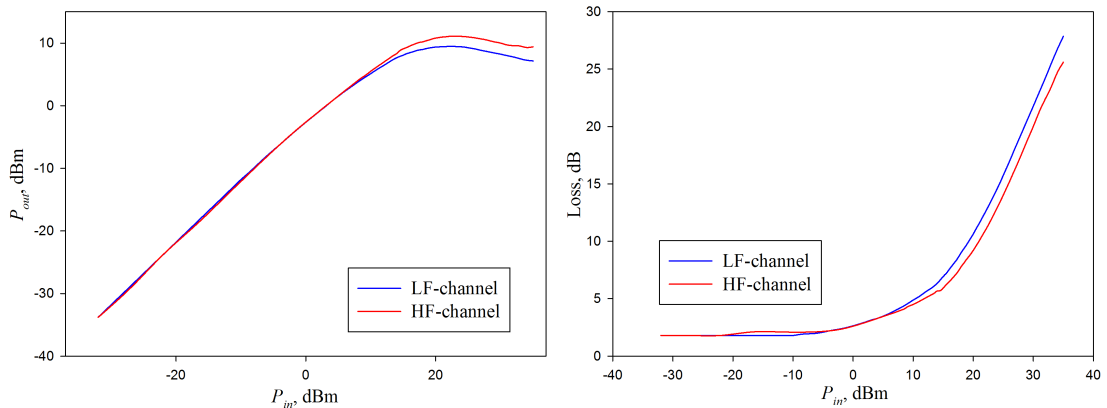


Fig. 4. Left — transfer characteristics of the fabricated device. Right — loss of power limiter versus input power. Blue curves are the results of LF-channel, red curves are the results of HF-channel

A new structure of microwave dual-band HTSC power limiter is presented. The device consists of two microstrip bandpass filters which have two quarter-wave resonators and the third composite one with HTSC-element. The prototype of the device has operation passbands being about 10% and 11% with central frequency being equal to 1.48 GHz and 2.03 GHz, the minimum loss in the passband is equal 1.9 dB and 1.7 dB for LF-channel and HF-channel correspondingly. The transfer characteristics of the device were investigated with microwave power level up to 3.15 W at the central frequencies of LF-channel and HF-channel.

References

- [1] F.Jahan, M.Gaevski, J.Deng, R.Gaska, M.Shur, G.Simin, RF power limiter using capacitively-coupled contacts III-nitride varactor, *Electronics Letterl*, **48**(2012), no. 23, 1480–1481. DOI: 10.1049/el.2012.3428
- [2] Yu.A.Budzinskiy, S.V.Bykovskiy, V.E.Kotov, O.A.Savrukhin, On the increase of the frequency band of cyclotron protective device, CriMiCo'2014, Sevastopol, Ukraine, September 2014.
- [3] A.T.Findikoglu, D.W.Reagor and etc., Electrodynamic properties of coplanar waveguides made from high-temperature superconducting YBaCuO electrodes on nonlinear dielectric SrTiO₃ substrates, *Journal of Applied Physics*, **86**(1999), no. 3, 1558–1568. DOI: 10.1063/1.370967
- [4] J.C.Booth, D.A.Rudman, R.H.Ono, Self-Attenuating Superconducting Transmission Line for Use as a Microwave Power Limiter, *IEEE Trans. on Appl. Supercond*, **13**(2003), no. 2, 305–310. DOI: 10.1109/TASC.2003.813716
- [5] B.A.Belyaev, I.V.Govorun, A.A.Leksikov, A.M.Serzhantov, Receiver Protecting Device Based on Microstrip Structure with High-Temperature Superconductor Film, *Technical Physics Letters*, **38**(2012), no. 3, 211–214. DOI: 10.1134/S1063785012030066
- [6] B.A.Belyaev, I.V.Govorun, A.A.Leksikov, A.M.Serzhantov, Investigation of the special features of the coupling coefficient microstrip asymmetric hairpin resonators at frequencies of the second passband, *Russian Physics Journal*, **55**(2013), no. 10, 1215–1221. DOI: 10.1007/s11182-013-9945-3
- [7] B.A.Belyaev, I.V.Govorun, A.A.Leksikov, A.M.Serzhantov, An.A.Leksikov, Reflective power limiter for X-band with HTSC Switching element, *IEEE Transactions on applied superconductivity*, **26**(2016), no. 6, 1–6. DOI: 10.1109/TASC.2016.2530700
- [8] I.V.Govorun, A.A.Leksikov, A.M.Serzhantov, Compact microwave power limiter with HTSC element, *Journal of Siberian Federal University. Mathematics&Physics*, **11**(2018), no. 1, 35–39. DOI: 10.17516/1997-1397-2018-11-1-35-39
- [9] J.Mateu, C.Collado and etc., Comprehensive circuit model of autolimiting superconductor devices, *IEEE Transactions on Applied Superconductivity*, **27**(2017), no. 4, 1–4. DOI: 10.1109/TASC.2016.2638419
- [10] A.V.Smirnov, M.S.Karmantsov and etc., Terahertz response of thin-film YBCO bolometers, *Technical Physics*, **57**(2012), no. 12, 1716–1719. DOI: 10.1134/S1063784212120250

ВТСП ограничитель мощности с двумя рабочими полосами

Алексей О. Афонин

Александр А. Александровский

Институт физики им. Л. В. Киренского СО РАН
Красноярск, Российская Федерация

Илья В. Говорун

Институт физики им. Л. В. Киренского СО РАН
Красноярск, Российская Федерация

Сибирский государственный университет науки и технологий им. М. Ф. Решетнева
Красноярск, Российская Федерация

Александр А. Лексиков

Андрей В. Угрюмов

Институт физики им. Л. В. Киренского СО РАН
Красноярск, Российская Федерация

Дмитрий К. Огородников

Сибирский федеральный университет
Красноярск, Российская Федерация

Аннотация. Предложена новая конструкция ВТСП ограничителя мощности с двумя рабочими полосами. Ограничитель содержит два микрополосковых полосно-пропускающих фильтра. Каждый фильтр состоит из двух четвертьволновых резонаторов, которые связаны между собой через составной полуволновый резонатор, содержащий пленку из высокотемпературного сверхпроводника. Макет устройства в открытом режиме имеет ширины рабочих полос пропускания 10% и 11% с центральными частотами 1.48 ГГц и 2.03 ГГц. Минимальные вносимые потери составили 1.9 дБ и 1.7 дБ для НЧ- и ВЧ-каналов соответственно. Передаточные характеристики устройства были исследованы до уровня СВЧ-мощности 3.15 Вт.

Ключевые слова: ограничитель мощности, СВЧ, ВТСП, микрополосковая структура.

EDN: UHYRGO
517.55+517.96

Difference Equations and Hadamard Composition of Multiple Power Series

Evgeny D. Leinartas*
Evgeny K. Leinartas†
Siberian Federal University
Krasnoyarsk, Russian Federation

Received 16.09.2023, received in revised form 10.11.2023, accepted 14.12.2023

Abstract. The sufficient conditions are given for the coefficients of two power series, which ensure the rationality of their Hadamard composition. Under certain additional constraints, the existence of a system of polynomial difference equations, satisfied by the coefficients of the composition, is proven.

Keywords: systems of polynomial linear equations with constant coefficients, multiple power series, Hadamard composition.

Citation: E.D. Leinartas, E.K. Leinartas, Difference Equations and Hadamard Composition of Multiple Power Series, J. Sib. Fed. Univ. Math. Phys., 2024, 17(2), 169–174. EDN: UHYRGO.



Introduction

Let $\mathbb{Z}_{\geq 0}^n$ denote the set of vectors with integer non-negative coordinates, and let $\varphi(x), \psi(x) : \mathbb{Z}_{\geq 0}^n \rightarrow \mathbb{C}$ be functions with integer arguments, where \mathbb{C} is the set of complex numbers. For power series,

$$\Phi(z) = \sum_{x \in \mathbb{Z}_{\geq 0}^n} \varphi(x) z^x \text{ and } \Psi(z) = \sum_{x \in \mathbb{Z}_{\geq 0}^n} \psi(x) z^x$$

the Hadamard composition of these power series is defined as

$$H(z) = \sum_{x \in \mathbb{Z}_{\geq 0}^n} \varphi(x) \psi(x) z^x. \tag{1}$$

For $n = 1$, the Hadamard theorem on multiplication of singularities states that the singular points of the composition $H(z)$ are given by the products of the singular points of the functions Φ and Ψ (see [1]), and the main tool for investigation is the integral representation, in which the composition is expressed in terms of Φ and Ψ . Note that if $\Phi(z)$ and $\Psi(z)$ are rational functions, direct calculation of the integral shows that the composition is also a rational function. However, for $n > 1$, this is no longer the case.

Example 1. $\Phi(z_1 z_2) = \frac{1}{1 - z_1 - z_2} = \sum_{(k_1, k_2) \in \mathbb{Z}_{\geq 0}^2} \frac{(k_1 + k_2)!}{k_1! k_2!} z_1^{k_1} z_2^{k_2}$, $\Psi(z_1 z_2) = \frac{1}{1 - z_1 z_2} = \sum_{k=0}^{\infty} z_1^k z_2^k$,

then $H(z_1 z_2) = \sum_{k=0}^{\infty} \frac{(2k)!}{(k!)^2} (z_1 z_2)^k = \frac{1}{\sqrt{1 - 4z_1 z_2}}$.

*elyaynartas@sfu-kras.ru

†leinartas@sfu-kras.ru

© Siberian Federal University. All rights reserved

We are interested in the question of the classes of rational functions whose Hadamard composition is a rational function (see, for example, [2]).

This paper considers the case when the coefficients of the series $\Phi(z)$ and $\Psi(z)$ satisfy systems of polynomial difference equations with constant coefficients. The main role here is played by the multidimensional analogue of the fundamental theorem of difference equations with constant coefficients [3].

Moreover, from the point of view of enumerative combinatorial analysis, the question of the system of difference equations satisfied by the product of the coefficients $\varphi(x)\psi(x)$ of the Hadamard composition of the series $\Phi(x)$ and $\Psi(x)$ is of interest.

We provide the necessary definitions and notations and formulate the main results.

Let δ_j be the shift operator with respect to the variable x_j

$$\begin{aligned}\delta_j f(x) &= \delta_j f(x_1, \dots, x_n) = f(x_1, \dots, x_{j+1}, \dots, x_n), \\ \delta &= (\delta_1, \dots, \delta_n), \quad \delta^\alpha = \delta_1^{\alpha_1} \cdots \delta_n^{\alpha_n}, \quad \alpha \in \mathbb{Z}_{\geq 0}^n.\end{aligned}$$

Consider a polynomial difference operator with constant coefficients of the form

$$Q(\delta) = \sum_{0 \leq \alpha \leq d} c_\alpha \delta^{d-\alpha}, \quad (2)$$

where $c_\alpha \in \mathbb{C}$ are some constants, and the notation $\alpha \geq \beta$ for multi-indices $\alpha = (\alpha_1, \dots, \alpha_n)$, $\beta = (\beta_1, \dots, \beta_n)$ means that $\alpha_j \geq \beta_j$, $j = 1, 2, \dots, n$.

The characteristic polynomial for the difference equation

$$Q(\delta)f(x) = 0, \quad x \in \mathbb{Z}_{\geq 0}^n \quad (3)$$

is defined as the polynomial

$$\sum_{0 \leq \alpha \leq d} c_\alpha \delta^{d-\alpha} = Q(z), \quad (4)$$

where $z = (z_1, \dots, z_n) \in \mathbb{C}^n$, $z^\alpha = z_1^{\alpha_1} \cdots z_n^{\alpha_n}$, $C_0 = 1$, $C_d \neq 0$.

The zeros of the polynomial Q are called characteristic roots, and the set

$$V = \{z \in \mathbb{C}^n : Q(z) = 0\}$$

of all these zeros of Q is called the characteristic set of the equation (3).

Let us consider a set of polynomials $Q = (Q_1, \dots, Q_n)$ of the form

$$Q_i(z) = \sum_{0 \leq \alpha \leq d_i} c_\alpha^i z^{d_i-\alpha}, \quad i = 1, 2, \dots, n, \quad (5)$$

where d^i are vectors from $\mathbb{Z}_{\geq 0}^n$. We assume that $c_0^i = 1$, $c_{d^i}^i \neq 0$.

We denote by V_Q the set of zeros of the system of equations:

$$Q_1(z) = Q_2(z) = \dots = Q_n(z) = 0, \quad (6)$$

which we will call the characteristic system.

In this paper, we will consider systems of difference equations of the form (3), which satisfy the following conditions:

- (*) the characteristic set V_Q is discrete and the characteristic roots do not lie on coordinate planes;

(**) the roots $a \in V_Q$ of the characteristic system (6) satisfy the following properties: there exists $d_\alpha = (d_{1,\alpha}, \dots, d_{n,\alpha}) \in \mathbb{Z}_{\geq}^n$ such that:

$$\frac{\partial^\alpha Q_i}{\partial z^\alpha}(a) = 0 \text{ for } 0 \leq \alpha \leq d_a - I, \quad i = 1, \dots, n, \tag{7}$$

$$\Delta_{d_a}(z) = \det \left\| \frac{\partial^{d_{l,a}} Q_i(z)}{\partial z_l^{d_{l,a}}} \right\|_{z=a} \neq 0. \tag{8}$$

In formula (8), the indices l and i take values $1, 2, \dots, n$.

For $d_a = I = (1, \dots, 1)$, these conditions are equivalent to the point $z = a$ being a simple root of the characteristic system of equations (6).

We state the main result of this paper.

Theorem. *Let $A(z) = (A_1(z), \dots, A_n(z))$ and $B(z) = (B_1(z), \dots, B_n(z))$ be two sets of polynomials and*

$$A(\delta)\varphi(x) = 0 \text{ and } B(\delta)\psi(x) = 0, \quad x \in \mathbb{Z}_{\geq}^n \tag{9}$$

be the corresponding systems of polynomial difference equations. If the roots of the characteristic systems V_A and V_B are discrete, do not lie on coordinate planes, and the characteristic polynomials $A(z)$ and $B(z)$ satisfy conditions (7) and (8), then:

- 1) *The generating function of the product $\varphi(x)\psi(x)$ of solutions to the system (9) of difference equations is rational.*
- 2) *If the characteristic roots of the systems of difference equations (9) are simple, then there exists a set of polynomial difference operators $R(\delta) = (R_1(\delta), \dots, R_n(\delta))$ such that the product $\varphi(x)\psi(x)$ satisfies the system of recurrence equations*

$$R_j(\delta)[\varphi(x)\psi(x)] = 0, \quad j = 1, 2, \dots, n.$$

The proof and an example

The main role in proving part 1) of the theorem is played by the multidimensional version of the fundamental theorem of difference equations with constant coefficients. We state this theorem (cf. [3]).

Theorem. *Let the polynomial vector $Q(z) = (Q_1(z), \dots, Q_n(z))$ have the form $Q_j(z) =$*

$$= \sum_{0 \leq \alpha \leq d^j} c_\alpha^j z^{d^j - \alpha} \text{ and satisfy the conditions } (*), (**), (7), \text{ and } (8).$$

For a function $f(x) = f(x_1, \dots, x_n) \rightarrow \mathbb{C}$, the following conditions are equivalent:

- (i) *The generating series for $f(x)$ is a rational function of the form*

$$F(z) = \sum_{x \geq 0} f(x)z^x = \sum_{j=1}^m \frac{b_j(z)}{(I - \gamma_{(j)}z)^{d_{(j)}}},$$

where

$$(I - \gamma_{(j)}z)^{d_{(j)}} = (1 - \gamma_{(j),1}z_1)^{d_{(j),1}}(1 - \gamma_{(j),2}z_2)^{d_{(j),2}} \dots (1 - \gamma_{(j),n}z_n)^{d_{(j),n}},$$

$b_j(z)$ are some polynomials of the form $\sum_{0 \leq \alpha < d_{(j)}} b_\alpha^j z^\alpha$, and $\gamma_{(j)}$ are the roots of the characteristic system (6).

(ii) For any $x \in \mathbb{Z}_{\geq}^n$, the function $f(x)$ satisfies the system of recurrence equations

$$\sum_{0 \leq \alpha \leq d^i} c_\alpha^i \delta^{d^i - \alpha} f(x) = 0, \quad i = 1, 2, \dots, n, \tag{10}$$

whose characteristic roots satisfy the conditions (7) and (8).

(iii) The function $f(x)$ has the form of an exponential polynomial

$$f(x) = \sum_{j=1}^m P_j(x) \gamma_{(j)}^x, \tag{11}$$

where $\gamma_{(j)}^x = \gamma_{(j),1}^{x_1} \cdot \dots \cdot \gamma_{(j),n}^{x_n}$ and $P_j(x)$ are polynomials of the form $\sum_{0 \leq k < d_{(j)}} P_k^{(j)} x^k$.

The proof of part 2 of the theorem is based on an algorithm for constructing a system of polynomial equations given the roots (see [4]), in the case where these roots are simple. The main element of the algorithm in [4] is the following proposition.

Proposition 1. Let $E = \{a^{(i)}\}_{i=1}^N$, where $a^{(i)} = (a_1^{(i)}, \dots, a_n^{(i)}) \in \mathbb{C}^n$ and $E_i, i = 1, 2$, is the set of zeros of the system of polynomial equations

$$P_j^{(i)}(z) = 0, \quad j = 1, 2, \dots, n,$$

where $P_l^{(1)} = P_l^{(2)}$ for $1 \leq l < r < n$, and the polynomials $P_l^{(1)}$ and $P_l^{(2)}$ have no common zeros. Let

$$q_j(z) = \begin{cases} P_j^{(1)}(z), & 1 \leq j < r, \\ P_j^{(1)}(z)P_j^{(2)}(z), & j = r, \\ P_r^{(1)}(z)P_j^{(2)}(z) + P_j^{(1)}(z)P_r^{(2)}(z), & r < j \leq n, \end{cases}$$

then the set of zeros of the system

$$q_j(z) = 0, \quad j = 1, 2, \dots, n$$

coincides with the set $E_1 \cup E_2$.

Proof of Theorem. $\gamma_{(j)} = (\gamma_{(j),1}, \dots, \gamma_{(j),n}) \in V_A$ and $\gamma_{(j)} = (\gamma_{(j),1}, \dots, \gamma_{(j),n}) \in V_B$ are the roots of the characteristic systems $A_1(z) = \dots = A_n(z)$ and $B_1(z) = \dots = B_n(z)$, respectively. Conditions (*) and (**) of the theorem are satisfied, therefore we can use the implication (ii) \Rightarrow (iii) of the multivariate version of the fundamental theorem of the theory of difference equations. For solutions $\varphi(x)$ and $\psi(x)$ of the difference equations systems, we obtain

$$\varphi(x) = \sum_j p_j(x) \gamma_{(j)}^x, \tag{12}$$

$$\psi(x) = \sum_i q_i(x) \nu_{(i)}^x, \tag{13}$$

where $\gamma_{(j)}^x = \gamma_{(j),1}^{x_1} \cdot \dots \cdot \gamma_{(j),n}^{x_n}$, $\nu_{(i)}^x = \nu_{(i),1}^{x_1} \cdot \dots \cdot \nu_{(i),n}^{x_n}$.

The polynomials $p_j(x)$ and $q_i(x)$ have the form

$$p_j(x) = \sum_{0 \leq \alpha \leq d} a_\alpha x^\alpha, \quad q_i(x) = \sum_{0 \leq \alpha \leq s} b_\alpha x^\alpha,$$

while the vectors $d_{(j)}$ and $s_{(i)}$ are determined by conditions (7) and (8).

Multiplying the exponential representations (12) and (13) for $\varphi(x)$ and $\psi(x)$, we obtain

$$h(x) = \varphi(x)\psi(x) = \sum_j p_j(x)\gamma_{(j)}^x \sum_i q_i(x)\nu_{(i)}^x = \sum_{j,i} p_j(x)q_i(x)(\gamma_{(j)}^x \cdot \nu_{(i)}^x),$$

where $(\gamma_{(j)}^x \cdot \nu_{(i)}^x) = (\gamma_{(j),1} \cdot \nu_{(i),1}, \dots, \gamma_{(j),n} \cdot \nu_{(i),n})$.

Thus $h(x)$ has an exponential representation, and due to the implication $(iii) \Rightarrow (i)$, we obtain that the generating function $H(z)$ for the product $\varphi(x) \cdot \psi(x)$ has the form

$$H(z) = \sum_{j,i} \frac{b_{ij}(z)}{(I - \gamma_{(j)}\nu_{(i)})^{d_{(ij)}}},$$

where $(I - \gamma_{(j)}\nu_{(i)})^{d_{(ij)}} = (1 - \gamma_{(j),1}\nu_{(i),1})^{d_{(ij)_1}} \dots (1 - \gamma_{(j),n}\nu_{(i),n})^{d_{(ij)_n}}$, $b_{ij}(z)$ are some polynomials of the form $\sum_{0 \leq \alpha \leq d_{(j)} \neq s_{(i)}} b_{\alpha}^{ij} z^{\alpha}$.

To prove the second part of the theorem, we will use the fact that the roots of the characteristic systems for the difference equations $A(\delta)\varphi(x) = 0$ and $B(\delta)\psi(x) = 0$ are simple. In this case, the exponential representations for $\varphi(x)$ and $\psi(x)$ have the form

$$\varphi(x) = \sum_j p_j \gamma_{(j)}^x \text{ and } \psi(x) = \sum_i q_i \nu_{(i)}^x,$$

where p_j, q_i are constants, and the exponential representation for the product $\varphi(x) \cdot \psi(x)$ has the form $\varphi(x) \cdot \psi(x) = \sum_{j,i} p_j q_i (\gamma_{(j)} \cdot \nu_{(i)})^x$.

This means that the difference equations system for the product $\varphi(x) \cdot \psi(x)$ (if it exists) has simple roots.

Using method from [4], we construct a system of polynomial equations

$$R_k(z) = 0, \quad k = 1, 2, \dots, n,$$

whose roots are the numbers $\{\gamma_{(j)}\nu_{(i)}\}$. For polynomial difference operators $R_k(\delta)$, we have the formula:

$$R_k(\delta)((\gamma_{(j)} \cdot \nu_{(i)})^x) = (\gamma_{(j)}\nu_{(i)})^x R_k(\gamma_{(j)}\nu_{(i)}) = 0$$

for $x \in \mathbb{Z}_{\geq}^n$. From the multivariate version of the fundamental theorem of the theory of difference equations, by the equivalence of $(ii) \approx (iii)$, it follows that $h(x) = \varphi(x)\psi(x)$ is a solution of the difference equations system

$$R_k(z) = 0, \quad k = 1, 2, \dots, n.$$

Example 2. Let us consider two difference equations systems

$$\begin{cases} \varphi(x_1 + 1, x_2) - \varphi(x_1, x_2) = 0 \\ \varphi(x_1, x_2 + 1) - \varphi(x_1, x_2) = 0 \end{cases} \quad (1, 1) \text{ is the root,}$$

$$\begin{cases} \psi(x_1 + 2, x_2) - a^2\psi(x_1, x_2) = 0 \\ \psi(x_1, x_2 + 1) - a^2\psi(x_1, x_2) = 0 \end{cases} \quad (a, a^2), (-a, a^2) \text{ are roots.}$$

The difference equations system for the product $h(x_1, x_2) = \varphi(x_1, x_2) \cdot \psi(x_1, x_2)$ has the form

$$\begin{cases} h(x_1 + 2, x_2) - a^2h(x_1, x_2) = 0 \\ h(x_1, x_2 + 1) - a^2h(x_1, x_2) = 0 \end{cases} \quad (a, a^2), (-a, a^2).$$

This is a very simple example, it can be complicated.

$$\begin{cases} \varphi(x_1 + 1, x_2) - \lambda_1 \varphi(x_1, x_2) = 0 \\ \varphi(x_1, x_2 + 1) - \lambda_2 \varphi(x_1, x_2) = 0 \end{cases} \quad (\lambda_1, \lambda_2) \text{ is the root,}$$

$$\begin{cases} \psi(x_1 + 2, x_2) - a^2 \psi(x_1, x_2) = 0 \\ \psi(x_1, x_2 + 1) - b \psi(x_1, x_2) = 0 \end{cases} \quad (a, b), (-a, b) \text{ are roots.}$$

As a result, the system of difference equations for the product $h(x_1, x_2) = \varphi(x_1, x_2) \cdot \psi(x_1, x_2)$ has the form

$$\begin{cases} h(x_1 + 2, x_2) - h(x_1, x_2 + 1) - (\lambda_1^2 a^2 - \lambda_2 b) h(x_1, x_2) = 0 \\ h(x_1, x_2 + 1) - \lambda_2 b h(x_1, x_2) = 0 \end{cases}.$$

Another example:

$$\begin{cases} h(x_1 + 2, x_2) - A h(x_1, x_2 + 1) - (\lambda_1^2 a^2 - A \lambda_2 b) h(x_1, x_2) = 0 \\ h(x_1, x_2 + 1) - \lambda_2 b h(x_1, x_2) = 0 \end{cases},$$

where A is an arbitrary constant, characteristic roots for the system of difference equations $(\lambda_1 a, \lambda_2 b), (-\lambda_1 a, b)$.

This work is supported by the Krasnoyarsk Mathematical Center and financed by the Ministry of Science and Higher Education of the Russian Federation (Agreement No. 075-02-2023-936).

References

- [1] L. Bieberbach, Analytische Fortsetzung, Springer-Verlag, Berlin, 1955, 400 S.
- [2] D.Ž.Djoković, A property of the Taylor expansion of a class of rational functions in several variables, *J. Math. Ann., Appl.*, **66**(1988), 679–685.
- [3] E.D.Leinartas, A.K.Tsikh, On a multidimensional version of the principal theorem of difference equations with constant coefficients, *J. Sib. Fed. Univ. Math. Phys.*, **15**(2022), no. 1, 125–132. DOI: 10.17516/1997-1397-2022-15-1-125-132
- [4] M.A.Mkrtchyan, Reconstruction of a system of algebraic equations from simple roots, *Nekotorye voprosy mnogomernogo kompleksnogo analiza*, Krasnoyarsk, KGU, 1980, 115–122 (in Russian).

Разностные уравнения и композиция Адамара кратных степенных рядов

Евгений Д. Лейнартас

Евгений К. Лейнартас

Сибирский федеральный университет

Красноярск, Российская Федерация

Аннотация. Приведены достаточные условия на коэффициенты двух кратных степенных рядов, которые обеспечивают рациональность композиции Адамара этих рядов, и при некоторых дополнительных ограничениях доказывается существование системы полиномиальных разностных уравнений, которой удовлетворяют коэффициенты композиции.

Ключевые слова: системы полиномиальных линейных уравнений с постоянными коэффициентами, кратные степенные ряды, композиция Адамара.

EDN: DSPWBH

УДК 517.9

On Hypergeometric Functions of Two Variables of Complexity One

Valerii K. Beloshapka*

Moscow Center of Fundamental and Applied Mathematics
Lomonosov Moscow State University
Moscow, Russian Federation

Received 10.09.2023, received in revised form 13.10.2023, accepted 20.12.2023

Abstract. For a series of examples of Horn systems and the Lauricella system for functions of two variables the description of solution of complexity one is given. Several questions are formulated.

Keywords: analytical complexity, hypergeometric functions, Horn system, Lauricella system, differential ring.

Citation: V.K. Beloshapka, On Hypergeometric Functions of Two Variables of Complexity One, J. Sib. Fed. Univ. Math. Phys., 2024, 17(2), 175–188. EDN: DSPWBH.



Introduction

The class of hypergeometric functions (HG-functions) of several variables is of considerable interest. It continues to be a subject of great attention [1]. On the other hand, there is the theory of analytical complexity, which is oriented to the study of questions about representability of functions of several variables with the help of superpositions of functions of lesser number of variables. In particular, the questions of representability of functions of two variables with the help of functions of one variable [2]. In the context of this theory, the simplest functions of two variables are the functions of complexity one (the functions of one variable have complexity zero). These are analytic functions of variables (x, y) , which can be locally represented as $z(x, y) = c(a(x) + b(y))$ (a, b, c are nonconstant analytic functions of one variable). These functions are of special interest. First, they are the functions, which have the stabilizer of the maximal dimension in the gauge group (the dimension is equal to three) [3]. Second, if we consider $z(x, y)$ as a function of a 3-web on the plane, then such web is equivalent to the hexagonal web if and only if z has the specified form [4].

The set of all such functions is, except for the functions of one variable, the set of analytic functions, which is the set of the solutions of a differential polynomial of order three. This polynomial is exactly the numerator of the following differential fraction: $(\ln(z'_x/z'_y))''_{xy}$, i.e., the defining condition for the functions of complexity one has the form:

$$d_1(z) = z'_x z'_y (z''_{xxy} z''_y - z''_{xyy} z'_x) + z''_{xy} ((z'_x)^2 z''_{yy} - (z'_y)^2 z''_{xx}) = 0, \quad z'_x z'_y \neq 0. \quad (1)$$

Note that the class of functions of complexity one includes all four arithmetic operations. If we remove the inequality, which excludes the functions of one variable, we obtain $Cl^1 = \{d_1(z) = 0\}$, which is the class of the functions of complexity not greater than one.

*vkb@strogino.ru <https://orcid.org/0000-0001-8253-0758>

© Siberian Federal University. All rights reserved

We think that the theory of hypergeometric functions of several (in particular, of two) variables differs qualitatively from the theory of hypergeometric functions of one variable by the fact that the class of hypergeometric functions of several variables is in a sense too large and the problem of the choice of a narrower class of the most interesting HG-functions arise. Which HG-functions are the most interesting? No doubt it is possible to give different answers to this question. For the functions of two variables we offer the following answer:

Good HG-functions are the HG-functions of complexity one.

We interpret a HG-function of two variables (Examples 1-7) as, following [1], a solution of a Horn system. To define the Horn system for functions of the variables (x, y) , we need four polynomials P, Q, R, S in two variables. Let $X = x \frac{\partial}{\partial x}$, $Y = y \frac{\partial}{\partial y}$ be the homogeneous partial differential operators. Then the Horn system corresponding to the given four polynomials is the system of two linear differential equations with nonconstant coefficients with respect to the function $z(x, y)$ of the form

$$\begin{aligned} G_x z &= (x P(X, Y) - Q(X, Y)) z = 0, \\ G_y z &= (y R(X, Y) - S(X, Y)) z = 0. \end{aligned} \quad (2)$$

What is the set of all solutions of complexity one of this system? The aim of this paper is to give the explicit description of the solutions of complexity one for a series of examples of systems of the form (2). Almost all examples are from [1]. With the growth of degrees of the defining equations and the number of free parameters the problem of the explicit description of the space of solutions quickly becomes computationally difficult even for polynomials of degree not greater than two. However, one can hope that the consideration of these examples will allow to formulate questions for the further study (some of them are given at the end of the paper).

In the theory of HG-functions there is an established approach, which suggests that an important characteristic of the Horn system is its holonomicity. The holonomicity of the system, in particular, guarantees the finite-dimensionality of the space of solutions. In our considerations we do not require holonomicity.

Since the Horn system is a system of linear differential equations, the set of its solutions is a linear space. Equation (1) is not linear. From the geometric point of view, the set of its solutions is an infinite-dimensional cone. In fact, the transformation $(z(x, y) \rightarrow \lambda z(x, y))$ maps the solutions to solutions. Hence, we can understand our question as the question about the construction of the intersection of the cone and a linear subspace.

Further we will need the following simple observation. Let two nonconstant functions $a(x)$ and $b(y)$ are given. For the existence of a function $c(t)$ for the function $w(x, y)$, such that in a neighbourhood of a generic point there is a local representation of the form $w = c(a(x) + b(y))$, it is necessary and sufficient that

$$V(w) = \left(\frac{1}{a'(x)} \frac{\partial}{\partial x} - \frac{1}{b'(y)} \frac{\partial}{\partial y} \right) (w) = 0. \quad (3)$$

The concrete computations were performed using Maple.

1. A set of examples

Example 1. Let

$$P = x^2, \quad Q = q_1 x + q_2 y, \quad R = y^2, \quad S = s_1 x + s_2 y, \quad q_1 q_2 s_1 s_2 \neq 0.$$

Then the system (2) for $z = c(a(x)+b(y))$ takes the form (low indexes are orders of derivatives)

$$\begin{aligned} G_x z &= x^3 a_1^2 c_2 + x^3 a_2 c_1 + x^2 a_1 c_1 - q_1 x c_1 a_1 - q_2 y c_1 b_1 = 0, \\ G_y z &= y^3 b_1^2 c_2 + y^3 b_2 c_1 - s_1 x c_1 a_1 + y^2 b_1 c_1 - s_2 y c_1 b_1 = 0. \end{aligned}$$

We can express the ratio c_2/c_1 from first equation and from second equation. We get two relations: the first is the equality of the both expressions, the second is the result of action of operator V on each of them. Thus,

$$\begin{aligned} e_1 &= x^3 y^3 a_1^2 b_2 - x^3 y^3 a_2 b_1^2 - x^4 a_1^3 s_1 + x^3 y^2 a_1^2 b_1 - x^3 y a_1^2 b_1 s_2 - \\ &\quad - x^2 y^3 a_1 b_1^2 + x y^3 a_1 b_1^2 q_1 + y^4 b_1^3 q_2 = 0, \\ e_2 &= -a_3 a_1 b_1 x^4 + 2 a_2^2 b_1 x^4 + a_2 a_1 b_1 x^3 - a_2 a_1 b_1 x^2 q_1 - a_1^2 b_2 x y q_2 - \\ &\quad - 2 a_2 b_1^2 x y q_2 + a_1^2 b_1 x^2 - 2 a_1^2 b_1 x q_1 - a_1^2 b_1 x q_2 - 3 a_1 b_1^2 y q_2 = 0. \end{aligned}$$

The expressions e_1 and e_2 are linear wrt b_2 . The coefficients of b_2 are not identically zero. It is possible to express b_2 from $e_1 = 0$ and from $e_2 = 0$. We get two relations: the first is the equality of the both expressions, the second is the result of the action of operator ∂/∂_x on each of them. Thus,

$$\begin{aligned} e_3 &= x^6 y^2 a_1 a_3 b_1 - 2 x^6 y^2 a_2^2 b_1 - x^5 y^2 a_1 a_2 b_1 + x^4 y^2 a_1 a_2 b_1 q_1 + \\ &\quad + 3 x^3 y^3 a_2 b_1^2 q_2 - x^4 y^2 a_1^2 b_1 + x^4 a_1^3 q_2 s_1 + 2 x^3 y^2 a_1^2 b_1 q_1 + \\ &\quad + x^3 y a_1^2 b_1 q_2 s_2 + 4 x^2 y^3 a_1 b_1^2 q_2 - x y^3 a_1 b_1^2 q_1 q_2 - y^4 b_1^3 q_2^2 = 0, \\ e_4 &= a_3 a_1 b_1^2 x^4 y^3 - 2 a_2^2 b_1^2 x^4 y^3 + a_2 a_1^3 x^5 s_1 - a_2 a_1 b_1^2 x^3 y^3 + a_2 a_1 b_1^2 x^2 y^3 q_1 + \\ &\quad + 2 a_2 b_1^3 x y^4 q_2 + a_1^4 x^4 s_1 - a_1^2 b_1^2 x^2 y^3 + 2 a_1^2 b_1^2 x y^3 q_1 + 3 a_1 b_1^3 y^4 q_2 = 0. \end{aligned}$$

The expressions e_3 and e_4 are quadratic wrt b_2 . The necessary condition for solvability is the equality to zero of the resultant of e_3 and e_4 with respect to b_1 . This resultant has the form

$$x^{11} y^{11} a_1^4 q_2^2 s_1 r(x, y, a_1, a_2, a_3),$$

hence, $r = 0$. And r is the polynomial of degree four with respect to y . The coefficient in r of y^4 is equal to

$$-x^2 a_1^5 q_2^3 s_2^3 (x a_2 + a_1) (2 x a_2 + 3 a_1)^2.$$

Thus, it is enough to consider two cases:

the first is $(2 x a_2 + 3 a_1) = 0$, and second is $(x a_2 + a_1) = 0$. We can solve these differential equations. In the first case we get $a_1 = k/x^{3/2}$ and in the second case we get $a_1 = k/x$. If we substitute the first solution in r , we can see that the equation $r = 0$ is impossible. If we substitute the second solution in r , we have

$$r = -\frac{k^8 q_2^3 s_1 (q_1 s_2 - q_2 s_1)}{x^7} y.$$

And we see that $r = 0$ iff $(q_1, q_2) = \lambda (s_1, s_2)$, $\lambda \neq 0$. We can substitute $a_1 = k/x$ in $e_3 = 0$ and we have $y b_1 q_2 + k q_1 = 0$. In such case we have $a(x) + b(y) = k \ln(x) - k \frac{q_1}{q_2} \ln(y) + const$ and $z = c(y/x^\alpha)$, where $\alpha = q_2/q_1 = s_2/s_1$. Then we can substitute such z in $G_x z = G_y z = 0$ and we get:

$c''(t) t + c'(t) = 0$, hence $c(t) = \lambda \ln(t) + \mu$. Thus, we have

Proposition 1 *The solutions of the Horn system of complexity one (i.e. of the kind $z = c(a(x) + b(y))$, a, b, c are nonconstant) for Example 1 exist iff $q_2/q_1 = s_2/s_1 = \alpha$. In this case the solutions have the form*

$$z = \lambda \ln \left(\frac{y}{x^\alpha} \right) + \mu, \quad \alpha \neq 0, \lambda \neq 0.$$

Example 2. Let

$$P = x + 1, \quad Q = 1, \quad R = y + 1, \quad S = 1.$$

Then the system (2) for $z = c(a(x) + b(y))$ takes the form

$$G_x z = x^2 a_1 c_1 + x c_0 - c_0 = 0, \quad G_y z = y^2 b_1 c_1 + y c_0 - c_0 = 0.$$

Then we have

$$\frac{c_1}{c_0} = -\frac{x-1}{x^2 a_1} = -\frac{y-1}{y^2 b_1} = \frac{1}{\lambda}.$$

Thus,

$$a_1 = -\frac{(x-1)\lambda}{x^2}, \quad b_1 = -\frac{(y-1)\lambda}{y^2}.$$

If we substitute these expressions in $G_x = 0$ and $G_y = 0$, we get

$$-(x-1)(\lambda c_1 - c_0) = -(y-1)(\lambda c_1 - c_0) = 0.$$

Hence $c(t) = \exp(-t/\lambda)$ and $z = \mu(x y \exp(1/x + 1/y))^{-1}$.

Proposition 2. *The solutions of the Horn system of complexity one for Example 2 have the form $z = \mu(x y \exp(1/x + 1/y))^{-1}$.*

Example 3. Let

$$P = 1, \quad Q = (x-1) \quad R = 1, \quad S = (y-1).$$

If $z = c(a(x) + b(y))$ we have

$$G_x z = -x c_1 a_1 + x c_0 + c_0 = 0, \quad G_y z = -y c_1 b_1 + y c_0 + c_0 = 0.$$

After elimination of c we obtain

$$-x a_1 y + y b_1 x - x a_1 + y b_1 = 0, \quad a_2 x^2 + a_2 x + a_1 = 0$$

Hence

$$a(x) = \frac{\lambda}{x} + \lambda \ln(x) + \ln(\alpha), \quad b(y) = \lambda \ln(y) + \frac{\lambda}{y} + \ln(\beta), \quad \lambda \neq 0.$$

Then we get the equation for the function c . When we solve this equation, we obtain the following proposition.

Proposition 3. *The solutions of the Horn system of complexity one for Example 3 have the form*

$$z = \mu x y e^{(x+y)}, \quad \mu \neq 0.$$

Example 4. Let

$$P = x^2 y + 1, \quad Q = 1 \quad R = y + 1, \quad S = 1.$$

For $z = c(a(x) + b(y))$ we have

$$G_x z = x^3 y a_1^2 b_1 c_3 + x^3 y a_2 b_1 c_2 + x^2 y a_1 b_1 c_2 + x c_0 - c_0 = 0, \\ G_y z = y^2 b_1 c_1 + y c_0 - c_0 = 0.$$

From the second equation we get $c_1 = (-b_2y^2 - yb_1 + b_2y + 2b_1)c_0$. After differentiation of this equation with respect to x we obtain such expressions for c_2 and c_3 . After the substitution of these expressions in $G_xz = 0$ we get:

$$l = x^3y^4a_2b_1 - x^3y^3a_1^2 - 2x^3y^3a_2b_1 + x^2y^4a_1b_1 + xy^5b_1^2 + 3x^3y^2a_1^2 + \\ + x^3a_2y^2b_1 - 2x^2y^3a_1b_1 - y^5b_1^2 - 3x^3ya_1^2 + x^2a_1y^2b_1 + x^3a_1^2 = 0.$$

From $V(c_1/c_0) = 0$ we get $e = -b_2y^2 - yb_1 + b_2y + 2b_1 = 0$. After differentiation of l with respect to y we obtain:

$$(l)'_y = x^3y^4a_2b_2 + 4x^3y^3a_2b_1 - 2x^3y^3a_2b_2 + x^2y^4a_1b_2 + 2xy^5b_1b_2 - 3x^3y^2a_1^2 - \\ - 6x^3a_2y^2b_1 + x^3a_2y^2b_2 + 4x^2y^3a_1b_1 - 2x^2y^3a_1b_2 + 5xy^4b_1^2 - 2y^5b_1b_2 + \\ + 6x^3ya_1^2 + 2x^3a_2yb_1 - 6x^2a_1y^2b_1 + x^2a_1y^2b_2 - 5y^4b_1^2 - 3x^3a_1^2 + 2x^2a_1yb_1 = 0.$$

The resultant of $(l)'_y$ and e with respect to b_2 equals

$$r_1 = 3x^3y^4a_2b_1 - 3x^3y^3a_1^2 - 6x^3y^3a_2b_1 + 3x^2y^4a_1b_1 + 3xy^5b_1^2 + 9x^3y^2a_1^2 + \\ + 3x^3a_2y^2b_1 - 6x^2y^3a_1b_1 - xy^4b_1^2 - 3y^5b_1^2 - 9x^3ya_1^2 + 3x^2a_1y^2b_1 + \\ + y^4b_1^2 + 3x^3a_1^2 = 0.$$

The resultant of r_1 and l with respect to b_1 equals

$$r_2 = x^6y^8a_1^4(y-1)^6(x-1)^2 = 0.$$

But r_2 is not equal to zero identically. Thus, we have:

Proposition 4. *The solutions of the Horn system of complexity one for Example 4 do not exist.*

Example 5. Let

$$P = x + y - p, \quad Q = x + q, \quad R = x + y - p, \quad S = y + s.$$

Case $p = 0$.

$$G_xz = x^2a_1c_1 + xyb_1c_1 - xa_1c_1 - qc_0 = 0, \\ G_yz = xya_1c_1 + y^2b_1c_1 - yb_1c_1 - sc_0 = 0.$$

From $c_1 \neq 0$ we get $q \neq 0$ and $s \neq 0$. After elimination of c we obtain

$$e_1 = qxya_1 + qy^2b_1 - sx^2a_1 - sxyb_1 - qyb_1 + sxa_1 = 0, \\ e_2 = -x^2a_2b_1 + xya_1b_2 - xa_1b_1 + xa_2b_1 - yb_1^2 + a_1b_1 = 0.$$

From $e_1 = 0$ we get b_1 . b_1 does not depend on x , hence

$$e_3 = -a_2q^2xy^2 + 2a_2qsx^2y - a_2s^2x^3 + a_2q^2xy - a_1q^2y^2 - a_2qsx^2 + 2a_1qksy - \\ a_2qksy - a_1s^2x^2 + a_2s^2x^2 + a_1q^2y - 2a_1qksx + a_2qksx - a_1qksy + a_1qs = 0.$$

This expression is quadratic in y . Write that the coefficient of y^2 is equal to zero, we get $q^2(xa_2 + a_1) = 0$. Hence $a(x) = \lambda \ln(x) + \alpha$ and $s = -q$, $b(y) = -\lambda \ln(y) + \beta$. As a result we get $z = \mu(y/x)^q$.

Case $p \neq 0$.

We have

$$\begin{aligned} G_x z &= x^2 a_1 c_1 + xy b_1 c_1 - p x c_0 - x c_1 a_1 - q c_0 = 0, \\ G_y z &= xy a_1 c_1 + y^2 b_1 c_1 - p y c_0 - y c_1 b_1 - s c_0 = 0. \end{aligned}$$

By elimination of c we get

$$\begin{aligned} e_1 &= p x y a_1 - p x y b_1 + q x y a_1 + q y^2 b_1 - s x^2 a_1 - s x y b_1 - q y b_1 + s x a_1 = 0, \\ e_2 &= -a_2 b_1 p x^3 + a_1 b_2 p x^2 y + a_2 b_1 p x^2 - a_2 b_1 q x^2 + a_1 b_2 q x y - a_1 b_1 q x + a_2 b_1 q x - \\ &\quad - b_1^2 q y + a_1 b_1 q = 0. \end{aligned}$$

Let us express b_2 from $e_2 = 0$ and b_1 from $e_1 = 0$. We have two conditions. The first: $(b_1)'_x = 0$ and the second: $(b_1)'_y = b_2$. After elimination the nonzero factors we can see that both conditions coincide and have the form

$$\begin{aligned} e_3 &= a_2 p^2 x^2 y + a_2 p q x^2 y - a_2 p q x y^2 - a_2 p s x^3 + a_2 p s x^2 y - a_2 q^2 x y^2 + 2 a_2 q s x^2 y - \\ &\quad - a_2 s^2 x^3 + a_2 p q x y - a_1 p q y^2 - a_1 p s x^2 + a_2 p s x^2 + a_2 q^2 x y - a_1 q^2 y^2 - a_2 q s x^2 + \\ &\quad + 2 a_1 q s x y - a_2 q s x y - a_1 s^2 x^2 + a_2 s^2 x^2 + a_1 p q y + a_1 q^2 y - 2 a_1 q s x + \\ &\quad + a_2 q s x - a_1 q s y + a_1 q s = 0. \end{aligned}$$

This expression is quadratic in y . Write that the coefficient of y^2 is equal zero, we get:

$$q(x a_2 + a_1)(p + q) = 0.$$

Case $p \neq 0, q = 0$.

Then e_3 has the form $x^2(p + s)(p y a_2 - s x a_2 - s a_1 + s a_2)$. We have two opportunities for this expression to be equal to zero: either $s = -p$ or $a_2 = s = 0$. The first case is impossible, because in this case $e_1 = p x a_1(x + y - 1)$. In the second case $a(x) = \lambda x + \alpha$, $b(y) = \lambda y + \beta$. Thus, we get:

$$z = \mu(1 - (x + y))^p, \quad q = s = 0, \quad p \neq 0.$$

Case $p \neq 0, q = -p, q \neq 0$. Then e_3 is divisible by s . But $s = 0$ is impossible, if $e_1 = 0$. Thus, we have $s = -p$ and:

$$z = \mu \left(\frac{(x-1)(y-1)}{xy} - 1 \right), \quad s = q = -p.$$

Case $p \neq 0, q \neq 0, (p + q) \neq 0$ ($x a_2 + a_1 = 0$). Then $a(x) = \lambda \ln(x) + \alpha$. From $e_2 = 0$ we get $s = -(p + q)$ and from $e_1 = 0$ we get $b_1 = -\lambda(p + q)/qy$, $b(y) = -\lambda(p + q)/q \ln(y) + \beta$. We have:

$$z = \mu \frac{y^{p+q}}{x^q}, \quad s = -(p + q), \quad q \neq 0, \quad (p + q) \neq 0.$$

Proposition 5. *The solutions of the Horn system of complexity one for Example 5 exist in three cases only:*

- (a) $q \neq 0, p + q \neq 0, s = -(p + q), z = \frac{\mu}{x^q y^s}$,
- (b) $p \neq 0, s = q = 0, z = \mu(1 - (x + y))^p$,
- (c) $s = q = -p \neq 0, z = \mu \left(\frac{(x-1)(y-1)}{xy} - 1 \right)$.

Example 6. Let

$$P = x(x + y), \quad Q = x^2, \quad R = y(x + y), \quad S = y^2.$$

For $z = c(a(x) + b(y))$ we have:

$$\begin{aligned} G_x z &= x^2 a_1^2 c_2 + x y a_1 b_1 c_2 + x^2 a_2 c_1 - x c_2 a_1^2 + x a_1 c_1 - x c_1 a_2 - c_1 a_1 = 0, \\ G_y z &= x y a_1 b_1 c_2 + y^2 b_1^2 c_2 + y^2 b_2 c_1 - y c_2 b_1^2 + y b_1 c_1 - y c_1 b_2 - c_1 b_1 = 0. \end{aligned}$$

After elimination of c we get

$$\begin{aligned} e_1 &= -x^3 y a_1 a_2 b_1 + x^2 y^2 a_1^2 b_2 - x^2 y^2 a_2 b_1^2 + x y^3 a_1 b_1 b_2 - x^2 y a_1^2 b_2 + \\ &+ x^2 y a_1 a_2 b_1 + x^2 y a_2 b_1^2 - x y^2 a_1^2 b_2 - x y^2 a_1 b_1 b_2 + x y^2 a_2 b_1^2 - x^2 a_1^2 b_1 + \\ &+ x y a_1^2 b_2 - x y a_2 b_1^2 + y^2 a_1 b_1^2 + x a_1^2 b_1 - y a_1 b_1^2 = 0, \\ e_2 &= -a_3 a_1^2 b_1 x^4 + 2 a_2^2 a_1 b_1 x^4 - a_2 a_1^2 b_2 x^3 y - a_3 a_1 b_1^2 x^3 y + a_2^2 b_1^2 x^3 y + \\ &+ 2 a_3 a_1^2 b_1 x^3 - 4 a_2^2 a_1 b_1 x^3 - a_1^3 b_2 x^2 y + a_2 a_1^2 b_2 x^2 y - a_2 a_1 b_1^2 x^2 y + a_3 a_1 b_1^2 x^2 y - \\ &- a_2^2 b_1^2 x^2 y - a_2 a_1^2 b_1 x^2 - a_3 a_1^2 b_1 x^2 + 2 a_2^2 a_1 b_1 x^2 + a_1^3 b_2 x y - \\ &- a_1^3 b_1 x + a_2 a_1^2 b_1 x - a_1^2 b_1^2 y + a_1^3 b_1 = 0. \end{aligned}$$

And we obtain two expression for b_2 . Then we have two conditions: equality of both expressions and their independence of x . We obtain $e_3(a_1, a_2, a_3, b_1) = e_4(a_1, a_2, a_3, b_1) = 0$ (e_3 contains 43 monomials, e_4 contains 45 monomials). If r is the resultant of e_3 and e_4 with respect to b_1 , we have:

$$r = y^2 a_1^4 (y - 1) (x - 1)^2 (x + y - 1)^2 r_1^2 r_2 r_3, \text{ where}$$

$$r_1 = (x a_2 + a_1), \quad r_2 = x^3 a_1 a_3 - x^3 a_2^2 + x^2 a_1 a_2 - x^2 a_1 a_3 + x^2 a_2^2 + a_1^2, \quad r_3 = r_{30} + y r_{31},$$

where

$$\begin{aligned} r_{30} &= x^7 a_1^2 a_3^2 - 4 x^7 a_1 a_2^2 a_3 + 4 x^7 a_2^4 - 2 x^6 a_1^2 a_2 a_3 - 3 x^6 a_1^2 a_3^2 + 4 x^6 a_1 a_2^3 + \\ &+ 12 x^6 a_1 a_2^2 a_3 - 12 x^6 a_2^4 - 2 x^5 a_1^3 a_3 + 5 x^5 a_1^2 a_2^2 + 6 x^5 a_1^2 a_2 a_3 + 3 x^5 a_1^2 a_3^2 - \\ &- 12 x^5 a_1 a_2^3 - 12 x^5 a_1 a_2^2 a_3 + 12 x^5 a_2^4 + 2 x^4 a_1^3 a_2 + 6 x^4 a_1^3 a_3 - 15 x^4 a_1^2 a_2^2 - \\ &- 6 x^4 a_1^2 a_2 a_3 - x^4 a_1^2 a_3^2 + 12 x^4 a_1 a_2^3 + 4 x^4 a_1 a_2^2 a_3 - 4 x^4 a_2^4 + x^3 a_1^4 - 6 x^3 a_1^3 a_2 - \\ &- 6 x^3 a_1^3 a_3 + 15 x^3 a_1^2 a_2^2 + 2 x^3 a_1^2 a_2 a_3 - 4 x^3 a_1 a_2^3 - 3 x^2 a_1^4 + 6 x^2 a_1^3 a_2 + \\ &+ 2 x^2 a_1^3 a_3 - 5 x^2 a_1^2 a_2^2 + 3 x a_1^4 - 2 x a_1^3 a_2 - a_1^4, \\ r_{31} &= 4 x^7 a_1 a_2^2 a_3 - 4 x^7 a_2^4 + 8 x^6 a_1^2 a_2 a_3 + x^6 a_1^2 a_3^2 - 4 x^6 a_1 a_2^3 - 12 x^6 a_1 a_2^2 a_3 + \\ &+ 12 x^6 a_2^4 + 4 x^5 a_1^3 a_3 + 4 x^5 a_1^2 a_2^2 - 16 x^5 a_1^2 a_2 a_3 - 2 x^5 a_1^2 a_3^2 + 12 x^5 a_1 a_2^3 + \\ &+ 12 x^5 a_1 a_2^2 a_3 - 12 x^5 a_2^4 + 4 x^4 a_1^3 a_2 - 8 x^4 a_1^3 a_3 + 3 x^4 a_1^2 a_2^2 + 10 x^4 a_1^2 a_2 a_3 + \\ &+ x^4 a_1^2 a_3^2 - 12 x^4 a_1 a_2^3 - 4 x^4 a_1 a_2^2 a_3 + 4 x^4 a_2^4 + 2 x^3 a_1^3 a_2 + 6 x^3 a_1^3 a_3 - \\ &- 11 x^3 a_1^2 a_2^2 - 2 x^3 a_1^2 a_2 a_3 + 4 x^3 a_1 a_2^3 + 3 x^2 a_1^4 - 6 x^2 a_1^3 a_2 - 2 x^2 a_1^3 a_3 + \\ &+ 5 x^2 a_1^2 a_2^2 - 3 x a_1^4 + 2 x a_1^3 a_2 + a_1^4. \end{aligned}$$

Thus, we need to consider three cases:

Case $r_1 = 0$. In this case $a(x) = \lambda \ln(x) + \alpha$. After the substitution of this expression in e_1 , we obtain

$$e_1 = \lambda (y - 1) (y b_2 + b_1) (x y b_1 + \lambda x - \lambda) = 0,$$

hence $(y b_2 + b_1) = 0$ and $b(y) = \mu \ln(y) + \beta$. Then we have $c_2 = 0$ and

$$z = \lambda \ln(x) + \mu \ln(y) + \nu, \quad \lambda \mu \neq 0.$$

Case $r_2 = 0$, $r_1 \neq 0$. If we solve $r_2 = 0$ with respect to a_3 and substitute this expression in $e_2 = 0$, we obtain:

$$\frac{b_2}{b_1} y = \frac{a_2}{a_1} (x - 1) = \lambda = \text{const.}$$

We solve these differential equations with respect to a and b , then we substitute these expressions in $e_1 = 0$. And we obtain a contradiction.

Case $r_3 = 0$, $r_1 \neq 0$, $r_2 \neq 0$. If $r_3 = 0$, then $r_{30} = r_{31} = 0$. Thus, the resultant of r_{30} and r_{31} with respect to a_3 is equal to zero and we have:

$$(x - 1)^6 (xa_2 + a_1)^4 x^{10} a_1^4 (2x^2 a_2 + 2a_1 x - 2xa_2 - a_1)^8 = 0.$$

From the equation $(2x^2 a_2 + 2a_1 x - 2xa_2 - a_1) = 0$ we get

$$a_2 = -1/2 \frac{a_1 (2x - 1)}{x(x - 1)}, \quad a_3 = 1/4 \frac{a_1 (8x^2 - 8x + 3)}{x^2 (x - 1)^2}.$$

After substitution of these expressions into $e_2 = 0$ we obtain $2xya_1 b_2 - 2yb_1^2 + a_1 b_1 = 0$. Then we have $a_1 = 2 \frac{yb_1^2}{2xyb_2 + b_1}$.

Let us substitute expressions for a_1, a_2, a_3 into $e_1 = 0$, then we extract the term without x and equate it to zero. We obtain $b_1^2 (y - 1) = 0$. The contradiction. We do not have such solutions. Thus, we have

Proposition 6. *The solutions of the Horn system of complexity one for Example 6 have the form:*

$$z = \lambda \ln(x) + \mu \ln(y) + \nu, \quad \lambda \mu \neq 0.$$

This example is from [1] (n. 8.1.9., p. 304). In this book there is the basis of 4-dimensional space of solutions. It is possible to get our result from this description. Also we can note that in this case the solutions of complexity one is the linear subspace of codimension one in the general solutions space of this Horn system.

Example 7. Let

$$P = (x + 2y + p), \quad Q = (x + y - q), \\ R = (x + 2y + p)(x + y + p + 1), \quad S = (x + y - q)(y - s).$$

For $z = c(a(x) + b(y))$ we have:

$$G_x z = x^2 a_1 c_1 + 2xyb_1 c_1 + pxc_0 + xc_1 a_1 + yc_1 b_1 - qc_0 = 0, \\ G_y z = x^2 y a_1^2 c_2 + xy^2 a_1 b_1 c_2 + pxy a_1 c_1 + x^2 y a_2 c_1 + xy a_1 b_1 c_2 + y^2 b_1^2 c_2 + \\ + pxa_1 c_1 + 3pyb_1 c_1 + qyb_1 c_1 + sxa_1 c_1 + syb_1 c_1 + 2xya_1 c_1 + \\ + y^2 b_2 c_1 + p^2 c_0 - qsc_0 + 3yc_1 b_1 + pc_0 = 0.$$

Let $f^{(n)}$ be (f_1, \dots, f_n) . After the elimination of c we obtain

$$e_1(a^{(2)}, b^{(2)}) = a_2 b_1 p x^3 - 2a_1 b_2 p x^2 y - a_1 b_1 p x^2 + a_2 b_1 p x^2 - a_1 b_2 p x y - a_2 b_1 q x^2 + \\ + 2a_1 b_2 q x y - b_1 a_1 p x - b_1^2 p y - a_2 b_1 q x + a_1 b_2 q y - 2b_1^2 q y = 0, \\ e_2(a^{(2)}, b^{(2)}) = 0 \quad \text{is the sum of 79 monomials.}$$

Thus, we obtain two expressions for b_2 : the first $b_2 = B_{21}(a^{(2)}, b_1)$ and the second $b_2 = B_{22}(a^{(2)}, b_1)$. Then we have two new conditions: equality of both expressions and their independence of x . We obtain $e_3(a^{(3)}, b_1) = 0$ (41 monomials) and $e_4(a^{(3)}, b_1) = 0$ (98 monomials). Here e_3 is linear with respect to b_1 , and e_4 is quadratic with respect to b_1 . If we express b_1 from $e_3 = 0$, then we get $b_1 = B_1(a^{(3)})$. The condition $(B_1)'_x = 0$ has the form $(px - q)e_5(a^{(4)}) = 0$ (e_5 is the sum of 55 monomials).

Our calculation is the tree of cases.

Case 1: $(px - q) \neq 0$, $e_5 = 0$.

If we substitute $b_1 = B_1(a^{(3)})$ into $e_4(a^{(3)}, b_1) = 0$ we obtain $ee_4(a^{(3)}) = ee_{40}(a^{(3)}) + yee_{41}(a^{(3)}) = 0$. Thus, we have $ee_{40}(a^{(3)}) = ee_{41}(a^{(3)}) = 0$, where ee_{40} consists of 489 monomials and ee_{41} consists of 215 monomials. Substitution of $b_1 = B_1(a^{(3)})$ in $B_{21}(a^{(2)}, b_1)$ yields $BB_{21}(a^{(3)})$. We can write $(B_1)'_y = BB_2$ and we get $e_6 = e_{61}e_{62} = 0$, where

$$\begin{aligned} e_{61} &= x^2a_3 + 4a_2x + xa_3 + 2a_1 + 2a_2, \\ e_{62} &= 2p^2x^5a_1a_3 - 2p^2x^5a_2^2 + 2p^2x^4a_1a_2 + 3p^2x^4a_1a_3 - 3p^2x^4a_2^2 - 4pqx^4a_1a_3 + \\ &\quad + 4pqx^4a_2^2 + 2p^2x^3a_1a_2 + p^2x^3a_1a_3 - p^2x^3a_2^2 - 4pqx^3a_1a_2 - 6pqx^3a_1a_3 + \\ &\quad + 6pqx^3a_2^2 + 2q^2x^3a_1a_3 - 2q^2x^3a_2^2 + a_1^2p^2x^2 + p^2x^2a_1a_2 + 2a_1^2pqx^2 - \\ &\quad - 4pqx^2a_1a_2 - 2pqx^2a_1a_3 + 2pqx^2a_2^2 + 2q^2x^2a_1a_2 + 3q^2x^2a_1a_3 - 3q^2x^2a_2^2 + \\ &\quad + 2pqa_1^2 - 2pqa_1a_2 + 2q^2xa_1a_2 + q^2xa_1a_3 - q^2xa_2^2 + pqa_1^2 + q^2a_1a_2. \end{aligned}$$

Case 1.1: $e_{61} = 0$, then $a(x) = \lambda \ln(x + 1) + \mu (\ln(x) - \ln(x + 1)) + \nu$. Substitution of this a in $e_3 = 0$ yields

$$\begin{aligned} &(2x^4p\lambda + 4x^3p\lambda + x^2p\lambda - \lambda x^2q + x^2p\mu + 2\mu x^2q + 2\mu xq + \mu q) \times \\ &\quad \times (pyb_1 + 2qyb_1 + \lambda q + p\mu) = 0. \end{aligned}$$

The set of coefficients of the first factor has the form:

$$\{\mu q, 2\lambda p, 4\lambda p, 2\mu q, \lambda p - \lambda q + p\mu + 2\mu q\}.$$

All of them can not vanish. Hence the second factor is zero.

Case 1.1.1: $p + 2q \neq 0$. From $(pyb_1 + 2qyb_1 + \lambda q + p\mu) = 0$ we get

$$b(y) = -\left(\frac{\lambda q + \mu p}{p + 2q}\right) \ln(y) + \beta.$$

Substitution of this a and b in $e_2 = 0$ yields $ee_2 = 0$, where ee_2 is the polynomial of degree 2 in (x, y) , the coefficients of which depend on (p, q, s, λ, μ) . One of them equals $\lambda(p + q + 1)(\lambda - 2\mu)$.

Case 1.1.1.1.: $(\lambda - 2\mu) = 0$. The analysis of coefficients of ee_2 shows us that $ee_2 = 0$ is impossible in this case.

Case 1.1.1.2.: $p + q + 1 = 0$.

Case 1.1.1.2.1.: $\lambda = \mu$. We have $ee_2 = 0$. Then we have $p = -1$, $q = 0$. The solution has the form $z = \nu(y/x)$.

Case 1.1.1.2.2.: $\lambda = -\mu p \neq 0$. We have $p = s = \lambda = 0$, $q = -1$, $\mu \neq 0$. The solution has the form $z = \nu(y/x^2)$.

Case 1.1.2: $p = 2q \neq 0$. From $e_4 = 0$ we obtain $b_1 = B_1(a^{(2)})$. After substitution of this expression in B_{21} we get BB_{21} . From $(B_1)'_y = BB_{21}$ we get $g_0(a^{(2)}) + y g_1(a^{(2)}) + y^2 g_2(a^{(2)}) = 0$ and hence $g_0(a^{(2)}) = g_1(a^{(2)}) = g_2(a^{(2)}) = 0$. The resultant of $g_1(a^{(2)})$ and $g_2(a^{(2)})$ with respect to a_2 is some polynomial in x of degree 11. The value of this polynomial for $x = 0$ is $(q - 1)^6$ and hence $q = 1$. Then we have

$$\forall s \quad r = -2 (2sx^2 + sx - 2x^2)^2 (-2x^2 - 2x)^3 x \neq 0.$$

A contradiction. Solutions are absent.

Case 1.2: $e_{62} = 0$. Let us express a_3 from this equation and substitute the result in $e_2 = 0$. We obtain $ee_2 = ee_{20}(a^{(3)}) + y ee_{21}(a^{(3)}) = 0$, then

$$\begin{aligned} g_1 &= (-psx - qsx + p^2 + qp + xp + p) g^3 = 0, \\ g_2 &= (xp^2 + pqx + x^2p - qp + 2xp - q^2 - q) g^3 = 0, \end{aligned}$$

where $g = (2px^2a_2 + 4pxa_1 + pxa_2 - 2qxa_2 + pa_1 - 2qa_1 - qa_2)$.

Case 1.2.1.: $g \neq 0$. In this case all coefficients of both factors must vanish. The set of these coefficients is:

$$\{p(p + q + 1), -ps - qs + p, p, p(p + q + 2), -q(p + q + 1)\}.$$

We see that $p = 0$, then $s = 0$ ($q \neq 0$) and $q = -1$. We have the solution $z = \nu(y/x^2)$ (this solution coincides with the solution of the case 1.1.1.2.2.).

Case 1.2.2.: $g = 0$. Let us express a_2 from this equation and substitute the result in $e_{62} = 0$. We obtain

$$2p^2x^3 + 4pqx^3 + 6pqx^2 + 6pqx + pq - q^2 = 0.$$

The set of coefficients of this polynomial is:

$$\{q(p - q), 6pq, 2p(p + 2q)\}.$$

The vanishing of all of them is impossible ($px - q \neq 0$).

Case 2: $p = q = 0$. The equation $G_x(z) = 0$ takes the form:

$$G_x z = x^2a_1 + 2xyb_1 + xa_1 + yb_1 = 0.$$

Hence

$$a_1 \frac{(x + 1)}{(2x + 1)} = \lambda = b_1 y, \quad \lambda \neq 0 \text{ is constant.}$$

And then we get

$$a(x) = \lambda(2x - \ln(x)) + \alpha, \quad b(y) = \lambda \ln(y) + \beta.$$

After elimination of c from

$$\begin{aligned} G_y z &= x^2ya_1^2c_2 + xy^2a_1b_1c_2 + x^2ya_2c_1 + xy a_1b_1c_2 + y^2b_1^2c_2 + \\ &+ sx a_1c_1 + sy b_1c_1 + 2xy a_1c_1 + y^2b_2c_1 + 3yc_1b_1 = 0 \end{aligned}$$

for our a and b we get:

$$8sx^3y - 12sx^2y - 8x^2y^2 + 2sxy + 4xy^2 - 10xy - y^2 + 4y - 2 = 0.$$

for all (x, y) . This is impossible for all s . A contradiction. Thus, we have:

Proposition 7. *The solutions of the Horn system of complexity one for Example 7 exist in two cases only:*

$$(a) \quad p = -1, \quad q = 0, \quad z = \nu \frac{y}{x},$$

$$(b) \quad p = s = 0, \quad q = -1, \quad z = \nu \frac{y}{x^2}.$$

Example 8. The Lauricella's functions are the subclass of the class of hypergeometric functions [5], [6]. They are the solutions of the Lauricella system (some generalization of the hypergeometric Gauss equation). If the number of the independent variables is two, this system is the system of two equations for the function $z(x, y)$ of the form

$$L_x(z) = x(1-x) \frac{\partial^2}{\partial x^2} z(x, y) + (1-x)y \frac{\partial^2}{\partial y \partial x} z(x, y) +$$

$$+ (q - (1 + p_1 + \rho)x) \frac{\partial}{\partial x} z(x, y) - p_1 y \frac{\partial}{\partial y} z(x, y) - p_1 \rho z(x, y) = 0,$$

$$L_y(z) = y(1-y) \frac{\partial^2}{\partial y^2} z(x, y) + (1-y)x \frac{\partial^2}{\partial y \partial x} z(x, y) +$$

$$+ (q - (1 + p_2 + \rho)y) \frac{\partial}{\partial y} z(x, y) - p_2 x \frac{\partial}{\partial x} z(x, y) - p_2 \rho z(x, y) = 0.$$

The parameters (p_1, p_2, ρ) are any complex numbers and $q \in \mathbf{C} \setminus \{0, -1, -2, \dots\}$. Our goal is to describe the solutions of the Lauricella system of complexity one (of kind $z = c(a(x) + b(y))$, where (a, b, c) are not constant). In order to simplify our calculation we will assume that $\rho = 0$. Thus, we have three complex parameters only (p_1, p_2, q) . The Lauricella system for $\rho = 0$, $z = c(a(x) + b(y))$ has the form:

$$L_x(z) = -x^2 a_1^2 c_2 - y c_2 a_1 b_1 x - x^2 a_2 c_1 + x a_1^2 c_2 - x a_1 c_1 p_1 +$$

$$+ y c_2 a_1 b_1 - p_1 y c_1 b_1 + q a_1 c_1 - x a_1 c_1 + x a_2 c_1 = 0,$$

$$L_y(z) = -y c_2 a_1 b_1 x - y^2 b_1^2 c_2 + x c_2 a_1 b_1 - p_2 x c_1 a_1 - y^2 b_2 c_1 +$$

$$+ y b_1^2 c_2 - y b_1 c_1 p_2 + q b_1 c_1 - y b_1 c_1 + y b_2 c_1 = 0.$$

Case 1. $x a_1 + y b_1 = 0$. We have

$$a(x) = -\lambda \ln(x) + \alpha, \quad b(y) = \lambda \ln(y) + \beta, \quad \lambda \neq 0$$

and our equations have the form

$$-\frac{\lambda c_1 (q-1)}{x} = \frac{\lambda c_1 (q-1)}{y} = 0.$$

The condition of solvability is $q = 1$ and we obtain $z = c(y/x)$, where $c(t)$ is any analytical function.

Case 2. $x a_1 + y b_1 \neq 0$. We can express c_2/c_1 from both equations. We have

$$c_2/c_1 = LC_{21}(a^{(2)}, b_1) = LC_{22}(a_1, b^{(2)}) = 0.$$

The solvability conditions are: $LC_{21} = LC_{22}$ and $V(LC_{21}) = 0$. This conditions are $e_1(a^{(2)}, b^{(2)}) = 0$ (20 monomials) and $e_2(a^{(3)}, b^{(2)}) = 0$ (39 monomials).

Case 2.1. $-x^2a_2 + qa_1 - xa_1 + xa_2 = 0$. Thus,

$$a_1 = \frac{(x-1)^{q-1}}{x^q}, \quad b_1 y = - \left(\frac{x-1}{x} \right)^{q-1}.$$

Hence $q = 1$, $a_1 = 1/x$ and $b_1 = -1/y$, and further $xa_1 + yb_1 = 0$. In this case it is impossible.

Case 2.2. $-x^2a_2 + qa_1 - xa_1 + xa_2 \neq 0$. The equations $e_1 = 0$ and $e_2 = 0$ are linear with respect to b_2 . We have two expressions for b_2 : $b_2 = B_{21}(a^{(2)}, b_1)$ and $b_2 = B_{22}(a^{(3)}, b_1)$. We get two conditions: $B_{21} = B_{22}$ yields $e_3(a^{(3)}, b_1) = 0$ (79 monomials), $(B_{21})'_x = 0$ yields $e_4(a^{(3)}, b_1) = 0$ (36 monomials). e_3 is cubic with respect to b_1 , e_4 is quadratic with respect to b_1 . We can divide e_3 by e_2 with the remainder (as polynomials with respect to b_1). We obtain that the remainder is zero. Thus, we have:

$$-yb_1 - \frac{(x^2a_2 + qa_1 + xa_1 - xa_2 - a_1)a_1}{xa_2 + a_1 - a_2} = 0.$$

Hence

$$yb_1 = \lambda = - \frac{(x^2a_2 + qa_1 + xa_1 - xa_2 - a_1)a_1}{xa_2 + a_1 - a_2}.$$

And further we get

$$b(y) = \lambda \ln(y) + \beta, \quad a_2 = - \frac{a_1(qa_1 + xa_1 + \lambda - a_1)}{x^2a_1 + \lambda x - xa_1 - \lambda}, \quad \lambda \neq 0.$$

After substitution of these expressions in $e_1 = e_2 = e_3 = e_4 = 0$ we get $ee_1(a_1) = ee_2(a_1) = ee_3(a_1) = ee_4(a_1) = 0$. The resultant of ee_1 and ee_2 with respect to a_1 is a polynomial with respect to (x, y) . The coefficient of x^6y in this polynomial is $(q-1)^4$, hence $q = 1$. For such q we have $xa_1 + yb_1 = 0$. In this case it's impossible. Thus, we have the following proposition.

Proposition 8. *The solutions of the Lauricella system of complexity one for $\rho = 0$ exist in the case $q = 1$ only. These solutions have the form:*

$$z = c\left(\frac{y}{x}\right), \quad \text{where } c(t) \text{ is any nonconstant analytical function.}$$

It is possible that the additional computational efforts would allow us to free ourselves from the constraint $\rho = 0$.

Conclusion

Both (2) and (1) are equalities to zero of differential polynomials, which are the elements of the differential ring \mathcal{R} , the ring of differential polynomials with complex coefficients and generators $(x, y, z, \partial_x, \partial_y)$ (and with obvious relations) [7], to which the field of fractions \mathcal{F} corresponds. The ring \mathcal{R} is a classical object of differential algebra. We can look at the common zeros of a system of differential-polynomial equations, i.e., at the solutions of these equations, from two different points of view. From a quite abstract algebraical point of view they are the elements of the differential-algebraic closure of the field \mathcal{F} . From the analytical point of view they are analytic functions, which gives solutions to the system of differential equations. In \mathcal{R} there is the subring $\mathbf{C}[x, y]$, which is the commutative ring of the polynomials in (x, y) . The set of the common zeros of a system of polynomials is an affine algebraic subvariety of two-dimensional space. This is the area of responsibility of algebraic geometry. If we move from $\mathbf{C}[x, y]$ to \mathcal{R} , then

the object arise, which is quite analogous to an algebraic variety: the set of the common zeros of a differential-polynomial system, which is a *differential-algebraic manifold* (DA-manifold). The term is not stable, there are variants, e.g., *diffiety* [8]. From this point of view the discussed above examples are examples of DA-manifolds, which are defined by three differential polynomials (two of them are the Horn system, and the third is the defining equation of the first class). The Horn systems from this point of view are not very interesting, the corresponding DA-manifold is a linear space. By adding the defining equation of the first class, we provide opportunities for a larger diversity. Studying an algebraic variety, one usually pays attention to a series of natural characteristics, namely: irreducible components, stratification of the points on the variety with respect to the dimension of the tangent space and so on. In the study of DA-manifolds these characteristics are also of interest. Nevertheless, there is a certain specifics.

For example, the dimension of the linear space of the solutions of system (2) can be either finite or infinite. In the case when it is infinite the question arise:

Question 9: (a) Under which condition the dimension of the intersection is finite? (b) If the dimension is finite, how to estimate it? (c) How to estimate the number of irreducible components?

DA-manifold defined by the equation $d_1(z) = 0$ is a cone, and DA-manifold defined by a Horn system is a linear space. However, when we speak about conic sections, we mean that the cutting plane does not necessary go through the vertex of the cone, as it is in our examples. We can easily avoid this limitation. Let $z_0(x, y)$ be an analytic function of complexity one, which is a solution of the Horn system, i.e., $G_x(z_0) = G_y(z_0) = 0$. Then we can consider the affine subspace, which consists of the functions of the form $\{z = z_0 + \delta z\}$, where δz is a solution of the Horn system, i.e., $G_x(\delta z) = G_y(\delta z) = 0$, and construct its intersection with the cone Cl^1 , which is certainly nonempty (there z_0 lies).

Some of the discussed examples of Horn systems are systems with parameters. This feature can be easily interpreted with the help of differential algebra. In the definition of the differential ring \mathcal{R} we should include these parameters in the field of constants.

Next, note that all our considerations can be adapted to functions of larger number of variables. The functions of complexity one in n variables are analytic functions of the form $z(x_1, \dots, x_n) = c(a_1(x_1) + \dots + a_n(x_n))$, where (a_1, \dots, a_n, c) are functions of one variable. The class of such functions, as in the case of two variables, is defined by a set of differential polynomials.

The consideration of examples with parameters allows us to note that in all discussed situations for the existence of solutions of complexity one there are necessarily restrictions on the parameters. I.e., solutions exist only for a proper algebraic subset of the space of parameters.

Question 10: Do there exist holonomic Horn systems with parameters, such that there are solutions of complexity one for all values of parameters?

Let a Horn system with parameters be given. And let solutions of complexity not greater than a fixed n of this system exist only under some nontrivial analytic conditions (for all natural n). Then it is easy to show that all solutions for generic values of parameters (outside solutions of some enumerable system of analytic equations) have infinite complexity. On the other hand, if we assume that for a Horn system with parameters all solutions are of finite complexity, then there exists a number N , such that *all* solutions for *all* values of parameters have complexity not greater than N .

The author is grateful to A. K. Tsikh and T.M. Sadykov for the discussion of this paper.

References

- [1] T.M. Sadykov, A.K. Tsikh, Hypergeometric and algebraic functions, Moscow, Nauka, 2014.
- [2] V.K.Beloshapka, Analytic Complexity of Functions of Two Variables, *Russian Journal of Mathematical Physics*, **14**(2007), no. 3, 243–249.
- [3] V.K.Beloshapka, Stabilizer of a Function in the Gauge Group, *Russian Journal of Mathematical Physics*, **24**(2017), no. 2, 1–10.
- [4] W.Blaschke, Einführung in die Geometrie der Waben, Birkhauser Verlag, Basel und Stuttgart, 1955; V.Blyashke, Vvedenie v geometriyu tkanej, Moscow, Fizmatgiz, 1959.
- [5] G.Lauricella, Sulle funzioni ipergeometriche a piu variabili, *Rend. Circ. Mat.Palermo*, **7**(1893), 111–158.
- [6] S.I.Bezrodnyk, The Lauricella hypergeometric function $F_D^{(N)}$, the Riemann–Hilbert problem, and some applications, *Russian Mathematical Survey*, **73**(2018), no. 6, 3–94.
DOI: 10.1070/RM9841
- [7] J.Ritt, Differential Algebra, American Mathematical Soc., 1950.
- [8] D.V.Alekseevsky, A.M.Vinogradov, V.V.Lychagin, Basic ideas and concepts of differential geometry, In: Itogi Nauki i Tekhniki. Ser. Sovrem. Probl. Mat. Fund. Napr., vol. 28, 1988, 5–289.

О гипергеометрических функциях двух переменных сложности один

Валерий К. Белошапка

Московский центр фундаментальной и прикладной математики
Московский государственный университет имени М. В. Ломоносова
Москва, Российская Федерация

Аннотация. Для серии примеров систем Горна и системы Лауричеллы для функций двух переменных дано описание решений, имеющих аналитическую сложность один. Ставится ряд вопросов.

Ключевые слова: аналитическая сложность, гипергеометрические функции, система Горна, система Лауричеллы, дифференциальное кольцо.

EDN: FEWHMQ

УДК 537.6

Hysteresis Effects in the Critical Behavior of Heisenberg Thin Films in an External Oscillating Field

Alexey V. Eikhler*

Vladimir V. Prudnikov[†]

Dostoevsky Omsk State University

Omsk, Russian Federation

Pavel V. Prudnikov[‡]

Center of New Chemical Technologies BIC

Boreskov Institute of Catalysis

Omsk, Russian Federation

Received 12.10.2023, received in revised form 22.11.2023, accepted 26.12.2023

Abstract. In this work, we simulated hysteresis effects in thin Heisenberg films subjected to an external oscillating field by Monte Carlo methods. It was observed that the system exhibits different types of phase transitions below the Curie temperature, depending on the rate of field influence. Relaxation features of the system have been identified, which may also impact the nature of the dynamic phase transition.

Keywords: Heisenberg model, dynamic phase transition, Monte Carlo methods, hysteresis effects.

Citation: A.V. Eikhler, V.V. Prudnikov, P.V. Prudnikov, Hysteresis Effects in the Critical Behavior of Heisenberg Thin Films in an External Oscillating Field, J. Sib. Fed. Univ. Math. Phys., 2024, 17(2), 189–194. EDN: FEWHMQ.



The phenomenon of dynamic phase transition is widespread across all fields of human activity. It has been observed that dynamic phase transitions can be used to describe biological [1, 2] and chemical systems [3], as well as processes associated with human social behavior [4]. The exploration of dynamic phase transitions in promising materials such as nanographene [5] or $\text{LiMn}_{0.5}\text{Fe}_{0.5}\text{PO}_4$ [6] opens new opportunities in energy engineering and design.

A dynamic phase transition in magnetic systems occurs when the speed of influence of an external oscillating field changes. At a high half-period of the external field, magnetization follows the cyclic changes in the field and remains in a dynamically disordered state. However, at a low half-period value, magnetization cannot qualitatively follow the oscillations and transitions into a dynamically ordered state. The transition between a dynamically ordered state and a dynamically disordered state is referred to as a dynamic phase transition.

The classic model for studying dynamic phase transitions is the Ising kinetic model. Work [7] was the first to prove the existence of a dynamic phase transition in magnetic structures.

In early experimental works [8, 9], a dynamic phase transition was observed in the hysteresis response with a change in the amplitude of the external field H_0 . Recent experimental studies on the magnetization reversal of thin films [10–14] have indicated that the system can undergo a qualitative transition from one ordered state to another by introducing an additional field in conjunction with an external oscillating field. As demonstrated in previous works [13, 14], this additional field in dynamic phase transitions is comparable to the influence of the field $H(t)$ in thermodynamic phase transitions.

*alexey987@bk.ru <https://orcid.org/0009-0002-7267-9705>

[†]prudnikov@univer.omsk.su <https://orcid.org/0000-0003-3078-6481>

[‡]prudnikp@ihcp.ru <https://orcid.org/0000-0002-6522-2873>

© Siberian Federal University. All rights reserved

Hysteresis effects in dynamic phase transitions are being actively studied numerically modeling and experimentally. However, many questions remain open and require additional study. The studies were carried out using the Heisenberg model, which is a more complex system compared to the Ising model [15], including the influence of anisotropy and three-dimensional spin. Considering the dynamic phase transition within a more complex model can provide additional insight into this phenomenon.

1. Model and methods

In this work, a thin magnetic film in an external oscillating field $H(t)$ with an amplitude H_0 below the Curie temperature was studied by Monte Carlo methods, in particular by the Metropolis algorithm using the anisotropic Heisenberg model.

The Hamiltonian of the anisotropic Heisenberg model was chosen as:

$$H = -J \sum_{i,j} [(1 - \Delta(N))(S_i^x S_j^x + S_i^y S_j^y) + S_i^z S_j^z] - H(t) \sum_i S_i^z, \quad (1)$$

where $S_i = (S_i^x, S_i^y, S_i^z)$ is the three-dimensional spin at the i -th node of all the systems; N is number of monolayers; $L \times L \times N$ — total number of spins of the system; J is the exchange integral of the interaction between nearest spins S_i .

$\Delta(N)$ is an anisotropy parameter depending on the number of monolayers, the value of which was chosen based on the article [16], the anisotropy value $\Delta(N = 5) = 0.75$. In this work, "easy axis" anisotropy was studied. The external magnetic field was directed perpendicular to the plane of the ferromagnetic film.

The dynamic order parameter Q is defined as:

$$Q = \frac{1}{2t_{1/2}} \int_0^{2t_{1/2}} m_z(t) dt. \quad (2)$$

In the dynamically disordered phase, the order parameter Q is close to zero, and in the ordered phase it is nonzero. The parameter that acts as an analogue of temperature in the transition is $\Theta = t_{1/2}/\langle\tau\rangle$, where $t_{1/2}$ is the half-period of the external field, $\langle\tau\rangle$ is the time of the metastable state, defined as the time at which the magnetization first crosses zero during the relaxation process. The magnetization of the z component was calculated using the formula:

$$m_z(t) = \frac{1}{L^2} \sum_{i=1}^{L^2} s_i^z. \quad (3)$$

The field bias value was introduced as a low additional field to the oscillating external field. As a result, uncompensation leads to asymmetrical oscillation of the field relative to zero:

$$H_b = \langle H(t) \rangle = \frac{1}{2t_{1/2}} \int_0^{2t_{1/2}} H(t) dt. \quad (4)$$

Simulation of the magnetic film was carried out for linear size $L = 128$ with external field amplitude $H_0 = 0.2$ and temperature $T = 0.6T_c(N)$, where $T_c(N = 5) = 1.31J$ [17]. The field bias H_b changed in steps of 0.001 and at time relaxation (the number of cycles) $P = 1000$. During the simulation, the number of monolayers $N = 5$ was considered. The spin system represents a cubic structure, based on the type of substrate anisotropy in experiments [12, 13].

2. Results and discussion

In this work, a thorough investigation of the various consequences of hysteresis in the critical region was carried out. The behavior of the order parameter $Q(H_b)$ is considered as the half-period $t_{1/2}$ increases to detect a dynamic phase transition. Figures 1 shows the change in the order parameter Q as a function of the field bias H_b at low field frequencies $t_{1/2} = 20$ MCS/s (Fig. 1(a)) with a clear existence of the first-order phase transition. With the appearance of the half-period $t_{1/2}$ (Fig. 1(b,c)), a sharp jump in the parameter was observed for a long time. A continuous phase transition occurs only at a critical half-period definition (Fig. 1(d)), when magnetization can follow a change in the oscillating field. In this case, collapse of the hysteresis loops is observed.

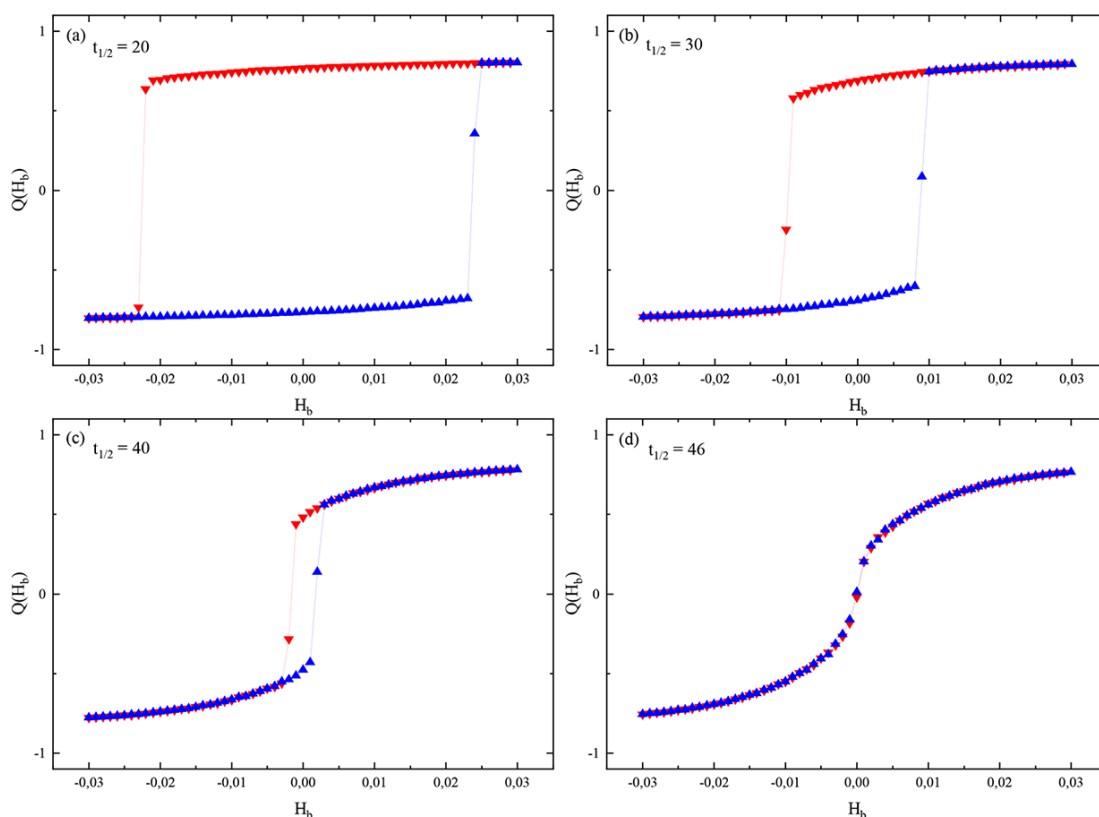


Fig. 1. Hysteresis loops for different values of half-period $t_{1/2}$. For case (a), a wide loop is formed, where the half-period is equal to $t_{1/2} = 20$ MCS/s, (b) an increase in the half-period $t_{1/2} = 30$ MCS/s contributes to the narrowing of the loop, as well as for case (c) $t_{1/2} = 40$ MCS/s, (d) $t_{1/2} = 46$ MCS/s the hysteresis loop collapses

The type of phase transition when considering hysteresis effects can also depend on the relaxation features of the model. Fig. 2 shows the relaxation dependence of the parameter Q on H_b on the oscillation cycles P of the system. A gradual increase in observation time leads to the fact that the hysteresis loops begin to collapse. In the region of dynamic phase transition, taking into account relaxation effects can play an important role. The simulation data qualitatively correlate with the experimental results of [11].

To consider the peculiarities of the behavior of the system after a dynamic phase transition (Fig. 3), a sufficiently large half-period $t_{1/2} = 100$ MCS/s for $H_0 = 0.2$ was chosen. We changed

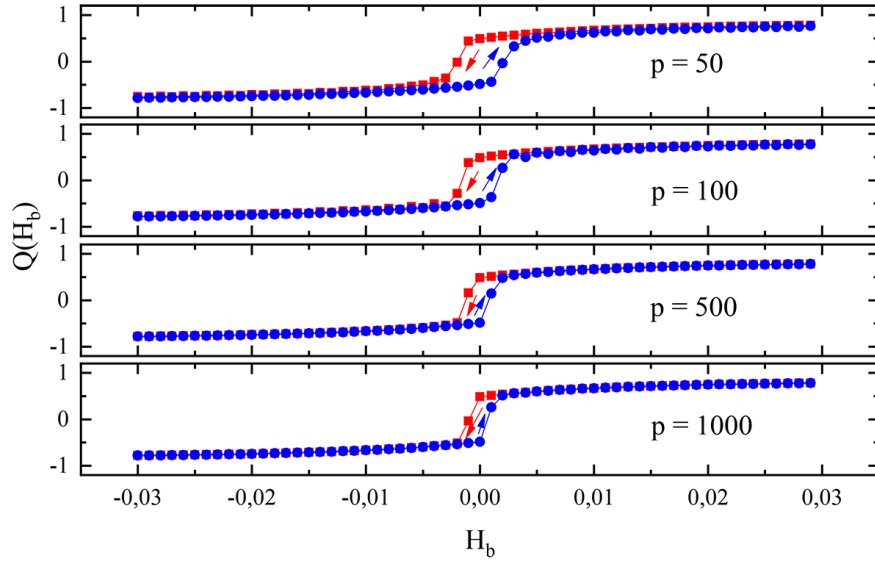


Fig. 2. Hysteresis effect depending on bias field H_b with increasing oscillation cycles P of the influence of the external field $H(t)$ at half-period $t_{1/2} = 40$ MCS/s

the value of the field amplitude from $H_0 = 0.16 \div 0.22$ in steps of 0.02 to more clearly show changes in the behavior of magnetization with distance from the multicritical point. Thus, at $H_0 = 0.16$ a collapsed hysteresis loop is represented, but fluctuations appear as the field increases. The magnitude of the field amplitude significantly affects the area of fluctuations and their magnitude.

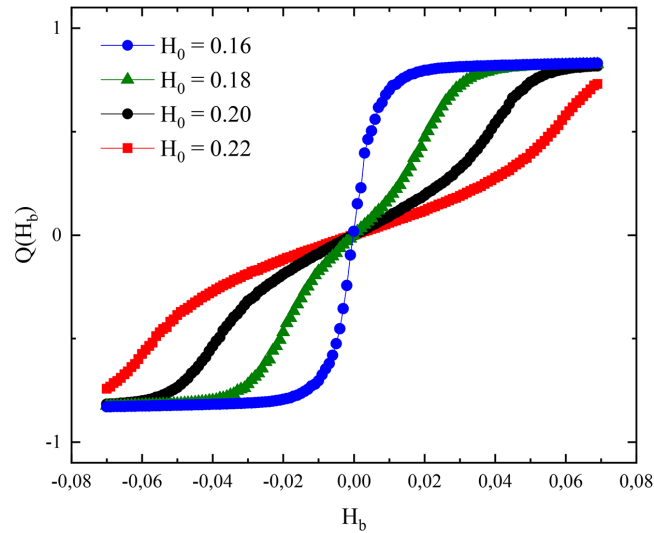


Fig. 3. Dependence of the hysteresis effect on changes in the field bias H_b for different field amplitudes $H_0 = 0.16 - 0.22$. Linear size of the system $L = 128$, half-period $t_{1/2} = 100$ MCS/s. At $H_0 = 0.16$ the hysteresis loop collapses (blue dots); at $H_0 = 0.20$ the loop bends (black dots)

Conclusion

We have carried out numerical modeling of hysteresis effects in a dynamic phase transition using the Heisenberg model in an external oscillating field by Monte Carlo methods. The dependence of the hysteresis loops on the $t_{1/2}$ was studied. As a result of which the existence of a first-order phase transition was revealed at less than values of the half-period $t_{1/2} = 46$ MCS/s, when the magnetization changes its state in an abrupt manner. A second-order phase transition occurs at higher values of $t_{1/2} = 46$ MCS/s. An increase in the half-period of the field leads to the fact that the magnetization of the system can follow the oscillations of the external field and consistently changes its values.

The collapse of the hysteresis loop occurs at a field amplitude $H_0 \geq H_0^c(t_{1/2}) = 0.16$ and $t_{1/2} = 100$ MCS/s. Curvature of the loops is observed with increasing H_0 [18]. This type indicates fluctuations that arise due to the stronger influence of $H(t)$ far from the critical region. The destruction of the phase transition with the formation of a metastable phase with a change in $H(t)$ is also observed, which also leads to a shift in the critical point.

Relaxation processes for hysteresis effects have been identified. The type of phase transition can be strongly influenced by the time of observation of the system. The results show a narrowing of the hysteresis loops with increasing oscillation cycles.

The reported study was supported by the Russian Science Foundation through project no. 23-22-00093. Pavel V. Prudnikov acknowledged for the supporting by the Ministry of Science and Higher Education of the Russian Federation within the governmental order for Boreskov Institute of Catalysis (project FWUR-2024-0039).

References

- [1] G.Schoner, J.Kelso, Dynamic Pattern Generation in Behavioral and Neural Systems, *Science*, **239**(1964), 1513–1520.
- [2] J.O.Dabiri, Landmarks and frontiers in biological fluid dynamics, *Physical Review Fluids*, **4**(2019), no. 110501. DOI:10.1103/PhysRevFluids.4.110501
- [3] C.E.Woodward, M.Campion, D.J.Isbister, Kinetics of a two-dimensional lattice gas mixture in a color field, *The Journal of Chemical Physics*, **116**(2002), 2983–2990. DOI:10.1063/1.1427719
- [4] B.Slavko, K.Glavatskiy, M.Prokopenko, Dynamic resettlement as a mechanism of phase transitions in urban configurations, *Physical Review E*, **99**(2019), no. 042143. DOI:10.1103/PhysRevE.99.042143
- [5] Y.Benhouria, I.Bouzi'ani, I.Essaoudi, A.Ainane, R.Ahuja, Quantum Monte Carlo study of dynamic magnetic properties of nano-graphene, *Journal of Magnetism and Magnetic Materials*, **460**(2018), 223–228. DOI:10.1016/j.jmmm.2018.04.007
- [6] S.Pleuksachat, P.Krabao, S.Pongha et al., Dynamic phase transition behavior of a $\text{LiMn}_{0.5}\text{Fe}_{0.5}\text{PO}_4$ olivine cathode material for lithium-ion batteries revealed through in-situ X-ray techniques, *Journal of Energy Chemistry*, **71**(2022), 452–459. DOI:10.1016/j.jechem.2022.04.016
- [7] T.Tome, M.J.de Oliveira, Dynamic phase transition in the kinetic Ising model under a time-dependent oscillating field, *Physical Review A*, **41**(1990), no. 4251.
- [8] Q.Jiang, H.-N.Yang, G.-C.Wang, Scaling and dynamics of low-frequency hysteresis loops in ultrathin Co films on a Cu(001) surface, *Physical Review B*, **52**(1995), no. 14911.

- [9] J.-S.Suen, J.L.Erskine, Magnetic Hysteresis Dynamics: Thin $p(1 \times 1)$ Fe Films on Flat and Stepped W(110), *Phys. Rev. Lett.*, **78**(1997), no. 3567. DOI: 10.1103/PhysRevLett.78.3567
- [10] D.T.Robb, Y.H.Xu, O.Hellwig, J.McCord, A.Berger, M.A.Novotny, P.A.Rikvold, Evidence for a dynamic phase transition in [Co/Pt3] magnetic multilayers, *Physical Review B*, **78**(2008), no. 134422. DOI: 10.1103/PhysRevB.78.134422
- [11] A.Berger, O.Idigoras, P.Vavassori, Transient Behavior of the Dynamically Ordered Phase in Uniaxial Cobalt Films, *Physical Review Lett.*, **111**(2013), no. 190602. DOI:10.1103/PhysRevLett.111.190602
- [12] P.Riego, P.Vavassori, A.Berger, Metamagnetic Anomalies near Dynamic Phase Transitions, *Physical Review E*, **118**(2017), no. 117202. DOI: 10.1103/PhysRevLett.118.117202
- [13] J.M.Marin Ramirez et al., Experimental exploration of dynamic phase transitions and associated metamagnetic fluctuations for materials with different Curie temperatures, *Physical Review E*, **102**(2020), no. 022804. DOI:https://doi.org/10.1103/PhysRevE.102.022804
- [14] P.Riego, P.Vavassori, A.Berger, Towards an understanding of dynamic phase transitions, *Physica B: Condensed Matter*, **549**(2018), 13–23. DOI: 10.1016/j.physb.2017.09.043
- [15] G.Korniss, C.J.White, P.A.Rikvold, M.A.Novotny, Dynamic phase transition, universality, and finite-size scaling in the two-dimensional kinetic Ising model in an oscillating field, *Physical Review E*, **63**(2000), no. 016120. DOI: 10.1103/PhysRevE.63.016120
- [16] P.V.Prudnikov, V.V.Prudnikov, M.V.Mamonova, N.I.Piskunova, Influence of anisotropy on magnetoresistance in magnetic multilayer structures, *Journal of Magnetism and Magnetic Materials*, **482**(2019), 201–205. DOI: 10.1016/j.jmmm.2019.03.061
- [17] M.A.Medvedeva, P.V.Prudnikov, Monte Carlo simulation of critical properties of ultrathin anisotropic Heisenberg films, *Journal of Physics: Conference Series*, **510**(2014), no. 012024. DOI:10.1088/1742-6596/510/1/012024
- [18] G.M.Buendia, P.A.Rikvold, Fluctuations in a model ferromagnetic film driven by a slowly oscillating field with a constant bias, *Physical Review B*, **96**(2017), no. 134306. DOI: 10.1103/PhysRevB.96.134306

Эффекты гистерезиса в критическом поведении тонких гейзенберговских пленок во внешнем осциллирующем поле

Алексей В. Ейхлер

Владимир В. Прудников

Омский государственный университет имени Достоевского
Омск, Российская Федерация

Павел В. Прудников

Центр новых химических технологий ИК СО РАН
Институт катализа имени Г.К. Борескова СО РАН
Омск, Российская Федерация

Аннотация. В данной работе методами Монте-Карло моделировались эффекты гистерезиса в тонких пленках Гейзенберга во внешнем осциллирующем поле. Было обнаружено, что в системе ниже температуры Кюри наблюдаются различные типы фазовых переходов в зависимости от скорости воздействия осциллирующего поля. Выявлены релаксационные особенности системы, которые влияют на характер динамического фазового перехода.

Ключевые слова: Модель Гейзенберга, динамический фазовый переход, методы Монте-Карло, эффекты гистерезиса.

EDN: FVESDY

УДК 517.9

Thermocapillary Convection of Immiscible Liquid in a Three-dimensional Layer at Low Marangoni Numbers

Viktor K. Andreev*

Institute of Computational Modelling SB RAS
Krasnoyarsk, Russian Federation

Received 26.08.2023, received in revised form 24.09.2023, accepted 20.12.2023

Abstract. The joint convection of two viscous heat-conducting liquids in a three-dimensional layer bounded by solid flat walls is studied. The upper wall is thermally insulated, and a non-stationary temperature field is set on the lower wall. Liquids are assumed to be immiscible and complex conjugation conditions are set at the flat interface between them. The evolution of this system is described by the Oberbeck-Boussinesq equations in each fluid. The solution of this problem is sought in the class of velocity fields linear in two coordinates, and temperature fields are quadratic functions of the same coordinates. In this case, the problem is reduced to a system of 10 nonlinear integro-differential equations. It is conjugate and inverse with respect to 4 functions of time. To find them, integral redefinition conditions are set. The physical meaning of these conditions is the closeness of the flow. The inverse initial-boundary value problem describes convection in a two-layer system that occurs near the temperature extremum point on the lower solid wall. For small Marangoni numbers, the problem is approximated by a linear one (the Marangoni number plays the role of the Reynolds number for the Navier-Stokes equations). A stationary solution to this problem has been found. The linear nonstationary problem is solved by the Laplace transform method, and the temperature can have discontinuities of the 1st kind (change by a jump). In Laplace images, the solution is obtained in quadratures. It is proved that with increasing time, it tends to stationary mode if the temperature on the lower wall stabilizes over time. The evolution of the behavior of the velocity field in the transformer oil-water system has been studied using the numerical inversion of the Laplace transform.

Keywords: Oberbeck-Boussinesq equations, interface, Marangoni number, thermocapillarity, inverse problem, Laplace transform.

Citation: Viktor K. Andreev, Thermocapillary Convection of Immiscible Liquid in a Three-dimensional Layer at Low Marangoni Numbers, *J. Sib. Fed. Univ. Math. Phys.*, 2024, 17(2), 195–206. EDN: FVESDY.



We consider the solution of the Oberbeck–Boussinesq equations of the form

$$\mathbf{u} = ((f(z, t) + h(z, t))x, (f(z, t) - h(z, t))y, -2 \int_0^z f(\xi, t) d\xi), \quad \bar{p} = \bar{p}(x, y, z, t), \quad (1)$$

$$\theta = a(z, t)x^2 + b(z, t)y^2 + q(z, t)$$

where \bar{p} is modified pressure.

The initial idea to search for exact solutions of the Navier-Stokes equations with a linear dependence of the velocity components on two spatial variables, apparently, was first proposed in [1]. It was shown that the general three-dimensional system of viscous magnetic hydrodynamics equations is reduced to a closed system of one-dimensional equations. A similar result for the

*andr@icm.krasn.ru

© Siberian Federal University. All rights reserved

gas dynamics equations was obtained in [2]. A more special case of the velocity field representation (1) for the motion of a single fluid is considered in [3, 4], and the pressure depended only on the vertical coordinate and time. The temperature is distributed according to the quadratic law (1) only at the free boundaries of the layer $z = \pm Z(t)$ and caused a thermocapillary effect. The numerical solution of the latter problem taking into account the general temperature distribution $\theta(x, y, z, t)$ in the layer $-Z(t) < z < Z(t)$ is carried out in the article [5]. A thorough review of the exact solutions of the Navier-Stokes system with a linear dependence of the velocity components on x and y is given in [6]. In [7], solution (1) was used to describe the slow convection of a single liquid in a layer with a free boundary. The paper [8] is devoted to the influence of interphase surface energy on stationary convection within the framework of solution (1). Unsteady creeping convection in the case of an isothermal interface for solution (1) was studied in the articles [9, 10]. The nonlinear stationary problem of two liquid media convection is numerically investigated in [11]. Note that similar two-dimensional problems (solution (1) can be called a three-dimensional analogue of the well-known Himenz solution) in various formulations are studied in the monograph [12].

In this paper, the quadratic dependence of x and y temperatures in (1) is an additional assumption and it agrees well with the conditions on the interface.

1. Statement of problem

Substituting the solution (1) into the system of convection equations and further compatibility analysis leads to the conclusion that the modified pressure in the layers is also a quadratic function of the coordinates x and y . Further, this solution is used to describe two-layer thermocapillary convection in the layer $-l_1 < z < l_2$, $|x| < \infty$, $|y| < \infty$. The boundaries of the layer $z = l_1$, $z = l_2$ are solid fixed walls, and $z = 0$ is a fixed interface between the layer $-l_1 < z < 0$, and the layer $0 < z < l_2$ of liquids "1", "2". These heat-conducting viscous liquids have constants: densities ρ_j , kinematic viscosities ν_j , thermal conductivity χ_j , thermal expansion coefficients β_j , $j = 1, 2$. At the interface $z = 0$, the surface tension depends linearly on temperature $\sigma(\theta_1) = \sigma_0 - \alpha\theta_1(x, y, 0, t)$ with constants σ_0 and $\alpha > 0$.

Remark 1. *In order for the interface to be flat, it is enough to assume the smallness of the Bond $Bo = g(\rho_1 - \rho_2)l_1^2/\sigma_0$ and the capillary $Ca = \mu_1\chi_1/\sigma_0l_1$ numbers, see [13].*

The unknowns, according to (1), are the functions $f_j(z, t)$, $h_j(z, t)$, $a_j(z, t)$, $b_j(z, t)$, $q_j(z, t)$, and $-l_1 \leq z \leq 0$ for $j = 1$, and $j = 2$ for $0 \leq z \leq l_2$. Suppose that the temperature is set on the substrate $z = -l_1$

$$\theta_1(x, y, -l_1, t) = \alpha_1(t)x^2 + \alpha_2(t)y^2 + \alpha_3(t) \quad (2)$$

with known functions $\alpha_i(t)$, $i = 1, 2, 3$, and the upper wall $z = l_2$ is thermally insulated: $\theta_{2z}(x, y, l_2, t) = 0$. For $\alpha_1(t) < 0$, $\alpha_2(t) < 0$, solution (1), (2) describes convection near the critical point $x = 0$, $y = 0$, when the temperature on the wall at this point has a maximum and with inverse values $\alpha_1(t)$, $\alpha_2(t)$ the temperature has a minimum.

Let $a^* = \max_{t \geq 0}(|\alpha_1(t)|, |\alpha_2(t)|)$, $\theta^* = \max_{t \geq 0}|\alpha_3(t)|$ is a characteristic temperature, so that a^*l_1 is a characteristic temperature gradient, $\tau = \chi_1 l_1^{-2} t$ is a characteristic thermal convection time.

For the first layer at $j = 1$ we put

$$\begin{aligned} \xi &= \frac{z}{l_1}, \quad -1 < \xi < 0, \quad f_1 = \frac{\chi_1}{l_1^2} M F_1(\xi, \tau), \quad h_1 = \frac{\chi_1}{l_1^2} M H_1(\xi, \tau), \\ a_1 &= a^* A_1(\xi, \tau), \quad b_1 = a^* B_1(\xi, \tau), \quad q_1 = \theta^* Q_1(\xi, \tau), \quad s_j = \frac{\chi_1^2}{l_1^4} M S_j(\tau), \\ M &= \frac{\varkappa_1 a^* l_1^3}{\mu_1 \chi_1}, \quad P_1 = \frac{\nu_1}{\chi_1}, \quad L_1 = \frac{\rho_1 \beta_1 g l_1^2}{\varkappa_1}, \quad d = \frac{a^* l_1^2}{\theta^*}, \end{aligned} \quad (3)$$

and for the second layer $j = 2$ we put

$$\begin{aligned} \xi &= \frac{z}{l_2}, \quad 0 < \xi < 1, \quad f_2 = \frac{\chi_1}{l_1^2} M F_2(\xi, \tau), \quad h_2 = \frac{\chi_1}{l_1^2} M H_2(\xi, \tau), \\ a_2 &= a^* A_2(\xi, \tau), \quad b_2 = a^* B_2(\xi, \tau), \quad q_2 = \theta^* Q_2(\xi, \tau), \quad s_i = \frac{\chi_1^2}{l_1^4} M S_k(\tau), \quad i = 3, 4, \\ P_2 &= \frac{\nu_2}{\chi_2}, \quad L_2 = \frac{\rho_1 \beta_2 g l_1 l_2}{\varkappa_1}, \quad \chi = \frac{\chi_1}{\chi_2}, \quad l = \frac{l_1}{l_2}, \quad \mu = \frac{\mu_1}{\mu_2}, \end{aligned} \quad (4)$$

where M is a Marangoni number, P_1, P_2 are the Prandtl numbers.

Suppose that $|M| \ll 1$ and we will look for a solution in the form

$$\begin{aligned} F_j &= F_j^{(0)} + M F_j^{(1)} + \dots, \quad H_j = H_j^{(0)} + M H_j^{(1)} + \dots, \\ A_j &= A_j^{(0)} + M A_j^{(1)} + \dots, \quad B_j = B_j^{(0)} + M B_j^{(1)} + \dots, \quad Q_j = Q_j^{(0)} + M Q_j^{(1)} + \dots, \\ S_i &= S_i^{(0)} + M S_i^{(1)} + \dots, \quad j = 1, 2, \quad i = \overline{1, 4}, \quad n = \overline{1, 3}. \end{aligned}$$

Assuming that $L_j = O(1)$ with $M \rightarrow 0$, we get a linear inverse problem in the zero approximation (index "0" is omitted)

$$\begin{aligned} F_{1\tau} &= P_1 F_{1\xi\xi} - P_1 L_1 \int_0^\xi (A_1(\xi, \tau) + B_1(\xi, \tau)) d\xi - S_1(\tau), \\ H_{1\tau} &= P_1 H_{1\xi\xi} - P_1 L_1 \int_0^\xi (A_1(\xi, \tau) - B_1(\xi, \tau)) d\xi - S_2(\tau), \\ A_{1\tau} &= A_{1\xi\xi}, \quad B_{1\tau} = B_{1\xi\xi}, \quad Q_{1\tau} = Q_{1\xi\xi} + 2d(A_1 + B_1), \quad -1 < \xi < 0, \quad \tau \in [0, \tau_0], \end{aligned} \quad (5)$$

$$\begin{aligned} F_{2\tau} &= \frac{P_2 l^2}{\chi} F_{2\xi\xi} - P_1 L_2 \int_0^\xi (A_2(\xi, \tau) + B_2(\xi, \tau)) d\xi - S_3(\tau), \\ H_{2\tau} &= \frac{P_2 l^2}{\chi} H_{2\xi\xi} - P_1 L_2 \int_0^\xi (A_2(\xi, \tau) - B_2(\xi, \tau)) d\xi - S_4(\tau), \\ A_{2\tau} &= \frac{l^2}{\chi} A_{2\xi\xi}, \quad B_{2\tau} = \frac{l^2}{\chi} B_{2\xi\xi}, \quad Q_{2\tau} = \frac{l^2}{\chi} Q_{2\xi\xi} + \frac{2d}{\chi} (A_2 + B_2), \quad 0 < \xi < 1, \quad \tau \in [0, \tau_0]. \end{aligned} \quad (6)$$

The boundary conditions on solid walls $\xi = -1, \xi = 1$ are ($\tau \in [0, \tau_0]$)

$$\begin{aligned} F_1(-1, \tau) &= H_1(-1, \tau) = 0, \quad A_1(-1, \tau) = \bar{\alpha}_1(\tau), \\ B_1(-1, \tau) &= \bar{\alpha}_2(\tau), \quad Q_1(-1, \tau) = \bar{\alpha}_3(\tau), \end{aligned} \quad (7)$$

$$F_2(1, \tau) = H_2(1, \tau) = 0, \quad A_{2\xi}(1, \tau) = B_{2\xi}(1, \tau) = Q_{2\xi}(1, \tau) = 0. \quad (8)$$

The conditions on interface are

$$\begin{aligned} F_1(0, \tau) &= F_2(0, \tau), \quad H_1(0, \tau) = H_2(0, \tau), \quad A_1(0, \tau) = A_2(0, \tau), \\ B_1(0, \tau) &= B_2(0, \tau), \quad Q_1(0, \tau) = Q_2(0, \tau), \\ l F_{2\xi}(0, \tau) - \mu F_{1\xi}(0, \tau) &= \mu(A_1(0, \tau) + B_1(0, \tau)), \\ l H_{2\xi}(0, \tau) - \mu H_{1\xi}(0, \tau) &= \mu(A_1(0, \tau) - B_1(0, \tau)), \\ l A_{2\xi}(0, \tau) - k A_{1\xi}(0, \tau) &= 0, \quad l B_{2\xi}(0, \tau) - k B_{1\xi}(0, \tau) = 0, \quad l Q_{2\xi}(0, \tau) - k Q_{1\xi}(0, \tau) = 0. \end{aligned} \quad (9)$$

In addition, the initial data are

$$\begin{aligned} F_j(\xi, 0) &= F_{0j}(\xi), & H_j(\xi, 0) &= H_{0j}(\xi), \\ A_j(\xi, 0) &= A_{0j}(\xi), & B_j(\xi, 0) &= B_{0j}(\xi), & Q_j(\xi, 0) &= Q_{0j}(\xi), \end{aligned} \quad (10)$$

where for $j = 1$ the variable $\xi \in (-1, 0)$, for $j = 2$ we have $\xi \in (0, 1)$; and the redefinition conditions

$$\int_{-1}^0 F_1(\xi, \tau) d\xi = \int_{-1}^0 H_1(\xi, \tau) d\xi = 0, \quad \int_0^1 F_2(\xi, \tau) d\xi = \int_0^1 H_2(\xi, \tau) d\xi = 0, \quad \tau \in [0, \tau_0]. \quad (11)$$

The equalities (11), meaning the closure of the flow, allow us to determine the unknown functions $S_i(\tau)$, $i = \overline{1, 4}$.

Functions $\bar{\alpha}_1(\tau) = \alpha_1(t)/a^*$, $\bar{\alpha}_2(\tau) = \alpha_2(t)/a^*$, $\bar{\alpha}_3(\tau)\alpha_3(t)/\theta^*$, $F_{0j}(\xi)$, $H_{0j}(\xi)$, $A_{0j}(\xi)$, $B_{0j}(\xi)$, $Q_{0j}(\xi)$ are defined on their definition domains. For a smooth solution, they must satisfy the compatibility conditions, for example,

$$F_{01}(-1) = H_{01}(-1) = 0, \quad F_{02}(1) = H_{02}(1) = 0, \quad F_{01}(0) = F_{02}(0), \quad H_{01}(0) = H_{02}(0) \text{ and so on.}$$

The modified pressures in the layers are determined by the formulas

$$\begin{aligned} \bar{p}_1 &= \frac{\rho_1 \nu_1 \chi_1}{l_1^2} M \Pi_1(\xi, \tau), \\ \Pi_1(\xi, \tau) &= \left[2L_1 \int_0^\xi A_1(\zeta, \tau) d\zeta + \frac{1}{P_1} (S_1(\tau) + S_2(\tau)) \right] \frac{\bar{x}^2}{2} + \left[2L_1 \int_0^\xi B_1(\zeta, \tau) d\zeta + \right. \\ &\quad \left. + \frac{1}{P_1} (S_1(\tau) - S_2(\tau)) \right] \frac{\bar{y}^2}{2} - \frac{2F_1}{P_1} + \frac{1}{P_1} \int_0^\xi (\xi - \zeta) F_{1\tau} d\zeta + \frac{L_1}{d} \int_0^\xi Q_1 d\zeta + \Pi_1(\tau), \\ \bar{p}_2 &= \frac{\rho_2 \nu_2 \chi_2}{l_2^2} M \Pi_2(\xi, \tau), \\ \Pi_2(\xi, \tau) &= \left[\frac{2\chi\nu L_2}{l^2} \int_0^\xi A_2 d\zeta + \frac{\chi^2}{l^2 P_2} (S_3(\tau) + S_4(\tau)) \right] \frac{\bar{x}^2}{2} + \left[\frac{2\chi\nu L_2}{l^2} \int_0^\xi B_2 d\zeta + \right. \\ &\quad \left. + \frac{\chi^2}{l^2 P_2} (S_3(\tau) - S_4(\tau)) \right] \frac{\bar{y}^2}{2} - \frac{2\chi F_2}{l^2} + \frac{2\chi^2}{l^4 P_2} \int_0^\xi (\xi - \zeta) F_{2\tau} d\zeta + \frac{\chi\nu L_2}{dl^2} \int_0^\xi Q_2 d\zeta + \Pi_2(\tau), \end{aligned}$$

where $\Pi_1(\tau)$, $\Pi_2(\tau)$ are arbitrary functions.

2. Stationary flow in layers

Let's find a stationary solution to the last problem $F_j^c(\xi)$, $H_j^c(\xi)$, $A_j^c(\xi)$, $B_j^c(\xi)$, $Q_j^c(\xi)$, $F_j^c(\xi)$, S_i^c ($j = 1, 2$; $i = \overline{1, 4}$). After some calculations, we get explicit expressions

$$\begin{aligned} A_1^c(\xi) &= \alpha_1^c, & B_1^c(\xi) &= \alpha_2^c, & Q_1^c(\xi) &= \alpha_3^c + d(\alpha_1^c + \alpha_2^c) \left[-\xi^2 + \frac{2\xi}{kl} + \frac{1}{3} \left(1 + \frac{2}{kl} \right) \right], \\ F_1^c(\xi) &= (\alpha_1^c + \alpha_2^c) \left[\left(\frac{3\xi^2}{4} + \xi + \frac{1}{4} \right) \gamma + L_1 \left(\frac{\xi^3}{6} + \frac{3\xi^2}{16} - \frac{1}{48} \right) \right], \\ H_1^c(\xi) &= (\alpha_1^c - \alpha_2^c) \left[\left(\frac{3\xi^2}{4} + \xi + \frac{1}{4} \right) \gamma + L_1 \left(\frac{\xi^3}{6} + \frac{3\xi^2}{16} - \frac{1}{48} \right) \right], \\ \gamma &= \frac{1}{\mu + l} \left(-\mu + \frac{lL_1}{12} + \frac{\nu}{12l} L_2 \right), \quad -1 \leq \xi \leq 0; \end{aligned} \quad (12)$$

$$\begin{aligned}
A_2^c(\xi) &= \alpha_1^c, & B_2^c(\xi) &= \alpha_2^c, & Q_2^c(\xi) &= \alpha_3^c + d(\alpha_1^c + \alpha_2^c) \left[\frac{2\xi - \xi^2}{l^2} + \frac{1}{3} \left(1 + \frac{2}{kl} \right) \right], \\
F_2^c(\xi) &= (\alpha_1^c + \alpha_2^c) \left[\left(\frac{3\xi^2}{4} - \xi + \frac{1}{4} \right) \gamma + \left(\frac{\xi^3}{6} - \frac{\xi^2}{4} + \frac{\xi}{12} \right) \frac{\nu L_2}{l^2} - \left(\frac{\xi^2}{16} - \frac{\xi}{12} + \frac{1}{48} \right) L_1 \right], \\
H_2^c(\xi) &= (\alpha_1^c - \alpha_2^c) \left[\left(\frac{3\xi^2}{4} - \xi + \frac{1}{4} \right) \gamma + \left(\frac{\xi^3}{6} - \frac{\xi^2}{4} + \frac{\xi}{12} \right) \frac{\nu L_2}{l^2} - \left(\frac{\xi^2}{16} - \frac{\xi}{12} + \frac{1}{48} \right) L_1 \right], \\
&0 \leq \xi \leq 1;
\end{aligned} \tag{13}$$

$$\begin{aligned}
S_1^c &= \frac{3P_1(\alpha_1^c + \alpha_2^c)}{2(\mu + l)} \left(-\mu + (4l + 3\mu)L_1 + \frac{\nu}{12l}L_2 \right), \\
S_2^c &= \frac{3P_1(\alpha_1^c - \alpha_2^c)}{2(\mu + l)} \left(-\mu + (4l + 3\mu)L_1 + \frac{\nu}{12l}L_2 \right), \\
S_3^c &= -\frac{3P_1l^2(\alpha_1^c + \alpha_2^c)}{2(\mu + l)} \left(\rho + \frac{\rho}{12}L_1 + \frac{(4\mu + 3l)}{12l^2}L_2 \right), \\
S_4^c &= -\frac{3P_1l^2(\alpha_1^c - \alpha_2^c)}{2(\mu + l)} \left(\rho + \frac{\rho}{12}L_1 + \frac{(4\mu + 3l)}{12l^2}L_2 \right).
\end{aligned} \tag{14}$$

The vertical velocities (dimensionless) are as follows

$$\begin{aligned}
W_1^c(\xi) &= -2 \int_0^\xi F_1^c(\zeta) d\zeta = -2(\alpha_1^c + \alpha_2^c) \left[\left(\frac{\xi^3}{4} + \frac{\xi^2}{2} + \frac{\xi}{4} \right) \gamma + \left(\frac{\xi^4}{24} + \frac{\xi^3}{16} - \frac{\xi}{48} \right) L_1 \right], \\
&-1 \leq \xi \leq 0, \\
W_2^c(\xi) &= -2 \int_0^\xi F_2^c(\zeta) d\zeta = -2(\alpha_1^c + \alpha_2^c) \left[\left(\frac{\xi^3}{4} - \frac{\xi^2}{2} + \frac{\xi}{4} \right) \gamma + \left(\frac{\xi^4}{24} - \frac{\xi^3}{12} + \frac{\xi^2}{24} \right) \frac{\nu L_2}{l^2} - \right. \\
&\left. - \left(\frac{\xi^3}{48} - \frac{\xi^2}{24} + \frac{\xi}{48} \right) L_1 \right], \quad 0 \leq \xi \leq 1,
\end{aligned} \tag{15}$$

Radial heating ($\alpha_1^c = \alpha_2^c$). When $H_1^c(\xi) = H_2^c(\xi) = 0$, $S_2^c = S_4^c = 0$ and the flow becomes axisymmetric. It is convenient to consider it in cylindrical coordinates (dimensionless) r, φ, ξ : $\mathbf{u}_j^c = (F_j^c(\xi)r, 0, W_j^c(\xi))$. Current functions $\Psi_j(r, \xi) : F_j^c(\xi)r = \frac{1}{r}\Psi_{j\xi}(r, \xi)$, $W_j^c(\xi) = -\frac{1}{r}\Psi_{jr}(r, \xi)$ and the mass conservation equation is fulfilled, so $\Psi_j(r, \xi) = r^2W_j^c(\xi)$.

Remark 2. For $\alpha_1 = -\alpha_2$ we have $F_1^c(\xi) = 0$, $F_2^c(\xi) = 0$, $W_1^c(\xi) = 0$, $W_2^c(\xi) = 0$ and the current will be plane parallel.

Figs. 1–3 show the results of calculations of velocity fields for the transformer oil ($j = 1$)-water ($j = 2$) [15] system. Moreover, with $l_1 = l_2 = 5$ mm, $g = 9.8$ m/c² we have $L_1 = 0.6$, $L_2 = 2.3$ and $M = 0.065a^*$. Fig. 1 shows the profile of the dimensionless vertical velocity component $W^c(\xi)$ (a) and velocity field in layers (b) at $\alpha_1^c = \alpha_2^c = 1^\circ\text{C}/\text{m}^2$, $l_1 = l_2 = 5$ mm, $g = 9.8$ m/c². It can be seen that in the first layer the flow is directed in the opposite direction of the z axis (ξ), and in the second layer the flow is directed in the direction of the z axis, as shown in Fig. 1b. A similar situation will occur for any case. Therefore, the results of calculations will be given below only for the vertical velocity component, since it gives an idea of the formed flows in the layers.

In Fig. 2 and the profiles of the dimensionless vertical velocity component $W^c(\xi)$ are given depending on α_2^c . If $\alpha_1^c + \alpha_2^c > 0$, then a return flow occurs in the first layer (the liquid moves

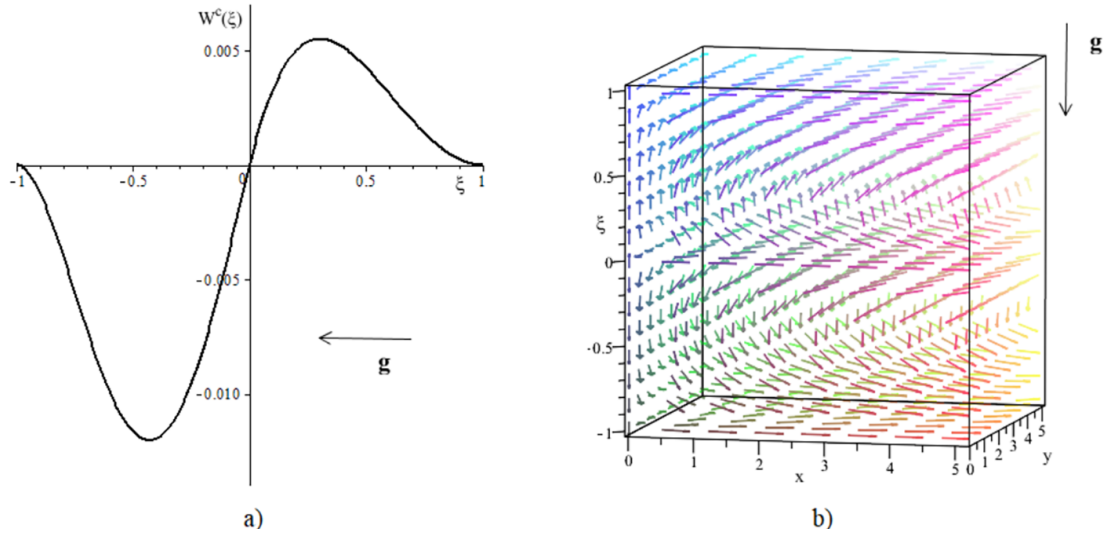


Fig. 1. Dimensionless vertical velocity component $W^c(\xi)$ (a) and the velocity field (b) at $\alpha_1^c = \alpha_2^c = 1$, $l_1 = l_2 = 5$ mm, $g = 9.8\text{M}/c^2$, $a^* = 1^\circ\text{C}/\text{M}^2$

in the opposite direction of the z axis), and in the second layer the flow is directed along the z axis. If $\alpha_1^c + \alpha_2^c < 0$, then the direction of currents in the layers changes to the opposite.

In Fig. 2b shows the profiles of the dimensionless vertical component of the velocity $W^c(\xi)$ depending on the acceleration of gravity g . It can be seen that gravity affects only the intensity of the flow. Moreover, in the first layer, the intensity increases with the growth of g , and in the second it decreases. So $\max_{\xi \in [-1,0]} |W^c(\xi, g = 0)| = 0.007$, $\max_{\xi \in [-1,0]} |W^c(\xi, g = 9.8)| = 0.012$ и $\max_{\xi \in [0,1]} |W^c(\xi, g = 0)| = 0.007$, $\max_{\xi \in [0,1]} |W^c(\xi, g = 9.8)| = 0.005$.

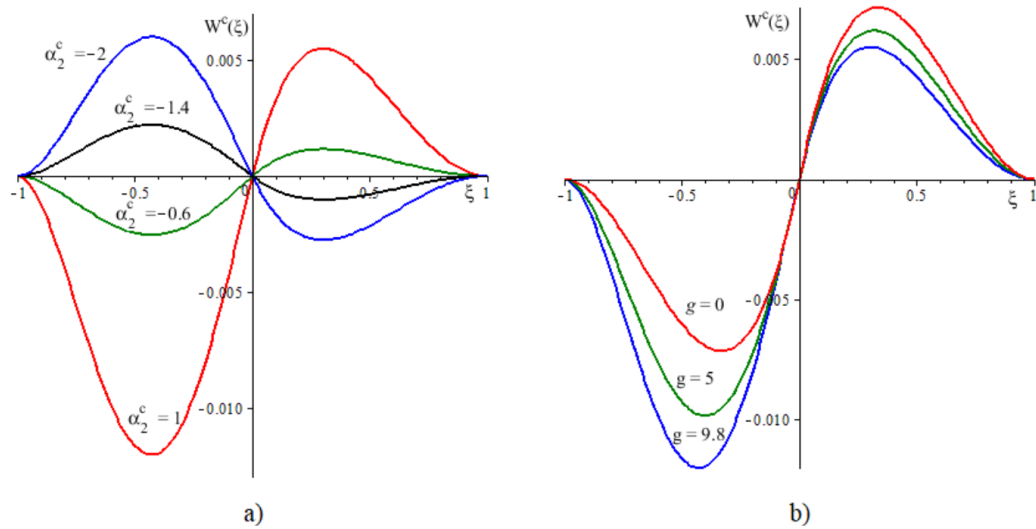


Fig. 2. Dimensionless vertical velocity component $W^c(\xi)$ depending on α_2^c (a) ($\alpha_1^c = 1$, $g = 9.8\text{M}/c^2$) and gravity acceleration g (b) ($\alpha_1^c = \alpha_2^c = 1$) at $l_1 = l_2 = 5$ mm

Fig. 3a shows the profiles of the dimensionless vertical velocity component $W^c(\xi)$ depending on the thickness of the first layer l_1 . It can be seen that with a decrease in l_1 , the flow in the first layer remains recurrent (only the intensity changes), and in the second layer, at $l_1 < 0.1$ mm, the flow becomes two-vortex (a return flow occurs near a solid wall). At $l_1 < 10^{-6}$ mm, the flow in the second layer becomes completely reversible.

Fig. 3b shows the profiles of the dimensionless vertical velocity component $W^c(\xi)$ depending on the thickness of the second layer l_2 . It can be seen that with a decrease in l_2 , the intensity of flows in the layers decreases. So $\max_{\xi \in [-1,0]} |W^c(\xi, l_2 = 5)| - \max_{\xi \in [-1,0]} |W^c(\xi, l_2 = 0.03)| = \max_{\xi \in [0,1]} |W^c(\xi, l_2 = 5)| - \max_{\xi \in [0,1]} |W^c(\xi, l_2 = 0.03)| \approx 0.006$.

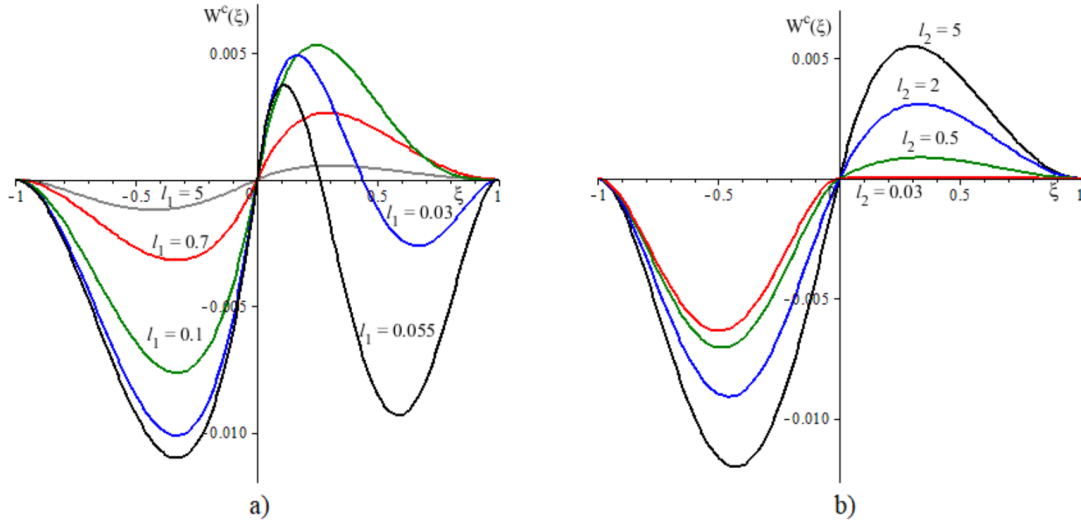


Fig. 3. Dimensionless vertical velocity component $W^c(\xi)$ depending on l_1 ($l_2 = 5$ mm)(a) and l_2 ($l_1 = 5$ mm) (b) at $\alpha_1 = \alpha_2 = 0.1$, $g = 9.8M/c^2$

Fig. 4 shows a dimensionless temperature field in layers at $\alpha_1 = \alpha_2$ (radial heating). In this case, the temperature at the point $x = 0$, $y = 0$ is minimal. The surface tension decreases in the direction of the axes x , y and the flow on the interface is directed in the direction opposite to the direction of the axes x , y (Fig. 4b).

2. Unsteady convection in layers

The inverse problem (6)–(11) in Laplace images is solved in quadratures, which allows us to obtain quantitative information about the solution. Let $U(\xi, \tau)$ be the original, $\tau \in [0, \infty)$, $\xi \in [-1, 0]$ (or $\xi \in [0, 1]$), its Laplace transform (image) is integral

$$\hat{U}(\xi, s) = \int_0^\infty U(\xi, \tau) e^{-s\tau} d\tau.$$

The definition and properties of the Laplace transform are described in many manuals, see for example [14]. It is applicable to a wide class of functions, in particular, having a finite number of discontinuity points of the first kind with respect to the variable τ .

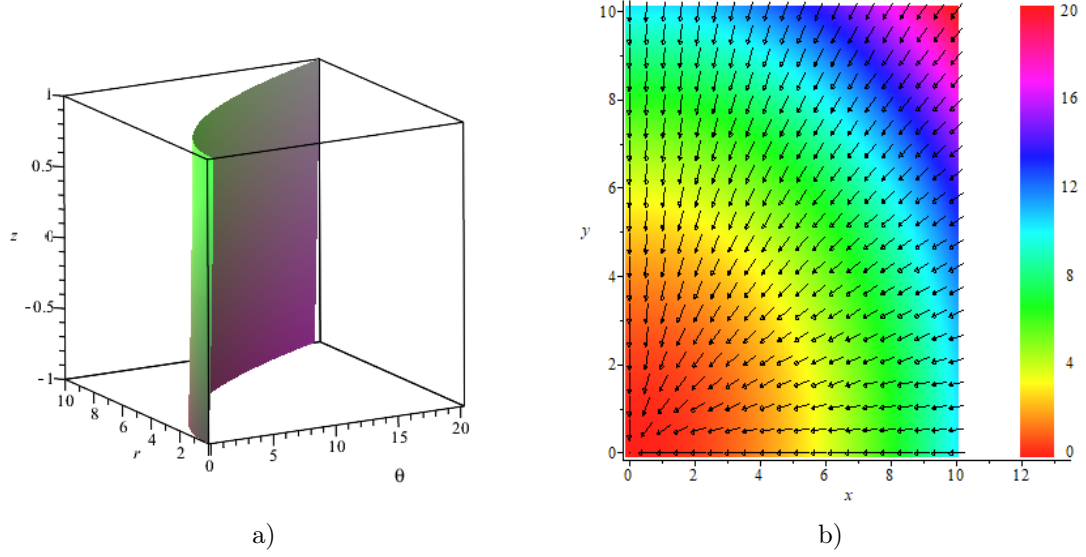


Fig. 4. The dimensionless temperature field θ in coordinates r, z in layers (a) and the temperature distribution on the interface $z = 0$ (b) at $\alpha_1^c = \alpha_2^c = 1$, $g = 9.8 \text{ m/c}^2$

The problem for $A_j(\xi, \tau)$ in Laplace images will be written like this

$$\begin{aligned} \hat{A}_{1\xi\xi} - s\hat{A}_1 &= -A_{01}(\xi), \quad \xi \in [-1, 0], \\ \hat{A}_{2\xi\xi} - \frac{\chi}{l^2}s\hat{A}_2 &= -\frac{\chi}{l^2}A_{02}(\xi), \quad \xi \in [0, 1], \\ \hat{A}_1(0, s) &= \hat{A}_2(0, s), \quad l\hat{A}_{2\xi}(0, s) - k\hat{A}_{1\xi}(0, s) = 0, \\ \hat{A}_1(-1, s) &= \hat{\alpha}_1(s), \quad \hat{A}_{2\xi}(1, s) = 0. \end{aligned}$$

The solution of this boundary value problem is written out without difficulty

$$\begin{aligned} \hat{A}_1(\xi, s) &= \frac{1}{\Delta} \left[\left(\hat{\alpha}_1(s) + \frac{1}{\sqrt{s}} \int_{-1}^0 A_{01}(\xi) \text{sh} \sqrt{s}(1 + \xi) d\xi \right) \left(\text{ch} \sqrt{\frac{s\chi}{l^2}} \text{ch} \sqrt{s}\xi - \right. \right. \\ &\quad \left. \left. - \frac{\sqrt{\chi}}{k} \text{sh} \sqrt{\frac{s\chi}{l^2}} \text{sh} \sqrt{s}\xi \right) - \frac{\chi}{kl\sqrt{s}} \text{sh}[\sqrt{s}(1 + \xi)] \int_0^1 A_{02}(\xi) \text{ch} \sqrt{\frac{s\chi}{l^2}}(1 - \xi) d\xi \right] - \\ &\quad - \frac{1}{\sqrt{s}} \int_0^\xi A_{01}(\zeta) \text{sh} \sqrt{s}(\xi - \zeta) d\zeta, \\ \hat{A}_2(\xi, s) &= \frac{1}{\Delta} \left[\left(\hat{\alpha}_1(s) + \frac{1}{\sqrt{s}} \int_{-1}^0 A_{01}(\xi) \text{sh} \sqrt{s}(1 + \xi) d\xi \right) \text{ch} \sqrt{\frac{s\chi}{l^2}}(\xi - 1) + \right. \\ &\quad \left. + \sqrt{\frac{\chi}{l^2s}} \left(\text{sh} \sqrt{\frac{s\chi}{l^2}} \xi \text{ch} \sqrt{s} + \frac{\sqrt{\chi}}{k} \text{sh} \sqrt{s} \text{ch} \sqrt{\frac{s\chi}{l^2}} \xi \right) \int_0^1 A_{02}(\xi) \text{ch} \sqrt{\frac{s\chi}{l^2}}(1 - \xi) d\xi \right] - \\ &\quad - \sqrt{\frac{\chi}{l^2s}} \int_0^\xi A_{02}(\zeta) \text{sh} \sqrt{\frac{s\chi}{l^2}}(\xi - \zeta) d\zeta, \\ \Delta &= \text{ch} \sqrt{\frac{s\chi}{l^2}} \text{ch} \sqrt{s} + \frac{\sqrt{\chi}}{k} \text{sh} \sqrt{\frac{s\chi}{l^2}} \text{sh} \sqrt{s}. \end{aligned} \quad (16)$$

The Laplace transform $\hat{B}_1(\xi, s)$, $\hat{B}_2(\xi, s)$ is defined by the formulas (16) with the replacement of $\hat{\alpha}_1(s)$ and $A_{0j}(\xi)$ by $\hat{\alpha}_2(s)$ and $B_{0j}(\xi)$, $j = 1, 2$ respectively. As for the functions $\hat{Q}_j(\xi, s)$, they

are from (16) with the replacement of $A_{01}(\xi)$ and $A_{02}(\xi)$ by $Q_{01}(\xi) - 2d(\hat{A}_1(\xi, s) + \hat{B}_1(\xi, s))$ and $[\chi Q_{20}(\xi) - 2d(\hat{A}_2(\xi, s) + \hat{B}_2(\xi, s))]/l^2$ respectively.

Inverse problem for functions $\hat{F}_j(\xi, s)$, $\hat{S}_1(s)$, $\hat{S}_2(s)$ has the form

$$\begin{aligned} \hat{F}_{1\xi\xi} - \frac{s}{P_1}\hat{F}_1 &= \frac{1}{P_1}\hat{S}_1(s) + L_1\hat{\Psi}_1(\xi, s) - \frac{1}{P_1}F_{01}(\xi), \quad \xi \in [-1, 0], \\ \hat{F}_{2\xi\xi} - \frac{s\chi}{P_2l^2}\hat{F}_2 &= \frac{\chi}{P_2l^2}\hat{S}_3(s) + \frac{\nu}{l^2}L_2\hat{\Psi}_2(\xi, s) - \frac{\chi}{P_2l^2}F_{02}(\xi), \quad \xi \in [0, 1], \\ \hat{F}_1(-1, s) &= 0, \quad \hat{F}_2(1, s) = 0, \quad \hat{F}_1(0, s) = \hat{F}_2(0, s), \\ \mu\hat{F}_{1\xi}(0, s) - l\hat{F}_{2\xi}(0, s) &= -\mu\hat{\Psi}_1\xi(0, s), \\ \int_{-1}^0 \hat{F}_1(\xi, s) d\xi &= 0, \quad \int_0^1 \hat{F}_2(\xi, s) d\xi = 0, \end{aligned} \quad (17)$$

where the functions $\hat{\Psi}_j$ are given by formulas $\hat{\Psi}_j = \int_0^\xi (\hat{A}_j(\xi, s) + \hat{B}_j(\xi, s)) d\xi$ with already known $\hat{A}_j, \hat{B}_j, j = 1, 2$. After some transformations, we find a solution to the problem (17):

$$\begin{aligned} \hat{F}_1(\xi, s) &= -\frac{\hat{S}_1}{s} + D_1 \operatorname{sh} \sqrt{\frac{s}{P_1}} \xi + D_2 \operatorname{ch} \sqrt{\frac{s}{P_1}} \xi + \\ &+ \sqrt{\frac{P_1}{s}} \int_0^\xi \left[L_1 \hat{\Psi}_1(\zeta, s) - \frac{1}{P_1} F_{01}(\zeta) \right] \operatorname{sh} \sqrt{\frac{s}{P_1}} (\xi - \zeta) d\zeta, \quad \xi \in [-1, 0], \\ \hat{F}_2(\xi, s) &= -\frac{\hat{S}_3}{s} + D_3 \operatorname{sh} \beta \xi + D_4 \operatorname{ch} \beta \xi + \frac{1}{\beta} \int_0^\xi \left[\frac{\nu}{l^2} L_2 \hat{\Psi}_2(\zeta, s) - \frac{\chi}{P_2 l^2} F_{02}(\zeta) \right] \operatorname{sh} \beta (\xi - \zeta) d\zeta, \\ \xi \in [0, 1], \quad \beta &= \sqrt{\frac{\chi s}{P_2 l^2}}, \end{aligned} \quad (18)$$

$$\begin{aligned} \hat{S}_1 &= -sD_1 \operatorname{sh} \sqrt{\frac{s}{P_1}} + sD_2 \operatorname{ch} \sqrt{\frac{s}{P_1}} + \sqrt{P_1 s} \int_{-1}^0 \left[L_1 \hat{\Psi}_1(\xi, s) - \frac{1}{P_1} F_{01}(\xi) \right] \operatorname{sh} \sqrt{\frac{s}{P_1}} (1 + \xi) d\xi, \\ \hat{S}_3 &= sD_3 \operatorname{sh} \beta + sD_4 \operatorname{ch} \beta + \frac{s}{\beta} \int_0^1 \left[\frac{\nu}{l^2} L_2 \hat{\Psi}_2(\xi, s) - \frac{\chi}{P_2 l^2} F_{02}(\xi) \right] \operatorname{sh} \beta (1 - \xi) d\xi. \end{aligned} \quad (19)$$

The values $D_i(s), i = \overline{1, 4}$ are determined from the boundary conditions (7)–(9), (11), they have a bulky appearance and are not listed here.

The solution of the inverse problem for $\hat{H}_1, \hat{H}_2, \hat{S}_2, \hat{S}_4$ is determined by the formulas (18), (19) with obvious substitutions of $F_{01}(\xi), F_{02}(\xi)$ and $\hat{\Psi}_1, \hat{\Psi}_2$ by $H_{01}(\xi), H_{02}(\xi)$ and $\hat{\Psi}_3 = \int_0^\xi (\hat{A}_1(\xi, s) - \hat{B}_1(\xi, s)) d\xi, \hat{\Psi}_4 = \int_0^\xi (\hat{A}_2(\xi, s) - \hat{B}_2(\xi, s)) d\xi$ respectively.

Let there be limits $\lim_{\tau \rightarrow \infty} \bar{\alpha}_j(\tau) = \alpha_j^c, j = 1, 2, 3$. Then [9] $\lim_{s \rightarrow 0} s\hat{\alpha}_j(s) = \alpha_j^c$. Using the asymptotic equalities $\operatorname{sh} x = x + x^3/3 + O(x^5), \operatorname{ch} x = 1 + x^2/2 + O(x^4), x \rightarrow 0$ and the obtained formulas (16), (18), (19), it can be proved that

$$\begin{aligned} \lim_{\tau \rightarrow \infty} A_j(\xi, \tau) &= \lim_{s \rightarrow 0} s\hat{A}_j(\xi, s) = \alpha_1^c, \quad \lim_{\tau \rightarrow \infty} B_j(\xi, \tau) = \lim_{s \rightarrow 0} s\hat{B}_j(\xi, s) = \alpha_2^c, \\ \lim_{\tau \rightarrow \infty} F_j(\xi, \tau) &= \lim_{s \rightarrow 0} s\hat{F}_j(\xi, s) = F_j^c(\xi), \quad \lim_{\tau \rightarrow \infty} H_j(\xi, \tau) = \lim_{s \rightarrow 0} s\hat{H}_j(\xi, s) = H_j^c(\xi), \\ \lim_{\tau \rightarrow \infty} Q_j(\xi, \tau) &= \lim_{s \rightarrow 0} s\hat{Q}_j(\xi, s) = Q_j^c(\xi), \quad \lim_{\tau \rightarrow \infty} S_i(\tau) = \lim_{s \rightarrow 0} s\hat{S}_i(s) = S_i^c, \quad j = 1, 2, \quad i = \overline{1, 4}, \end{aligned}$$

which confirms the theoretical conclusions.

Fig. 5 shows, for example, dimensionless velocity profiles $W(\xi, \tau)$ (Fig. 5a) for the case when

$$\bar{\alpha}_1(\tau) = \bar{\alpha}_2(\tau) = \begin{cases} \varepsilon_1 \sin \varepsilon_2 \tau & \text{при } 0 \leq \tau \leq \tau_1; \\ \alpha_1^c + e^{-\varepsilon_3 \tau} & \text{при } \tau > \tau_1 \end{cases}$$

and $\varepsilon_1 = 1.5$, $\varepsilon_2 = 0.1$, $\varepsilon_3 = 0.02$, $\tau_1 = 68$. At $0 < \tau \leq 68$, the temperature gradients on the lower wall change their sign, and at $\tau > 68$ they reach a constant value of $\alpha_1^c = \alpha_2^c = 1$ (Fig. 5 b). With $\tau = 20$, the real time is $t \approx 3500$ with.

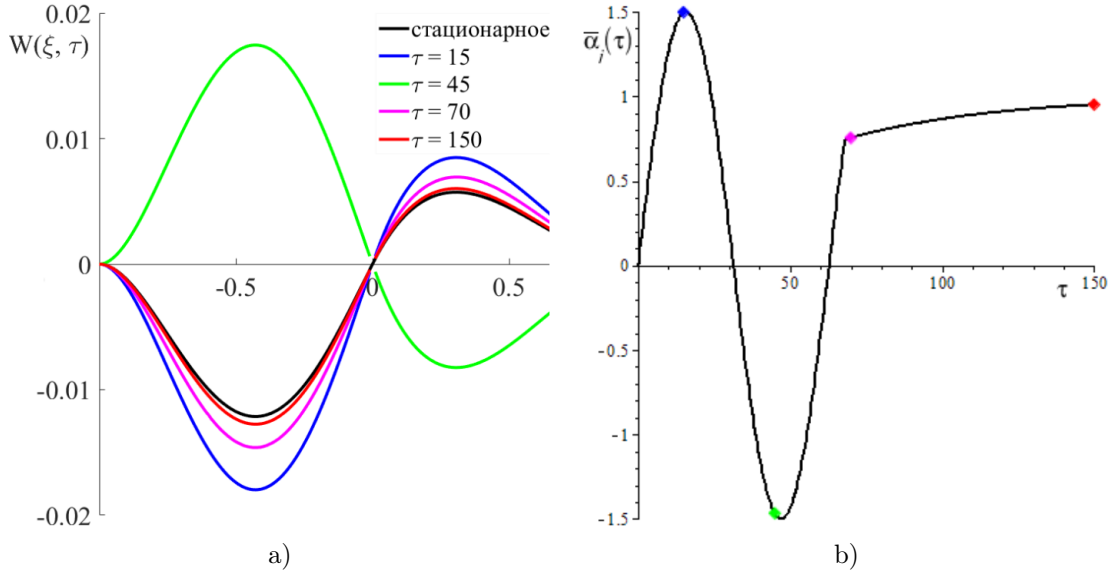


Fig. 5. Vertical component of the velocity vector $W(\xi, \tau)$ (a) and temperature gradients $\bar{\alpha}_j(\tau)$ (b)

Conclusion

A linear model describing slow two-layer convection in a 3D layer is constructed. It takes into account both the influence of thermocapillary forces and the change in buoyancy forces in the layers. From a mathematical point of view, the resulting initial-boundary value problem is the inverse. Its stationary solution has been found, which makes it possible to trace the influence of dimensionless parameters on the structure of flows in layers. The solution of the non-stationary problem is obtained in Laplace images in the form of quadratures. It is proved that if the set temperature on the lower wall stabilizes with time, then the non-stationary solution goes to a stationary mode with increasing time. Which means its stability.

This work is supported by the Krasnoyarsk Mathematical Center and financed by the Ministry of Science and Higher Education of the Russian Federation in the framework of the establishment and development of regional Centers for Mathematics Research and Education (Agreement No. 075-02-2023-912).

References

- [1] C.C.Lin, Note on a class of exact solutions in magnetohydrodynamics, *Arch. Rational Mech. Anal.*, **1**(1958), 391–395.

-
- [2] A.F.Sidorov, On two classes of solutions of equations of fluid and gas mechanics and their connection with the theory of traveling waves, *Applied Mechanics and Technical Physics*, (1989), no. 2, 34–40.
- [3] V.V.Pukhnachev, Model of viscous layer deformation by thermocapillary forces, *Eur. Journal Appl. Math.*, **13**(2002), no. 2, 205–224. DOI: 10.1017/S0956792501004776
- [4] V.K.Andreev, Yu.A.Gaponenko, O.N.Goncharova, V.V.Pukhnachev, *Mathematical Models of Convection*, Berlin/Boston: De Gruyter, 2020.
- [5] E.V.Rezanova, Numerical modelling of heat transfer in the layer of viscous incompressible liquid with free boundaries, *EPJ Web of Conference*, (2017), no. 159, 00047. DOI: 10.1051/epjconf/201715900047
- [6] S.N.Aristov, D.V.Knyazev, A.D.Polyanin, Exact solutions of the Navier-Stokes equations with linear dependence of the velocity components on two spatial variables, *Theoretical Foundations of Chemical Engineering*, **43**(2009), no. 5, 547–566. DOI:10.1134/S0040579509050066
- [7] A.A.Azanov, V.K.Andreev, Solving the problem of the creeping motion of a fluid with a free boundary with a special velocity field in a three-dimensional strip, Some actual problems of modern mathematics and mathematical education. Herzen Readings — 2021. Materials of the scientific conference. St. Petersburg: Publishing House of the A.I. Herzen State Pedagogical University. Publishing House of the VVM, 2021, 42–54.
- [8] V.K.Andreev, E.N.Lemeshkova, Two-layer steady creeping thermocapillary flow in a three-dimensional channel, *Journal of Applied Mechanics and Technical Physics*, **63**(2022), no. 1, 82–88. DOI:10.1134/S0021894422010138
- [9] V.K.Andreev, On a creeping 3D Convective Motion of Fluids with an Isothermal Interface, *Journal of Siberian Federal University. Mathematics & Physics*, **13**(2020), no. 6, 661–669. DOI: 10.17516/1997-1397-2020-13-6-661-669
- [10] V.K.Andreev, The solution of three-dimensional equations of thermal convection and its interpretation, Some actual problems of modern mathematics and mathematical education. Herzen Readings — 2020. Materials of the scientific conference. St. Petersburg: Publishing House of the A. I. Herzen State Pedagogical University, VVM, 2021, 4–8.
- [11] V.K.Andreev, E.N.Lemeshkova, Thermal convection of two immiscible liquids in a three-dimensional channel with a velocity field of a special type, *PMM*, **87**(2023), no. 2, 200–210 (in Russian). DOI: 10.31857/S0032823523020029
- [12] V.K.Andreev, E.N.Lemeshkova, *Linear problems of convective motions with interface surfaces*, Krasnoyarsk: Sib. Fed. Univ, 2018.
- [13] R.H.Zeitunyan, The problem of thermocapillary instability of Benara-Marangoni, *UFN*, **168**(1998), 259–286 (in Russian). DOI: 10.3367/UFNr.0168.199803b.0259
- [14] M.A.Lavrentiev, B.V.Shabat, *Methods of the theory of functions of a complex variable*, Moscow, Nauka, 1973.
- [15] N.B.Vargaftik, *Handbook of Thermophysical Properties of Gases and Liquids*, Nauka, 1972.

Термокапиллярная конвекция несмешивающихся жидкостей в трехмерном слое при малых числах Марангони

Виктор К. Андреев

Институт вычислительного моделирования СО РАН
Красноярск, Российская Федерация

Аннотация. Изучается совместная конвекция двух вязких теплопроводных жидкостей в трёхмерном слое, ограниченном твердыми плоскими стенками. Верхняя стенка теплоизолирована, а на нижней стенке задано нестационарное поле температур. Жидкости предполагаются несмешивающимися, и на плоской границе раздела между ними заданы сложные условия сопряжения. Эволюция этой системы описывается уравнениями Обербека-Буссинеска в каждой жидкости. Решение указанной задачи ищется в классе полей скоростей, линейных по двум координатам, а поля температур — квадратичные функции тех же координат. В этом случае задача редуцируется к системе 10-ти нелинейных интегродифференциальных уравнений. Она является сопряженной и обратной относительно 4-х функций времени. Для их нахождения ставятся интегральные условия переопределения, имеющие ясный физический смысл — замкнутость потока. Поставленная обратная начально-краевая задача описывает конвекцию в двухслойной системе, возникающую вблизи точки экстремума температуры на нижней твердой стенке. При малых числах Марангони задача аппроксимируется линейной (число Марангони играет роль числа Рейнольдса для уравнений Навье-Стокса). Найдено стационарное решение этой задачи. Линейная нестационарная задача решена методом преобразования Лапласа, причем температура может иметь разрывы 1-го рода — изменяться скачком. В образах по Лапласу решение получено в квадратурах. Доказано, что с ростом времени оно выходит на стационарный режим, если температура на нижней стенке стабилизируется со временем. С помощью численного обращения преобразования Лапласа изучена эволюция поведения поля скоростей в системе трансформаторное масло – вода.

Ключевые слова: уравнения Обербека-Буссинеска, поверхность раздела, число Марангони, термокапиллярность, обратная задача, преобразование Лапласа.

EDN: GTRJTD

УДК 532.5.013.3

On One Exact Solution of an Evaporative Convection Problem with the Dirichlet Boundary Conditions

Victoria B. Bekezhanova*

Institute of Computational Modelling SB RAS

Krasnoyarsk, Russian Federation

Olga N. Goncharova†

Altai State University

Barnaul, Russian Federation

Received 16.10.2023, received in revised form 07.12.2023, accepted 08.01.2024

Abstract. Characteristics of steady-state convective flows of a liquid and a co-current gas flux under the conditions of inhomogeneous evaporation of the diffusive type in a flat horizontal channel are studied. A partially-invariant exact solution of equations of the thermosolutal convection is used to describe the flows within the framework of the Oberbeck–Boussinesq approximation. It is derived as the solution of the evaporative convection problem with the Dirichlet boundary conditions on the outer channel walls. The influence of the external thermal load on the structure of the velocity and temperature fields, evaporation mass flow rate and vapor content in the gas layer was investigated in the HFE-7100–nitrogen system.

Keywords: mathematical model, boundary-value problem, exact solution, evaporative convection.

Citation: V.B. Bekezhanov, O.N. Goncharova, On One Exact Solution of an Evaporative Convection Problem with the Dirichlet Boundary Conditions, *J. Sib. Fed. Univ. Math. Phys.*, 2024, 17(2), 207–219. EDN: GTRJTD.



Introduction

Traditional approach to describe the evaporative convection in two-phase systems is based on the use of the Navier–Stokes equations (or their approximations) supplemented by the heat transfer and molecular transport equations [1]. The set of governing relations for determining kinematic, temperature and concentration characteristics presents the thermosolutal convection equations. Due to the group properties the system of equation admits a partially invariant solution belonging to the Birikh class [2, 3]. Such type of solutions can be used for describing the evaporative convection in a bilayer liquid–gas system with a sharp interface in plane channels with solid impermeable walls in the frame of the two-sided approach [1]. Various well-posed statements of the boundary value problems for the thermosolutal convection equations were analysed [4, 5]. It was shown that the use of the Dirichlet boundary conditions for all the required functions on the external boundaries of the flow domain allows one to derive the informative Birikh type exact solution. It correctly takes into account the impact of the thermocapillary and thermodiffusion effects, non-uniform character of diffusion-limited evaporation on the phase

*vbek@icm.krasn.ru <https://orcid.org/0000-0003-2068-6364>

†gon@math.asu.ru <https://orcid.org/0000-0002-9876-4177>

© Siberian Federal University. All rights reserved

boundary as well as the influence of the thermal load applied on the channel walls. It should be noted that non-constant evaporation rate along the liquid surface was fixed in physical experiments [6]. In the present paper, the mentioned above solution of the Dirichlet problem is used to study characteristics of gas sheared liquid flows in a horizontal channel under various intensity of the external thermal load. Applicability conditions of the exact solution to model steady-state convective flows of a liquid and a co-current gas flux are specified.

1. Statement of the problem and anzatz of solution

Let us consider the combined convection in a system of two viscous heat-conducting incompressible fluids (liquid and gas-vapour mixture) in a flat horizontal mini-channel with solid impermeable walls $y = -l$ and $y = h$ (Fig. 1). The two-phase system is in the terrestrial conditions with the vector of the gravity force acceleration $\mathbf{g} = (0, -g)$, $g = 9.81 \text{ m/s}^2$. Basic characteristics of this system are the velocity \mathbf{v}_i , temperature T_i , pressure p_i of both media, and vapour concentration C in the gas. Here and below, the subscript or superscript $i = 1$ and $i = 2$ corresponds to the characteristics of the fluids in the lower and upper layers, respectively.

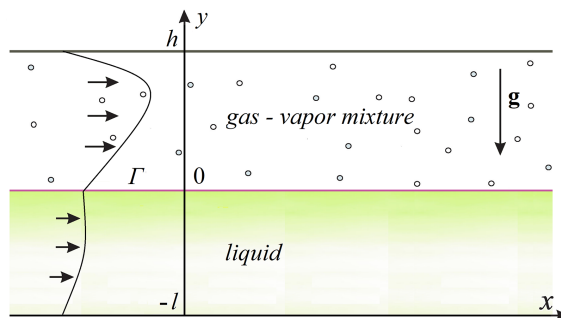


Fig. 1. The sketch of a two-phase system in the Cartesian coordinates

When posing the problem, the following assumptions are supposed to be satisfied.

(i) Surface between the liquid and gas phases is the thermocapillary interface Γ enabling the mass transfer due to evaporation/condensation. Only diffusive type evaporation occurs, and convective mass transfer through Γ is not considered. Here, the surface remains in the non-deformed state $y = 0$. The tangential forces, induced by the thermocapillary effect and shear stresses due to the gas pumping, act on Γ . The surface tension of the phase boundary is specified by the function $\sigma = \sigma_0 - \sigma_T(T - T_0)$, where σ_0 , T_0 are the characteristic values of the surface tension and liquid temperature, respectively, σ_T is the temperature coefficient of surface tension.

(ii) The liquid volatilizes across the interface at a rate M so that the mixture of the carrier gas and liquid vapour fills the upper layer. Vapour is considered as a passive admixture. The Soret and Dufour effects appear in the gas phase due to presence of the volatile component.

(iii) The reference values T_0 , p_0 , C_0 characterize the thermodynamic equilibrium state of the two-phase system. The ground state of the system described by the above-mentioned basic functions is close to the thermodynamic equilibrium state or slightly deviates from it, i.e., convection under the Boussinesq conditions is considered.

(iv) Thermal load distributed according to the linear law with respect to the longitudinal coordinate is applied on channel walls.

Basic factors governing regimes of convective flows in the strip confined by fixed walls are the buoyancy force, the Marangoni effect, gas pumping and linear heating of the outer boundaries. To describe the stationary flows of each medium the Navier – Stokes equations in the Oberbeck – Boussinesq approximation are used:

$$\begin{aligned} \frac{\partial u}{\partial x} + \frac{\partial v}{\partial y} &= 0, & u \frac{\partial u}{\partial x} + v \frac{\partial u}{\partial y} &= -\frac{1}{\rho_0} \frac{\partial p}{\partial x} + \nu \left(\frac{\partial^2 u}{\partial x^2} + \frac{\partial^2 u}{\partial y^2} \right), \\ u \frac{\partial v}{\partial x} + v \frac{\partial v}{\partial y} &= -\frac{1}{\rho_0} \frac{\partial p}{\partial y} + \nu \left(\frac{\partial^2 v}{\partial x^2} + \frac{\partial^2 v}{\partial y^2} \right) + g(\beta T + \gamma C), \\ u \frac{\partial T}{\partial x} + v \frac{\partial T}{\partial y} &= \chi \left(\frac{\partial^2 T}{\partial x^2} + \frac{\partial^2 T}{\partial y^2} + \delta \left(\frac{\partial^2 C}{\partial x^2} + \frac{\partial^2 C}{\partial y^2} \right) \right). \end{aligned} \quad (1.1)$$

The vapour transfer in the background gas is governed by the convection-diffusion equation [7]:

$$u \frac{\partial C}{\partial x} + v \frac{\partial C}{\partial y} = D \left(\frac{\partial^2 C}{\partial x^2} + \frac{\partial^2 C}{\partial y^2} + \alpha \left(\frac{\partial^2 T}{\partial x^2} + \frac{\partial^2 T}{\partial y^2} \right) \right). \quad (1.2)$$

Terms γC and $\delta \Delta C$ in the momentum and energy transport equations, respectively, as well as equation (1.2) are taken into account to model the flow in the upper gas layer only. The following notations are used: u, v are the projections of the velocity vector \mathbf{v} on the Ox and Oy axes, p is the modified pressure, ρ_0 is the average fluid density, ν is the coefficient of kinematic viscosity, β is the thermal expansion coefficient, γ is the coefficient of concentration expansion, χ is the coefficient of heat diffusivity, D is the coefficient of vapour diffusion in the gas, and the coefficients δ and α characterize the diffusive thermal effect and the thermodiffusion effect in the gas-vapour layer, correspondingly. It is worth noting that within the frame of the Oberbeck – Boussinesq approximation function p describes deviation of the physical (true) fluid pressure P from the hydrostatic one. Taking into account the hydrostatic component and equilibrium characteristics of each fluid, one can obtain $p_i = P_i - \tilde{\rho}_i \mathbf{g} \cdot \mathbf{x}$. Here, $\tilde{\rho}_1 = \rho_{01}(1 + \beta_1 T_0)$, $\rho_2 = \rho_{02}(1 + \beta_2 T_0 + \gamma C_0)$.

System of equations (1.1), (1.2) admits a stationary exact solution of the form

$$\begin{aligned} u_i &= u_i(y), & v_i &= 0, & T_i &= T_i(x, y) = (a_1^i + a_2^i y)x + \vartheta_i(y), \\ C &= C(x, y) = (b_1 + b_2 y)x + \phi(y), & p_i &= p_i(x, y). \end{aligned} \quad (1.3)$$

Here, a_j^i, b_j ($j = 1, 2$) are parameters of the solution. They satisfy some compatibility relations dictated by the boundary conditions. Solution (1.3) as the solution of an evaporative convection problem was first proposed in [8]. Its treatment as the partially invariant exact solution of rank 1 and defect 3 was given in [2]. Below, conditions on the outer boundaries $y = -l$ and $y = h$ and on the internal interface $y = 0$ are formulated with regard to the solution form.

The Dirichlet boundary conditions are set on the channel walls for all required functions:

$$\begin{aligned} y = -l, & \quad u_1 = 0, \quad T_1 = A_1 x + \vartheta_1, \\ y = h : & \quad u_2 = 0, \quad T_2 = A_2 x + \vartheta_2, \quad C = 0. \end{aligned} \quad (1.4)$$

Here, A_i are given constant longitudinal temperature gradients that determines intensity and type (heating or cooling) of the thermal load applied on the walls, ϑ_1, ϑ_2 are constants setting an average temperature of the wall. In the general case when $\vartheta_1 \neq \vartheta_2$, the transverse temperature drop is formed in the channel. Then, temperature field in the entire flow domain is characterized by resulting non-uniform gradient with respect to y . Relations for velocity functions present the

no-slip conditions. If vapour concentration is equal to zero then it is interpreted as the condition of full vapour absorption on the upper wall. For the first time this condition was considered in [8]. Later, it was tested in analogical problem within the frame of three-dimensional statement [9]. The comparison of modelling results with experimental data showed that the use of such type of condition allowed one to describe the influence of edge effects. The effects presents as significant growth of evaporation rate near the three-phase contact line [10]. Condition $C = 0$ can be realized in experiments by the vapour freezing.

The following conditions are to be satisfied on the common internal boundary Γ

$$\begin{aligned}
 y = 0 : \quad \rho_1 \nu_1 \frac{du_1}{dy} &= \rho_2 \nu_2 \frac{du_2}{dy} - \sigma_T \frac{\partial T_1}{\partial x}, \quad p_1 = p_2, \\
 \kappa_1 \frac{\partial T_1}{\partial y} - \kappa_2 \frac{\partial T_2}{\partial y} - \delta \kappa_2 \frac{\partial C}{\partial y} &= -LM, \\
 u_1 = u_2 = u_\Gamma, \quad T_1 = T_2 = T_\Gamma, \quad C &= C_0[1 + \varepsilon(T_2 - T_0)].
 \end{aligned} \tag{1.5}$$

The first two expressions present projections of the dynamic condition on the unit tangential and normal vectors to Γ . The third condition is the heat balance relation when transfer through the interface takes place. The fourth and fifth equalities set the continuity conditions for the velocity and temperature. The last relation gives the concentration of saturated vapour. Taking into account the solution form and assumption on the diffusive character of evaporation, the kinematic condition is satisfied identically. The following notations are used in (1.5): κ is the heat conductivity coefficient, L is the latent heat of vaporization, u_Γ and T_Γ are common values of velocity and temperature on the interface, respectively, $\varepsilon = L\mu/(RT_0^2)$, μ is the molar mass of evaporating liquid, and R is the universal gas constant. The mass balance condition is used to evaluate evaporation rate M . In the present paper, the case when M is not constant is considered. It varies along the channel according to the linear law

$$M = -D\rho_2 \left(\frac{\partial C}{\partial y} + \alpha \frac{\partial T_2}{\partial y} \right), \quad M = M(x) = M_0 + M_x x. \tag{1.6}$$

Positive values of M refer to evaporation of the liquid into the gas flux, and negative ones correspond to vapour condensation.

Additional condition that defines the gas flow rate in the upper layer closes the problem statement:

$$Q = \int_0^h \rho_2 u_2(y) dy. \tag{1.7}$$

Explicit expressions for all required functions derived in the frame of the problem statement under consideration are presented in [4]. Therein, the physical interpretation of exact solution (1.3) is given, and the domain of its applicability for describing two-phase flows in real physical systems is discussed. Complete analysis of the applicability conditions of this solution for all possible problem statement was carried out [5].

It should be noted that solution (1.3) can be derived without using any assumption about shape of the interface. The second equality in (1.5) can be considered as the first term of the expansion of the dynamical condition for the normal stresses with respect to small capillary number Ca . The structure of the exact solution dictates the rectilinear shape of the interface within the framework of the problem statement under study when the leading term of the expansion leads to zero mean curvature of the interface (for details see [9]). Experimental possibility to maintain the plane form of the phase boundary of an evaporating liquid layer blown by a gas flux was described in [11].

2. Calculation of the solution parameters characterizing temperature, evaporation rate and vapour content

Substituting required functions (1.3) in governing equations (1.1), (1.2), functional representations for velocity u_j , temperature T_j , pressure p_j and concentration C can be we found (see [4]). Constants M_0 and M_x that determine evaporation rate as well as solution parameters a_j^i, b_j satisfy relations based on the boundary conditions.

First of all parameters a_1^1 and a_1^2 are equal to each other, $a_1^i = A$ as it follows from the continuity condition for the temperature on the phase boundary. Therefore, temperature functions in the layers take the form $T_i = (A + a_2^i y)x + \vartheta_i(y)$. Here, A is the longitudinal temperature gradient on Γ that determines the intensity of the thermocapillary convection and evaporation process.

Conditions of linear temperature distribution on the rigid channel walls $y = -l$ and $y = h$ result in the following relations for a_2^i : $a_2^1 = (A - A_1)l^{-1}$, $a_2^2 = (A_2 - A)h^{-1}$.

Taking into account the condition of zero vapour concentration on the upper wall $y = h$, one can obtain the following equality that relates parameter b_1 to parameter b_2 : $b_1 + b_2 h = 0$. The Clapeyron–Clausius equation in the linearised form gives the saturated vapour concentration on Γ (the last condition in (1.5)). The consequence of this equation entails relationship $b_1 = C_0 \varepsilon A$. Then, $b_2 = C_0 \varepsilon A / h$.

Further, the gradient of evaporative mass flow rate M_x can be directly calculated with the help of mass balance condition (1.6):

$$M_x = -D\rho_2(b_2 + \alpha a_2^2) = -D\rho_2 h^{-1}(-A(C_0 \varepsilon - \alpha) + \alpha A_2), \quad (2.1)$$

whereas the relation for M_0 that defines the average value of evaporation rate contains integration constants included in expressions for temperature and concentration functions.

Using the heat transfer condition at the interface and expression (2.1), the following relationship between a_2^1 and a_2^2 is obtained

$$a_2^2 = K a_2^1 + \bar{K} M_x, \quad K = \frac{\kappa_1}{\kappa_2(1 - \alpha\delta)}, \quad \bar{K} = \frac{D\rho_2\lambda + \delta\kappa_2}{D\rho_2\kappa_2(1 - \alpha\delta)}.$$

Since a_2^1, a_2^2 and M_x depend on A, A_1, A_2 , condition on constraint is

$$A_2(1 + \alpha D\rho_2 \bar{K}) = A(1 + hl^{-1}K + (C_0 \varepsilon + \alpha)D\rho_2 \bar{K}) - A_1 hl^{-1}K. \quad (2.2)$$

Expression (2.2) establishes relation between longitudinal temperature gradients A, A_1 and A_2 on system boundaries. Two coefficients defining temperature gradients are prescribed arbitrarily; the third one is found according to (2.2). One should note that in a real physical system evaporation results in cooling of the liquid surface and formation of longitudinal temperature gradient at the interface. Thus, this gradient can be evaluated on the basis of the exact solution. According to (2.2), interfacial temperature gradient A depends on boundary gradients A_i , geometric parameters of the system and physical parameters of the fluids.

In view of the form of the exact solution, the vapour concentration function increases with x . Since function C is treated as mass fraction of the volatile component in the gas phase, it has a physical meaning only if its values belong to the interval $[0; 1]$. The extent of the flow domain L_h where C takes on feasible values can be determined in the terms of input data of the problem. According to the last condition in (1.5), changes in vapour content along the

longitudinal coordinate x can be evaluated as follows: $C \sim C_0(1 + \varepsilon Ax)$. Then, the length L_h can be evaluated as follows $L_h \leq (1 - C_0)/\varepsilon AC_0$.

Below, the obtained solution of the Dirichlet problem is used to study the influence of the applied thermal load on the characteristics of flow regimes in two-phase systems.

3. Characteristics of convective regimes with non-uniform evaporation

***** Let us consider the bilayer system with HFE-7100 liquid and nitrogen gas as working media. Physical parameters of fluids are given in the order {HFE-7100, nitrogen} or only for one of the media: $\rho = \{1.5 \cdot 10^3, 1.2\}$ kg/m³; $\nu = \{0.38 \cdot 10^{-6}, 0.15 \cdot 10^{-4}\}$ m²/s; $\beta = \{1.8 \cdot 10^{-3}, 3.67 \cdot 10^{-3}\}$ K⁻¹; $\chi = \{0.4 \cdot 10^{-7}, 0.3 \cdot 10^{-4}\}$ m²/s; $\kappa = \{0.07, 0.027\}$ W/(m·K), $\sigma_T = 1.14 \cdot 10^{-4}$ N/(m·K), $\gamma = -0.5$, $D = 0.7 \cdot 10^{-5}$ m²/s, $\alpha = 5 \cdot 10^{-3}$ K⁻¹, $\delta = 10^{-5}$ K, $L = 1.11 \cdot 10^5$ W·s/kg. The equilibrium characteristics of the bilayer system are $C_0 = 0.45$, $T_0 = 293.15$ K; here, $\varepsilon = 0.04$ K⁻¹, $\mu = 0.25$ kg/mol.

Velocity and temperature fields in the system, vapour content in the gas layer and evaporation rate that depend on the character and intensity of the thermal load applied on the external boundaries of the flow domain are analysed. Parameters defining the external thermal action are the longitudinal temperature gradients A_1 , A_2 and ϑ_1 , ϑ_2 (see (1.4)). Relation (2.2) is used to evaluate the interface gradient A at various boundary gradients A_i . Values of A_i vary from -10 to 10 K/m, and ϑ_1 , ϑ_2 are equal to 293.15 K unless otherwise specified. If $A_i < 0$ ($A_i > 0$) then the channel wall is cooled (heated) in the direction of the longitudinal axes. For the working media used and heating conditions under consideration, the length L_h should be within 0.4 m. The thickness of the liquid layer $l = 0.0025$ m, the thickness of the gas layer $h = 0.005$ m and gas flow rate $Q = 9.6 \cdot 10^{-6}$ kg/(m²·s) are fixed for all cases under consideration.

Influence of the longitudinal temperature gradient. One of the important factors that defines the pattern of the arising convective regime is the interface temperature gradient A . It is this parameter which governs the intensity of the surface tension-driven convection. Considering data listed in Tabs. 1, 2, one can conclude that interfacial gradient A and other parameters of the system are more sensitive to variations of boundary gradient A_1 than variations of A_2 . In the tables, ΔT denotes the temperature drop in the whole system, T_{\max} and $|u|_{\max}$ are the maximum values of the temperature and the absolute value of velocity in the system, respectively, C_{\max} is the maximum value of the vapour concentration in the gas layer. In all considered cases the solution predicts relative variations of the temperature and deviations of maximum values of the vapour concentration from the equilibrium values T_0 , C_0 retained within 15% which can be considered to be moderate ones.

Significant alterations in flow topology and thermal field occur with the change in A_i . When analysing basic characteristics of convective regimes, the Napolitano classification of flow types is used in the two-layer systems on the basis of the flow topology [12]. Three basic classes are distinguished: mixed type flows (MF), Poiseuille-type regimes (PF) and pure thermocapillary flows (TKF). Additionally, subclasses of MF and PF that are specific to two-phase systems with evaporation are considered. Detailed description of specific features and mechanisms causing all possible flow regimes as well as examples of velocity, temperature and vapour concentration fields for each mode can be found in [5]. The first form of mixed type flows (MF-1) is defined by the specific “negative lamination” of the velocity contour near the liquid–gas boundary and

Table 1. Parameters of the two-phase system at fixed $A_2 = 5$ K/m for different values of A_1

A_1 , K/m	A , K/m	ΔT , K	T_{\max} , K	C_{\max}	$ u _{\max} \times$, $\times 10^{-3}$, m/s	$M_0 \cdot 10^4$, kg/(m ² ·s)	$M_x \cdot 10^4$, kg/(m·s)
-10	-6.596	1.628	293.15	0.4216	2.423	6.9407	-2.909
-5	-2.875	2.097	293.15	0.4134	2.171	6.7669	-1.5049
0	0.846	2.23	293.15	0.4111	2.428	6.7193	-0.1008
5	4.567	2.024	293.15	0.4147	2.78	6.798	1.3034
10	8.289	1.482	293.15	0.4241	3.164	7.0028	2.7075

Table 2. Parameters of the two-phase system at fixed $A_1 = 5$ K/m for different values of A_2

A_2 , K/m	A , K/m	ΔT , K	T_{\max} , K	C_{\max}	$ u _{\max} \times$, $\times 10^{-3}$, m/s	$M_0 \cdot 10^4$, kg/(m ² ·s)	$M_x \cdot 10^4$, kg/(m·s)
-10	2.029	2.204	293.15	0.4115	2.51	6.7295	1.6056
-5	2.875	2.158	293.15	0.4123	2.598	6.7468	1.5049
0	3.721	2.098	293.15	0.4134	2.688	6.7697	1.4041
5	4.567	2.024	293.15	0.4147	2.78	6.798	1.3034
10	5.413	1.935	293.15	0.4162	2.873	6.8317	1.2026

formation of near-surface reverse flow (Fig. 2(a-c)). The second type mixed flow (MF-2) is characterized by the "positive stratification" of the velocity profile along the interface. Here, the longitudinal velocity component is positive in both fluids (Fig. 2(d-f)). Mixed flows of the third type (MF-3) have the velocity field similar to the Couette structure in one of the layers (Fig. 2(g-i)) or concurrently in both layers. It was found that all three classes of mixed type flows could be realized in the system under considered conditions.

In the general case, three subclasses of flows among the Poiseuille-type regimes were identified [5]. However, in the considered range of boundary gradients A_i , one can observe only flows with the velocity distribution close to the parabolic one through the whole height of the channel or simultaneously in both phases, where the longitudinal velocity component is positive everywhere. Such a flow regime presents the PF-1 regime (Fig. 3(a-c)). Finally, pure thermocapillary flows (TKF, Fig. 3(d-f)) which are characterized by global liquid counterflow can be also realized in the two-phase system under conditions of temperature pumping with gradients A_i from the specified range. Several consecutive transitions from one type of flows to another can occur with an increase in A_i from -10 to 10 K/m. Topological regimes arising in the bilayer system under study are specified on the map of flow regimes in Fig. 4(a) according to the given classification. Along with the topology of the flow, the intensity of the motion also varies. It is characterized by maximum values of the modulus of velocity $|u|$ (see Tabs. 1, 2) and it can be varied by more than 40%. As previously mentioned, the system is less sensitive to variations in A_2 . When A_2 is changed from -10 K/m to 10 K/m, a smaller number of successive transitions between regimes is observed in comparison with corresponding variations in A_1 . The intensity of the flow slightly responds to changes in the thermal load caused by variations in A_2 (compare values of $|u|_{\max}$ in Tabs. 1 and 2). One should note that all three basic types of flows are observed in real systems with evaporating liquid driven by the co-current gas flux [13].

The change of intensity of temperature driving forces leads not only to transformation of the velocity field but also to alteration of the thermal picture. The solution predicts formation of the non-uniform temperature gradient in the vertical direction for all observed convective regimes.

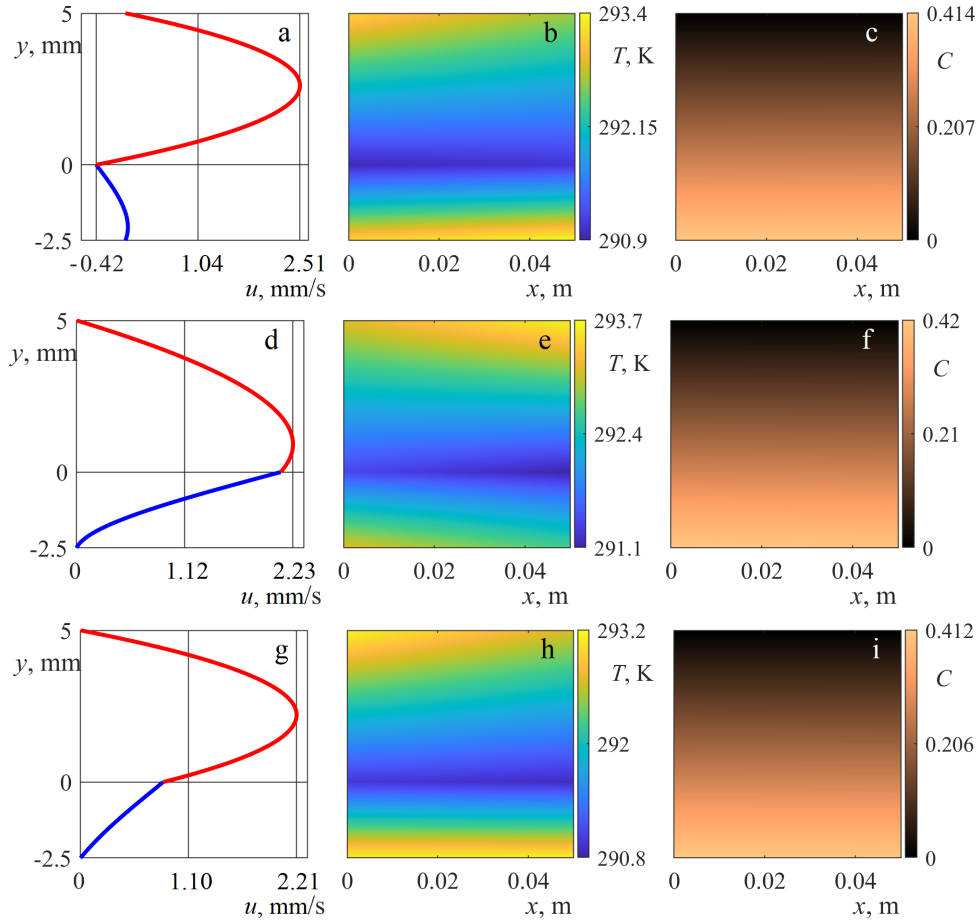


Fig. 2. Velocity (a, d, g), temperature (b, e, h) and vapour concentration (c, f, i) fields for mixed type flows: MF-1, $A_1 = 5$ K/m, $A_2 = -10$ K/m (a-c); MF-2, $A_1 = -10$ K/m, $A_2 = 10$ K/m (d-f); MF-3, $A_1 = 0$ K/m, $A_2 = -10$ K/m (g-i)

Two typical thermal patterns with a substantial "cold" zone on both sides of the phase boundary (CNsZ) and with a cold thermocline along the interface (CThI) can emerge. The regimes with the cool near-surface zone (CNsZ) are characterized by unstable temperature stratification of the entire liquid layer. In this case, the gas layer is steadily stratified (Figs. 2(b, e, h), 3(b)). The evaporation effect prevails over the thermocapillary effect in these modes. Formation of the distinctive cold thermocline on the interface (CThI) is caused by the competition of the Marangoni effect which gives rise to the thermocapillary motion of the liquid from the region with higher temperature into the cool domain along the interface with the evaporation process resulting in cooling of the liquid surface (Fig. 3(e)). The possibility of formation of convective modes with the cool boundary layer near the liquid surface in the two-layer systems with evaporation was confirmed in experiments [14]. Figure 4(b) presents a "map" of thermal regimes that depend on the longitudinal temperature gradients A_i .

The pattern of the vapour concentration field in the gas layer remains the same for all considered cases (see distributions of the vapour concentration functions in Figs. 2, 3). The vapour

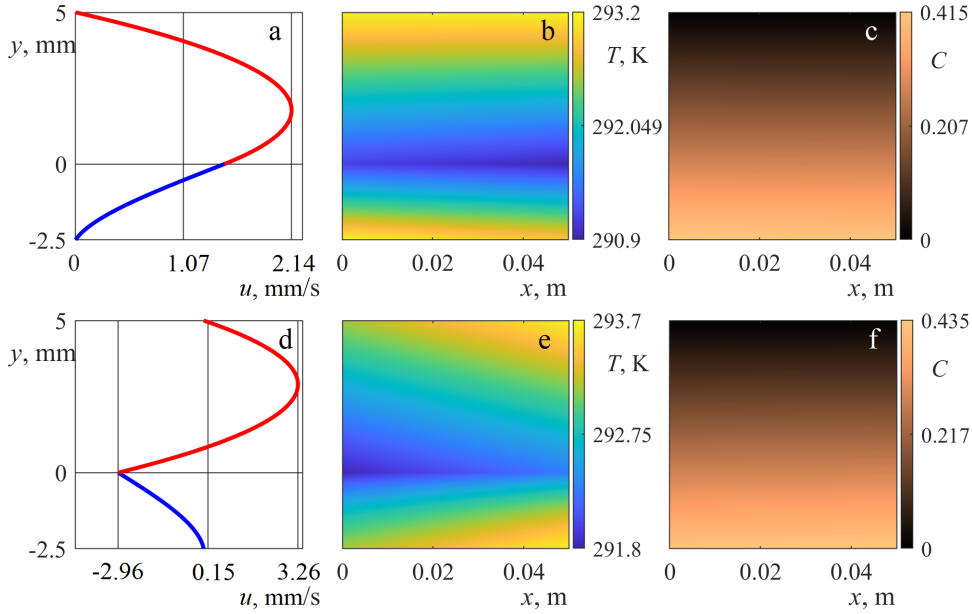


Fig. 3. Velocity (a,d), temperature (b,e) and vapour concentration (c,f) fields: PF-1, $A_1 = -5$ K/m, $A_2 = 0$ K/m (a-c); TKF, $A_1 = A_2 = 10$ K/m (d-f)

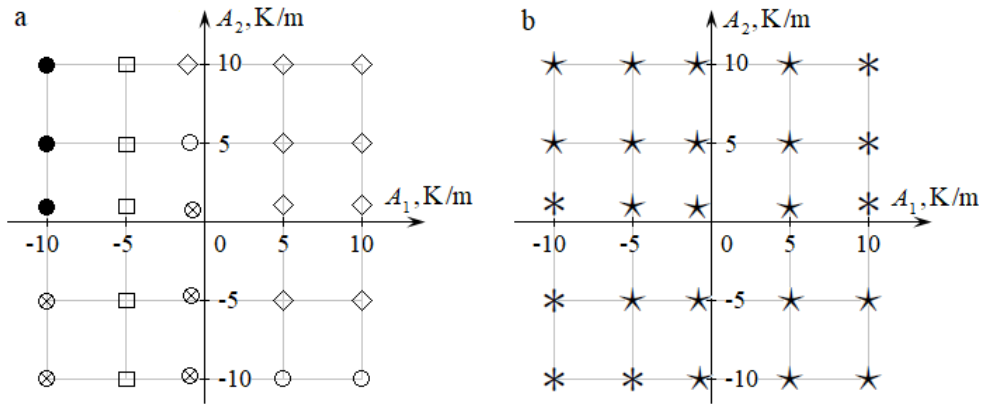


Fig. 4. Maps of flow regimes (a) and temperature patterns (b) in the HFE-7100–nitrogen system subjected to external thermal load: (a) – \circ – MF-1, \bullet – MF-2, \otimes – MF-3, \square – PF-1, \diamond – TKF; (b) – \star – regime with CNsZ, $*$ – regime with CThI

content is close to the concentration of saturated vapour C_0 near the interface, and it varies here depending on changes in the interfacial temperature gradient A whereas near the upper wall the values of C drop to zero. The behaviour of the vapour concentration function is caused by changes in the evaporation mass flow rate M which significantly depends on temperature characteristics of the interface. Since temperature gradient A is more sensitive to variations of the thermal load applied to the substrate then similar behaviour is inherent to M (compare the variation range for M_0 , M_x in Tabs. 1, 2 and the character of their relation with changes in A

related to changes in boundary temperature gradients A_i presented in Fig. 5). If M_x is negative then the evaporation rate M decreases along the channel and the vapour concentration in the gas diminishes (Tab. 1). The higher is the temperature, the higher is the saturation pressure on the gas side of the phase interface. Therefore, more liquid evaporates at the same gas pressure. If the surface tension-driven motion is co-directional with the gas flow then evaporation is induced by both the thermal load and the effect associated with the shear stress. The gas flux encourages the vapour motion in the gas. It results in higher concentration gradient at the liquid–gas interface and ensures higher evaporation rate.

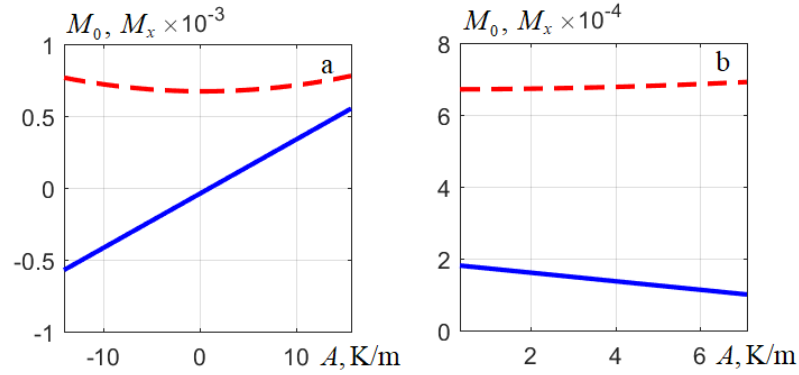


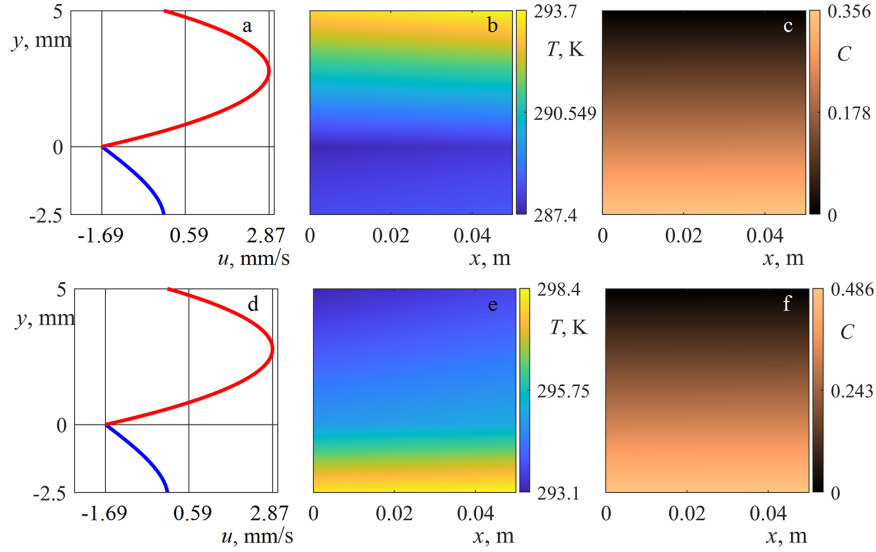
Fig. 5. Relationship between parameters M_0 (dashed lines) and M_x (solid curves) and interface temperature gradient with changes in A_1 (a) and A_2 (b): $A_2 = 20$ K/m; $A_1 = 20$ K/m

Thus, one can exert control over the evaporation rate and flow regimes with the intensity of thermal pumping defined by boundary gradients A_i . If it is necessary to retain the given temperature head on one of the walls then one can maintain acceptable variations of the evaporation rate by means of the thermal regime on other wall and forecast potential changes in the vapour content.

Influence of the vertical temperature gradient. The structure of the thermal field can be considerably transformed with conditions of thermal load with non-zero gradients A_i and various ϑ_1 and ϑ_2 . It depends on the value and orientation of the resulting temperature gradient. Since the system behaviour is more responsive to variations of the thermal load applied on the substrate the influence of the vertical temperature drop on the bilayer flow characteristics is investigated when parameter ϑ_1 varies from 288.15 to 298.15 K. Formation of regimes with stable (Fig. 6(b)) and unstable (Fig. 6(e)) temperature stratification is studied in the transverse direction of the whole system. One should note that solution predicts only reconstruction of the thermal field whereas the velocity profile is not transformed with the changes in ϑ_1 . According to (2.2) and (1.6), both interface temperature gradient A and gradient M_x defining the variation rate of M along the longitudinal axes do not depend on ϑ_1 . It remains the same for corresponding fixed values of A_i for all vertical temperature drops (quantitative characteristics for configurations under consideration are exemplified in Tab. 3). It is regarded as a imperfection of solution (1.3) as in this case the exact solution does not reflect the impact of the Marangoni effect. One can conclude that the presence of non-zero transverse temperature drop does not lead to the formation of topologically new classes of flows that differ from those described earlier and presented in Figs. 2, 3.

Table 3. Parameters of the two-phase system at $A_1 = -5$ K/m, $A_2 = 5$ K/m with changes in ϑ_1

ϑ_1 , K	ΔT , K	T_{\max} , K	C_{\max}	$ u _{\max} \times$, $\times 10^{-3}$, m/s	$M_0 \cdot 10^4$, kg/(m ² ·s)	$M_x \cdot 10^4$, kg/(m·s)
288.15	5.818	293.15	0.3484	2.171	5.3628	-1.5049
293.15	2.097	293.15	0.4134	2.171	6.7669	-1.5049
298.15	5	298.15	0.4784	2.171	8.171	-1.5049

Fig. 6. Velocity (a, d), temperature (b, e) and vapour concentration (c, f) fields in the bilayer system at $A_1 = 5$ K/m, $A_2 = 10$ K/m for $\vartheta_1 = 288.15$ K (a–c) and $\vartheta_1 = 298.15$ K (d–f)

Despite the mentioned above defect this solution feasibly describes the qualitative interrelation of the variations of the evaporative mass flow rate and the vapour content in the gas with changes in the vertical temperature drop. The growth of deviation of the liquid temperature from the equilibrium value T_0 and significant deviation of vapour concentration in the gas phase from C_0 with an increase in the transverse temperature drop is observed. If $\vartheta_1 < T_0$ then the vapour content in the gas drops. The lower is the temperature of the liquid the lower is the average kinetic energy of the liquid volume and, therefore, the smaller is the quantity of the volatilizing fluid. Along with this, the lower is the vapour concentration in the background gas, the faster is the volatilization from the liquid phase [15]. With the rising temperature the average kinetic energy of the liquid volume increases. Therefore, vapour concentration C also grows accompanied by the inhibition of growth of the vaporization rate M . If $\vartheta_1 > T_0$ then the maximum vapour concentration is above the equilibrium concentration C_0 . The solution precisely specifies this relationship between evaporation rate and characteristics of the vapour content in the gas phase and temperature drop in the whole system. Thus, the qualitative behaviour of evaporation characteristics that depends on the transverse temperature drop in the bilayer system is adequately described by the exact solution under study.

The applicability of solution (1.3) that describes characteristics of the bilayer system with the transverse temperature drop is limited by values of ϑ_1 and ϑ_2 providing moderate deviations of

C_{\max} from C_0 , namely, no more than 20–25%. For the considered two-layer system the transverse temperature drop should be within 10 degrees, where the average temperature of duct walls ϑ_1 and ϑ_2 have to be close to the temperature of the local thermodynamic equilibrium T_0 .

The work of O. N. Goncharova was carried out in accordance with the State Assignment of the Russian Ministry of Science and Higher Education entitled "Modern methods of hydrodynamics for environmental management, industrial systems and polar mechanics" (Government contract code FZMW-2020-0008).

References

- [1] V.B.Bekezhanova, O.N.Goncharova, Problems of the evaporative convection (review), *Fluid Dyn.*, **53**(2018), suppl. 1, S69-S102.
- [2] V.K.Andreev, The Birikh Solution of Convection Equations and Some Its Generalization, Preprint no. 1-10, ICM SB RAS, Krasnoyarsk, 2010 (in Russian).
- [3] V.V.Pukhnachev, Group-theoretical methods in convection theory, *AIP Conf. Proc.*, **1404**(2011), 27–38. DOI: 10.1063/1.3659901
- [4] V.B.Bekezhanova, O.N.Goncharova, I.A.Shefer, Solution of a two-layer flow problem with inhomogeneous evaporation at the thermocapillary interface, *J. Sib. Fed. Univ. Math. Phys.*, **14**(2021), no. 4, 404–413. DOI: 10.17516/1997-1397-2021-14-4-404-413
- [5] V.B.Bekezhanova, O.N.Goncharova, Comparative characteristic of evaporative convection regimes in different statements of boundary value problem for convection equations, *J. Math. Sci.*, **267**(2022), no. 4, 444–456. DOI:10.1007/s10958-022-06149-4
- [6] Y.V.Lyulin et al., The effect of the interface length on the evaporation rate of a horizontal liquid layer under a gas flow, *Thermophys. Aeromech.*, **27**(2020), no. 1, 117–121. DOI: 10.1134/S0869864320010114
- [7] L.D.Landau, E.M.Lifshitz, Course of Theoretical Physics, Vol. 6, Fluid Mechanics, second ed., ButterworthHeinemahh, 1987.
- [8] M.I.Shliomis, V.I.Yakushin, Convection in a two-layers binary system with an evaporation, *Collected papers: Uchenye zapiski Permskogo Gosuniversiteta, seriya Gidrodinamika*, **4**(1972), 129–140 (in Russian).
- [9] V.B.Bekezhanova, O.N.Goncharova, Modeling of three dimensional thermocapillary flows with evaporation at the interface based on the solutions of a special type of the convection equations, *Applied Mathematical Modelling*, **62**(2018), 145–162. DOI: 10.1016/j.apm.2018.05.021
- [10] V.S.Ajaev, O.A.Kabov. Heat and mass transfer near contact lines on heated surfaces, *Int. J. Heat Mass Transf.*, **108**(2017), 918–932. DOI: 10.1016/j.ijheatmasstransfer.2016.11.079
- [11] Yu.Lyulin, O.A.Kabov. Thermal effect in the evaporation process from the interface of the horizontal liquid layer under ashear gas flow, *Interfacial Phenom. Heat Transf.*, **11**(2023), no. 1, 55–64. DOI: 10.1615/InterfacPhenomHeatTransfer.2023046985

- [12] L.G.Napolitano, Plane Marangoni – Poiseuille flow two immiscible fluids, *Acta Astronaut.*, **7**(1980), 461–478.
- [13] Yu.Lyulin, O.Kabov, Evaporative convection in a horizontal liquid layer under shear-stress gas flow, *Int. J. Heat Mass Transfer*, **70**(2014), 599–609.
DOI: 10.1016/j.ijheatmasstransfer.2013.11.039
- [14] V.P Reutov et al., Convective structures in a thin layer of an evaporating liquid under an airflow, *J. Appl. Mech. Techn. Phys.*, **48**(2007), no. 4, 469–478.
DOI: 10.1007/s10808-007-0059-y
- [15] P.I.Voropai, A.A.Shlepov, Enhancement of Reliability and Efficiency of Reciprocating Compressors, Nedra, Moscow, 1980 (in Russian).

Об одном точном решении задачи испарительной конвекции с граничными условиями Дирихле

Виктория Б. Бекежанова

Институт вычислительного моделирования СО РАН
Красноярск, Российская Федерация

Ольга Н. Гончарова

Алтайский государственный университет
Барнаул, Российская Федерация

Аннотация. Изучаются характеристики стационарных конвективных течений жидкости и спутного потока газа в плоском горизонтальном канале в условиях неоднородного испарения диффузионного типа. Для описания течений в рамках приближения Обербека – Буссинеска используется частично-инвариантное точное решение уравнений термоконцентрационной конвекции, полученное как решение задачи испарительной конвекции с граничными условиями Дирихле на внешних стенках канала. На примере системы сред HFE-7100 – азот исследовано влияние внешней тепловой нагрузки на структуру полей скорости и температуры, массовый расход испарения и паросодержание в газе.

Ключевые слова: математическая модель, краевая задача, точное решение, испарительная конвекция.

EDN: HZSBXR

УДК 519.218.2

Further Remarks on the Explicit Generating Function Expression of the Invariant Measure of Critical Galton-Watson Branching Systems

Azam A. Imomov*

Karshi State University

Karshi, Uzbekistan

Sarvar B. Iskandarov†

Urgench State University

Urgench, Uzbekistan

Received 20.04.2023, received in revised form 14.09.2023, accepted 22.12.2023

Abstract. Consider the critical Galton-Watson branching system with infinite variance of the offspring law. We provide an alternative arguments against what Slack [9] did when it seeked for a local expression in the neighborhood of point 1 of the generating function for invariant measures of the branching system. So, we obtain the global expression for all $s \in [0, 1)$ of this generating function. A fundamentally improved version of the differential analogue of the basic Lemma of the theory of critical branching systems is established. This assertion plays a key role in the formulation of the local limit theorem with explicit terms in the asymptotic expansion of local probabilities. We also determine the decay rate of the remainder term in this expansion.

Keywords: Galton–Watson branching system, generating functions, slow variation, basic lemma, transition probabilities, invariant measures, limit theorems, convergence rate.

Citation: A.A. Imomov, S.B. Iskandarov, Further Remarks on the Explicit Generating Function Expression of the Invariant Measure of Critical Galton–Watson Branching Systems, *J. Sib. Fed. Univ. Math. Phys.*, 2024, 17(2), 220–228. EDN: HZSBXR.



1. Background, assumptions and purpose

Let Z_n be the population size in the Galton–Watson Branching (GWB) System at time $n \in \mathbb{N}_0$, where $\mathbb{N}_0 = \{0\} \cup \mathbb{N}$ and $\mathbb{N} = \{1, 2, \dots\}$. An evolution of the system will occur by the following scheme. Each individual lives a unit lifespan and at the end of his life produces j progeny with probability p_j , $j \in \mathbb{N}_0$, independently of each other at that $p_0 > 0$. Newborn individuals subsequently undergo reproduction obeying the offspring law $\{p_j\}$. The population sizes sequence can be represented by the following recurrent random sum of random variables:

$$Z_{n+1} = \xi_{n1} + \xi_{n2} + \dots + \xi_{nZ_n} \tag{1.1}$$

for any $n \in \mathbb{N}$, where ξ_{nk} are independent random variables with the common distribution $\mathbb{P}\{\xi_{nk} = j\} = p_j$ for all $k \in \mathbb{N}$. These variables are interpreted as the number of descendants of the k th individual in the n th generation. The GWB system defined above forms a reducible, homogeneous-discrete-time Markov chain with a state space consisting of two classes: $\mathcal{S}_0 =$

*imomov_azam@mail.ru <https://orcid.org/0000-0003-1082-0144>

†sarvar.i@urdu.uz

© Siberian Federal University. All rights reserved

$\{0\} \cup \mathcal{S}$, where $\mathcal{S} \subset \mathbb{N}$, therein the state $\{0\}$ is absorbing, and \mathcal{S} is the class of possible essential communicating states. Its n -step transition probabilities

$$P_{ij}(n) := \mathbb{P} \{ Z_{n+k} = j \mid Z_k = i \} \quad \text{for any } k \in \mathbb{N}$$

are completely given by the offspring law $\{p_j\}$. In fact, denoting $\mathbf{p}_j(n) := P_{1j}(n)$, we observe that a probability Generating Function (GF) $\sum_{j \in \mathcal{S}_0} P_{ij}(n)s^j = [f_n(s)]^i$ for any $i \in \mathcal{S}$ and $s \in [0, 1)$, where $f_n(s) = \sum_{j \in \mathcal{S}_0} \mathbf{p}_j(n)s^j$. At that the GF $f_n(s)$ is the n -fold iteration of the GF $f(s) := \sum_{j \in \mathcal{S}_0} p_j s^j$.

The classification of \mathcal{S} depends on the value of the parameter $m := \sum_{j \in \mathcal{S}} jp_j = f'(1-)$, the mean per-capita offspring number. The chain $\{Z_n\}$ is classified as sub-critical, critical and supercritical if $m < 1$, $m = 1$ and $m > 1$ respectively. Needless to say that $f_n(0) = \mathbf{p}_0(n)$ is a vanishing probability of the system initiated by one individual, which is monotone and $\lim_{n \rightarrow \infty} \mathbf{p}_0(n) = q$, where q is called an extinction probability of the system and it is smallest nonnegative root of the fixed-point equation $f(s) = s$ on the domain of $\{s : s \in [0, 1]\}$. Furthermore $f_n(s) \rightarrow q$ as $n \rightarrow \infty$ uniformly in $s \in [0, 1)$; see [1, Ch.I, §§1–5].

In the paper we focus on the critical case in which $q = 1$. We assume that the offspring GF $f(s)$ for $s \in [0, 1)$ has the following form:

$$f(s) = s + (1 - s)^{1+\nu} \mathcal{L} \left(\frac{1}{1 - s} \right), \tag{[f_\nu]}$$

where $0 < \nu < 1$ and $\mathcal{L}(\cdot)$ is slowly varying (SV) function at infinity. By the criticality of the system, the assumption $[f_\nu]$ implies that $2b := f''(1-) = \infty$. If $0 < b < \infty$ then $\nu = 1$ and $\mathcal{L}(t) \rightarrow b$ as $t \rightarrow \infty$.

Further, putting into practice the function

$$\Lambda(y) := \frac{f(1 - y) - (1 - y)}{y} = y^\nu \mathcal{L} \left(\frac{1}{y} \right)$$

for $y \in (0, 1]$, we rewrite and will use the condition $[f_\nu]$ in the following form:

$$f(s) - s = (1 - s)\Lambda(1 - s). \tag{[f_\Lambda]}$$

Slack [9] has shown (see, also [8]) that

$$\widehat{U}_n(s) := \frac{f_n(s) - f_n(0)}{f_n(0) - f_{n-1}(0)} \longrightarrow U(s) \quad \text{as } n \rightarrow \infty \tag{1.2}$$

for $s \in [0, 1]$, where the limit function $U(s)$ is the GF of the invariant measure for the system $\{Z_n\}$, and it satisfies the Abel equation

$$U(f(s)) = U(s) + 1. \tag{1.3}$$

Moreover, in the case when $[f_\nu]$ attends SV-function $L(\cdot)$ at zero instead of $\mathcal{L}(\cdot)$, Slack [9] found that $U(s)$ admits a local expression

$$U(s) \sim \frac{1}{\nu(1 - s)^\nu L(1 - s)} \quad \text{as } s \uparrow 1.$$

The mean value theorem implies that $f_{n+1}(0) - f_n(0) \sim f_n(0) - f_{n-1}(0)$ as $n \rightarrow \infty$ and hence altering Slack's definition of $\widehat{U}_n(s)$ to

$$U_n(s) := \frac{f_n(s) - f_n(0)}{f_{n+1}(0) - f_n(0)}, \tag{S_U}$$

we see that $\lim_{n \rightarrow \infty} U_n(s) = U(s)$. Then Slack's [9] arguments, in contrast to the method in [5], made it easy to prove the following statement, called the Basic Lemma of the theory of critical GWB systems, which clearly shows an explicit asymptotic expression for the function $R_n(s) := 1 - f_n(s)$.

Lemma 1 (Basic Lemma [6]). *If the condition $[f_\Lambda]$ holds then*

$$R_n(s) = \frac{\mathcal{N}(n)}{(\nu n)^{1/\nu}} \cdot \left[1 - \frac{\mathcal{U}_n(s)}{\nu n} \right], \tag{1.4}$$

where the function $\mathcal{N}(x)$ is SV at infinity and

$$\mathcal{N}(n) \cdot \mathcal{L}^{1/\nu} \left(\frac{(\nu n)^{1/\nu}}{\mathcal{N}(n)} \right) \rightarrow 1 \quad \text{as } n \rightarrow \infty, \tag{1.5}$$

and the function $\mathcal{U}_n(s)$ has the following properties:

- $\mathcal{U}_n(s) \rightarrow U(s)$ as $n \rightarrow \infty$ so that the equation (1.3) holds;
- $\lim_{s \uparrow 1} \mathcal{U}_n(s) = \nu n$ for each fixed $n \in \mathbb{N}$;
- $\mathcal{U}_n(0) = 0$ for each fixed $n \in \mathbb{N}$.

First direct result of the statement of the Basic Lemma 1 is certainly an expression of survival probability of the family of one individual in a form of

$$Q_n := \mathbb{P} \{ Z_n > 0 \} = R_n(0) = \frac{\mathcal{N}(n)}{(\nu n)^{1/\nu}}.$$

In our discussions an important role plays the following assertion, which we call the differential analogue of the Basic Lemma 1.

Lemma 2 ([6]). *Let the condition $[f_\Lambda]$ holds. Then the following relation is true:*

$$R'_n(s) = -\psi_n(s) \frac{R_n(s)\Lambda(R_n(s))}{(1-s)\Lambda(1-s)}, \tag{1.6}$$

where the function $\psi_n(s)$ has following properties:

- $\psi_n(s)$ is continuous in $s \in [0, 1)$, for all $n \in \mathbb{N}$ and

$$\frac{f'(s)}{f'(f_n(s))} \leq \psi_n(s) \leq 1;$$

- $\psi(s) := \lim_{n \rightarrow \infty} \psi_n(s)$ exists for $s \in [0, 1)$ and

$$f'(s) \leq \psi(s) \leq 1 \quad \text{and} \quad \psi(1-) = 1.$$

By definition $\mathcal{L}(\lambda x)/\mathcal{L}(x) \rightarrow 1$ as $x \rightarrow \infty$ for each $\lambda > 0$. Then it is natural that

$$\alpha_\lambda(x) := \frac{\mathcal{L}(\lambda x)}{\mathcal{L}(x)} - 1$$

decreases to zero with a certain speed rate at infinity. With a known rate of decrease of $\alpha_\lambda(x)$, the function $\mathcal{L}(\cdot)$ is called SV at infinity with remainder; see [2, p. 185].

The following statement is also known, which is an improved analogue of the Basic Lemma 1.

Lemma 3 ([4]). *Let the condition $[f_\Lambda]$ holds and $\alpha_\lambda(x) = o(\mathcal{L}(x)/x^\nu)$. Then*

$$\frac{1}{\Lambda(R_n(s))} - \frac{1}{\Lambda(1-s)} = \nu n + \frac{1+\nu}{2} \cdot \ln[\Lambda(1-s)\nu n + 1] + \rho_n(s), \tag{1.7}$$

where $\rho_n(s) = o(\ln n) + \sigma_n(s)$ and, $\sigma_n(s)$ is bounded uniformly for $s \in [0, 1)$ and converges to the limit $\sigma(s)$ as $n \rightarrow \infty$ which is a bounded function for all $s \in [0, 1)$.

The peculiarity of the Lemma 2 is that it perfectly generalizes an analogous statement established in [7, Theorem 1], in which the offspring law variance was assumed to be finite and later refined under a third finite moment assumption in [3, p. 20]. In both papers just mentioned, $\nu = 1$ and $\Lambda(y) \equiv y$, and thereat $f''(1-)n/2$ appeared instead of the first term νn and moreover, the subsequent tail terms are found on the right-hand side of (1.7).

In accordance with our purpose, we now recall the following theorem, which shows the explicit-integral form of the invariant measure GF $U(s)$.

Theorem 1.1 ([6]). *If condition $[f_\Lambda]$ holds and $\alpha_\lambda(x) = o(\mathcal{L}(x)/x^\nu)$, then*

(1) *the GF $U(s)$ is*

$$U(s) = \int_0^s \frac{\psi(y)}{(1-y)\Lambda(1-y)} dy, \tag{1.8}$$

where $\psi(s)$ is continuous in $s \in [0, 1]$, and $f'(s) \leq \psi(s) \leq 1$;

(2) *the derivative $U'(s)$ has the following representation:*

$$U'(s) = \frac{\psi(s)}{(1-s)\Lambda(1-s)}, \tag{1.9}$$

where $\psi(s) = 1 + \mathcal{O}(\Lambda(1-s))$ as $s \uparrow 1$.

In the last statements inequality estimations for the functions $\psi_n(s)$ and $\psi(s)$ were announced, but explicit expressions were not obtained for them.

In this paper, in addition to the assumption $[f_\Lambda]$, we adopt the remainder term rate of the SV-function $\mathcal{L}(\cdot)$ to be

$$\alpha_\lambda(x) = \mathcal{O}\left(\frac{\mathcal{L}(x)}{x^\nu}\right) \quad \text{as } x \rightarrow \infty, \tag{R_L}$$

that is more exact decreasing speed rate condition, than it was assumed in contents of the Lemma 3 and in the Theorem 1.1.

Our purpose is as follows. First, we improve the result of Theorem 1.1 by finding an explicit expression for the function $U(s)$ that is more exactly than in (1.8) and an explicit expression for the “undesirable” function $\psi(s)$ in the equality (1.9) depending on GF $f(s)$ and $f'(s)$. This contributes to the refinement of the formula (1.6), pointing to the explicit form of the function $\psi_n(s)$. In this issue we propose another proof of the Lemma 2 that improves its content. Next, using condition $[R_L]$, we find the main part term in the asymptotic expansion of the right-hand side of (1.6) with an estimate for the remainder term. All these results facilitate to refine some limit theorems.

The rest of this paper is organized as follows. Section 2. contains main results. Section 3. provides the proof of main results.

2. Main results

In this section we present our main results. Let

$$\mathcal{V}(s) := \frac{1}{\nu\Lambda(1-s)} \quad \text{and} \quad J(s) := \frac{1-f'(s)}{\Lambda(1-s)} - 1.$$

Theorem 2.1. *If condition $[f_\Lambda]$ holds, then*

(1) *the GF $U(s)$ has the following form:*

$$U(s) = \mathcal{V}(s) - \mathcal{V}(0); \tag{2.1}$$

(2) *the derivative $U'(s)$ has the following expression:*

$$U'(s) = J(s) \frac{\mathcal{V}(s)}{1-s}. \tag{2.2}$$

Remark 1. *Undoubtedly, the function $U(s)$, as the limit of the generating function, admits the form of a power series expansion $U(s) = \sum_{j \in \mathcal{S}} u_j s^j$, where $u_j = \sum_{k \in \mathcal{S}} u_k P_{kj}(1)$ and $\sum_{k \in \mathcal{S}} u_k p_0^k = 1$; see [9, Lemma 4]. Then relation (2.2) immediately implies that*

$$u_1 = U'(0) = \frac{J(0)}{\nu p_0} = \frac{1-p_0-p_1}{\nu p_0^2}. \tag{2.3}$$

Next, differentiating the Slack's altered definition $[\mathcal{S}_U]$ we have

$$U'_n(s) = -\frac{R'_n(s)}{Q_n \Lambda(Q_n)}.$$

Thus, we can interpret the statement of the Lemma 2 in terms of the convergence $U'_n(s) \rightarrow U'(s)$ as $n \rightarrow \infty$. So we provide its refinement in the following theorem.

Theorem 2.2. *If conditions $[f_\Lambda]$ and $[\mathcal{R}_\mathcal{L}]$ hold, then*

$$U'_n(s) = U'(s) \left(1 + \mathcal{O}\left(\frac{1}{n}\right) \right) \quad \text{as } n \rightarrow \infty, \tag{2.4}$$

where $U'(s)$ has the form of (2.2).

The assertion of Theorem 2.2 provides the following important limit result. Let

$$\mathcal{N}_\nu(n) := \mathcal{L}^{-1/\nu} \left(\frac{1}{Q_n} \right) \quad \text{and} \quad \mathcal{P}_\nu^{\{j\}}(n) := (\nu n)^{(1+\nu)/\nu} \mathbf{p}_j(n).$$

Theorem 2.3. *If conditions $[f_\Lambda]$ and $[\mathcal{R}_\mathcal{L}]$ hold, then the sequence $\{\mathcal{P}_\nu(n) := \mathcal{P}_\nu^{\{1\}}(n)\}$ is SV at infinity such that*

$$\frac{\mathcal{P}_\nu(n)}{\mathcal{N}_\nu(n)} = u_1 \cdot \left(1 - \frac{(1+\nu)^2 \ln n}{2\nu^2 n} + o\left(\frac{\ln n}{n}\right) \right) \quad \text{as } n \rightarrow \infty, \tag{2.5}$$

where u_1 is given in (2.3). Moreover

$$\mathcal{N}_\nu(n) \cdot \mathcal{L}^{1/\nu} \left(\frac{(\nu n)^{1/\nu}}{\mathcal{N}_\nu(n)} \right) \rightarrow 1 \quad \text{as } n \rightarrow \infty$$

and

$$\mathcal{N}_\nu(n) = C_\mathcal{N} + \mathcal{O}(n^{-\nu}) \quad \text{as } n \rightarrow \infty,$$

where $C_\mathcal{N} = C_\mathcal{L}^{-1/\nu}$ and $C_\mathcal{L} := \mathcal{L}(\infty-) < \infty$.

The statement of this theorem can be generalized for all $j \in \mathcal{S}$ as follows.

Proposition. *If conditions $[f_\Lambda]$ and $[\mathcal{R}_\mathcal{L}]$ hold, then*

$$\frac{\mathcal{P}_\nu^{\{j\}}(n)}{\mathcal{N}_\nu(n)} = u_j \cdot (1 + \mathfrak{U}_n),$$

where

$$\mathfrak{U}_n = -\frac{(1 + \nu)^2 \ln n}{2\nu^2 n} + o\left(\frac{\ln n}{n}\right) \quad \text{as } n \rightarrow \infty.$$

We leave the proof of Proposition until our next works.

3. Proof of results

We will need the following auxiliary statement.

Lemma 4. *Let condition $[f_\Lambda]$ holds.*

1. Then

$$\rho(s) := \left| \nu - J(s) \right| \rightarrow 0 \quad \text{as } s \uparrow 1. \tag{3.1}$$

2. If, in addition $[\mathcal{R}_\mathcal{L}]$ holds, then

$$\rho(s) = \mathcal{O}\left((1 - s)^\nu\right) \quad \text{as } s \uparrow 1. \tag{3.2}$$

Proof. From representation $[f_\Lambda]$ we have

$$1 - f'(s) = \Lambda(1 - s) + (1 - s)\Lambda'(1 - s). \tag{3.3}$$

On the other hand, it was proved in the book [2, p. 401] that

$$\frac{y\Lambda'(y)}{\Lambda(y)} \rightarrow \nu \quad \text{as } y \downarrow 0.$$

Then it follows

$$J(s) = \frac{1 - f'(s)}{\Lambda(1 - s)} - 1 = \frac{(1 - s)\Lambda'(1 - s)}{\Lambda(1 - s)} \rightarrow \nu \quad \text{as } s \uparrow 1$$

which implies (3.1).

To prove the second part we first write

$$\frac{y\Lambda'(y)}{\nu\Lambda(y)} = 1 + \delta(y), \tag{3.4}$$

with some continuous $\delta(y)$ being that $\delta(y) \rightarrow 0$ as $y \downarrow 0$. And then we follow the corresponding arguments in [6, p.126], relying, in contrast to them, on the condition $[\mathcal{R}_\mathcal{L}]$. Then we obtain in this issue that

$$\delta(y) = \mathcal{O}(\Lambda(y)) \quad \text{as } y \downarrow 0.$$

Continuing discussions in accordance with [6, p.126], we see that $C_\mathcal{L} := \mathcal{L}(\infty-) < \infty$ and

$$[\mathcal{R}_\mathcal{L}] \iff \mathcal{L}(x) = C_\mathcal{L} + \mathcal{O}(x^{-\nu}) \quad \text{as } x \rightarrow \infty. \tag{3.5}$$

Therefore it follows $\delta(y) = \mathcal{O}(y^{-\nu})$ as $y \downarrow 0$. Then using this conclusion, combining relations (3.3) and (3.4), we get to the estimation (3.2).

The lemma is proved. □

Proof of Theorem 2.1. Put

$$\mathcal{M}_n(s) := 1 - \frac{\Lambda(R_n(s))}{\Lambda(Q_n)}. \tag{3.6}$$

Using relations (1.2) and (1.4), in [6, p.131] proved that

$$n\mathcal{M}_n(s) \longrightarrow U(s) \quad \text{as } n \rightarrow \infty.$$

Moreover, it was shown there [6, p.130] that

$$\lim_{n \rightarrow \infty} \frac{1}{\nu n} \left[\frac{1}{\Lambda(R_n(s))} - \frac{1}{\Lambda(1-s)} \right] = 1. \tag{3.7}$$

Combining (3.6) and (3.7), we obtain

$$\begin{aligned} U(s) &= \lim_{n \rightarrow \infty} n\mathcal{M}_n(s) \\ &= \lim_{n \rightarrow \infty} n \left[1 - \frac{\Lambda(1-s)}{p_0} \frac{p_0\nu n + 1}{\Lambda(1-s)\nu n + 1} \right] = \mathcal{V}(s) - \mathcal{V}(0). \end{aligned}$$

We accounted for $\Lambda(1) = \mathcal{L}(1) = p_0$ in the last step. The relation (2.1) is proved.

The proof content of second part is short due to (3.3). Write

$$U'(s) = \mathcal{V}'(s) = \frac{\Lambda'(1-s)}{\nu\Lambda^2(1-s)} = \frac{1-f'(s) - \Lambda(1-s)}{\nu(1-s)\Lambda^2(1-s)}.$$

The right-hand side is easily transformed to the form of those part of (2.2).

The theorem is proved completely. □

Remark 2. Repeatedly use of Abel equation (1.3), with considering of relation (2.1), yields

$$\frac{1}{\Lambda(R_n(s))} - \frac{1}{\Lambda(1-s)} = \nu n.$$

It more exact refines the well-known statement mentioned in (3.7), indicating the absence of the limit operation as $n \rightarrow \infty$ on the left-hand side. Then under the condition $[f_\Lambda]$ it follows that

$$Q_n = \frac{\mathcal{N}_\nu(n)}{(\nu n)^{1/\nu}} \left(1 - \frac{1}{p_0\nu n} (1 + o(1)) \right) \quad \text{as } n \rightarrow \infty,$$

where $\mathcal{N}_\nu(n) = \mathcal{L}^{-1/\nu}(1/Q_n)$.

Proof of Theorem 2.2. Repeatedly using (1.3) entails $U(f_n(s)) = U(s) + n$ and hence

$$f'_n(s) = \frac{U'(s)}{U'(f_n(s))}.$$

Using relation (2.2) in last equality, in our notation we have

$$R'_n(s) = -\frac{J(s)}{J(R_n(s))} \frac{R_n(s)\Lambda(R_n(s))}{(1-s)\Lambda(1-s)}. \tag{3.8}$$

We recall now to relation (2.2) and the Lemma 4. Then

$$\left. \begin{aligned} J(R_n(s)) &= \nu + \mathcal{O}(R_n^\nu(s)) = \nu + \mathcal{O}\left(\frac{1}{n}\right) \quad \text{as } n \rightarrow \infty \\ \text{and} \\ \frac{J(s)}{\nu(1-s)\Lambda(1-s)} &= U'(s). \end{aligned} \right\} \quad (3.9)$$

Formulas (3.8) and (3.9) complete the proof of the theorem. \square

Proof of Theorem 2.3. First, in our assumptions, we rewrite (2.4) as follows:

$$R'_n(s) = -U'(s)R_n(s)\Lambda(R_n(s)) \left(1 + \mathcal{O}\left(\frac{1}{n}\right)\right) \quad \text{as } n \rightarrow \infty.$$

Then, since $R'_n(0) = -\mathfrak{p}_1(n)$, letting $s = 0$ implies

$$\mathfrak{p}_1(n) = U'(0)Q_n\Lambda(Q_n) \left(1 + \mathcal{O}\left(\frac{1}{n}\right)\right) \quad \text{as } n \rightarrow \infty. \quad (3.10)$$

Using Lemma 3 we obtain

$$\Lambda(Q_n) = \frac{1}{\nu n} \left(1 - \frac{1 + \nu \ln n}{2\nu} \frac{1}{n} + o\left(\frac{\ln n}{n}\right)\right) \quad \text{as } n \rightarrow \infty \quad (3.11)$$

and

$$Q_n = \frac{\mathcal{L}^{-1/\nu}(1/Q_n)}{(\nu n)^{1/\nu}} \left(1 - \frac{1 + \nu \ln n}{2\nu^2} \frac{1}{n} + o\left(\frac{\ln n}{n}\right)\right) \quad \text{as } n \rightarrow \infty. \quad (3.12)$$

Further, combining (3.10)–(3.12) produces

$$\mathfrak{p}_1(n) = u_1 \frac{\mathcal{N}_\nu(n)}{(\nu n)^{(1+\nu)/\nu}} \left(1 - \frac{(1 + \nu)^2 \ln n}{2\nu^2} \frac{1}{n} + o\left(\frac{\ln n}{n}\right)\right) \quad \text{as } n \rightarrow \infty, \quad (3.13)$$

where $\mathcal{N}_\nu(n) = \mathcal{L}^{-1/\nu}(1/Q_n)$ and u_1 is defined in (2.3). It is known that $Q_n = \mathcal{N}(n)/(\nu n)^{1/\nu}$ which is a result of Lemma 1, where $\mathcal{N}(\ast)$ is SV at infinity with the asymptotic property (1.5). In accordance with this property we write that

$$1 = \mathcal{N}_\nu(n) \cdot \mathcal{L}^{1/\nu} \left(\frac{1}{Q_n}\right) = \mathcal{N}_\nu(n) \cdot \mathcal{L}^{1/\nu} \left(\frac{(\nu n)^{1/\nu}}{\mathcal{N}(n)}\right) \sim \frac{\mathcal{N}_\nu(n)}{\mathcal{N}(n)} \quad \text{as } n \rightarrow \infty.$$

Then it follows

$$\mathcal{N}_\nu(n) \cdot \mathcal{L}^{1/\nu} \left(\frac{(\nu n)^{1/\nu}}{\mathcal{N}_\nu(n)}\right) \rightarrow 1 \quad \text{as } n \rightarrow \infty.$$

But by virtue of (3.5)

$$\mathcal{N}_\nu(n) = C_{\mathcal{N}} + \mathcal{O}(n^{-\nu}) \quad \text{as } n \rightarrow \infty,$$

where $C_{\mathcal{N}} = C_{\mathcal{L}}^{-1/\nu}$. Recalling now denotation $\mathcal{P}_\nu(n) := (\nu n)^{(1+\nu)/\nu} \mathfrak{p}_1(n)$, we transform the asymptotic relation (3.13) to the form of (2.5).

The proof is completed. \square

References

- [1] K.B.Athreya, P.E.Ney, *Branching processes*, Springer, New York, 1972.
- [2] N.H.Bingham, C.M.Goldie, J.L.Teugels, *Regular variation*, Cambridge, 1987.
- [3] T.E.Harris, *The theory of branching processes*, Springer-Verlag, 1963.
- [4] A.A.Imomov, E.E.Tukhtaev, On application of slowly varying functions with remainder in the theory of Galton-Watson branching process. *Jour. Siber. Fed. Univ.: Math. Phys.* **12**(2019), no. 1, 51–57. DOI: 10.17516/1997-1397-2019-12-1-51-57
- [5] A.A.Imomov, On a limit structure of the Galton-Watson branching processes with regularly varying generating functions, *Prob. and math. stat.*, **39**(2019), no. 1, 61–73. DOI: 10.19195/0208-4147.39.1.4
- [6] A.A.Imomov, E.E.Tukhtaev, On asymptotic structure of critical Galton-Watson branching processes allowing immigration with infinite variance, *Stochastic Models* **39**(2023), no. 1, 118–140. DOI: 10.1080/15326349.2022.2033628
- [7] H.Kesten, P.E.Ney, F.L.Spitzer, The Galton-Watson process with mean one and finite variance, *Jour. Appl. Prob.*, **11**(1966), no. 4, 579–611.
- [8] E.Seneta, The Galton-Watson process with mean one, *Jour. Appl. Prob.*, **4**(1967), 489–495.
- [9] R.S.Slack, A branching process with mean one and possible infinite variance, *Wahrscheinlichkeitstheor und Verw. Geb.*, **9**(1968), 139–145.

Дальнейшие замечания о явном выражении производящей функции инвариантной меры критических ветвящихся систем Гальтона-Ватсона

Азам А. Имомов

Каршинский государственный университет
Карши, Узбекистан

Сарвар Б. Искандаров

Ургенчский государственный университет
Ургенч, Узбекистан

Аннотация. Рассмотрим критическую ветвящуюся систему Гальтона-Ватсона с бесконечной дисперсией закона превращения одной частицы. Предлагаем аргументы, альтернативные аргументам Слейка [9], который нашел локальное выражение в окрестности точки 1 производящей функции для инвариантных мер ветвящейся системы. Мы получаем глобальное выражение для всех $s \in [0, 1)$ этой производящей функции. Устанавливаем улучшенный вариант дифференциального аналога основной леммы теории критических ветвящихся систем. Это утверждение играет ключевую роль в формулировке локальной предельной теоремы с явными членами в асимптотическом разложении локальных вероятностей. Мы также определяем скорость убывания остаточного члена в этом разложении.

Ключевые слова: ветвящиеся системы Гальтона-Ватсона, производящие функции, медленное изменение, основная лемма, переходные вероятности, инвариантные меры, предельные теоремы, скорость сходимости.

EDN: LOHSKC

УДК 532.517.4

Approximate Solution to a Model of the far Momentumless Axisymmetric Turbulent Wake

Alexey V. Shmidt*

Institute of Computational Modelling SB RAS

Krasnoyarsk, Russian Federation

Received 10.09.2023, received in revised form 28.10.2023, accepted 26.12.2023

Abstract. The flow in the far axisymmetric momentumless turbulent wake is described with the use of a mathematical model based on $k - \varepsilon$ semi-empirical model of turbulence. A group-theoretical analysis of the mathematical model of the wake is performed. The similarity reduction of the model to a system of ordinary differential equations is obtained. Asymptotic expansion of the solution in the vicinity of a singular point is used to construct approximate solution of corresponding boundary value problem.

Keywords: far momentumless axisymmetric turbulent wake, approximate solution, asymptotic expansion.

Citation: A. V. Shmidt, Approximate Solution to a Model of the far Momentumless Axisymmetric Turbulent Wake, J. Sib. Fed. Univ. Math. Phys., 2024, 17(2), 229–237. EDN: LOHSKC.



Introduction

Turbulent momentumless wake behind body of revolution was considered in many publications (see, e.g., [1–17] and references therein). The turbulent axisymmetric wake has been studied experimentally [1–6]. These experiments showed that wake asymptotically tends to self-similarity at a relatively small distance from the body.

Theoretical analysis of the self-similarity of the wake was performed in [7–12]. In these works asymptotic behaviour of the far wake was investigated. The non-linear eigenvalue problem for turbulent energy, its dissipation rate and velocity deficit was solved numerically Hassid [10]. Exponents in the power law were also obtained. The asymptotic behaviour of the wake was analysed [12] using the theory of self-similar solutions of the second kind [18]. The similarity solution of the second-order turbulence model was obtained analytically and the process of transition to self-similarity was studied numerically. It was found that a single-point spectrum of solutions of corresponding eigenvalue problem for turbulent energy and dissipation rate exists. Moreover, it was shown that wake parameters is weakly dependent on empirical constant $C_{\varepsilon 2}$.

Numerical modelling of the axisymmetric momentumless turbulent wake was carried out using different semi-empirical turbulence models [13–17].

Mathematical model based on $k - \varepsilon$ semi-empirical model of axisymmetric momentumless wake was used to tackle the problem of degeneration of the far turbulent wake behind a self-propelled body in a passively stratified medium [19–22]. The model was reduced [20–22] to a system of ordinary differential equations using group-theoretical analysis [23] and the B -determining equations method [24]. The boundary-value problem for the reduced system was solved numerically

*schmidt@icm.krasn.ru

using shooting method. Self-similarity index was determined during calculation process. An approach to determine self-similarity index has been suggested [25] where approximate solution to a model of the far plane momentumless turbulent wake was constructed using asymptotic expansion of the solution in a vicinity of the singular point.

This work is a continuation of studies presented in [20–22, 25]. In this paper an approximate solution was constructed to describe flow in the far axisymmetric momentumless turbulent wake.

1. Similarity reduction

The following semi-empirical model of turbulence is used to describe flow in the far axisymmetric momentumless turbulent wake

$$U_0 \frac{\partial U_1}{\partial x} = \frac{1}{r} \frac{\partial}{\partial r} \left(C_\mu r \frac{e^2}{\varepsilon} \frac{\partial U_1}{\partial r} \right), \quad (1)$$

$$U_0 \frac{\partial e}{\partial x} = \frac{1}{r} \frac{\partial}{\partial r} \left(C_\mu r \frac{e^2}{\varepsilon} \frac{\partial e}{\partial r} \right) - \varepsilon, \quad (2)$$

$$U_0 \frac{\partial \varepsilon}{\partial x} = \frac{1}{r} \frac{\partial}{\partial r} \left(\frac{C_\mu}{\sigma} r \frac{e^2}{\varepsilon} \frac{\partial \varepsilon}{\partial r} \right) - C_{\varepsilon 2} \frac{\varepsilon^2}{e}. \quad (3)$$

Here $U_1 = U - U_0$ is the deficit of the mean longitudinal velocity component, k is the kinetic energy of turbulence, and ε is the kinetic energy dissipation rate. It is assumed that fluid is incompressible and the flow is steady. Moreover, in what follows the undisturbed flow velocity U_0 is taken to be unity.

The empirical constants are as follows

$$C_\mu = 0.136, \quad \sigma = 1.3, \quad C_{\varepsilon 2} = 1.92.$$

The empirical constant C_μ has a modified value of 0.136 because model (1)–(3) was constructed as a simplification of more complicated algebraic model of Reynolds stresses [26–29].

The consequences of equation (1) is the following law of conservation of total excess momentum

$$J = \int_0^\infty r U_1 dr = 0. \quad (4)$$

A theoretical-group analysis [23] is used to construct self-similar solution. The Lie algebra basis of equations (1)–(3) consists of the following infinitesimal generators

$$X_1 = \frac{\partial}{\partial x}, \quad X_2 = \frac{\partial}{\partial U_1}, \quad X_3 = U_1 \frac{\partial}{\partial U_1}, \quad X_4 = x \frac{\partial}{\partial x} - 2e \frac{\partial}{\partial e} - 3\varepsilon \frac{\partial}{\partial \varepsilon}, \quad X_5 = r \frac{\partial}{\partial r} + 2e \frac{\partial}{\partial e} + 2\varepsilon \frac{\partial}{\partial \varepsilon}.$$

Using linear combination of operators X_3 , X_4 and X_5 it is not difficult to obtain the following representation for solution of (1)–(3)

$$U_1 = x^\beta U_2(t), \quad e = x^{2\alpha-2} K(t), \quad \varepsilon = x^{2\alpha-3} E(t), \quad t = r/x^\alpha, \quad (5)$$

here t is the self-similar variable, α and β are arbitrary constants appearing in the linear combination of operators X_3 , X_4 and X_5 .

Using representation (5) the initial mathematical model (1)–(3) can be reduced to the following system of ordinary differential equations

$$C_\mu \frac{K^2 U_2''}{E} + \left(C_\mu \frac{K}{E} \left(2K' - \frac{KE'}{E} + \frac{K}{t} \right) + \alpha t \right) U_2' - \beta U_2 = 0, \quad (6)$$

$$C_\mu \frac{K^2 K''}{E} + 2C_\mu \frac{KK'^2}{E} - \left(C_\mu \frac{K^2}{E} \left(\frac{E'}{E} - \frac{1}{t} \right) + \alpha t \right) K' - 2(\alpha - 1)K - E = 0, \quad (7)$$

$$\frac{C_\mu}{\sigma} \frac{K^2 E''}{E} - \frac{C_\mu}{\sigma} \frac{K^2 E'^2}{E^2} + \left(\frac{C_\mu}{\sigma} \frac{K}{E} \left(2K' + \frac{K}{t} \right) + \alpha t \right) E' - C_{\varepsilon 2} \frac{E^2}{K} - (2\alpha - 3)E = 0. \quad (8)$$

Solution of reduced system (6)–(8) has to satisfy the following conditions

$$U_2'(0) = K'(0) = E'(0) = 0, \quad (9)$$

$$U_2(a) = K(a) = E(a) = 0. \quad (10)$$

The first group of conditions take into account that flow is symmetric with respect to the Ox axis. The second group of conditions follow from the requirement that flow is undisturbed outside the turbulent wake domain. The value of a is related to the turbulent wake semi-width and it can be set equal to unity in the following calculations by virtue of the invariance of equations of reduced system (6)–(8) with respect to the scaling transformation. It should also be noted that coefficients of system (6)–(8) have singularities in the boundary conditions.

2. Approximate solution

According to the results presented in [25] to construct approximate solution of boundary-value problem (6)–(10) asymptotic expansion of a solution of equations (6)–(8) near the singular point $t = 1$

$$U_2 = u_1(1-t)^{10/7} + u_2(1-t)^{17/7} + u_3(1-t)^{20/7} + u_4(1-t)^{24/7} + u_5(1-t)^{27/7} + u_6(1-t)^{30/7} + u_7(1-t)^{31/7} + o(|1-t|^{31/7}), \quad (11)$$

$$K = k_1(1-t)^{10/7} + k_2(1-t)^{17/7} + k_3(1-t)^{20/7} + k_4(1-t)^{24/7} + k_5(1-t)^{27/7} + k_6(1-t)^{30/7} + k_7(1-t)^{31/7} + o(|1-t|^{31/7}), \quad (12)$$

$$E = e_1(1-t)^{13/7} + e_2(1-t)^{20/7} + e_3(1-t)^{23/7} + e_4(1-t)^{27/7} + e_5(1-t)^{30/7} + e_6(1-t)^{33/7} + e_7(1-t)^{34/7} + o(|1-t|^{34/7}) \quad (13)$$

is patched at the point $t = 0$ with an expansion of the solution near $t = 0$

$$U_2 = U_0 + \alpha_2 t^2 + \alpha_4 t^4 + \alpha_6 t^6 + \alpha_8 t^8 + o(t^8), \quad (14)$$

$$K = K_0 + \beta_2 t^2 + \beta_4 t^4 + \beta_6 t^6 + \beta_8 t^8 + o(t^8), \quad (15)$$

$$E = E_0 + \gamma_2 t^2 + \gamma_4 t^4 + \gamma_6 t^6 + \gamma_8 t^8 + o(t^8), \quad (16)$$

where

$$\alpha_2 = \frac{125\beta U_0 E_0}{68K_0^2}, \quad \alpha_4 = \frac{125\beta U_0 E_0^2}{18496K_0^4} \left(\frac{124E_0}{K_0} - 600\alpha + 125\beta + 25 \right),$$

$$\alpha_6 = -\frac{125\beta U_0 E_0^3}{45278208K_0^6} \left(469488 \frac{E_0^2}{K_0} + \frac{100E_0(30062\alpha - 2480\beta - 20481)}{K_0} - 4185000\alpha^2 + 1075000\alpha\beta - 62500\beta^2 - 868750\alpha - 50000\beta + 1344375 \right),$$

$$\begin{aligned}
\alpha_8 = & -\frac{125\beta U_0 E_0^4}{49262690304 K_0^8} \left(149379072 \frac{E_0^3}{K_0^3} - \frac{400 E_0^2 (15958860\alpha - 911685\beta - 5144117)}{K_0^2} - \right. \\
& - \frac{2500 E_0 (10062956\alpha^2 - 1156330\alpha\beta + 31000\beta^2 - 12644966\alpha + 724275\beta + 3240202)}{K_0} + \\
& + 13444250000\alpha^3 - 3935625000\alpha^2\beta + 312500000\alpha\beta^2 - 7812500\beta^3 + 15625187500\alpha^2 - \\
& \left. - 707656250\alpha\beta - 15625000\beta^2 - 23595718750\alpha + 1174453125\beta + 5909437500 \right), \\
\beta_2 = & \frac{125 E_0}{68 K_0^2} (2K_0(\alpha - 1) + E_0), \\
\beta_4 = & \frac{125 E_0^2}{36992 K_0^3} \left(\frac{872 E_0^2}{K_0^2} + \frac{E_0}{K_0} (446\alpha - 1921) - 100(14\alpha + 9)(\alpha - 1) \right), \\
\beta_6 = & \frac{125 E_0^3}{22639104 K_0^5} \left(\frac{386136 E_0^3}{K_0^3} - 2 \frac{E_0^2}{K_0^2} (1091094\alpha + 44131) - 25 \frac{E_0}{K_0} (97608\alpha^2 - 262642\alpha + \right. \\
& \left. + 61109) + 625(\alpha - 1)(3656\alpha^2 + 4190\alpha - 1911) \right), \\
\beta_8 = & \frac{125 E_0^4}{24631345152 K_0^7} \left(\frac{113548800 E_0^4}{K_0^4} - 4 \frac{E_0^3}{K_0^3} (464953518\alpha - 134090393) + \right. \\
& + 25 \frac{E_0^2}{K_0^2} (582220340\alpha^2 - 282803792\alpha + 15406827) + 625 \frac{E_0}{K_0} (31897184\alpha^3 - 87603958\alpha^2 \\
& \left. + 49562507\alpha - 7217483) - 31250(\alpha - 1)(216336\alpha^3 + 630596\alpha^2 - 596608\alpha + 113937) \right), \\
\gamma_2 = & \frac{13 E_0^2}{136 K_0^2} \left(\frac{48 E_0}{K_0} + 50\alpha - 75 \right), \\
\gamma_4 = & \frac{13 E_0^3}{73984 K_0^4} \left(\frac{59808 E_0^2}{K_0^2} + \frac{200 E_0}{K_0} (86\alpha - 663) - 625(28\alpha + 37)(2\alpha - 3) \right), \\
\gamma_6 = & \frac{13 E_0^4}{45278208 K_0^6} \left(\frac{52068864 E_0^3}{K_0^3} - \frac{600 E_0^2}{K_0^2} (176050\alpha + 179049) - \frac{1250 E_0}{K_0} (56324\alpha^2 - \right. \\
& \left. - 234744\alpha - 26877) + 15625(2\alpha - 3)(1912\alpha^2 + 3460\alpha - 471) \right), \\
\gamma_8 = & \frac{13 E_0^4}{45278208 K_0^6} \left(\frac{52068864 E_0^4}{K_0^4} - \frac{19200 E_0^3}{K_0^3} (13948348\alpha + 4637301) + \frac{2500 E_0^2}{K_0^2} (226322592\alpha^2 + \right. \\
& \left. + 144240370\alpha + 705225) + \frac{15625 E_0}{K_0} (35006416\alpha^3 - 122923916\alpha^2 + 29552956\alpha - 1486725) - \right. \\
& \left. - (390625(2\alpha - 3))(236544\alpha^3 + 833020\alpha^2 - 455825\alpha + 49755) \right).
\end{aligned}$$

Representing (11)–(13) as a power series at $t = 0$

$$U_2 = \bar{\alpha}_0 + \bar{\alpha}_1 t + \bar{\alpha}_2 t^2 + \bar{\alpha}_3 t^3 + \bar{\alpha}_4 t^4 + \bar{\alpha}_5 t^5 + \bar{\alpha}_6 t^6 + \bar{\alpha}_7 t^7 + \bar{\alpha}_8 t^8 + o(t^8), \quad (17)$$

$$K = \bar{\beta}_0 + \bar{\beta}_1 t + \bar{\beta}_2 t^2 + \bar{\beta}_3 t^3 + \bar{\beta}_4 t^4 + \bar{\beta}_5 t^5 + \bar{\beta}_6 t^6 + \bar{\beta}_7 t^7 + \bar{\beta}_8 t^8 + o(t^8), \quad (18)$$

$$E = \bar{\gamma}_0 + \bar{\gamma}_1 t + \bar{\gamma}_2 t^2 + \bar{\gamma}_3 t^3 + \bar{\gamma}_4 t^4 + \bar{\gamma}_5 t^5 + \bar{\gamma}_6 t^6 + \bar{\gamma}_7 t^7 + \bar{\gamma}_8 t^8 + o(t^8), \quad (19)$$

where

$$\bar{\alpha}_0 = u_1 + u_2 + u_3 + u_4 + u_5 + u_6 + u_7, \quad \bar{\alpha}_1 = -\frac{1}{7}(10u_1 + 17u_2 + 20u_3 + 24u_4 + 27u_5 + 30u_6 + 31u_7),$$

$$\bar{\alpha}_2 = \frac{1}{49}(15u_1 + 85u_2 + 130u_3 + 204u_4 + 270u_5 + 345u_6 + 372u_7),$$

$$\begin{aligned}
\bar{\alpha}_3 &= \frac{1}{343}(20u_1 - 85u_2 - 260u_3 - 680u_4 - 1170u_5 - 1840u_6 - 2108u_7), \\
\bar{\alpha}_4 &= \frac{1}{2401}(55u_1 - 85u_2 - 65u_3 + 510u_4 + 1755u_5 + 4140u_6 + 5270u_7), \\
\bar{\alpha}_5 &= \frac{1}{16807}(198u_1 - 187u_2 - 104u_3 + 408u_4 + 351u_5 - 1656u_6 - 3162u_7), \\
\bar{\alpha}_6 &= \frac{1}{117649}(825u_1 - 561u_2 - 260u_3 + 748u_4 + 468u_5 - 1380u_6 - 2108u_7), \\
\bar{\alpha}_7 &= \frac{1}{5764801}(26400u_1 - 14025u_2 - 5720u_3 + 13464u_4 + 7020u_5 - 16560u_6 - 23188u_7), \\
\bar{\alpha}_8 &= \frac{1}{40353607}(128700u_1 - 6100u_2 - 20735u_3 + 42075u_4 + 19305u_5 - 39330u_6 - 52173u_7), \\
\bar{\beta}_0 &= k_1 + k_2 + k_3 + k_4 + k_5 + k_6 + k_7, \quad \bar{\beta}_1 = -\frac{1}{7}(10k_1 + 17k_2 + 20k_3 + 24k_4 + 27k_5 + 30k_6 + 31k_7), \\
\bar{\beta}_2 &= \frac{1}{49}(15k_1 + 85k_2 + 130k_3 + 204k_4 + 270k_5 + 345k_6 + 372k_7), \\
\bar{\beta}_3 &= \frac{1}{343}(20k_1 - 85k_2 - 260k_3 - 680k_4 - 1170k_5 - 1840k_6 - 2108k_7), \\
\bar{\beta}_4 &= \frac{1}{2401}(55k_1 - 85k_2 - 65k_3 + 510k_4 + 1755k_5 + 4140k_6 + 5270k_7), \\
\bar{\beta}_5 &= \frac{1}{16807}(198k_1 - 187k_2 - 104k_3 + 408k_4 + 351k_5 - 1656k_6 - 3162k_7), \\
\bar{\beta}_6 &= \frac{1}{117649}(825k_1 - 561k_2 - 260k_3 + 748k_4 + 468k_5 - 1380k_6 - 2108k_7), \\
\bar{\beta}_7 &= \frac{1}{5764801}(26400k_1 - 14025k_2 - 5720k_3 + 13464k_4 + 7020k_5 - 16560k_6 - 23188k_7), \\
\bar{\beta}_8 &= \frac{1}{40353607}(128700k_1 - 6100k_2 - 20735k_3 + 42075k_4 + 19305k_5 - 39330k_6 - 52173k_7), \\
\bar{\gamma}_0 &= e_1 + e_2 + e_3 + e_4 + e_5 + e_6 + e_7, \quad \bar{\gamma}_1 = -\frac{1}{7}(13e_1 + 20e_2 + 23e_3 + 27e_4 + 30e_5 + 33e_6 + 34e_7), \\
\bar{\gamma}_2 &= \frac{1}{49}(39e_1 + 130e_2 + 184e_3 + 270e_4 + 345e_5 + 429e_6 + 459e_7), \\
\bar{\gamma}_3 &= \frac{1}{343}(13e_1 - 260e_2 - 552e_3 - 1170e_4 - 1840e_5 - 2717e_6 + 3060e_7), \\
\bar{\gamma}_4 &= \frac{1}{2401}(26e_1 - 65e_2 + 276e_3 + 1755e_4 + 4140e_5 + 8151e_6 + 9945e_7), \\
\bar{\gamma}_5 &= \frac{1}{16807}(78e_1 - 104e_2 + 276e_3 + 351e_4 - 1656e_5 - 8151e_6 - 11934e_7), \\
\bar{\gamma}_6 &= \frac{1}{117649}(286e_1 - 260e_2 + 552e_3 + 468e_4 - 1380e_5 - 2717e_6 - 1989e_7), \\
\bar{\gamma}_7 &= \frac{1}{5764801}(8294e_1 - 5720e_2 + 10488e_3 + 7020e_4 - 16560e_5 - 24453e_6 - 15912e_7), \\
\bar{\gamma}_8 &= \frac{1}{40353607}(37323e_1 - 20735e_2 + 34086e_3 + 19305e_4 - 39330e_5 - 48906e_6 - 29835e_7),
\end{aligned}$$

and equating like powers of t in (14)–(16) and (17)–(19), the system of 27 algebraic equations with 20 unknowns α , β , U_0 , K_0 , E_0 , u_i , k_i , e_i , $i = 1, \dots, 7$ is obtained. The equation for E at t^8 is omitted. This system of algebraic equations is solved numerically. The solution of this system is facilitated because (6) is split off from (7) and (8). The described procedure is initially applied to equations (7) and (8) to find

$$\alpha = 0.2208287460, \quad K_0 = 0.7998977201, \quad E_0 = 0.9205281496, \quad k_1 = 4.111142059,$$

$$\begin{aligned}
k_2 &= -22.05686118, & k_3 &= 40.76497218, & k_4 &= -49.00284702, & k_5 &= 43.42154950, \\
k_6 &= -31.82206053, & k_7 &= 15.38400271, & e_1 &= 10.09175704, & e_2 &= -85.15426605, \\
e_3 &= 173.9330323, & e_4 &= -224.1225187, & e_5 &= 205.3920322, & e_6 &= -154.4430672, \\
e_7 &= 75.22355867.
\end{aligned}$$

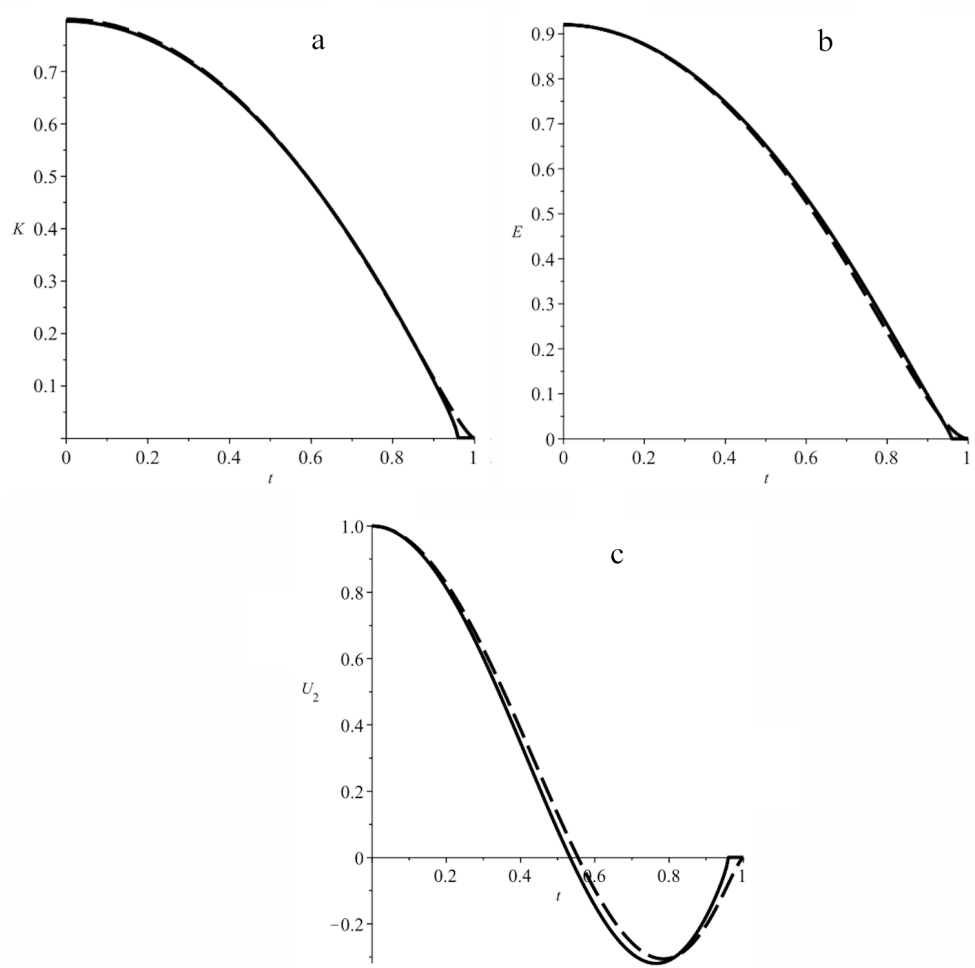


Fig. 1. Profiles of approximate and numerical solutions: a — the kinetic energy of turbulence; b — the kinetic energy dissipation rate; c — the deficit of the longitudinal averaged velocity component; solid lines — numerical solution, dotted lines — approximate solution

Obtained values are unique, taking into account (9), (10) and conditions

$$\alpha, K_0, E_0 > 0; \quad K'(t), E'(t) < 0, \quad t \in (0, 1).$$

Further, equation (6) is considered in a similar way and the following values are determined:

$$\begin{aligned}
U_0 &= 1, & \beta &= -1.698508059, & u_1 &= -10.17461628, & u_2 &= 101.0215753, & u_3 &= -191.1549873, \\
u_4 &= 238.1557643, & u_5 &= -197.6563167, & u_6 &= 79.67680195, & u_7 &= -18.86822130.
\end{aligned}$$

In order to increase accuracy one of the algebraic equations for determining coefficients of asymptotic expansion (11) is replaced by integral relation (4).

The obtained values α , K_0 , and E_0 are used to solve boundary value problem (6)–(10) by the shooting method. As a result of numerical calculations the following values were found: $K_0 = 0.79617$, $E_0 = 0.92053$, and $\beta = -1.822$. The difference between approximate and numerical solutions does not exceed 5% (see Fig. 1).

Thus, at large distance behind the body the flow in an axisymmetric momentumless turbulent wake is characterized by the following laws of similarity degeneration: $U_1(x, 0) \sim x^{-1.822}$, $e(x, 0) \sim x^{-1.558}$, $\varepsilon(x, 0) \sim x^{-2.558}$, $l \sim x^{0.221}$ (l is the width of the wake). The established laws are consistent with those presented in [12,17,21,22,].

The author is grateful to Professor O. V. Kaptsov and Professor G. G. Chernykh for their attention to the work.

This work is supported by the Krasnoyarsk Mathematical Center and financed by the Ministry of Science and Higher Education of the Russian Federation in the framework of the establishment and development of regional Centers for Mathematics Research and Education (Agreement no. 075-02-2023-912).

References

- [1] E.Naudascher, Flow in the wake of self-propelled bodies and related sources of turbulence, *J. Fluid Mech.*, **22**(1965), no. 4, 625–656.
- [2] A.S.Ginevskiy, Theory of turbulent wakes and jets (Teoriya turbulentnyh sledov i struy), Moscow, Mashinostroenie, 1969 (in Russian).
- [3] N.V.Alekseenko, V.A.Kostomaha, Experimental research axisymmetric momentumless turbulent jet flow, *Prikl. Mekh. i Tekhn. Fiz.*, (1987), no. 1, 65–69 (in Russian).
- [4] H.Higuchi, T.Kubota, Axysymmetric wakes behind a slender body including zeromomentum configurations, *Phys. Fluids*, **2**(1990), no. 9, 1615–1623.
- [5] A.I.Sirviente, V.Patel, Wake of a self-propelled body. Part 1: Momentumless wake, *AIAA J.*, **38**(2000), no. 4, 613–619. DOI:10.2514/2.1032
- [6] J.A.Schetz, Injection and mixing in turbulent flow, Progr. In Astronautics and Aeronautics, Vol. 68, 1980.
- [7] M.L.Finson, Similarity behaviour of momentumless turbulent wakes, *J. Fluid Mech.*, **71**(1975), no. 3, 465–479.
- [8] V.A.Sabelnikov, On some features of turbulent flows with zero excess momentum (O nekotoryh osobennostyah turbulentnyh techeniy s nulevym izbytochnym impulsom), *Uch. Zap. TsAGI*, **6**(1975), no. 4, 71–74 (in Russian).
- [9] V.A.Gorodtsov, Similarity and weak closing relations for symmetric free turbulence, *Fluid Dyn.*, **14**(1979), no. 1, 31–37.
- [10] S.Hassid, Similarity and decay laws of momentumless wakes, *Phys. Fluids*, **23**(1980), no. 2, 404–405.

-
- [11] J.Piquet, Turbulent flows. Models and physics, Berlin, Heidelberg: Springer-Verlag, 1999.
- [12] V.Maderich, S.Konstantinov, Asymptotic and numerical analysis of momentumless turbulent wakes, *Fluid Dyn. Res.*, **41**(2010), 25. DOI: 10.1088/0169-5983/42/4/045503
- [13] B.A.Kolovandin, N.N.Luchko, Numerical modeling of the turbulent velocity field of an axisymmetric impulse-free wake (Chislennoe modelirovanie turbulentnogo polya skorosti osesimmetrichnogo bezypulsnogo sleda), *Teplomassoobmen-6*, Minsk, ITMO AN BSSR, **1**(1980), no. 2, 126–135 (in Russian).
- [14] G.G.Chernykh, N.N.Fedorova, V.A.Kostomakha, N.V. Lesnova, Experimental and numerical simulation of turbulent axisymmetric momentumless wake behind sphere, Proc. of ICMAR 92, Novosibirsk, Inst. of Theor. and Appl. Mech., 1992, no. 1, 30–33.
- [15] G.G.Chernykh, A.G.Demenkov, N.N.Fedorova, Numerical models of a plane and axisymmetric turbulent wakes in homogeneous fluid, Proc. of ICMAR 94, Novosibirsk, 1994, Pt. 2, 76–81.
- [16] O.F.Voropaeva, The numerical investigation of momentumless turbulent wakes behind sphere based on semi-empirical turbulence models of second order, *Computational Technology*, **7**(2002), no. 2, 11–23 (in Russian).
- [17] O.F.Voropaeva, The numerical modelling of the far momentumless axisymmetric turbulent wake, *Computational Technology*, **8**(2003), no. 2, 36–52 (in Russian).
- [18] G.I.Barenblatt, Similarity, self-similarity and intermediate asymptotics, New York, Plenum, 2003.
- [19] O.F.Voropaeva, Far momentumless turbulent wake in a passively stratified medium, *Computational Technology*, **8**(2003), no. 3, 32–46 (in Russian).
- [20] O.V.Kaptsov, A.V.Schmidt, Application of the B-determining equations method to one problem of free turbulence, *SIGMA*, **8**(2012), 073. DOI: 10.3842/SIGMA.2012.073
- [21] O.V.Kaptsov, A.V.Fomina, G.G.Chernykh, et al., Self-similar decay of the momentumless turbulent wake in a passive stratified medium, *Math. Modell.*, **27**(2015), no. 1, 84–98 (in Russian).
- [22] O.V.Kaptsov, A.V.Schmidt, A three-dimensional semi-empirical model of a far turbulent wake, *J. of Appl. Math. and Mech.*, **79**(2015), no. 5, 459–466.
DOI: 10.1016/J.JAPPMATHMECH.2016.03.007
- [23] L.V.Ovsyannikov, Group analysis of differential equations, New York, Academic Press, 1982.
- [24] O.V.Kaptsov, B-determining equations: applications to nonlinear partial differential equations, *Euro. J. Appl. Math.*, **6**(1995), 265–286. DOI: 10.1017/S0956792500001832
- [25] A.V.Schmidt, Approximate solution for a flow in the far flat momentumless turbulent wake, *Prikl. Mekh. i Tekhn. Fiz.*, **64**(2023), 53–59 (in Russian). DOI: 10.15372/PMTF202215204
- [26] W.Rodi, Examples of calculation methods for flow and mixing in stratified fluids, *J. Geophys. Res.*, **92**(1987), no. 5, 5305–5328.

- [27] O.F.Voropaeva, Yu.D.Chashechkin, G.G. Chernykh, Diffusion of a passive admixture from a local source in a turbulent mixing zone, *Fluid Dyn.*, **32**(1997), no. 2, 212–218.
- [28] G.G.Chernykh., O.F.Voropayeva, Numerical modeling of momentumless turbulent wake dynamics in a linearly stratified medium, *Computers and Fluids*, **28**(1999), no. 3, 281–306.
- [29] N.P.Moshkin, A.V.Fomina, G.G.Chernykh, Numerical modeling of the dynamics of a turbulent wake behind a towed body in a linearly stratified medium (Chislenoe modelirovanie dinamiki turbulentnogo sleda za buksiruемым телом в линейно stratifitsirovannoi srede), *Matem. Modelirovanie*, **19**(2007), no. 1, 29–56.

Приближенное решение модели дальнего безымпульсного осесимметричного турбулентного следа

Алексей В. Шмидт

Институт вычислительного моделирования СО РАН
Красноярск, Российская Федерация

Аннотация. Для описания течения в дальнем осесимметричном безымпульсном турбулентном следе привлекается модель, основанная на $k - \varepsilon$ модели турбулентности. Выполнен теоретико-групповой анализ модели. Получена автомодельная редукция уравнений модели к системе обыкновенных дифференциальных уравнений. Для построения приближенного решения соответствующей краевой задачи используется асимптотическое разложение решения в окрестности особой точки.

Ключевые слова: дальний безымпульсный осесимметричный турбулентный след, приближенное решение, асимптотическое разложение.

EDN: MDLPVA

УДК 538.9

A Study of the Scaling Behavior of the Two-dimensional Ising Model by Methods of Machine Learning

Alina A. Chubarova*

Marina V. Mamonova[†]

Dostoevsky Omsk State University
Omsk, Russian Federation

Pavel V. Prudnikov[‡]

Center of New Chemical Technologies BIC
Boreskov Institute of Catalysis SB RAS
Omsk, Russian Federation

Received 10.09.2023, received in revised form 30.10.2023, accepted 27.01.2024

Abstract. In the field of condensed matter physics, machine learning methods have become an increasingly important instrument for researching phase transitions. Here we present a method for calculating the universal characteristics of spin models using an Ising model that is exactly solvable in two dimensions. The method is based on a convolutional neural network (CNN) with controlled learning. The scaling functions prove the continuing type of phase transition for the 2D Ising model. As a result of the proposed technique, it has been possible to calculate correlation length directly.

Keywords: machine learning, convolutional neural networks, Monte Carlo methods, Ising model, scaling, correlation length, magnetic susceptibility.

Citation: A.A. Chubarova, M.V. Mamonova, P.V. Prudnikov, A Study of the Scaling Behavior of the Two-dimensional Ising Model by Methods of Machine Learning, J. Sib. Fed. Univ. Math. Phys., 2024, 17(2), 238–245. EDN: MDLPVA.



Machine learning methods over the last few years have proved as a good tool for analysing multicomponent complex systems [1–3]. Different machine learning methods have been developed for study such systems [4–6]. Convolutional neural networks (CNN) [7] are traditionally used to investigate phase transition classification problems where no prior knowledge is assumed. This method is well applicable to any spin models [8,9] also.

Machine learning methods look like a "black box" and the typical problem is "how to prove CNN classification without traditional methods". Machine learning can test a fundamental features of critical phenomena [10, 11], such as the long-range ordering and scaling.

Using the two-dimensional Ising model [12] as a basis for analysing the critical behavior of a spin system, we propose an alternative methodology for studying the critical behaviour of spin systems through the use of machine learning techniques [12].

*ChubarovaAA@omsu.ru <https://orcid.org/0009-0009-0414-1963>

[†]MamonovaMV@omsu.ru <https://orcid.org/0000-0001-7466-086X>

[‡]prudnikp@ihcp.ru <https://orcid.org/0000-0002-6522-2873>

© Siberian Federal University. All rights reserved

1. Model and methods

We calculate the system using the classical representation. Ising model Hamiltonian with spin states $S = \pm 1$ on a square lattice.

$$H = -\frac{J}{2} \sum_{\langle i,j \rangle}^N S_i S_j, \tag{1}$$

where $J = 1$ is the exchange interaction constant, $J > 0$ for the ferromagnetic model. A linear lattice size of L determines the number of spins in the system, and $N = L \times L$.

We used a CNN model with controlled learning to study the universal characteristics of spin systems. This CNN model is divided into two sets of convolutional layers by a pooling layer — followed by a dense layer with a softmax activation function. The neural network output layer contains two nodes whose values are real numbers in the interval $[0;1]$ and correspond to the probability of detecting the system state in the high-temperature (HT, $T > T_C$) or low-temperature (LT, $T < T_C$) phases.

$$M^\infty = \begin{cases} 1, & T < T_c - \text{low-temperature phase, (LT)} \\ 0, & T > T_c - \text{high-temperature phase, (HT)} \end{cases}. \tag{2}$$

A supervised type of training is used, for which a large number of configurations are generated. The neural network training process was performed on the data set of correlation matrices, the values of which were determined for each spin configuration. The correlation matrices were obtained using the next equation (3).

$$C_i = \frac{1}{2} (S_{x,y} S_{x+L/2,y} + S_{x,y} S_{x,y+L/2}), \tag{3}$$

where the correlation function takes into account the interaction of spins at a distance equal to half of the lattice.

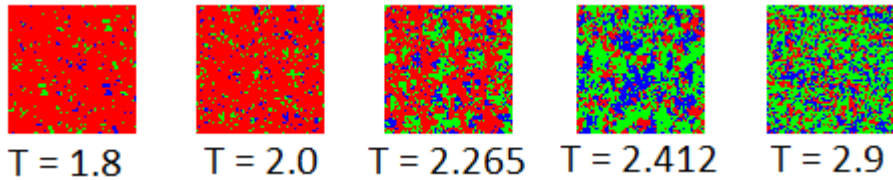


Fig. 1. Example of correlation matrices for training a neural network at different temperatures for linear size $L = 64$

The Binder cumulant of 4-th order (4), which is commonly used to find the critical temperature, was taken to construct the scaling relationship by Monte Carlo methods.

$$U_4(T) = \frac{1}{2} \left[3 - \frac{\langle m^4 \rangle}{\langle m^2 \rangle^2} \right]. \tag{4}$$

The methodology proposed for the calculation of universal characteristics using CNNs allows us to calculate the correlation length function [10] describing the stepped recession near the critical point of the phase transition.

The results obtained with CNN were compared with the results of classical Monte Carlo calculations to confirm the correctness of the results obtained with the help of CNN. The correlation length function is presented in the equation (5).

$$\xi/L = \frac{1}{2 \sin \frac{\pi}{2}} \sqrt{\frac{\langle M^2 \rangle}{\langle \Phi \rangle}}, \quad (5)$$

where

$$\Phi = \frac{1}{2} \sum_{n=1}^2 \left| \sum_i S_i e^{iq_n x_{nj}} \right|^2. \quad (6)$$

The method proposed by us also allowed us to calculate the temperature dependence of the magnetic susceptibility

$$\chi(T) = \frac{1}{N} \frac{\langle m^2 \rangle - \langle m \rangle^2}{T} \quad (7)$$

a comparison with the classical calculations (eq. 7) was also carried out to check the correctness of the CNN results [10].

The calculation of two cases was carried out to verify the successful applicability of the proposed methodology and to identify the distinctive features of machine learning techniques:

- A low number of temperature steps (150) and a large number of Monte Carlo steps for relaxation (30 000 MCS/s) and averaging (50 000 MCS/s).
- A large number of temperature steps (2 000) and a small number of Monte Carlo steps for relaxation (3 000 MCS/s) and averaging (5 000 MCS/s).

The training dataset consisted of 200 statistical configurations, of which training was performed on 100 configurations.

2. Result of machine learning technique

Using the predicted values from the low-temperature phase, the scaling function, correlation lengths, and magnetic susceptibility calculations have been developed based on the low-temperature phase. We carried out the calculations using classical Monte Carlo methods, including the Metropolis algorithm, simultaneously with the derivation of the correlation matrices [13].

Fig. 2 and Fig. 3 show the scaling functions for different modeling cases. It can be clearly seen that for the two cases, the constructed scaling dependencies reflect the universal behavior of the model at different linear dimensions. It is worth noting that the smoothest function is observed in the case of a large number of temperature steps and small Monte Carlo times.

As a result of the calculations of scaling dependency, we have been able to demonstrate that machine learning methods are able to demonstrate universality in the same way that Monte Carlo calculations can demonstrate universality. The convolutional neural network on the other hand requires more temperature steps for smooth dependence as well as a small number of time steps, which results in a significant reduction in the calculation time of the model.

Using machine learning methods, we studied universal features of the spin model, and were able to find dependences between correlation length and magnetic susceptibility. These thermodynamic quantities provide a detailed description of the behavior of the system near the phase transition.

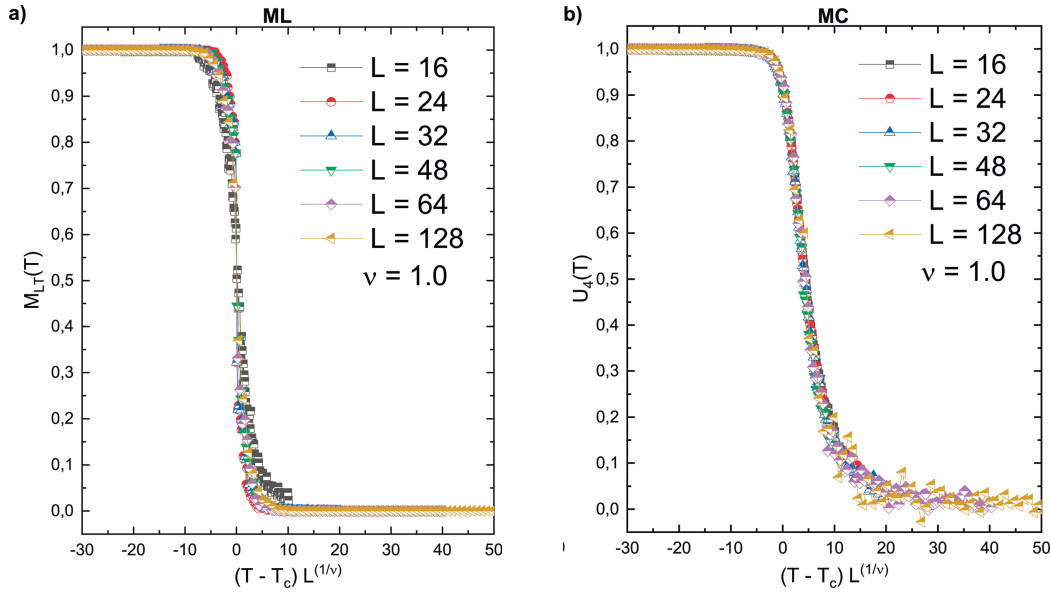


Fig. 2. The scaling relationships of the two-dimensional Ising model for 150 temperature steps constructed: a) by machine learning methods; b) by Monte Carlo methods

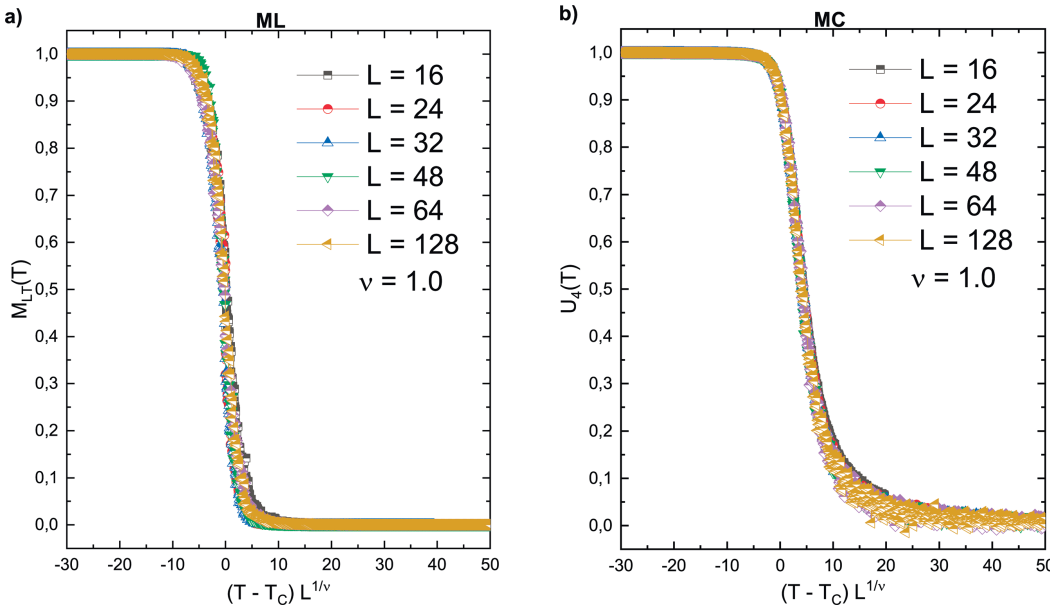


Fig. 3. The scaling relationships of the two-dimensional Ising model for 2000 temperature steps, constructed: a) by machine learning methods; b) by Monte Carlo methods

Figs. 4 and 5 show the correlation length calculations for each linear dimension for the two cases considered. It is worth noting that in both cases considered, the machine learning method performs well, although it is subject to fluctuation effects. The influence of fluctuations is much smaller in the case of a large number of temperature steps.

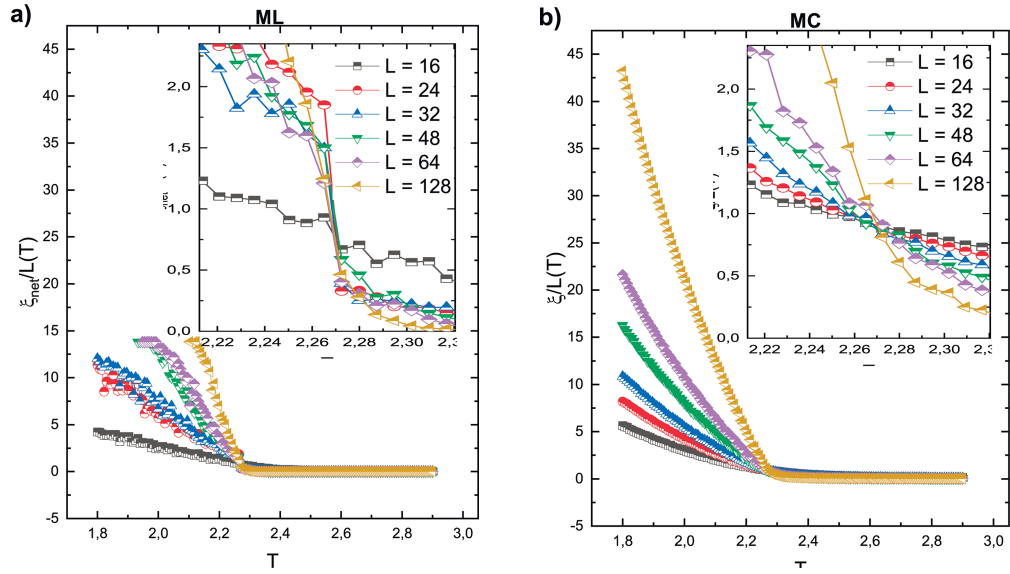


Fig. 4. The temperature relationships of the functions ξ_{net}/L and ξ/L for 150 temperature steps, plotted using: a) machine learning methods; b) Monte Carlo methods

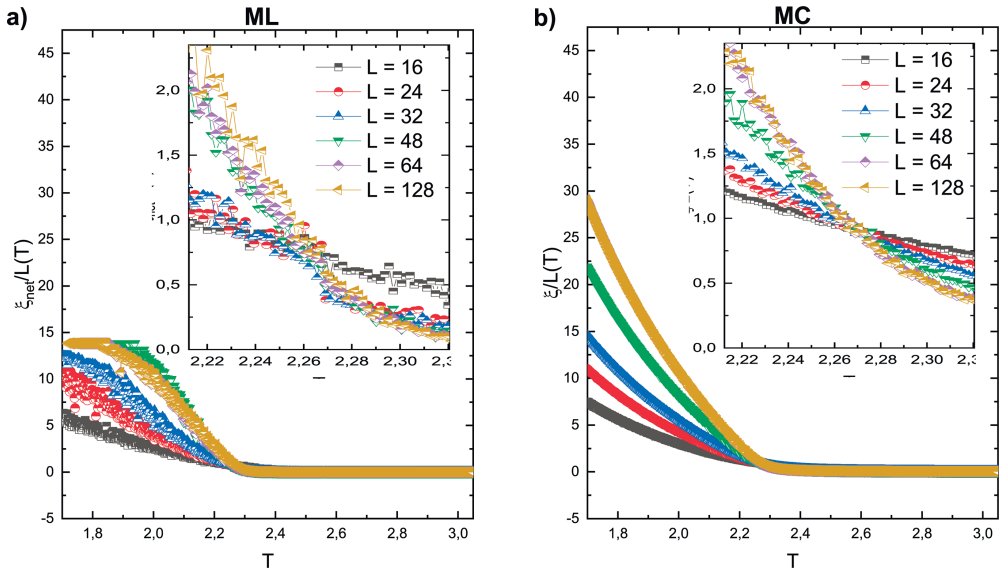


Fig. 5. The temperature relationships of the functions ξ_{net}/L and ξ/L for 2000 temperature steps, plotted using: a) machine learning methods; b) Monte Carlo methods

In constructing the temperature dependence of magnetic susceptibility (Fig. 6 and Fig. 7), it was noticed that CNNs show rather high peaks in the critical temperature region compared to the Monte Carlo results. It is worth noting that the machine learning results weakly demonstrate a property of the two-dimensional Ising model — as the linear size increases, there is a noticeable shift on the temperature scale to the exact value.

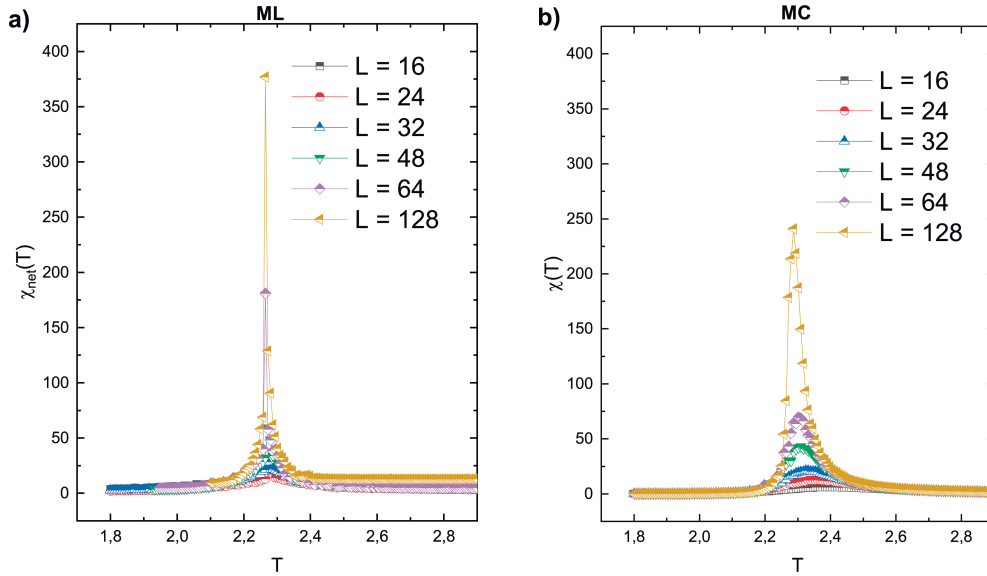


Fig. 6. The temperature relationships of the susceptibility $\chi_{net}(T)$ and $\chi(T)$ near the critical temperature for 150 temperature steps, constructed a) by machine learning methods; b) by Monte Carlo methods

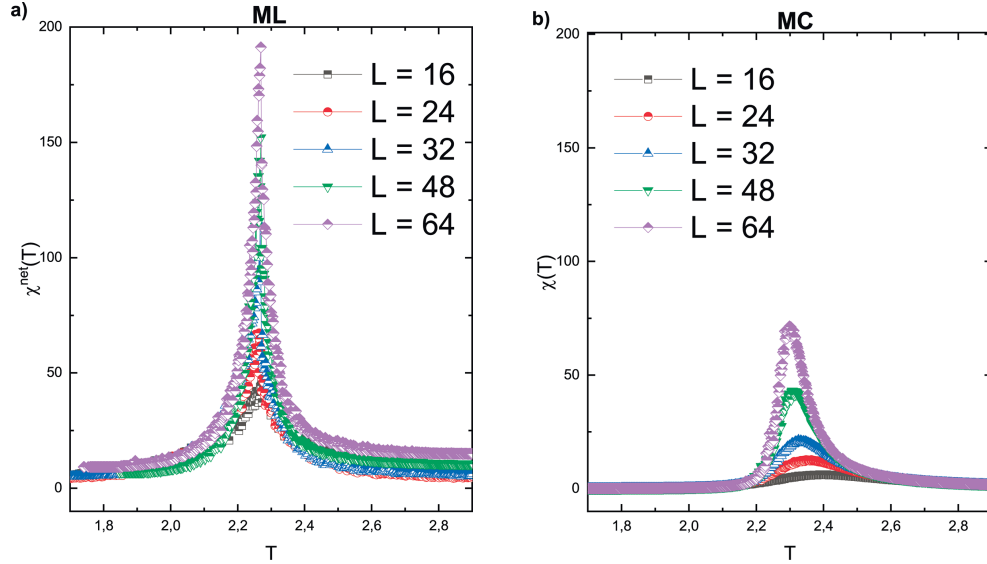


Fig. 7. The temperature relationships of the susceptibility $\chi_{net}(T)$ and $\chi(T)$ near the critical temperature for 2000 temperature steps, constructed a) by machine learning methods; b) by Monte Carlo methods

Conclusion

A universal technique for calculating the universal characteristics of spin systems is presented in the paper by using the method of convolutional neural networks on the example of a two-dimensional Ising model to calculate the universal characteristics of spin systems. A study that

was carried out on spin systems uncovered that machine learning methods were an excellent tool for studying those systems. It was found that when classical calculations were compared to machine learning methods, it took significantly less time for the machine learning methods to make the universal characteristics calculations compared to classical calculations. Using the proposed method, in order to reflect the continuity of the phase transition, a scaling dependence was developed in order to reflect the continuity of the phase transition. This study was carried out using the CNN method in order to calculate the thermodynamic dependence of the correlation length and magnetic susceptibility.

The reported study was supported by the Russian Science Foundation through project no. 23-22-00093. Pavel V. Prudnikov acknowledged for the supporting by the Ministry of Science and Higher Education of the Russian Federation within the governmental order for Boreskov Institute of Catalysis (project FWUR-2024-0039).

References

- [1] F.A.Gomez Albarracin, H.D.Rosales, Machine learning techniques to construct detailed phase diagrams for skyrmion systems, *Phys. Rev. B*, **105**(2022), 214423.
DOI: 10.1103/PhysRevB.105.214423
- [2] W.Wang, Z.Wang, Y.Zhang, B.Sun, K.Xia, Learning Order Parameters from Videos of Skyrmion Dynamical Phases with Neural Networks, *Phys. Rev. V.*, **16**(2021), 014005.
DOI: 10.1103/PhysRevApplied.16.014005
- [3] M.Kumar, V.Banerjee, S.Puri, M.Weigel, Critical behavior of the three-state random-field Potts model in three dimensions, *Phys. Rev. Res.*, **4**(2022), L042041.
DOI: 10.1103/PhysRevResearch.4.L042041
- [4] C.W.Glass, A.R.Oganov, N.Hansen, USPEX – evolutionary crystal structure prediction, *Comp. Phys. Comm.*, **175**(2006), 713-720. DOI: 10.1016/j.cpc.2006.07.020
- [5] C.W.Glass, A.R.Oganov, Crystal structure prediction using ab initio evolutionary techniques: Principles and application, *J. Chem. Phys.*, **124**(2006), 244704. DOI: 10.1063/1.2210932
- [6] K.Shiina, H.Mori, Y.Okabe, H.K.Lee, Machine-Learning Studies on Spin Models, *Sci. Rep.*, **10**(2020), 2177. DOI: 10.1038/s41598-020-58263-5
- [7] A.Azizi, M.Pleimling, A cautionary tale for machine learning generated configurations in presence of a conserved quantity, *Sci. Rep.*, **11**(2021), 6395.
DOI: 10.1038/s41598-021-85683-8
- [8] A.Tanaka, A.Tomiya, A cautionary tale for machine learning generated configurations in presence of a conserved quantity, *J. Phys. Soc. Jpn.*, **86**(2017), 063001.
- [9] S.J.Wetzel, M.Scherzer, Machine Learning of Explicit Order Parameters: From the Ising Model to SU(2) Lattice Gauge Theory, *Phys. Rev. B*, **96**(2017), 184410.
DOI: 10.1103/PhysRevB.96.184410
- [10] N.Maskara, M.Buchhold, M.Endres, E. van Nieuwenburg, Learning algorithm relecting universal scaling behavior near phase transitions, *Phys. Rev. Res.*, **4**(2022), L022032.
DOI: 10.1103/PhysRevResearch.4.L022032

- [11] D.A.Martin, T.L.Ribeiro, and etc., Box-scaling as a proxy of finite-size correlations, *Sci. Rep.*, **11**(2020), 15937. DOI: 10.1038/s41598-021-95595-2
- [12] Ju.V.Mikhailova, V.P.Krainov, R.O.Zaitsev, Two-dimensional Ising model (exact solution), Moscow: MIPT, 2015.
- [13] N.Metropolis, A.W.Rosenbluth, M.N.Rosenbluth, A.H.Teller, E.Teller, Equations of State Calculations by Fast Computing Machines, *J. Chem. Phys.*, **21**(1953), 1087.

Исследование скейлингового поведения двумерной модели Изинга методами машинного обучения

Алина А. Чубарова
Марина В. Мамонова

Омский государственный университет им. Ф. И. Достоевского
Омск, Российская Федерация

Павел В. Прудников

Центр новых химических технологий
Институт катализа им. Г. К. Борескова СО РАН
Омск, Российская Федерация

Аннотация. Методы машинного обучения стали новым быстро набирающим инструментом для исследования фазовых переходов в физике конденсированного состояния. В данной работе представлен метод расчета универсальных характеристик спиновых моделей на основе двумерной модели Изинга. Метод основан на использовании сверточной нейронной сети (CNN) с контролируемым обучением. Функции скейлинга доказывают непрерывный тип фазового перехода для двумерной модели Изинга. В результате применения предложенной методики стало возможным вычисление корреляционной длины.

Ключевые слова: машинное обучение, сверточные нейронные сети, методы Монте–Карло, модель Изинга, скейлинг, корреляционная длина, магнитная восприимчивость.

EDN: NUTSKE

УДК 621.38

Analysis of the Electric Current Distribution in a Three-Layer Conductive Structure

Alexey A. Levitskiy*
Pavel S. Marinushkin†
Valentina A. Bakhtina‡
Siberian Federal University
Krasnoyarsk, Russian Federation

Received 18.09.2023, received in revised form 24.10.2023, accepted 14.01.2024

Abstract. The paper presents an analytical model allowing to investigate the electric current distribution in a three-layer conductive structure. The proposed model takes into account the characteristics of the three conductive layers and the transient resistances between them. Expressions for the current distribution and electric potential variation along the structure, as well as its total resistance are obtained. In addition, quantitative estimates showing the features of the electric current redistribution between the layers with alteration of the layers parameters are presented.

Keywords: three-layer conductive structure, current distribution, resistance, specific contact resistivity, transmission line method.

Citation: A.A. Levitskiy, P.S. Marinushkin, V.A. Bakhtina, Analysis of the Electric Current Distribution in a Three-Layer Conductive Structure, J. Sib. Fed. Univ. Math. Phys., 2024, 17(2), 246–256. EDN: NUTSKE.



The study of the current flow processes in multilayer conductive structures is of great interest in a number of areas, both in scientific and applied terms. The papers [1–10] present an analysis of the electric current distribution in two-layer conductive structures as applied to semiconductor devices based on analytical one-dimensional models using the so-called transmission line method (TLM). In most of these works, the main objects of analysis are planar metal-semiconductor contacts and the static current distribution, and the dependence of the contact resistance on the geometric and electrical parameters of the structure are studied. One of the layers of the model is a metal, which is usually considered as an ideal conductor having zero resistance. The second layer is a semiconductor, which conductive properties are described by the specific volume resistance. These models also take into account the specific contact resistance between metal and semiconductor layers.

In [2] an attempt is made to take into account in the TLM model the contribution of capacitance between a metal and a semiconductor separated by an interface layer. In [3] a sufficiently detailed description of TLM models of semiconductor structures is given both in the region of planar metal-semiconductor contacts and a two-layer silicide-semiconductor structure in the interelectrode region. Model for integrated circuit contacts in [4] is built taking into account the resistance of the metal layer. In [5–10] a planar contact model taking into account the longitudinal resistance of the metal-semiconductor transition layer is presented. Accordingly, the resistance of the metal-transition layer and the transition layer-semiconductor are taken into account separately.

*alevitskiy@sfu-kras.ru <https://orcid.org/0000-0003-3179-9743>

†pmarinushkin@sfu-kras.ru <https://orcid.org/0000-0001-7510-526X>

‡vbachtina@sfu-kras.ru

Similar problems of constructing models of the electric current flow are also of interest in the study of processes in the human skin and muscle tissues in relation to electromyography and electrical stimulation [11–14]. In this case, the human skin is considered as a multilayer conductive structure. An attempt to build an analytical model of current flow for the skin, similar to the TLM models described above, is presented in [12, 13]. However, the results of the distribution of electric current in the human skin in [11–14] were obtained only on the basis of a numerical model.

In this paper, an analytical model is proposed that describes the flow of electric current in a three-layer conducting structure. Such analytical formulation has not been discussed previously and is suitable for solving research problems associated with any of the mentioned applied fields.

1. Problem Formulation

Consider the model of a three-layer structure shown in Fig. 1. Three conductive layers are highlighted in the figure. The indexes of the variables in the figure are assigned in accordance with the conditional numbers of the conductive layers: 1 is the top layer; 2 – the second (middle) layer; 3 – the third (the lowest) layer.

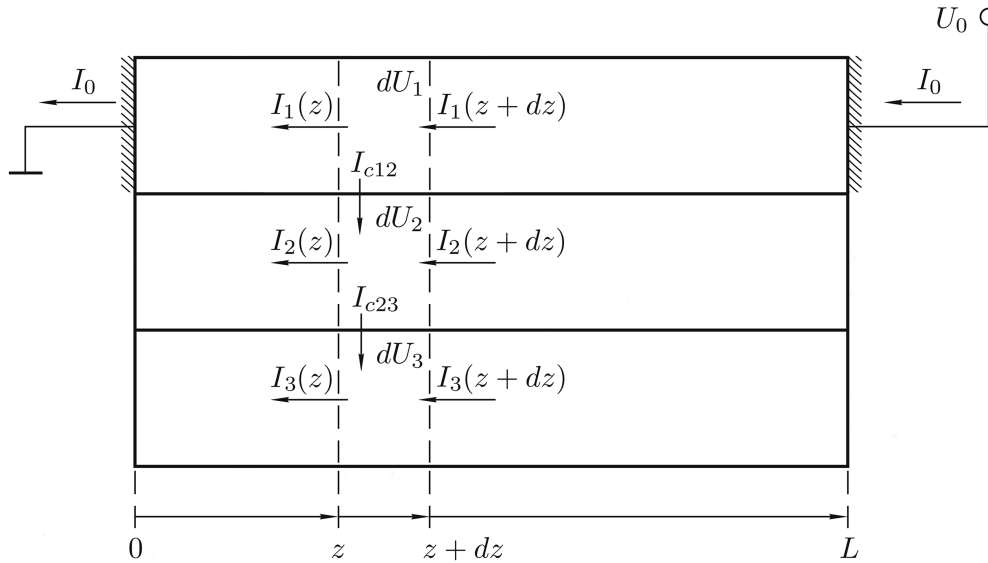


Fig. 1. Three-layer conductive structure

The layers of the structure are characterized by specific volume resistances ρ_1, ρ_2, ρ_3 and thicknesses h_1, h_2 and h_3 for the first, second and third layers, respectively. Layer parameters do not alter along the longitudinal coordinate z . The length of the structure is L . In the direction perpendicular to the plane of the figure, the three-layer structure is also homogeneous and its width is equal to W .

When considering the structure mentioned above, the following assumptions are used.

a) The length of the three-layer structure L much greater than the thicknesses of the layers h_1, h_2 and h_3 . Taking into account the conditions $h_1 \ll L, h_2 \ll L, h_3 \ll L$ the transverse current distribution in each of the layers can be assumed to be uniform. Therefore, we will use a one-dimensional model, where all variables in each of the layers may vary along z axis only.

b) The interfaces between the layers are characterized by specific contact resistivities ρ_{c12}

between the first and second layers, and ρ_{c23} between the second and third layers. In practice, this assumption corresponds to the case when the thickness of the transition region between the resistive layers is much less than the values h_1, h_2 and h_3 .

Without loss of generality, we assume that a constant voltage U_0 is applied to the upper layer of the structure. At the same time, on the left boundary (at $z = 0$) the electric potential is equal to zero, and on the right boundary (at $z = L$) the potential is positive and equal to U_0 .

The boundary conditions for the considered model have the form:

$$\begin{aligned} I_1(z = 0) &= I_0, I_1(z = L) = I_0, \\ I_2(z = 0) &= 0, I_2(z = L) = 0, \\ I_3(z = 0) &= 0, I_3(z = L) = 0, \end{aligned} \quad (1)$$

where I_1, I_2, I_3 are the currents in the first, second and third layers, respectively. The total current I_0 flowing through a three-layer structure depends on the parameters of this structure and the applied voltage U_0 . Obviously, $I_0 = I_1 + I_2 + I_3$.

2. Mathematical model

Equations for the currents flowing in the layers can be expressed as follows:

$$I_1(z) = \frac{Wh_1}{\rho_1} \frac{dU_1(z)}{dz}, \quad (2.1)$$

$$I_2(z) = \frac{Wh_2}{\rho_2} \frac{dU_2(z)}{dz}, \quad (2.2)$$

$$I_3(z) = \frac{Wh_3}{\rho_3} \frac{dU_3(z)}{dz}, \quad (2.3)$$

where dU_1, dU_2 and dU_3 are the voltage drops in the elementary sections dz in the first, second and third layers, respectively.

Part of the current $I_1(z)$ flowing in the upper layer of the structure branches off into the adjacent (second) layer, so that the current $I_1(z)$ in the section dz decreases by $dI_{c12}(z)$, where $dI_{c12}(z)$ is the current flowing through the interface between the layers. In this case, the current $I_2(z)$ in the second layer increases correspondingly by $dI_{c12}(z)$. Similarly, the current is redistributed between the second and third layers.

Therefore, it is correct to write the current balance ratios in the form:

$$I_1(z + dz) - I_1(z) = -dI_{c12}(z), \quad (3.1)$$

$$I_2(z + dz) - I_2(z) = dI_{c12}(z) - dI_{c23}(z), \quad (3.2)$$

$$I_3(z + dz) - I_3(z) = dI_{c23}(z). \quad (3.3)$$

On the other hand, the currents $dI_{c12}(z)$ and $dI_{c23}(z)$ flowing through the interface between the layers depend on the difference in electric potentials in adjacent layers

$$U_{c12}(z) = U_2(z) - U_1(z), \quad (4.1)$$

$$U_{c23}(z) = U_3(z) - U_2(z), \quad (4.2)$$

so

$$dI_{c12}(z) = \frac{W}{\rho_{c12}} U_{c12}(z) dz \quad \text{or} \quad \frac{dI_{c12}(z)}{dz} = \frac{W}{\rho_{c12}} U_{c12}(z), \quad (5.1)$$

$$dI_{c23}(z) = \frac{W}{\rho_{c23}} U_{c23}(z) dz \quad \text{or} \quad \frac{dI_{c23}(z)}{dz} = \frac{W}{\rho_{c23}} U_{c23}(z). \quad (5.2)$$

To find the currents flowing in the layers in the cross section $(z + dz)$, we write down the equations obtained by expanding expressions (2.1), (2.2) and (2.3) in a Taylor series, keeping the first two terms of the series:

$$I_1(z + dz) \approx \frac{Wh_1}{\rho_1} \left[\frac{dU_1(z)}{dz} + \frac{d^2U_1(z)}{dz^2} dz \right], \quad (6.1)$$

$$I_2(z + dz) \approx \frac{Wh_2}{\rho_2} \left[\frac{dU_2(z)}{dz} + \frac{d^2U_2(z)}{dz^2} dz \right], \quad (6.2)$$

$$I_3(z + dz) \approx \frac{Wh_3}{\rho_3} \left[\frac{dU_3(z)}{dz} + \frac{d^2U_3(z)}{dz^2} dz \right]. \quad (6.3)$$

Let's get the equation for distribution $U_1(z)$ in the first layer. To do this we substitute the right side of (6.1) in (3.1) instead of the first term $I_1(z + dz)$, and replace the second term $I_1(z)$ by (2.1), and the right side $-dI_{c12}(z)$ by (5.1) :

$$\frac{Wh_1}{\rho_1} \left[\frac{dU_1(z)}{dz} + \frac{d^2U_1(z)}{dz^2} dz \right] - \frac{Wh_1}{\rho_1} \frac{dU_1(z)}{dz} = -\frac{W}{\rho_{c12}} U_{c12}(z) dz \quad \text{or} \quad \frac{d^2U_1(z)}{dz^2} = -\frac{\rho_1}{h_1} \frac{U_{c12}(z)}{\rho_{c12}}.$$

Similarly, we obtain expressions for the second and third layers. Then the system of equations for all three layers has the form:

$$\frac{d^2U_1(z)}{dz^2} = -\frac{\rho_1}{h_1} \frac{U_{c12}(z)}{\rho_{c12}}, \quad (7.1)$$

$$\frac{d^2U_2(z)}{dz^2} = \frac{\rho_2}{h_2} \left[\frac{U_{c12}(z)}{\rho_{c12}} - \frac{U_{c23}(z)}{\rho_{c23}} \right], \quad (7.2)$$

$$\frac{d^2U_3(z)}{dz^2} = \frac{\rho_3}{h_3} \frac{U_{c23}(z)}{\rho_{c23}}. \quad (7.3)$$

Let us take into account that $U_{c12}(z) = U_1(z) - U_2(z)$, whence, using (7.1) and (7.2), we obtain

$$\frac{d^2U_{c12}(z)}{dz^2} = \frac{d^2U_2(z)}{dz^2} - \frac{d^2U_1(z)}{dz^2} = \frac{\rho_2}{h_2} \left[\frac{U_{c12}(z)}{\rho_{c12}} - \frac{U_{c23}(z)}{\rho_{c23}} \right] + \frac{\rho_1}{h_1} \frac{U_{c12}(z)}{\rho_{c12}}.$$

Combining this relation with a similar expression for $U_{c23}(z)$, we write down the general system of equations

$$\begin{aligned} \frac{d^2U_{c12}(z)}{dz^2} &= \frac{1}{\rho_{c12}} \left[\frac{\rho_1}{h_1} + \frac{\rho_2}{h_2} \right] U_{c12}(z) - \frac{1}{\rho_{c23}} \frac{\rho_2}{h_2} U_{c23}(z), \\ \frac{d^2U_{c23}(z)}{dz^2} &= -\frac{1}{\rho_{c12}} \frac{\rho_2}{h_2} U_{c12}(z) + \frac{1}{\rho_{c23}} \left[\frac{\rho_2}{h_2} + \frac{\rho_3}{h_3} \right] U_{c23}(z). \end{aligned} \quad (8)$$

The solution of this system of equations makes it possible to determine the distribution of electric currents in a three-layer structure.

3. Analytical solution

To simplify the notations, we represent the system (8) in the following form:

$$\begin{aligned} \frac{d^2U_{c12}(z)}{dz^2} &= AU_{c12} + BU_{c23}, \\ \frac{d^2U_{c23}(z)}{dz^2} &= CU_{c12} + DU_{c23}. \end{aligned} \quad (9)$$

where $A = [(\rho_1/h_1) + (\rho_2/h_2)]/\rho_{c12}$, $B = -\rho_2/(\rho_{c23}h_2)$, $C = -\rho_2/(\rho_{c12}h_2)$, $D = [(\rho_2/h_2) + (\rho_3/h_3)]/\rho_{c23}$.

For the resulting system, the characteristic equation with respect to the parameter λ describing its particular solutions, has the form

$$\lambda^4 - (A + D)\lambda^2 + (AD - BC) = 0. \quad (10)$$

This biquadratic equation has four roots $\lambda_1, \lambda_2, \lambda_3, \lambda_4$. Since the characteristic equation has two pairs of roots λ that differ in sign, and they are real simple, the solution of the system for U_{c12} can be written in the following form:

$$U_{c12} = C_1 \exp(\lambda_1 z) + C_2 \exp(\lambda_2 z) + C_3 \exp(\lambda_3 z) + C_4 \exp(\lambda_4 z), \quad (11)$$

where C_1, C_2, C_3, C_4 are constants, which values are determined by the boundary conditions (1). It is obvious that the terms containing $\lambda > 0$ make an increasing contribution to (11) along the z axis, while the terms with $\lambda < 0$ make a decreasing one.

Accordingly, the solution for U_{c23} (including $B = -\rho_2/(\rho_{c23}h_2) \neq 0$) will also contain four constants of integration:

$$U_{c23} = \frac{1}{B} \left(\frac{d^2 U_{c23}(z)}{dz^2} - A U_{c12} \right) = \frac{1}{B} \sum_{i=1}^4 C_i \lambda_i^2 \exp(\lambda_i z) - \frac{A}{B} \sum_{i=1}^4 C_i \exp(\lambda_i z). \quad (12)$$

To determine the constants C_1, C_2, C_3 and C_4 we use the boundary conditions. Using (1) and expressions (2.1), (2.2) and (2.3), we relate $I_1(z), I_2(z), I_3(z)$ and $U_{c12}(z), U_{c23}(z)$ on the boundaries of the structure $z = 0$ and $z = L$ through $U_1(z), U_2(z), U_3(z)$ using the formulas

$$\frac{dU_{c12}}{dz} = \frac{dU_2}{dz} - \frac{dU_1}{dz}, \quad (13.1)$$

$$\frac{dU_{c23}}{dz} = \frac{dU_3}{dz} - \frac{dU_2}{dz}. \quad (13.2)$$

The derivatives of U_1, U_2 , and U_3 on the right-hand sides of (13.1) and (13.2) are expressed using the boundary conditions (1).

On the left boundary of the structure at $z = 0$, taking into account (2.1), (2.2), and (2.3), we have the relations

$$I_1(z=0) = \frac{Wh_1}{\rho_1} \frac{dU_1(z=0)}{dz} = I_0 \quad \text{or} \quad \frac{dU_1(z=0)}{dz} = I_0 \frac{\rho_1}{Wh_1}, \quad (14.1)$$

$$I_2(z=0) = \frac{Wh_2}{\rho_2} \frac{dU_2(z=0)}{dz} = 0 \quad \text{or} \quad \frac{dU_2(z=0)}{dz} = 0, \quad (14.2)$$

$$I_3(z=0) = \frac{Wh_3}{\rho_3} \frac{dU_3(z=0)}{dz} = I_0 \quad \text{or} \quad \frac{dU_3(z=0)}{dz} = 0. \quad (14.3)$$

Similarly, for the right boundary at $z = L$ we get :

$$I_1(z=L) = \frac{Wh_1}{\rho_1} \frac{dU_1(z=L)}{dz} = I_0 \quad \text{or} \quad \frac{dU_1(z=L)}{dz} = I_0 \frac{\rho_1}{Wh_1}, \quad (15.1)$$

$$I_2(z=L) = \frac{Wh_2}{\rho_2} \frac{dU_2(z=L)}{dz} = 0 \quad \text{or} \quad \frac{dU_2(z=L)}{dz} = 0, \quad (15.2)$$

$$I_3(z=L) = \frac{Wh_3}{\rho_3} \frac{dU_3(z=L)}{dz} = I_0 \quad \text{or} \quad \frac{dU_3(z=L)}{dz} = 0. \quad (15.3)$$

Using the obtained relations (14.1)–(14.3) and (15.1)–(15.3), we form a system of equations allowing us to find the constants C_i included in the solutions (11) and (12) for $U_{c12}(z)$ and $U_{c23}(z)$.

First equation of the system for U_{c12} at $z = 0$ (and, accordingly, taking into account $e^{\lambda,0} \equiv 0$) we obtain by substituting (14.1), (14.2) and dU_{c12}/dz , obtained by differentiation of (11), into (13.1). Similarly, we obtain the second equation for U_{c23} at $z = 0$ by substituting (14.2), (14.3) and dU_{c12}/dz , obtained by differentiation of (12), into (13.2). Following the same logic, we get the third equation for U_{c12} at $z = L$ by substituting (15.1), (15.2) and dU_{c12}/dz into (13.1). Finally, the fourth equation for U_{c23} at $z = L$ we obtain by substituting (15.2), (15.3) and dU_{c12}/dz into (13.2). Resulting four relations allow us to form a system of equations for the unknowns C_1, C_2, C_3, C_4 :

$$\begin{aligned} C_1\lambda_1 + C_2\lambda_2 + C_3\lambda_3 + C_4\lambda_4 &= -\frac{I_0\rho_1}{Wh_1}, \\ C_1(\lambda_1^3 - A\lambda_1) + C_2(\lambda_2^3 - A\lambda_2) + C_3(\lambda_3^3 - A\lambda_3) + C_4(\lambda_4^3 - A\lambda_4) &= 0, \\ C_1\lambda_1 \exp(\lambda_1 z) + C_2\lambda_2 \exp(\lambda_2 z) + C_3\lambda_3 \exp(\lambda_3 z) + C_4\lambda_4 \exp(\lambda_4 z) &= -\frac{I_0\rho_1}{Wh_1}, \\ C_1\lambda_1(\lambda_1^3 - A\lambda_1) + C_2\lambda_2(\lambda_2^3 - A\lambda_2) + C_3\lambda_3(\lambda_3^3 - A\lambda_3) + C_4\lambda_4(\lambda_4^3 - A\lambda_4) &= 0. \end{aligned} \quad (16)$$

Solving this system, one can find the constants C_1, C_2, C_3, C_4 . Such a solution can be implemented analytically by any of the direct methods or numerically using built-in computational procedures of mathematical software systems.

So, from (10) and (16) one can find all λ_i and all C_i . This allows, using (11) and (12), to determine the dependences $U_{c12}(z)$ and $U_{c23}(z)$, and on their basis it is possible to calculate the distributions $I_1(z), I_2(z), I_3(z)$.

To determine the dependence $I_1(z)$, we use (2.1)–(2.3) and (7.1), (7.2), (7.3), pairwise connecting I_1 and U_1, I_2 and U_2 , and also I_3 and U_3 .

For the current I_1 on the basis of (2.1) we write $d^2U_1(z)/dz^2 = (\rho_1/Wh_1)/[dI_1(z)/dz]$. By replacing the $U_1(z)$ in this relation with the right side of (7.1), we obtain an expression relating $U_{c12}(z)$ and the first derivative $I_1(z)$:

$$\frac{\rho_1}{Wh_1} \frac{dI_1(z)}{dz} = -\frac{\rho_1}{h_1} \frac{U_{c12}(z)}{\rho_{c12}} \quad \text{or} \quad \frac{dI_1(z)}{dz} = -\frac{W}{\rho_{c12}} U_{c12}(z).$$

Integrating the last relation and taking into account $I_1(0) = I_0$, we determine the current variation in the first layer $I_1(z)$:

$$I_1(z) = I_0 - \frac{W}{\rho_{c12}} \int_0^z U_{c12}(z) dz = I_0 - \frac{W}{\rho_{c12}} \sum_{i=1}^4 \frac{C_i}{\lambda_i} [\exp(\lambda_i z) - 1]. \quad (17)$$

For current I_3 on the basis of (2.3) we write $d^2U_3(z)/dz^2 = (\rho_3/Wh_3)/[dI_3(z)/dz]$. Based on equation (7.3), which expresses the second derivative of $U_3(z)$ in terms of $U_{c23}(z)$, we can write

$$\frac{\rho_3}{Wh_3} \frac{dI_3(z)}{dz} = \frac{\rho_3}{h_3} \frac{U_{c23}(z)}{\rho_{c23}} \quad \text{or} \quad \frac{dI_3(z)}{dz} = \frac{W}{\rho_{c23}} U_{c23}(z).$$

Integrating the last relation, taking into account $I_3(0) = 0$, we determine the current variation in the third layer $I_3(z)$:

$$I_3(z) = \frac{W}{\rho_{c23}} \int_0^z U_{c23}(z) dz = \frac{1}{B} \frac{W}{\rho_{c23}} \sum_{i=1}^4 C_i [\exp(\lambda_i z) - 1] \left(\lambda_i - \frac{A}{\lambda_i} \right). \quad (18)$$

Using (2.2) for the current I_2 we obtain $d^2U_2(z)/dz^2 = (\rho_2/Wh_2)/[dI_2(z)/dz]$. On the other hand, according to (7.2) $d^2U_2(z)/dz^2 = (\rho_2/h_2)/[(U_{c12}/\rho_{c12}) - (U_{c23}/\rho_{c23})]$. Then

$$\frac{\rho_2}{Wh_2} \frac{dI_2(z)}{dz} = \frac{\rho_2}{h_2} \left[\frac{U_{c12}(z)}{\rho_{c12}} - \frac{U_{c23}(z)}{\rho_{c23}} \right] \quad \text{or} \quad \frac{dI_2(z)}{dz} = W \left[\frac{U_{c12}(z)}{\rho_{c12}} - \frac{U_{c23}(z)}{\rho_{c23}} \right].$$

Integrating the last relation, one can find $I_2(z)$ and, taking into account (17) and (18), obtain:

$$I_2(z) = \frac{W}{\rho_{c12}} \int_0^z U_{c12}(z) dz - \frac{W}{\rho_{c23}} \int_0^z U_{c23}(z) dz = I_0 - I_1(z) - I_3(z). \quad (19)$$

Relation (19) shows that in any section of the three-layer structure the equality $I_0 = I_1 + I_2 + I_3$ and the dependence of the current $I_2(z)$ for the middle layer can be found if the distributions of $I_1(z)$ and $I_3(z)$ are known.

Integration (2.1) allows us to find the distribution $U_1(z)$ in the upper layer of the structure:

$$U_1(z) - U_1(0) = \frac{\rho_1}{Wh_1} \int_0^z I_1(z) dz. \quad (20)$$

By substituting in (20) the dependence of $I_1(z)$ from (17) and taking into account $U_1(0) = 0$, we obtain

$$U_1(z) = \frac{\rho_1}{Wh_1} \int_0^z I_1(z) dx - U_1(0) = \frac{\rho_1 I_0}{Wh_1} z - \frac{\rho_1}{\rho_{c12} h_1} \sum_{i=1}^4 \frac{C_i}{\lambda_i} \left[\frac{\exp(\lambda_i z)}{\lambda_i} - z \right] - \sum_{i=1}^4 \frac{C_i}{\lambda_i^2}. \quad (21)$$

The total voltage drop over the entire length of the three-layer structure is determined from (21) as $U_0 = U_1(L)$. Accordingly, the total resistance of the structure is equal to

$$R = [U_1(L) - U_1(0)]/I_0 = U_1(L)/I_0. \quad (22)$$

4. Simulation results

The distributions of voltages and currents along the three-layer structure obtained as a result of the calculations are shown in Fig. 2. Taking into account the fact that the value of I_0 , as well as the width of the structure W , does not affect the nature of the distribution of currents and voltages (this can be seen from the calculated relations (17)–(19), (21)), graphs are given in a normalized form: for voltages $\tilde{U}_{c12} = U_{c12}/U_0$, $\tilde{U}_{c23} = U_{c23}/U_0$, $\tilde{U}_1 = U_1/U_0$, $\tilde{U}_2 = U_2/U_0$, $\tilde{U}_3 = U_3/U_0$ and currents $\tilde{I}_1 = I_1/I_0$, $\tilde{I}_2 = I_2/I_0$, $\tilde{I}_3 = I_3/I_0$ relative to the reduced coordinate $\tilde{z} = z/L$.

Dependences $U_{c12}(z)$ and $U_{c23}(z)$ are calculated on the basis of (11) and (12). The distributions $U_1(z), U_2(z), U_3(z)$ are obtained using (21) and using (4.1) and (4.2): $U_2(z) = U_1(z) + U_{c12}(z)$; $U_3(z) = U_2(z) + U_{c23}(z)$. Dependences $I_1(z), I_2(z)$ and $I_3(z)$ are constructed in accordance with (17), (18) and (19).

Calculations were made for the following parameters: $L = 0.01$ m; $W = 0.01$ m; $\rho_1 = 2 \cdot 10^{-6}$ Ohm·m; $\rho_2 = 1 \cdot 10^{-6}$ Ohm·m; $\rho_3 = 4 \cdot 10^{-6}$ Ohm·m. Specific contact resistivities ρ_{c12} and ρ_{c23} were chosen from the condition: $\rho_{c12} = \min(\rho_1, \rho_2) \times 1$ m; $\rho_{c23} = \min(\rho_2, \rho_3) \times 1$ m, so that for the specified layer parameters $\rho_{c12} = \rho_{c23} = 1 \cdot 10^{-6}$ Ohm·m². The layer thicknesses were set equal: $h_1 = h_2 = h_3/2 = L \times 10^{-3} = 10^{-5}$ m (Fig. 2, a) and $h_1 = h_2 = h_3/2 = L \times 10^{-4} = 10^{-6}$ m (Fig. 2, b). Such thicknesses are typical in works on thin-film microelectronics [1–10].

The intensity of redistribution of the total current I_0 between the layers of the structure can be judged from the gradients of $I_1(z), I_2(z)$ and $I_3(z)$. As can be seen from Fig. 2, this process is most active in areas near the left and right boundaries. As a result, for $z = 0$ and $z = L$ (in Fig. 2 $\tilde{z} = 0$ and $\tilde{z} = 1$) voltages U_{c12} and U_{c23} have maximum absolute values, which is

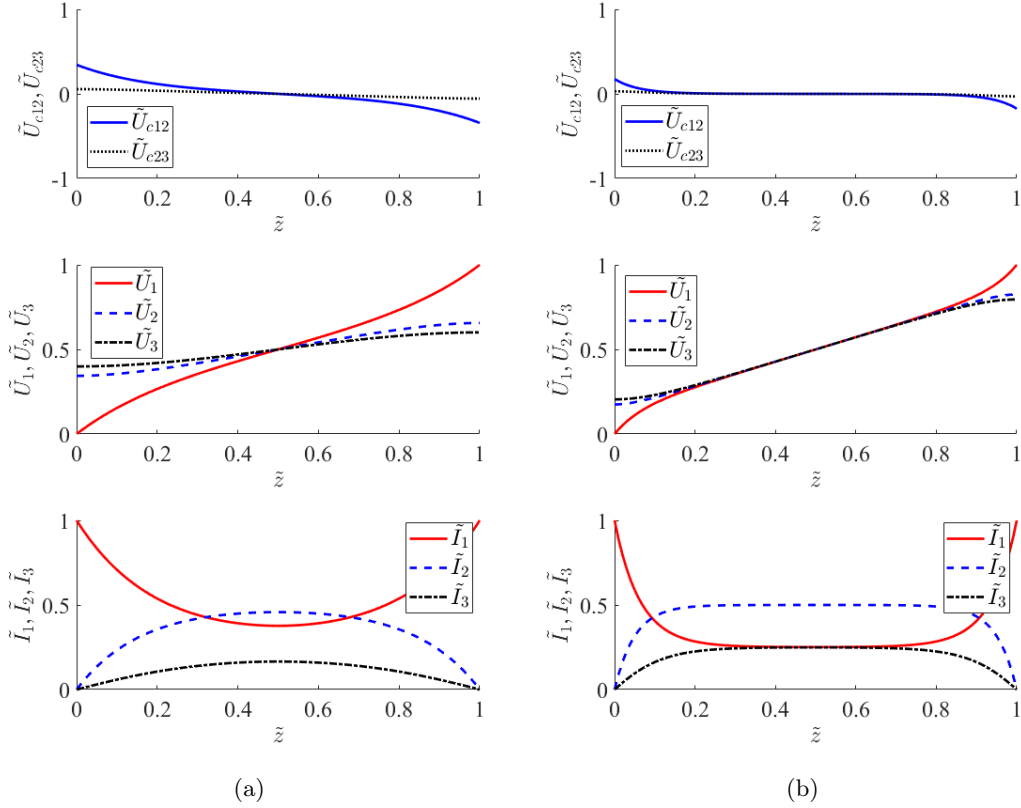


Fig. 2. Voltage and current distributions along a three-layer structure: a) $h_1 = h_2 = h_3/2 = L \times 10^{-3} = 10 \mu\text{m}$; b) $h_1 = h_2 = h_3/2 = L \times 10^{-4} = 1 \mu\text{m}$

consistent with (5.1) and (5.2), from which it follows that $U_{c12} \sim dI_{c12}$ and $U_{c23} \sim dI_{c23}$. The slope of the curves $U_1(z)$, $U_2(z)$ and $U_3(z)$ also changes along the coordinate z , and near the left and right boundaries of the structure, the gradient $U_1(z)$ is maximum, and the gradients $U_2(z)$ and $U_3(z)$ are minimal as U_{c12} and U_{c23} increase.

Dependencies in Fig. 2, a, corresponding to the ratio $h_i/L \sim 10^{-3}$, show that the redistribution of the current and the variation in voltages are observed over the entire length of the structure. In the middle part of the structure, the current I_1 has a minimum value, while the currents I_2 and I_3 , on the contrary, reach maximum values due to the branching of a part of the total current I_0 into the lower layers. In this case, in any section, \tilde{z} the relation is fulfilled $\tilde{I}_1 + \tilde{I}_2 + \tilde{I}_3 = 1$, which is similar to the condition $I_1 + I_2 + I_3 = I_0$.

Current and voltage distributions presented in Fig. 2, b are obtained for thinner conductive layers ($h_i/L \sim 10^{-4}$), while keeping other initial calculated parameters unchanged. It can be seen that the length of the segments in which the redistribution of currents I_1 , I_2 , and I_3 mainly occurs does not exceed half the length of the structure. It is also worth noting that a similar result can be obtained not only by decreasing the layer thickness, but also by increasing the length L .

The difference in the character of dependences in Fig. 2, a and Fig. 2, b can be attributed to the fact that the variation in currents I_1 , I_2 and I_3 , according to (17), (19) and (18), is determined by the roots λ_i of equation (10), depending on the specific contact resistances ρ_{c12} , ρ_{c23} and parameters that, for a given structure width W characterize the longitudinal conductivity of the

layers – $\rho_1/h_1, \rho_2/h_2, \rho_3/h_3$. Therefore, an increase or decrease in $\rho_1/h_1, \rho_2/h_2, \rho_3/h_3$ leads to a change in the parameters λ_i and, accordingly, to a reduction or increase in the length of the regions in which the redistribution of currents I_1, I_2 mainly occurs and I_3 .

Due to the fact that in Fig. 2, b, the regions of growth and decay of currents in the layers make up a relatively small part of the total length L , in the middle part of the structure, the dependences $I_1(z), I_2(z)$ and $I_3(z)$ have flat sections, within which $dI_1(z)/dz \approx dI_2(z)/dz \approx dI_3(z)/dz \approx 0$ and, respectively, $I_{c12}(z) \approx 0, I_{c23}(z) \approx 0, U_{c12}(z) \approx 0, U_{c23}(z) \approx 0, U_1(z) \approx U_2(z) \approx U_3(z)$. For the given design parameters, these sections are located in the range approximately from $\tilde{z} \approx 0.4$ to $\tilde{z} \approx 0.6$. Obviously, with an increase in the length of the structure, the extent of these flat sections will increase.

It should be noted that the contribution of each of the currents I_1, I_2 and I_3 in the total current I_0 at (that is, at $z = L/2$) is inversely proportional to the ratio $\rho_1/h_1, \rho_2/h_2$ and ρ_3/h_3 respectively for each of the layers. From the dependencies in Fig. 2, b, for example, it can be seen that the currents in the first and third layers are equal, since $\rho_1/h_1 = \rho_3/h_3$.

An analysis of the influence of geometric factors on the nature of the distribution of currents and voltages shows that for the considered three-layer structure, a nonlinear dependence of its total resistance R on the length L can be observed. Fig. 3 shows the dependences $R(L)$ calculated in the range of L from 10^{-4} m to 10^{-2} m for three options corresponding to the layer thicknesses: $h_1 = h_2 = h_3/2 = 10^{-6}$ m; $h_1 = h_2 = h_3/2 = 3 \cdot 10^{-6}$ m; $h_1 = h_2 = h_3/2 = 10^{-5}$ m. The values of the other parameters of the structure were set the same as in the previous calculations.

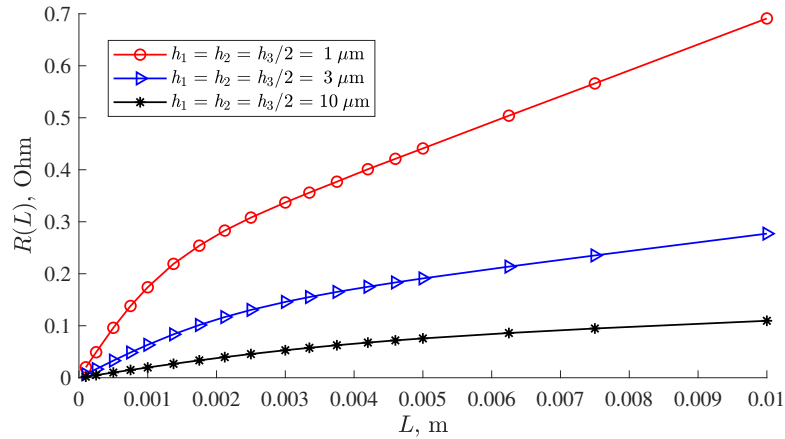


Fig. 3. Length dependence of the three-layer structure resistance $R(L)$ for different layers thicknesses

On the entire length of the upper curve, the condition of smallness of the layer thickness $h_i/L \leq 0.02$ is satisfied, and on the second curve located below it, – $h_i/L \leq 0.02$. For the lower dependence in the range of L from 0.001 m to 0.01 m, this condition corresponds to $h_i/L \leq 0.02$. At $L < 0.001$ m, the ratio h_3/L can reach 0.2, so this section can be considered as an extrapolation of the dependence based on the proposed model.

Plots in Fig. 3 show that for the given design parameters, the dependence $R(L)$ in its initial section is non-linear, approximately up to $L \sim (2 \dots 3) \cdot 10^3 \times h_1$. The non-linear nature of the curves at small values of the structure length is due to the fact that in this range of L variation, the redistribution of the current between the layers occurs over its entire length.

It can be shown that for a structure length not exceeding approximately $L \sim 1/\lambda_i$ (see (10), (17)), the current flowing through the structure is mainly concentrated in the upper layer, while the fraction of the current in the two lower layers is very small. As L increases, the part of the

current branched into the second and third layers of the structure increases, which leads to a decrease in the rate of increase in the resistance of the structure $dR(L)/dL$ with an increase in its length.

With an increase in the length of the structure, approximately from $L \sim (2 \dots 3) \cdot 10^3 \times h_1$, the resistance R begins to increase linearly. At large values of L , the most significant influence on the nature of the $R(L)$ dependence is exerted by the middle part of the structure, within which the distributions of $I_1(z)$, $I_2(z)$, and $I_3(z)$ have flat areas. In this case, an increment in the length L leads to a corresponding increase in the length of these flat sections, which determines the linear nature of the dependence $R(L)$.

Conclusion

The analysis of the current flow mechanism in a three-layer conductive structure made it possible to obtain a model that describes the regularities in the distribution of electric current and voltage in the structure. The analysis of the obtained relations describing the three-layer structure, as well as the calculations performed on their basis, allow us to draw the following conclusions.

1. The length of the sections of current redistribution between the layers of the structure within the framework of the proposed model is determined by the specific contact resistances ρ_{c12}, ρ_{c23} at the interfaces of the conductive layers and the ratios of the volume resistivity of the layers to their thicknesses — $\rho_1/h_1, \rho_2/h_2, \rho_3/h_3$.

2. For "short" three-layer structures, in which the redistribution of current between the layers occurs over their entire length L , the dependence of the total resistance R on L is non-linear.

3. For "long" three-layer structures, in which the regions of growth and decay of currents in the layers make up a relatively small part of the total length L , in the middle part of the structure, the dependences $I_1(z), I_2(z)$ and $I_3(z)$ have low slope graphs. For such structures, a linear dependence of the resistance R on the length L is observed .

The approach used in this work can be applied to the construction of similar models of multilayer structures, for example, for other boundary conditions that determine their connection to an external circuit.

The study was carried out within the framework of the state task of the Federal State Autonomous Educational Institution of Higher Education Siberian Federal University (no. FSRZ-2023-0008).

References

- [1] H.Murrmann, D.Widmann, Current Crowding on Metal Contacts to Planar Devices, *IEEE Transactions on Electron Devices*, **16**(1969), no. 12, 1022–1024.
- [2] H.H.Berger, Models for Contacts to Planar Devices, *Solid-State Electronics*, **15**(1972), 145–158.
- [3] D.B.Scott, W.R.Hunter, H.Shichijo, A Transmission Line Model for Silicided Diffusions: Impact on the Performance of VLSI Circuits, *IEEE Transactions on Electron Devices*, **ED-29**(1982), no. 4, 651–661.
- [4] G.Reeves, B.Harrison, Determination of Contact Parameters of Interconnecting Layers in VLSI Circuits, *IEEE Transactions on Electron Devices*, **ED-33**(1986), no. 3, 328–334.

- [5] G.K.Reeves, P.W.Leech, H.B.Harrison, A new Electrical Model for Calculation the Sheet Resistance Parameter in Alloyed Ohmic Contacts, *MRS Mat. Res. Symp. Proc.*, **337**(1994), 275–280.
- [6] G.K.Reeves, P.W.Leech, H.B.Harrison, Understanding the Sheet Resistance Parameter of Alloyed Ohmic Contacts Using a Transmission Line Model, *Solid-State Electronics*, **38**(1995), no. 4, 745–751.
- [7] G.K.Reeves, H.B.Harrison, An Analytical Model for Alloyed Ohmic Contacts Using a Tri-layer Transmission Line Mode, *IEEE Transactions on Electron Devices*, **42**(1995), no. 8, 1536–1547.
- [8] G.K.Reeves, H.B.Harrison, P.W.Leech, Modeling Geometrical Effects of Parasitic and Contact Resistance of FET Devices, *MRS Mat. Res. Symp. Proc.*, **427**(1996), 147–152.
- [9] G.K.Reeves, H.B.Harrison, Using TLM Principles to Determine MOSFET Contact and Parasitic Resistance, *Solid-State Electronics*, **41**(1997), no. 8, 1067–1074.
- [10] N.Shrestha, G.K.Reeves, P.W.Leech, Y.Pan, A.S.Holland, Analytical test structure model for determining lateral effects of tri-layer ohmic contact beyond the contact edge, *Facta Universitatis, Series: Electronics and Energetics*, **30**(2017), no. 2, 257–265.
- [11] N.Sha, L.P.J.Kenney, B.Heller, M.Moatamedi, A Finite Element Model to Identify Electrode Influence on Current Distribution in the Skin, *Artificial Organs*, **32**(2008), no. 8, 639–643.
- [12] T.Keller, A.Kuhn, Electrodes for transcutaneous (surface) electrical stimulation, *Journal of Automatic Control*, University of Belgrade, **18**(2008), no. 2, 35–45.
- [13] T.Keller, A.Kuhn, Skin properties and the influence on electrode design for transcutaneous (surface) electrical stimulation, *Chapter in IFMBE proceedings*, **25**(2010), no. 9, 492–495. DOI:10.1007/978-3-642-03889-1_131
- [14] M.Prodanovic, J.Malesevic, M.Filipovic, T.Jevtic, G.Bijelic, N.Malesevic, Numerical Simulation of the Energy Distribution in Biological Tissues During Electrical Stimulation, *Serbian Journal of Electrical Engineering*, **10**(2013), no. 1, 165–173. DOI: 10.2298/SJEE1301165P

Анализ распределения электрического тока в трехслойной проводящей структуре

Алексей А. Левицкий
Павел С. Маринушкин
Валентина А. Бахтина

Сибирский федеральный университет
Красноярск, Российская Федерация

Аннотация. В работе представлена аналитическая модель, позволяющая исследовать характер распределения электрического тока в трехслойной проводящей структуре. Предложенная модель учитывает характеристики трех проводящих слоев и переходных сопротивлений между ними. Также получены выражения для распределения тока и изменения электрического потенциала вдоль структуры, а также её общего сопротивления. Кроме того, представлены количественные оценки, показывающие особенности перераспределения электрического тока между слоями при изменении параметров слоев.

Ключевые слова: трехслойная проводящая структура, распределение тока, сопротивление, удельное контактное сопротивление, TLM-метод.

EDN: OEJOOF

УДК 530

Cylindrically Symmetric Generalized Ghost Pilgrim Dark Energy Cosmological Univers

Mandala Krishna*

Raghu Engineering Collage, Visakhapatnam
AndhraPradesh, India-531162

Sobhanbabu Kappala†

University Collage of Engineering Kakinada, Narasaraopeta
AndhraPradesh, India-522616

Rajamahanthi Santhikumar‡

Aditya Institute of Technology and Management
Tekkali, Srikakulam Dist
Andhra Pradesh, India-532203

Received 10.07.2023, received in revised form 29.08.2023, accepted 24.01.2024

Abstract. The solution of the cylindrically symmetric Einstein Rosen universe is investigated and occupied with generalized ghost pilgrim dark energy and matter. To obtain the exact solutions of Einstein's field equations, we discussed the GGPDE model and determined the EoS parameter, Regions of the model to be identified by the $\omega_d-\dot{\omega}_d$ plane analysis, Phantom and quintessence phases to be discussed by state finder, and Stability of the model to be discussed by squared speed of sound. The physical properties of the model are discussed. The results obtained are to be useful with the current observations.

Keywords: phantom, quintessence, Stability, cylindrically, symmetric.

Citation: M. Krishna, S.B. Kappala, R. Santhikumar, Cylindrically Symmetric Generalized Ghost Pilgrim Dark Energy Cosmological Univers, J. Sib. Fed. Univ. Math. Phys., 2024, 17(2), 257–265. EDN: OEJOOF.



Introduction

The present challenging problem shows that the universe is expanding rapidly. It is big mystic problem today. Through supernova I_a , the expansion phenomenon of the universe was explained by authors (Riess et al. [1]; Permutter et al [2]; Copeland et al. [3]). The Negative pressure of the universe causes e accelerating expansion of the universes caused Dark Energy The galactic curved and structure formation of the universe was explained by the absence of pressure, the dark matter. Several dark energy models have been proposed by many authors which can be characterized by the equation of parameter ω . For fine-tuning there are many cosmological constants are considered for dark energy like holographic (Cohen et al.[4]; Hooft [5]), Pilgrim (Wei [6]), k-essence (Armendariz [7]), h-essence (Wei [8]), phantom (Caldwell [9]), quintom (Guo et al.[10]), quitessence (Ratra e.al., [11]), tachyon (Sen [12]), dilation (Gasperini et al. [13]), and DBIessence (Gumjudpai et al. [14]; Martin et al. [15]) etc.

It is observed the ordinary ghost Dark energy model only the leading term (i.e., H) has been deliberated and sub leading term (i.e, H^2) is introduced by "Cai et al.[16]" in the ordinary ghost

*mandala.krishna.phd@gmail.com <https://orcid.org/0000-0003-1975-8930>

†ksobhanjntu@gmail.com <https://orcid.org/0000-0002-2991-7651>

‡skrmahanthi@gmail.com <https://orcid.org/0000-0001-5122-3800>

© Siberian Federal University. All rights reserved

dark energy it helps to describing early-stage evolution of the universe and the energy density is called generalized ghost dark energy density defined as $\rho_\Lambda = a_1 H + b_1 H^2$. The vacuum energy from the Veneziano ghost field in QCD is obtained as $H + O(H^2)$ (Zhitnitsky [17]), it shows the accelerated expansion of the universe. Several authors (Karami [18]; Malekjani [19];) has been developed different cosmological parameters like Eos parameter, deceleration, investigated different, state finder and squared speed of sound, etc. The stability of this type of model has been investigated by authors ‘Ebrahimi and Sheykhi [20]’. Therefore, the Generalized Ghost Pilgrim Dark Energy(GGPDE) is defined as (Sharif and Nazir [21]) $\rho_\Lambda = (\alpha_1 H + \alpha_2 H^2)^\beta$.

Vijayashanti et al. [22] studied bianchi type GGPDE and Anisotropic GGPDED respectively. Tazmin[23] studied GGPDE with Sign-Changeable Integration. Sharif et at[24] developed GG-PDE in f(R,T) gravity. Prianka et al. [25] studied GGPDE in Saez-Ballester theory. Wajihajavad et al. [26] studied Interacting GGDE anisotropic scalar field models. Bharali et al. [27] studied dynamics of GGPDE. By the motivation of all the above study of researchers, we studied in this reach article ‘cylindrically symmetric GGPDE’. The physical and general properties are also discussed.

1. Metric and field equations

The Einstein Rosen metric is in the form

$$ds^2 = e^{(2A-2B)} [dt^2 - dr^2] - r^2 e^{-2B} d\psi^2 - e^{2B} dz^2 \quad (1)$$

where A and B are time dependent only and $x^1 = r$, $x^2 = \varphi$, $x^3 = z$ and $x^4 = t$. The field equation is

$$R_{ij} - \frac{1}{2} R g_{ij} = -8\pi (T_{ij} + \bar{T}_{ij}). \quad (2)$$

Since the momentum of energy is conservative

$$(T_{ij} + \bar{T}_{ij})_{;j} = 0 \quad (3)$$

Here, R_{ij} is the Ricci tensor, g_{ij} is metric tensor, R is Ricci scalar.

Take $8\pi G = c = 1$.

The EMT for DE and DM are given by

$$T_i^j = \text{diag} [1, 0, 0, 0] \rho_m \quad (4)$$

$$\bar{T}_i^j = \text{diag} [\rho_d, -p_d, -p_d, -p_d] = \text{diag} [1, -\omega_d, -\omega_d, -\omega_d] \rho_d \quad (5)$$

where ρ_m, ρ_d are ED of DM and DE, p_d is pressure of DM,

The EoS parameter of DE is defined by

$$\omega_d = \frac{p_d}{\rho_d} \quad (6)$$

The ED for dark energy \bar{T}_i^j can be reduced to

$$\bar{T}_i^j = \text{diag} [1, -\omega_d, -(\omega_d + \delta), -(\omega_d + \delta)] \rho_d \quad (7)$$

Here, δ is skewness parameter deviated from ω_d on y and z axes.

By eqs. (1), (4) and (7) The field eq. (2) can reduced to the following equations

$$\left(\dot{B}\right)^2 = (-\omega_d \rho_d) e^{(2A-2B)} \quad (8)$$

$$\ddot{A} + \left(\dot{B}\right)^2 = -(\omega_d + \delta_y) \rho_d e^{(2A-2B)} \quad (9)$$

$$\ddot{A} + \left(\dot{B}\right)^2 - 2\left(\ddot{B}\right) = -(\omega_d + \delta_z) \rho_d e^{(2A-2B)} \quad (10)$$

$$\left(\dot{B}\right)^2 = -(\rho_m + \rho_d) e^{(2A-2B)} \quad (11)$$

$$\frac{1}{e^{(2A-2B)}} \left(\frac{\dot{A}}{r}\right) = 0 \quad (12)$$

By the law of conservation for DM and DE can be reduced as

$$\begin{aligned} \dot{\rho}_m + \left(\dot{A} - \dot{B}\right) \left[2 + e^{(-2A+2B)}\right] \rho_m - \dot{\rho}_d + \left\{ \left(\dot{A} - \dot{B}\right) \left(2 + (1 + \omega_d) e^{(-2A+2B)}\right) + \right. \\ \left. + (\omega_d + \delta_y) r^{-2} e^{2B} + (\omega_d + \delta_z) e^{-2B} \right\} \rho_d = 0 \end{aligned} \quad (13)$$

Here, overhead dot stands for ODE w.r.t t

2. Solution of the filed equations

The filed equations (8)–(12) form is a system of five independent equations with six unknowns $A, B, \rho_d, \rho_m, \omega_d$ and δ . The system is initially undetermined. So, we can require extra physical conditions to solve the above equations.

The DM and DE components are

$$\dot{\rho}_m + \left(\dot{A} - \dot{B}\right) \left[2 + e^{(-2A+2B)}\right] \rho_m = 0 \quad (14)$$

$$\dot{\rho}_d = \left\{ \left(\dot{A} - \dot{B}\right) \left(2 + (1 + \omega_d) e^{(-2A+2B)}\right) + (\omega_d + \delta_y) r^{-2} e^{2B} + (\omega_d + \delta_z) e^{-2B} \right\} \rho_d \quad (15)$$

By eq. (12)

$$A = \text{constant} = \vartheta(\text{say}) \quad (16)$$

By Berman (1983) applying the law of variation for the Hubbles parameter with constant decelerating parameter.

The average scale factor for Einstein–Rosen metric is

$$a = (re^{2A-2B})^{\frac{1}{3}} \quad (17)$$

The special Volume V is

$$V = \sqrt{(-g)} = re^{2A-2B} \quad (18)$$

The mean Hubble's parameter H is

$$H = \frac{1}{3} \left(\frac{\dot{V}}{V}\right) = \left(\frac{\dot{a}}{a}\right) = \frac{2}{3} (\dot{A} - \dot{B}) = \frac{2}{3} (-\dot{B}) \quad (19)$$

We considered the relation

$$H = \frac{k_1}{(a)^n} \quad (20)$$

where k_1 and n are non-negative constants.

The decelerating parameter is q is

$$q = -\frac{a \ddot{a}}{(\dot{a})^2} \quad (21)$$

By Eq. (19) and (20) $\left(\frac{\dot{a}}{a}\right) = H = \frac{k_1}{(a)^n}$, we have

$$\dot{a} = k_1 a^{(1-n)} \quad (22)$$

$$\ddot{a} = k_1^2 (1-n) a^{(1-2n)} \quad (23)$$

Using Eqs. (21)–(23), the " q " is reduced to

$$q = n - 1 \quad \text{for } n \neq 0, \quad q = -1 \quad \text{for } n = 0. \quad (24)$$

Using eq. (22), the average scale factor for two conditions obtained as

$$a = (c_1 t + c_2)^{\frac{1}{n}} \quad \text{for } n \neq 0 \quad (25)$$

$$a = c_3 e^{k_1 t} \quad \text{for } n = 0 \quad (26)$$

Where c_1, c_3 are constants and c_2 is integration constants

The ED of GGDE in terms of pilgrim dark energy is defined by (sharif et al. [28])

$$\rho_d = (\alpha_1 H + \alpha_2 H^2)^\beta \quad (27)$$

Where β pilgrim dark energy parameter

The state finder pair $\{r, s\}$ are defined as (Sahni et al. [39])

$$r = \frac{1}{H^3} \left(\frac{\ddot{a}}{a} \right) \quad (28)$$

$$s = \frac{r - 1}{3 \left(q - \frac{1}{2} \right)} \quad (29)$$

The state finders represent the distance between CDM to DE model. If $(r,s)=(1,0)$ indicate CDM limit and $(r,s)=(1,1)$ indicate CDM . Also, if $r < 1$ and $s > 0$ represents the region of quintessence and phantom.

Square speed sound is obtained for this model is

$$v^2 = \frac{\dot{\rho}_d}{\rho_d} \quad (30)$$

The stability of background evolution of the model is analyzed based on the sign of Squared speed sound. The (-)ve and (+)ve sign indicates the model is unstable and stable respectively..

$\omega_d - \dot{\omega}_d$ Plane analysis :

By Caldwell and Linder(2005) to estimate the nature of the quintessence scalar field DE model. The model splits into two regions i.e., If $\omega_d < 0, \dot{\omega}_d > 0$ the region of the model is the throwing region, where as $\omega_d < 0, \dot{\omega}_d < 0$ the region is the freezing region.

Case (i) : Model for $n \neq 0$ or $q \neq -1$

By Eqs(12), (16), (19) and (25)

$$B = \log \left(c_4 (c_1 t + c_2)^{\left(\frac{-3}{2n}\right)} \right) \quad (31)$$

Where c_4 are constants

The metric (1) can be reduced to

$$ds^2 = c_4(c_1t + c_2)^{\left(\frac{3}{n}\right)} \left[e^{(2v)} [dt^2 - dr^2] - r^2 d\psi^2 \right] - \frac{dz^2}{c_4(c_1t + c_2)^{\left(\frac{3}{n}\right)}} \quad (32)$$

By Eq. (20) and (25)

The Hubble's parameter,

$$H = \frac{k_1}{(a)^n} = \frac{k_1}{(c_1t + c_2)} \quad (33)$$

By eqs. (27) and (33) The ED is

$$\rho_d = \left(\alpha_1 \frac{k_1}{(c_1t + c_2)} + \alpha_2 \left(\frac{k_1}{(c_1t + c_2)} \right)^2 \right)^\beta \quad (34)$$

By Eq. (11) The MD is

$$\rho_m = \frac{c_5}{(c_1t + c_2)^{\left(2 + \frac{3}{n}\right)}} - \left(\alpha_1 \frac{k_1}{(c_1t + c_2)} + \alpha_2 \left(\frac{k_1}{(c_1t + c_2)} \right)^2 \right)^\beta \quad (35)$$

Where $c_5 = \frac{3c_1}{2ne^{2\vartheta}c_4^2}$

By Eq. (8) and (31) the pressure is

$$p_d = \frac{c_5}{(c_1t + c_2)^{\left(2 + \frac{3}{n}\right)}} \quad (36)$$

The EoS parameter is

$$\omega_d = \frac{p_d}{\rho_d} = \frac{c_5}{(c_1t + c_2)^{\left(2 + \frac{3}{n}\right)} \left(\alpha_1 \frac{k_1}{(c_1t + c_2)} + \alpha_2 \left(\frac{k_1}{(c_1t + c_2)} \right)^2 \right)^\beta} \quad (37)$$

$$\begin{aligned} \dot{\omega}_d = & \frac{-c_1c_5 \left(2 + \frac{3}{n}\right)}{(c_1t + c_2)^{\left(3 + \frac{3}{n}\right)} \left(\alpha_1 \frac{k_1}{(c_1t + c_2)} + \alpha_2 \left(\frac{k_1}{(c_1t + c_2)} \right)^2 \right)^\beta} + \\ & + \frac{c_1c_5\beta \left(\frac{\alpha_1 k_1}{(c_1t + c_2)^2} - \frac{2\alpha_2 k_1^2}{(c_1t + c_2)^3} \right)}{(c_1t + c_2)^{\left(2 + \frac{3}{n}\right)} \left(\alpha_1 \frac{k_1}{(c_1t + c_2)} + \alpha_2 \left(\frac{k_1}{(c_1t + c_2)} \right)^2 \right)^{-\beta-1}} \end{aligned} \quad (38)$$

The state finder pair { r, s} are defined as

$$r = \frac{1}{H^3} \left(\frac{\ddot{a}}{a} \right) = \frac{(1 - 2n)(1 - n)c_1^3}{n^3 k_1} \quad (39)$$

$$s = \frac{r - 1}{3 \left(q - \frac{1}{2} \right)} = \left[\frac{(1 - 2n)(1 - n)c_1^3 - n^3 k_1}{n^3 k_1 3 \left(n - \frac{3}{2} \right)} \right] \quad (40)$$

Square speed sound is obtained for this model is

$$v^2 = \frac{\dot{p}_d}{\dot{\rho}_d} = \frac{-c_1c_5 \left(2 + \frac{3}{n}\right)}{(c_1t + c_2)^{\left(3 + \frac{3}{n}\right)} \left(\alpha_1 \frac{k_1}{(c_1t + c_2)} + \alpha_2 \left(\frac{k_1}{(c_1t + c_2)} \right)^2 \right)^\beta} \frac{\left(\frac{-c_1\alpha_1 k_1}{(c_1t + c_2)^2} - \frac{2c_1\alpha_2 k_1^2}{(c_1t + c_2)^3} \right)}{\left(\alpha_1 \frac{k_1}{(c_1t + c_2)} + \alpha_2 \left(\frac{k_1}{(c_1t + c_2)} \right)^2 \right)^{\beta-1}} \quad (41)$$

By Eq. (8)–(10) and (31) we have the Skewness parameter is

$$\delta_y = 0 \quad (42)$$

and

$$\delta_z = \frac{3c_1^2 c_4}{ne^{2\vartheta}(c_1 t + c_2)^{\left(2 + \frac{3}{n}\right)} \left(\alpha_1 \frac{k_1}{(c_1 t + c_2)} + \alpha_2 \left(\frac{k_1}{(c_1 t + c_2)} \right)^2 \right)^\beta} \quad (43)$$

Case (ii) : Model for $n = 0$ or $q = -1$

By Eqs. (12), (16), (19) and (25)

$A = \text{constant} = \vartheta$ and

$$B = c_6 t + c_7 \quad (44)$$

Where $c_6 = \frac{-3k_1}{2}$ and c_7 is integral constants

The metric (1) can be reduced to

$$ds^2 = e^{-2(c_6 t + c_7)} \left[e^{(2\nu)} [dt^2 - dr^2] - r^2 d\psi^2 \right] - \frac{dz^2}{e^{2\nu - 2(c_6 t + c_7)}} \quad (45)$$

By Eqs.(20) and (25)

The Hubble's parameter

$$H = k_1 \quad (46)$$

By Eqs. (27) and (46) The ED is

$$\rho_d = \left(\alpha_1 k_1 + \alpha_2 (k_1)^2 \right)^\beta \quad (47)$$

By Eq.(11) The MD is

$$\rho_m = -c_6^2 e^{2(c_6 t + c_7 - \nu)} - \left(\alpha_1 k_1 + \alpha_2 (k_1)^2 \right)^\beta \quad (48)$$

By Eq.(8) and (44) the pressure is

$$p_d = -c_6^2 e^{2(c_6 t + c_7 - \nu)} \quad (49)$$

The EoS parameter is

$$\omega_d = \frac{p_d}{\rho_d} = \frac{-c_6^2 e^{2(c_6 t + c_7 - \nu)}}{\left(\alpha_1 k_1 + \alpha_2 (k_1)^2 \right)^\beta} \quad (50)$$

$$\dot{\omega}_d = \frac{-2c_6^3 e^{2(c_6 t + c_7 - \nu)}}{\left(\alpha_1 k_1 + \alpha_2 (k_1)^2 \right)^\beta} \quad (51)$$

Since $\omega_d < 0$, $\dot{\omega}_d < 0$, so the region of the model is freezing region

The state finder pair $\{r, s\}$ is

$$r = \frac{1}{H^3} \left(\frac{\ddot{a}}{a} \right) = 1 \quad (52)$$

$$s = \frac{r - 1}{3 \left(q - \frac{1}{2} \right)} = 0 \quad (53)$$

Clearly $(r,s)=(1,0)$ indicate CDM limit so that the state finders represents the distance from CDM to dark energy model.

Square speed sound is obtained for this model is

$$v^2 = \frac{\dot{p}_d}{\dot{\rho}_d} = \text{does not exist} \quad (54)$$

By Eq.(8)–(10) and (44) we have the skewness parameter are

$$\delta_y = 0 \quad \text{and} \quad \delta_z = 0 \quad (55)$$

Conclusions

We obtained the solution of cylindrically symmetric Einstein Rosen universe with GGPDE & DM. The aim of PDE shows interest as it indicates one of the opinions about the universe due to phantom energy in the late time. The volume of the model does not vanish throughout the evolution of the universe has no singularity. We identified with clearly evidence "q" is time dependent, we also discussed Λ with $\omega_d = -1$. The $\omega_d - \dot{\omega}_d$ plane analyzed the throwing and freezing regions. The state finder splits the model into Phantom and Quintessence regions. The squared speed of sound indicates the stability of the universe. Since here ω_d is consistent it represents that the universe is accelerating. The model developed r-s plane possesses the region of Chaplayin gas models. At the end of conclusion, this model favors the PDE phenomenon. The results obtained are to be compatible with the present-day observations.

References

- [1] A.G.Riess, Observational Evidence from Supernovae for an Accelerating Universe and a Cosmological Constant, *Astron. J.*, **116**(1998), 1009.
- [2] S.Perlmutter, et al., Measurements of Ω and Λ from 42 High-Redshift Supernovae, *Astrophys. J.*, **517**(1999), 565.
- [3] E.J.Copeland, Dynamics of dark energy, *Int. J. Mod. Phys. D*, **15**(2006), 1753.
DOI: 10.1142/S021827180600942X
- [4] A.G.Cohen, et al., Effective Field Theory, Black Holes, and the Cosmological Constant, *Phys. Rev. Lett.*, **82**(1999), 4971.
- [5] G.'t.Hooft, Dimensional Reduction In Quantum Gravity, 2009. arXiv:gr-qc/9310026.
- [6] H.Wei, Pilgrim dark energy, *Class. Quantum Grav.*, **29**(2012), 175008.
DOI: 10.1088/0264-9381/29/17/175008
- [7] C.Armendariz-Picon, Dynamical Solution to the Problem of a Small Cosmological Constant and Late-Time Cosmic Acceleration, *Phys. Rev. Lett.*, **85**(2000), 4438.
DOI: 10.1103/PhysRevLett.85.4438
- [8] H.Wei, et al., A new view of Quintom Dark Energy, *Class. Quantum Grav.*, **22**(2005), 3189.
DOI: 10.1088/0264-9381/22/16/005
- [9] R.R.Caldwell, A phantom menace? Cosmological consequences of a dark energy component with super-negative equation of state, *Phys. Lett. B*, **545**(2002), 23.
DOI: 10.1016/S0370-2693
- [10] Z.K.Guo, Cosmological Evolution of a Quintom Model of Dark Energy, *Phys. Lett. B* **608**, **177**(2005). DOI: 10.1016/j.physletb.2005.01.017

-
- [11] B.Ratra, Cosmological consequences of a rolling homogeneous scalar field, *Phys. Rev. D*, **37**(1988), 3406.
- [12] A.Sen, Tachyon Matter, *J. High Energy Phys.*, **0207**(2002), 065.
DOI: 10.1088/1126-6708/2002/07/065
- [13] M.Gasperini, et al., Quintessence as a run-away dilaton, *Phys. Rev. D*, **65**(2002), 023508.
DOI: PhysRevD.65.023508
- [14] B.Gumjudpai, J.Ward, Generalised DBI-Quintessence, *J. Phys. Rev. D*, **80**(2009), 023528.
DOI: 10.1103/PhysRevD.80.023528
- [15] J.Martin, M.Yamaguchi, DBI-essence, *Phys. Rev. D*, **77**(2008), 123508.
DOI: 10.1103/PhysRevD.77.123508
- [16] R.-G.Cai, et al., More on QCD ghost dark energy, *Phys. Rev. D*, **86**(2012), 023511.
DOI: PhysRevD.86.023511
- [17] A.R.Zhitnitsky, Contact term, its holographic description in QCD and dark energy, *Phys. Rev. D*, **86**(2012), 045026. DOI: 10.1103/PhysRevD.86.045026
- [18] K.Karami, et al., Qcd Modified Ghost Scalar Field Dark Energy Models, *Int. J. Mod. Phys. D*, **22**(2013), 1350018. DOI: 10.1142/S0218271813500181
- [19] M.Malekjani, Cosmography of interacting generalized QCD ghost dark energy, *Int. J. Mod. Phys. D*, **22**(2013), 1350084. DOI: 10.1142/S0218271813500843
- [20] E.Ebrahimi, et al., Interacting generalized ghost dark energy in a non-flat universe, *Eur. J. Phys.*, **11**(2013), 949. DOI: 10.2478/s11534-013-0253-x
- [21] M.Sharif, K.Nazir, Cosmological evolution of generalized ghost pilgrim dark energy in $f(T)$ gravity, *Astrophys. Space Sci.*, **360**(2015), 57. DOI: 10.1007/s10509-015-2572-4
- [22] M.Vijaya Santhi, et al., Some Bianchi type generalized ghost pilgrim dark energy models in general relativity, *Astrophys. Space Sci.*, **361**(2016), 142. DOI: 10.1007/s10509-016-2731-2
- [23] Tazmin Sultana, Generalized Ghost Pilgrim Dark Energy with Sign-Changeable Interaction, *Prespacetime Journal*, **8**(2017), 798.
- [24] M.Sharif, Generalized ghost pilgrim dark energy in $f(G,T)$ gravity, *Int. J. Mod. Phys. D*, **28**(2019), no. 06.
- [25] Prianka Garg, et al., Cosmological models of generalized ghost pilgrim dark energy (GG-PDE) in the gravitation theory of Saez–Ballester, *Int. Jor. Geo. Med. Mod. Phy*, **18**(2021), no. 14, 2150221. DOI: 10.1142/S0219887821502212
- [26] Wajiha Javed, et al., Interacting generalized anisotropic scalar field models, *Eur. Phys. J. C*, **81**(2021), 149. DOI: 10.1140/epjc/s10052-020-08555-x
- [27] J.Bharali, Abdul Jawad, Hyperbolic Scenario of Accelerating Universe in Modified Gravity, *Bul. Jor. Phys.*, **50**(2023). DOI: 10.1007/s10509-014-1833...
- [28] M.Sharif, Analysis of generalized ghost version of pilgrim dark energy, *Astrophysics. Space Sci.*, **351**(2014), 321. DOI: 10.1007/s10509-014-1833-y
- [29] V.Sahni, et al., Statefinder — a new geometrical diagnostic of dark energy, *JETP Lett.*, **77**(2003), 201.

Цилиндрически-симметричный обобщенный призрачный странник, темная энергия космологических вселенных

Мандала Кришна

Инженерный колледж Рагху, Вишакхапатнам
Андхра-Прадеш, Индия-531162

Собханбабу Каппала

Университетский инженерный колледж, Нарасараопет
Андхра-Прадеш, Индия-522616

Раджамаханти Санतिकумар

Институт технологий и менеджмента Адити
Шрикакулам Dist

Теккали, Андхра-Прадеш, Индия-53220

Аннотация. Решение цилиндрически-симметричной вселенной Эйнштейна Розена исследовано и связано с обобщенной темной энергией и материей призрачного странника. Чтобы получить точные решения уравнений поля Эйнштейна, мы обсудили модель GGPDE и определили параметр EoS. Области модели, которые необходимо идентифицировать с помощью анализа плоскости $\omega_d - \dot{\omega}_d$, Phantom и фазы квинтэссенции, которые будут обсуждаться с помощью средства поиска состояний, и стабильность модели, которая будет обсуждаться посредством квадрата скорости звука. Обсуждаются физические свойства модели. Полученные результаты будут полезны при текущих наблюдениях.

Ключевые слова: фантом, квинтэссенция, стабильность, цилиндрический, симметричный.

EDN: UODEBV
УДК 517.5

On a New Class of Integrals Involving Generalized Hypergeometric Functions

Adem Kilicman*

Department of Mathematics
Institute for Mathematical Research
University Putra Malaysia (UPM)
Selangor, Malaysia

Shantha Kumari Kurumujji†

Department of Mathematics
A J Institute of Engineering and Technology
Visvesvaraya Technological University (VTU), Belagavi
Karnataka, India

Arjun K. Rathie‡

Department of Mathematics
Vedant College of Engineering and Technology
Rajasthan Technical University
Rajasthan State, India

Received 27.04.2023, received in revised form 20.08.2023, accepted 11.01.2024

Abstract. In the theory of hypergeometric and generalized hypergeometric series, classical summation theorems such as those of Gauss, Gauss second, Bailey and Kummer for the series ${}_2F_1$; Watson, Dixon, Whipple and Saalshüz play a key role. Applications of the above mentioned summation theorems are well known. In our present investigation, we aim to evaluate twenty five new class of integrals involving generalized hypergeometric function in the form of a single integral of the form:

$$\int_0^1 x^{c-1}(1-x)^{c-1} {}_3F_2 \left[\begin{matrix} a, b, c + \frac{1}{2} \\ \frac{1}{2}(a+b+i+1), 2c+j \end{matrix} ; 4x(1-x) \right] dx$$

for $i, j = 0, \pm 1, \pm 2$.

The results are established with the help of the generalizations of the classical Watson's summation theorem obtained earlier by Lavoie et al. [2]. Fifty interesting integrals in the form of two integrals (twenty five each) have also been given as special cases of our main findings.

Keywords: generalized hypergeometric function, Watsons theorem, definite integral, beta integral.

Citation: A. Kilicman, S.K. Kumari, A.K. Rathie, On a New Class of Integrals Involving Generalized Hypergeometric Functions, J. Sib. Fed. Univ. Math. Phys., 2024, 17(2), 266–271. EDN: UODEBV.



1. Introduction and preliminaries

The natural generalization of the Gauss's hypergeometric function ${}_2F_1$ is called the generalized hypergeometric function ${}_pF_q$, where $p, q \in \mathbb{N}_0$ defined by [1, 5]

$${}_pF_q \left[\begin{matrix} a_1, \dots, a_p \\ b_1, \dots, b_q \end{matrix} ; z \right] = \sum_{n=0}^{\infty} \frac{(a_1)_n \dots (a_p)_n}{(b_1)_n \dots (b_q)_n} \frac{z^n}{n!} \quad (1)$$

*akilicman@putra.edu.my <https://orcid.org/0000-0002-1217-963X>

†shanthakk99@gmail.co <https://orcid.org/0000-0002-2153-0524>

‡arjunkumarrathie@gmail.com <https://orcid.org/0000-0003-3902-3050>

© Siberian Federal University. All rights reserved

where $(a)_n$ is the well known Pochhammer symbol (or the raised factorial or the shifted factorial since $(1)_n = n!$) defined for any complex $a \in \mathbb{C}$ by

$$(a)_n = \frac{\Gamma(a+n)}{\Gamma(a)}, \quad (a \in \mathbb{C} \setminus \mathbb{Z}_0^-) = \begin{cases} a(a+1)\dots(a+n-1), & (n \in \mathbb{N}) \\ 1, & (n = 0) \end{cases} \quad (2)$$

where Γ is the well known Gamma function.

For a detailed study about hypergeometric and generalized hypergeometric functions, we refer the standard texts [1, 5].

In the theory of hypergeometric and generalized hypergeometric functions, classical summation theorems such as those of Gauss, Gauss second, Kummer and Bailey for the series ${}_2F_1$; Watson, Dixon, Whipple and Saalschütz for the series ${}_3F_2$ play a key role.

Later, the above mentioned classical summation theorems have been generalized by Lavoie et al. [2-4].

However, in our present investigation, we are interested in the following classical Watson's summation theorem [1].

$${}_3F_2 \left[\begin{matrix} a, b, c \\ \frac{1}{2}(a+b+1), 2c \end{matrix}; 1 \right] = \frac{\Gamma(\frac{1}{2}) \Gamma(c + \frac{1}{2}) \Gamma(\frac{1}{2}a + \frac{1}{2}b + \frac{1}{2}) \Gamma(c - \frac{1}{2}a - \frac{1}{2}b + \frac{1}{2})}{\Gamma(\frac{1}{2}a + \frac{1}{2}) \Gamma(\frac{1}{2}b + \frac{1}{2}) \Gamma(c - \frac{1}{2}a + \frac{1}{2}) \Gamma(c - \frac{1}{2}b + \frac{1}{2})} \quad (3)$$

provided $\Re(2c - a - b) > -1$, and its following generalization due to Lavoie et al. [2].

$$\begin{aligned} & {}_3F_2 \left[\begin{matrix} a, b, c \\ \frac{1}{2}(a+b+i+1), 2c+j \end{matrix}; 1 \right] = \\ & = \mathcal{A}_{i,j} \frac{2^{a+b+i-2} \Gamma(\frac{1}{2}a + \frac{1}{2}b + \frac{1}{2}i + \frac{1}{2}) \Gamma(c + [\frac{j}{2}] + \frac{1}{2}) \Gamma(c - \frac{1}{2}(a+b+|i+j|-j-1))}{\Gamma(\frac{1}{2}) \Gamma(a) \Gamma(b)} \times \\ & \times \left\{ \mathcal{B}_{i,j} \frac{\Gamma(\frac{1}{2}a + \frac{1}{4}(1 - (-1)^i)) \Gamma(\frac{1}{2}b)}{\Gamma(c - \frac{1}{2}a + \frac{1}{2} + [\frac{j}{2}] - \frac{1}{4}(-1)^j (1 - (-1)^i)) \Gamma(c - \frac{1}{2}b + \frac{1}{2} + [\frac{j}{2}])} + \right. \\ & \left. + \mathcal{C}_{i,j} \frac{\Gamma(\frac{1}{2}a + \frac{1}{4}(1 + (-1)^i)) \Gamma(\frac{1}{2}b + \frac{1}{2})}{\Gamma(c - \frac{1}{2}a + [\frac{j+1}{2}] + \frac{1}{4}(-1)^j (1 - (-1)^i)) \Gamma(c - \frac{1}{2}b + [\frac{j+1}{2}])} \right\} = \\ & = \Omega \quad (\text{let}) \end{aligned} \quad (4)$$

for $i, j = 0, \pm 1, \pm 2$.

For $i = j = 0$, the result (4) reduces to classical Watson's summation theorem (3).

Here, $[x]$ denotes the greatest integer less than or equal to x and the modulus is denoted by $|x|$. For the expressions of the coefficients $\mathcal{A}_{i,j}$, $\mathcal{B}_{i,j}$ and $\mathcal{C}_{i,j}$, one can refer [2].

The aim of this paper is to evaluate twenty five integrals involving generalized hypergeometric function in the form of a single integral of the form

$$\int_0^1 x^{c-1} (1-x)^{c-1} {}_3F_2 \left[\begin{matrix} a, b, c + \frac{1}{2} \\ \frac{1}{2}(a+b+i+1), 2c+j \end{matrix}; 4x(1-x) \right] dx$$

for $i, j = 0, \pm 1, \pm 2$.

The results are derived with the help of generalized Watson's summation theorem on the sum of a ${}_3F_2$ given by (4). Fifty interesting integrals in the form of two integrals (twenty five each) have also been given as special cases of our main findings.

2. Main integrals

The twenty five integrals in the form of a single integral to be evaluated in this paper is given in the following theorem.

Theorem 2.1. For $\Re(c) > 0$, $\Re(2c - a - b + i + 2j + 1) > 0$, for $i, j = 0, \pm 1, \pm 2$, the following integral formula holds.

$$\int_0^1 x^{c-1}(1-x)^{c-1} {}_3F_2 \left[\begin{matrix} a, b, c + \frac{1}{2} \\ \frac{1}{2}(a+b+i+1), 2c+j \end{matrix}; 4x(1-x) \right] dx = \frac{\Gamma(c) \Gamma(c)}{\Gamma(2c)} \Omega \quad (5)$$

where Ω is the same as given in (4).

Proof: The proof of our theorem is quite straight forward. For this, we proceed as follows. Denoting the left hand side of (5) by I , we have

$$I = \int_0^1 x^{c-1}(1-x)^{c-1} {}_3F_2 \left[\begin{matrix} a, b, c + \frac{1}{2} \\ \frac{1}{2}(a+b+i+1), 2c+j \end{matrix}; 4x(1-x) \right] dx \quad (6)$$

Now expressing ${}_3F_2$ as a series, changing the order of integration and summation, which is easily seen to be justified due to the uniform convergence of the series in the interval $(0, 1)$, we have

$$I = \sum_{n=0}^{\infty} \frac{(a)_n (b)_n (c)_n 2^{2n}}{\left(\frac{1}{2}(a+b+i+1)\right)_n (2c+j)_n} \int_0^1 x^{c+n-1}(1-x)^{c+n-1} dx \quad (7)$$

Evaluating the Beta integral and using the result

$$(a)_n = \frac{\Gamma(a+n)}{\Gamma(a)}$$

we have, after some simplification

$$I = \frac{\Gamma(c) \Gamma(c)}{\Gamma(2c)} \sum_{n=0}^{\infty} \frac{(a)_n (b)_n (c)_n}{\left(\frac{1}{2}(a+b+i+1)\right)_n (2c+j)_n n!} \quad (8)$$

Now summing up the series, we have

$$I = \frac{\Gamma(c) \Gamma(c)}{\Gamma(2c)} = {}_3F_2 \left[\begin{matrix} a, b, c \\ \frac{1}{2}(a+b+i+1), 2c+j \end{matrix}; 4x(1-x) \right] \quad (9)$$

We now observe that the ${}_3F_2$ appearing can be evaluated with the help of known result (4) and we easily arrive at the right hand side of (5).

This completes the proof of the theorem. \square

3. Special cases

In this section, we shall mention a large number of very interesting special cases of our main findings.

For this, we observe here that, in (5), we let $b = -2n$ and replace a by $a + 2n$ or we let $b = -2n - 1$ and replace a by $a + 2n + 1$. In each case, one of the two terms appearing on the right-hand side of (5) will vanish and we get fifty interesting special cases (twenty five each) given below in the form of two corollaries.

Corollary 3.1. For $i, j = 0, \pm 1, \pm 2$, the following twenty five results holds.

$$\int_0^1 x^{c-1}(1-x)^{c-1} {}_3F_2 \left[\begin{matrix} -2n, a+2n, c+\frac{1}{2} \\ \frac{1}{2}(a+i+1), 2c+j \end{matrix}; 4x(1-x) \right] dx =$$

$$= D_{i,j} \frac{\Gamma(c) \Gamma(c)}{\Gamma(2c)} \frac{\left(\frac{1}{2}\right)_n \left(\frac{1}{2}a - c + \frac{3}{4} - \frac{(-1)^i}{4} - \left[\frac{1}{2}j + \frac{1}{4}(1 + (-1)^i)\right]\right)_n}{\left(c + \frac{1}{2} + \left[\frac{j}{2}\right]\right)_n \left(\frac{1}{2}a + \frac{1}{4}(1 + (-1)^i)\right)_n} \tag{10}$$

where the coefficients $D_{i,j}$ are as in Tables (1) and (2) given below.

Table 1. Table for $D_{i,j}$, $i = 0, \pm 1, \pm 2$ and $j = -2, -1, 0$

$i \setminus j$	-2	-1	0
2	$\frac{(a+1)[(c-1)(a-1)+2n(a+2n)]}{(c-1)(a+4n-1)(a+4n+1)}$	$\frac{(a+1)(a-1)}{(a+4n+1)(a+4n-1)}$	$\frac{(a+1)[(a-1)(2c-a-1)-4n(a+2n)]}{(2c-a-1)(a+4n+1)(a+4n-1)}$
1	$\frac{a(c+2n-1)}{(c-1)(a+4n)}$	$\frac{a}{a+4n}$	$\frac{a}{a+4n}$
0	$1 - \frac{2n(a+2n)}{(c-1)(2c-a-3)}$	1	1
-1	$1 - \frac{2n(2c+a+4n-2)}{(c-1)(2c-a-4)}$	$1 - \frac{4n}{(2c-a-2)}$	1
-2	$D_{-2,-2}$	$1 - \frac{8n(a+2n)}{(a-1)(2c-a-3)}$	$1 - \frac{4n(a+2n)}{(a-1)(2c-a-1)}$

$$D_{-2,-2} = 1 - \frac{2an(6c+a-7)(2c-a-3) - 4n^2[5a^2 - 4a - 21 - 4c(3c-a-8)] - 64n^3(a+n)}{(c-1)(a-1)(2c-a-3)(2c-a-5)}$$

Table 2. Table for $D_{i,j}$, $i = 0, \pm 1, \pm 2$ and $j = 1, 2$

$i \setminus j$	1	2
2	$\frac{(a+1)[(a-1)(2c-a-1)-8n(a+2n)]}{(2c-a-1)(a+4n+1)(a+4n-1)}$	$D_{2,2}$
1	$\frac{a(2c-a-4n)}{(2c-a)(a+4n)}$	$\frac{a[(c+1)(2c-a)-2n(2c+a+4n+2)]}{(c+1)(2c-a)(a+4n)}$
0	1	$1 - \frac{2n(a+2n)}{(c+1)(2c-a+1)}$
-1	1	$1 + \frac{2n}{(c+1)}$
-2	1	$1 + \frac{2n(a+2n)}{(c+1)(a-1)}$

$$D_{2,2} = \frac{(a+1) \left((a-1)(c+1)(2c-a+1)(2c-a-1) - 2an(6c+a+5)(2c-a+1) + 4n^2(5a^2+4a-5-4c(3c-a+4)) + 64n^3(a+n) \right)}{(c+1)(2c-a+1)(2c-a-1)(a+4n+1)(a+4n-1)}$$

Corollary 3.2. For $i, j = 0, \pm 1, \pm 2$, the following twenty five results holds.

$$\int_0^1 x^{c-1}(1-x)^{c-1} {}_3F_2 \left[\begin{matrix} -2n-1, a+2n+1, c+\frac{1}{2} \\ \frac{1}{2}(a+i+1), 2c+j \end{matrix}; 4x(1-x) \right] dx =$$

$$= E_{i,j} \frac{\Gamma(c) \Gamma(c)}{\Gamma(2c)} \frac{\left(\frac{3}{2}\right)_n \left(\frac{1}{2}a - c + \frac{5}{4} + \frac{(-1)^i}{4} - \left[\frac{1}{2}j + \frac{1}{4}(1 + (-1)^i)\right]\right)_n}{\left(c + \frac{1}{2} + \left[\frac{j+1}{2}\right]\right)_n \left(\frac{1}{2}a + \frac{1}{4}(3 - (-1)^i)\right)_n} \tag{11}$$

where the coefficient $E_{i,j}$ are as in Tables (3) and (4) given below.

Table 3. Table for $E_{i,j}$ $i = 0, \pm 1, \pm 2$ and $j = -2, -1, 0$

$i \setminus j$	-2	-1	0
2	$\frac{(a+1)(2c-a-3)}{(c-1)(a+4n+1)(a+4n+3)}$	$\frac{(a+1)(4c-a-3)}{(a+4n+1)(a+4n+3)(2c-1)}$	$\frac{2(a+1)}{(a+4n+1)(a+4n+3)}$
1	$\frac{(c-a-2n-2)}{(c-1)(a+4n+2)}$	$\frac{2c-a-2}{(a+4n+2)(2c-1)}$	$\frac{1}{a+4n+2}$
0	$\frac{-1}{(c-1)}$	$\frac{-1}{(2c-1)}$	0
-1	$E_{-1,-2}$	$\frac{-(2c+a+4n)}{a(2c-1)}$	$\frac{-1}{a}$
-2	$\frac{-(2c+a+4n-1)(2c-a-4n-5)}{(a-1)(c-1)(2c-a-5)}$	$E_{-2,-1}$	$\frac{-2}{(a-1)}$

$$E_{-2,-1} = - \frac{[(4c + a - 1)(2c - a - 3) - 8n(a + 2n + 2)]}{(a - 1)(2c - 1)(2c - a - 3)}$$

$$E_{-1,-2} = - \frac{[(c + a)(2c - a - 4) - 2n(3a - 2c + 4n + 6)]}{a(c - 1)(2c - a - 4)}$$

Table 4. Table for $E_{i,j}$ $i = 0, \pm 1, \pm 2$ and $j = 1, 2$

$i \setminus j$	1	2
2	$E_{2,1}$	$\frac{(a+1)(2c+a+4n+3)(2c-a-4n-1)}{(c+1)(2c-a-1)(a+4n+1)(a+4n+3)}$
1	$\frac{(2c+a+4n+2)}{(2c+1)(a+4n+2)}$	$\frac{(c+a+2)(2c-a)-2n(3a-2c+4n+2)}{(c+1)(2c-a)(a+4n+2)}$
0	$\frac{1}{(2c+1)}$	$\frac{1}{(c+1)}$
-1	$\frac{-(2c-a)}{a(2c+1)}$	$\frac{-(c-a-2n)}{a(c+1)}$
-2	$\frac{-(4c-a+1)}{(a-1)(2c+1)}$	$\frac{-(2c-a+1)}{(a-1)(c+1)}$

$$E_{2,1} = \frac{(a + 1)[(4c + a + 3)(2c - a - 1) - 8n(a + 2n + 2)]}{(a + 4n + 1)(a + 4n + 3)(2c + 1)(2c - a - 1)}$$

In particular, in (10), if we take $i = j = 0$, we get the following interesting result.

$$\int_0^1 x^{c-1}(1-x)^{c-1} {}_3F_2 \left[\begin{matrix} -2n, a+2n, c+\frac{1}{2} \\ \frac{1}{2}(a+b+1), 2c \end{matrix}; 4x(1-x) \right] dx =$$

$$= \frac{\Gamma(c) \Gamma(c)}{\Gamma(2c)} \frac{\left(\frac{1}{2}\right)_n}{\left(c+\frac{1}{2}\right)_n} \frac{\left(\frac{1}{2}a-c+\frac{1}{2}\right)_n}{\left(\frac{1}{2}a+\frac{1}{2}\right)_n}$$
(12)

Similarly, in (11), if we take $i = j = 0$, we get the following elegant result.

$$\int_0^1 x^{c-1}(1-x)^{c-1} {}_3F_2 \left[\begin{matrix} -2n-1, a+2n+1, c+\frac{1}{2} \\ \frac{1}{2}(a+b+1), 2c \end{matrix}; 4x(1-x) \right] dx = 0$$
(13)

Similarly, we can obtain other results. We, however, prefer to omit the details.

Conclusions

In this paper, we have evaluated twenty five interesting integrals involving generalized hypergeometric function in the form of a single integral.

The results are established with the help of generalization of classical Watson's summation theorem obtained earlier by Lavoie et al. [2].

Fifty interesting integrals in the form of two integrals (twenty five each) have also been evaluated as special cases of our main findings.

We conclude this paper by remarking that the interesting applications of the integrals obtained in this paper are under investigations and will be published soon.

References

- [1] W.N.Bailey, Generalized Hypergeometric Series, Cambridge Tracts in Mathematics and Mathematical Physics, no. 32, Stechert-Hafner, New York, NY, USA, 1964.
- [2] J.L.Lavoie, F.Groncin, A.K.Rathie, Generalizations of Watson's theorem on the sum of a ${}_3F_2$, *Indian J. Math.*, **34**(1992), no. 2, 23–32.
- [3] J.L.Lavoie, F.Groncin, A.K.Rathie, K.Arora, Generalizations of Dixon's theorem on the sum of a ${}_3F_2$, *Math. Comput.*, **62**(1994), 267–276, .
- [4] J.L.Lavoie, F.Groncin, A.K.Rathie, Generalizations of Whipple's theorem on the sum of a ${}_3F_2$, *J. Comput. Appl. Math.*, **72**(1996), 293–300.
- [5] E.D.Rainville, *Special Functions*, Macmillan Company, New York, 1960; Reprinted by Chelsea Publishing Company, Bronx, New York, 1971.

О новом классе интегралов, включающих обобщенные гипергеометрические функции

Адем Киликман

Институт математических исследований
Университет Путра Малайзия (UPM)
Селангор, Малайзия

Шанта Кумари Курумуджи

АИ Институт инженерии и технологий
Висвесварайский технологический университет (VTU), Белагави
Карнатака, Индия

Арджун К. Рати

Ведантский инженерно-технологический колледж
Технический университет Раджастана
Штат Раджастан, Индия

Аннотация. В теории гипергеометрических и обобщенных гипергеометрических функций классические теоремы суммирования, такие как теоремы Гаусса, Бейли и Каммера для серии ${}_2F_1$; Уотсона, Диксона, Уиппла и Саалшуз, играют ключевую роль. Приложения вышеупомянутых теорем о суммировании хорошо известны. В нашем настоящем исследовании мы стремимся оценить двадцать пять новых классов интегралов, включающих обобщенную гипергеометрическую функцию в форме единого интеграла:

$$\int_0^1 x^{c-1}(1-x)^{c-1} {}_3F_2 \left[\begin{matrix} a, b, c + \frac{1}{2} \\ \frac{1}{2}(a+b+i+1), 2c+j \end{matrix} ; 4x(1-x) \right] dx$$

for $i, j = 0, \pm 1, \pm 2$.

Результаты устанавливаются с помощью обобщений теоремы классической суммы Уотсона, полученной ранее Лавойе и др. [2]. Пятьдесят интересных интегралов в форме двух видов интегралов (двадцать пять каждый) также были даны в качестве особых случаев наших основных результатов.

Ключевые слова: обобщенная гипергеометрическая функция, теорема Уотсона, определенный интеграл, бета-интеграл.

EDN: VEGZRT

УДК 519.688

Analysis of the Unstable State of a Nematic Liquid Crystal Based on a Simplified Dynamic Model

Irina V. Smolekho*

Institute of Computational Modelling SB RAS
Krasnoyarsk, Russian Federation

Received 18.05.2023, received in revised form 01.11.2023, accepted 14.02.2024

Abstract. The Fréedericksz effect consisting in the reorientation of liquid crystal molecules in an extended layer under the action of inhomogeneous electric field is simulated in the paper. The constitutive equations for tangential stress, angular velocity, and electric potential are obtained from the equations of a simplified dynamic model of a 5CB nematic liquid crystal in the acoustic approximation. The algorithm for numerical solution of the constitutive equations is constructed on the basis of finite-difference schemes. The algorithm is implemented with the use of CUDA technology for computers with graphics accelerators.

Keywords: liquid crystal, dynamics, electric potential, Fréedericksz effect, method of straight lines, Laplace equation, parallel programming, CUDA technology.

Citation: I.V. Smolekho, Analysis of the Unstable State of a Nematic Liquid Crystal Based on a Simplified Dynamic Model, J. Sib. Fed. Univ. Math. Phys., 2024, 17(3), 272–281. EDN: VEGZRT.



Introduction

Liquid crystals (LCs) have in a certain temperature range both fluidity (the property of liquids) and anisotropy (the property of solid crystals). There is an order in the spatial orientation of liquid crystal molecules which significantly affects their properties. To characterize the order a unit vector “director” is introduced. It specifies the preferred direction of the molecules. Depending on the order of orientation of molecules there are three classes of LCs: nematic (molecules are oriented in the direction of the vector-director and located randomly), smectic (molecules form layers, and each layer has its own orientation of molecules) and cholesteric (molecules are form into layers, creating a spiral). Liquid crystals are sensitive to external influences which make it possible to control their properties by changing their spatial orientation. That is why the liquid crystal state of matter is of scientific interest to researchers. Liquid crystals are widely used in creating displays of various digital devices. Due to anisotropy of the permittivity weak electric field causes the liquid crystal molecules to rotate, and it results in the change of optical properties. The reorientation of liquid crystal molecules under the action of electric field was first observed and studied by Fréedericksz and his colleagues [1]. The orientation was changed when strong enough field was applied to the liquid crystal. This effect was called the Fréedericksz transition, and it has a threshold character. Theoretically, it was studied using the elastic free energy of Frank and the energy of interaction with electric field. The Oseen–Frank model [2,3] describes

*ismol@icm.krasn.ru <https://orcid.org/0000-0002-9852-9310>

© Siberian Federal University. All rights reserved

the static state of liquid crystals. According to the theory, the field causes such deformation of the liquid crystal that distribution of molecules corresponds to minimum of the free energy which is equal to the sum of elastic and dielectric components. The elastic energy is a quadratic form in terms of derivatives of the vector-director with respect to spatial coordinates. However, this model cannot be generalized for the analysis of dynamic processes. It does not take into account translational motion because only rotational motion is considered. By now universal dynamic model has been developed by Eriksen [4] and Leslie [5]. It is based on conservation laws and takes into account translational and rotational degrees of freedom of molecules. This theory describes the flow of nematic liquid crystal from the hydrodynamic point of view, and it is reduced to the Oseen–Frank theory in the static case. The need to create new dynamic models of liquid crystal is dictated by the complexity of the existing universal Eriksen–Leslie model that requires construction of state functions using specific experiments. A simplified dynamic model in the acoustic approximation was proposed [6]. It includes equations of acoustics and heat conduction. These equations are based on conservation laws and the Cosserat continuum model, and they include small independent rotations of particles in addition to translational motion. The model describes the dynamic behaviour of nematic liquid crystals under the action of mechanical, thermal and electrical external factors.

Analysis of an unstable state in statics was carried out in [7], where the governing equations of the model are non-linear variational Euler equations for the electric potential and the orientation angle of molecules in the problem of minimizing the potential energy functional.

This work is devoted to modelling the reorientation of molecules in an extended liquid crystal layer located in the electric field of a capacitor with short plates arranged periodically. The governing equations are obtained from the simplified dynamic model of the liquid crystal in the acoustic approximation. The developed parallel numerical algorithm is based on an explicit difference scheme of the second order of approximation. The accuracy of numerical solution can be improved by choosing a finer grid due to the distribution of computational load. The computational algorithm is implemented as a software package written in C++ by means of CUDA technology using video card graphics accelerators.

1. Formulation of the problem

The governing partial differential equations for the angular velocity ω and tangential stress q are obtained by differentiating the equations of the simplified dynamic model of the nematic liquid crystal:

$$\begin{aligned} \frac{\partial^2 q}{\partial t^2} + \frac{2\alpha}{\eta} \frac{\partial q}{\partial t} + 2\alpha \frac{\partial \omega}{\partial t} &= \frac{\alpha}{\rho} \left(\Delta q + \frac{\partial f_2}{\partial x_1} - \frac{\partial f_1}{\partial x_2} \right), \\ \frac{\partial^2 \omega}{\partial t^2} - \frac{2}{j} \frac{\partial q}{\partial t} &= \frac{\gamma}{j} \Delta \omega + \frac{1}{j} \frac{\partial m}{\partial t}. \end{aligned} \tag{1}$$

Here ρ is the density, j is the moment of inertia, η is the viscosity coefficient, α is the modulus of elastic resistance to rotation, γ is the modulus of elastic resistance to curvature change. Equations (1) describe moment interactions of liquid crystal molecules under the action of inhomogeneous electric field in a two-dimensional formulation. This model of the effect of the Fréedericksz reorientation have a fewer number of equations in comparison with the general model. The initial data for q and ω are

$$q\Big|_{t=0} = q^0, \quad \omega\Big|_{t=0} = \omega^0, \quad \frac{\partial q}{\partial t}\Big|_{t=0} = -2\alpha\left(\omega^0 + \frac{q^0}{\eta}\right), \quad \frac{\partial \omega}{\partial t}\Big|_{t=0} = \frac{2q^0 + m}{j},$$

where q^0, ω^0 are the values of the required quantities at the initial moment of time. The initial linear velocities and moment stresses are assumed to be equal to zero. The boundary conditions are formulated in terms of q and ω . The symmetry conditions for stress state of the liquid crystal are given in terms of derivatives q_{x_1}, ω_{x_1} or q_{x_2}, ω_{x_2} (depending on the symmetry line).

During the action of electric field bulk forces $f = (P \cdot \nabla) E$ and moment of forces $m = P \times E$ arise. Here $E = -\nabla\varphi$ is the electric field vector, $P = \varepsilon_0 \chi E$ is the electric polarization vector, $\chi = \varepsilon - I$ is the dielectric susceptibility tensor, and ε is the dielectric susceptibility tensor. In a 2D formulation of the problem bulk forces and moment of forces are defined as follows

$$\begin{aligned} f_1 &= \varepsilon_0 \left(\chi_{11} \frac{\partial \varphi}{\partial x_1} + \chi_{12} \frac{\partial \varphi}{\partial x_2} \right) \frac{\partial^2 \varphi}{\partial x_1^2} + \varepsilon_0 \left(\chi_{12} \frac{\partial \varphi}{\partial x_1} + \chi_{22} \frac{\partial \varphi}{\partial x_2} \right) \frac{\partial^2 \varphi}{\partial x_1 \partial x_2}, \\ f_2 &= \varepsilon_0 \left(\chi_{11} \frac{\partial \varphi}{\partial x_1} + \chi_{12} \frac{\partial \varphi}{\partial x_2} \right) \frac{\partial^2 \varphi}{\partial x_1 \partial x_2} + \varepsilon_0 \left(\chi_{12} \frac{\partial \varphi}{\partial x_1} + \chi_{22} \frac{\partial \varphi}{\partial x_2} \right) \frac{\partial^2 \varphi}{\partial x_2^2}, \\ m &= \varepsilon_0 (\chi_{11} - \chi_{22}) \frac{\partial \varphi}{\partial x_1} \frac{\partial \varphi}{\partial x_2} - \varepsilon_0 \chi_{12} \left(\left(\frac{\partial \varphi}{\partial x_1} \right)^2 - \left(\frac{\partial \varphi}{\partial x_2} \right)^2 \right). \end{aligned} \quad (2)$$

The permittivity along molecules ε_{\parallel} and permittivity across molecules ε_{\perp} are different. Components of ε tensor depend on rotation angle of molecules θ :

$$\varepsilon_{11} = \varepsilon_{\parallel} \cos^2 \theta + \varepsilon_{\perp} \sin^2 \theta, \quad \varepsilon_{22} = \varepsilon_{\parallel} \sin^2 \theta + \varepsilon_{\perp} \cos^2 \theta, \quad \varepsilon_{12} = \varepsilon_{21} = (\varepsilon_{\parallel} - \varepsilon_{\perp}) \cos \theta \sin \theta,$$

Relations for calculating components of the permittivity tensor contain rotation angle that changes each time step when solving dynamic problem. Thus, it is necessary to add an equation for the rotation angle to system of equations (1):

$$\frac{\partial \theta}{\partial t} = \omega. \quad (3)$$

Bulk forces and moment of forces (2) are taken into account in the right parts of governing equations (1). In turn, a change in the spatial orientation of molecular domains due to the action of forces and moment of forces leads to a change in the permittivity tensor. Then, electric field is changed.

The perturbation by the electric field occurs as follows. A horizontally infinite flat liquid crystal layer located between short capacitor plates is considered. Potential difference is set between upper and bottom plates: $\varphi^+ = \varphi^0, \varphi^- = -\varphi^0$. Conditions for the continuity of the electric potential (between the dielectric and air) and the continuity of the normal component of the electric induction vector are set at the interface:

$$\begin{aligned} \varphi^+ &= \varphi, \quad \frac{\partial \varphi^+}{\partial x_2} = \varepsilon_{12} \frac{\partial \varphi}{\partial x_1} + \varepsilon_{22} \frac{\partial \varphi}{\partial x_2} \quad \text{if } x_2 = h, \\ \varphi &= \varphi^-, \quad \varepsilon_{12} \frac{\partial \varphi}{\partial x_1} + \varepsilon_{22} \frac{\partial \varphi}{\partial x_2} = \frac{\partial \varphi^-}{\partial x_2} \quad \text{if } x_2 = 0. \end{aligned}$$

The initial distribution of orientation angles θ_0 relative to the x_1 axis is known inside the layer. It is given, for example, as shown in Fig. 1. Angle θ is calculated in succeeding time steps using the difference analogue of equation (3).

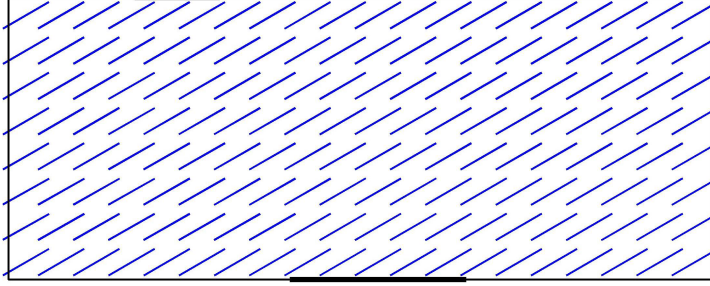


Fig. 1. Scheme of perturbation of the liquid crystal layer by an electric field

2. Computational algorithm

The solution of the problem includes several stages. At the first stage, it is necessary to calculate the values of the electric potential included in (2). The electric potential satisfies the anisotropic equation $\nabla \cdot (\varepsilon \cdot \nabla \varphi) = 0$ in the LC layer. To solve this equation the finite difference method is used to implement an iterative process in which the Poisson equation is recursively solved using fast Fourier transform with respect to new approximation of the potential φ^{n+1} :

$$\tilde{\varepsilon} \Delta \varphi^{n+1} = \tilde{\varepsilon} \Delta \varphi^n - \nabla \cdot (\varepsilon \cdot \nabla \varphi^n).$$

Here the right hand side is calculated using approximation from the previous time step φ^n , constant $\tilde{\varepsilon}$ is chosen in such a way that iterative process converges. The process continues until the relative error defined as the uniform difference norm becomes sufficiently small. Calculations showed that no more than 10 iterations are required for the convergence of the iterative process with a relative error of 10^{-5} for $\tilde{\varepsilon} = (\varepsilon_{\parallel} + \varepsilon_{\perp})/2$.

The Laplace equation $\Delta \varphi = 0$ is satisfied outside the LC layer. It is solved by the method of straight lines. The segment is uniformly partitioned in the direction x_1 , and derivatives with respect to x_2 are replaced by finite differences. Thus, function φ is discrete in the direction x_1 and continuous in the direction x_2 . Further, the solution is constructed using the Fourier transform. To calculate the solution, the same rectangular grid is considered for both solutions. The algorithm of calculation of electrical action on the liquid crystal layer is described in detail in [8]. After finding the values of the electric potential, bulk forces and moment of forces are calculated using (2) where partial derivatives are replaced with finite differences. At the last stage, using the explicit second order of accuracy finite-difference scheme “cross” values of q and ω are determined:

$$\begin{aligned} \omega_{i_1, i_2}^{n+1} &= 2\omega_{i_1, i_2}^n - \omega_{i_1, i_2}^{n-1} + \frac{\Delta t}{j} (q_{i_1, i_2}^{n+1} - q_{i_1, i_2}^{n-1}) + \\ &+ \frac{\gamma (\Delta t)^2}{j} \left(\frac{\omega_{i_1+1, i_2}^n - 2\omega_{i_1, i_2}^n + \omega_{i_1-1, i_2}^n}{(\Delta x_1)^2} + \frac{\omega_{i_1, i_2+1}^n - 2\omega_{i_1, i_2}^n + \omega_{i_1, i_2-1}^n}{(\Delta x_2)^2} \right) + \\ &+ \frac{\Delta t}{2j} (m_{i_1, i_2}^n - m_{i_1, i_2}^{n-1}), \end{aligned} \quad (4)$$

$$\begin{aligned}
& \left(\frac{\alpha}{j} + \frac{\alpha}{\eta \Delta t} + \frac{1}{(\Delta t)^2} \right) q_{i_1, i_2}^{n+1} = \frac{2}{(\Delta t)^2} q_{i_1, i_2}^n + \frac{2\alpha}{\Delta t} \left(\omega_{i_1, i_2}^{n-1} - \omega_{i_1, i_2}^n \right) + \\
& + \left(\frac{\alpha}{j} + \frac{\alpha}{\eta \Delta t} - \frac{1}{(\Delta t)^2} \right) q_{i_1, i_2}^{n-1} + \frac{\alpha}{\rho} \left(\frac{q_{i_1+1, i_2}^n - 2q_{i_1, i_2}^n + q_{i_1-1, i_2}^n}{(\Delta x_1)^2} + \right. \\
& + \frac{q_{i_1, i_2+1}^n - 2q_{i_1, i_2}^n + q_{i_1, i_2-1}^n}{(\Delta x_2)^2} + \frac{f_{2i_1+1, i_2}^n - f_{2i_1-1, i_2}^n}{2\Delta x_1} - \\
& \left. - \frac{f_{1i_1, i_2+1}^n - f_{1i_1, i_2-1}^n}{2\Delta x_2} \right) + \frac{\alpha}{2j} \left(m_{i_1, i_2}^n - m_{i_1, i_2}^{n-1} \right) - \\
& - \frac{\alpha \gamma \Delta t}{j} \left(\frac{\omega_{i_1+1, i_2}^n - 2\omega_{i_1, i_2}^n + \omega_{i_1-1, i_2}^n}{(\Delta x_1)^2} + \frac{\omega_{i_1, i_2+1}^n - 2\omega_{i_1, i_2}^n + \omega_{i_1, i_2-1}^n}{(\Delta x_2)^2} \right).
\end{aligned} \tag{5}$$

Then rotation angle is recalculated as follows

$$\theta_{i_1, i_2}^{n+1} = \theta_{i_1, i_2}^n + \frac{\Delta t}{2} \left(\omega_{i_1, i_2}^{n+1} + \omega_{i_1, i_2}^n \right).$$

3. Analysis of the unstable state of LC based on the Oseen–Frank model

When the potential difference is below of some threshold value, an oscillatory motion of molecules occurs with a small deviation from the initial position. The static Oseen–Frank theory is used to estimate the instability of the equilibrium of the liquid crystal. In accordance with the theory, the distribution of orientation angles of molecules in the equilibrium state of the LC layer under the action of electric field created by charges on the plates satisfies the stationarity condition for the potential energy functional:

$$J = \int_V \left(F - \frac{1}{2} D \cdot E \right) dV.$$

Here V is the rectangular area selected in accordance with the symmetry of the problem, $E = - (0, \varphi_{x_2}, 0)$, $D = \varepsilon_0 \varepsilon_{\perp} E + \varepsilon_0 \Delta \varepsilon (n \cdot E) n$, $\Delta \varepsilon = \varepsilon_{\parallel} - \varepsilon_{\perp}$. The Frank free energy F in the one-constant approximation takes the form

$$F = \frac{1}{2} \gamma \left(|\nabla \cdot n|^2 + |\nabla \times n|^2 \right). \tag{6}$$

The vector-director responsible for the predominant direction of liquid crystal molecules depends in this case only on x_2 : $n = (\cos \theta(x_2), \sin \theta(x_2), 0)$. The equilibrium of liquid crystal molecules is achieved by minimizing the Oseen–Frank free energy functional:

$$\int_V \left(F - \frac{1}{2} D \cdot E \right) dV \rightarrow \min, \tag{7}$$

where

$$D \cdot E = \varepsilon_0 \varepsilon_{\perp} E^2 + \varepsilon_0 \Delta \varepsilon (n \cdot E)^2. \tag{8}$$

Taking into account that the first term in expression (8) does not depend on n and n in turn does not depend on x_1 , this expression takes the form

$$D \cdot E = \varepsilon_0 \varepsilon_{\perp} \left(\frac{d\varphi}{dx_2} \right)^2 + \varepsilon_0 \Delta \varepsilon \left(\frac{d\varphi}{dx_2} \right)^2 \sin^2 \theta.$$

After substituting (6) and (8) into (7) and taking into account that $\sin \theta \approx \theta$, one can obtain

$$\int_0^h \left[\frac{\gamma}{2} \left(\frac{d\theta}{dx_2} \right)^2 - \frac{1}{2} \varepsilon_0 \varepsilon_{\perp} \left(\frac{d\varphi}{dx_2} \right)^2 - \frac{1}{2} \varepsilon_0 \Delta\varepsilon \left(\frac{d\varphi}{dx_2} \right)^2 \theta^2 \right] dx_2 \rightarrow \min.$$

Varying the functional and integrating it by parts, one can obtain that

$$\int_0^h \left[-\gamma \frac{d^2\theta}{dx_2^2} - \varepsilon_0 \Delta\varepsilon \left(\frac{d\varphi}{dx_2} \right)^2 \theta \right] \delta\theta dx_2 = 0.$$

Thus, the Euler equation is obtained:

$$\gamma \frac{d^2\theta}{dx_2^2} = -\varepsilon_0 \Delta\varepsilon \left(\frac{d\varphi}{dx_2} \right)^2 \theta. \quad (9)$$

The following chain of transformations is valid

$$\theta = e^{\lambda x_2}, \quad \gamma \lambda^2 = -\varepsilon_0 \Delta\varepsilon \left(\frac{d\varphi}{dx_2} \right)^2, \quad \lambda = \pm i \sqrt{\frac{\varepsilon_0 \Delta\varepsilon \left(\frac{d\varphi}{dx_2} \right)^2}{\gamma}};$$

$$\theta = \sin \sqrt{\frac{\varepsilon_0 \Delta\varepsilon \left(\frac{d\varphi}{dx_2} \right)^2}{\gamma}} x_2 \Big|_0^h = 0 \quad \Rightarrow \quad \sqrt{\frac{\varepsilon_0 \Delta\varepsilon \left(\frac{d\varphi}{dx_2} \right)^2}{\gamma}} h = \pi.$$

Minimization of the functional gives an estimate of the instability at which the functional loses its convexity. Corresponding Euler equation (9) with boundary conditions $\theta(0) = \theta(h) = 0$ has non-trivial solutions

$$\varphi^+ - \varphi^- = \pi \sqrt{\frac{\gamma}{\varepsilon_0 \Delta\varepsilon}}.$$

For a 5CB liquid crystal with $\gamma = 6 \cdot 10^{-12}$ H, $\varepsilon_{\parallel} = 16.7$, $\varepsilon_{\perp} = 7$ the threshold value the potential difference is about 1 V. Above this value, the molecules lose their stability and turn along the direction of the field, forming swarms of identically oriented molecules.

4. Calculation results

A parallel program implementing the described algorithms is written in C++ using CUDA technology for computing systems with graphics accelerators. The calculations were carried out on the high-performance Flagman server of ICM SB RAS.

In all calculations, the coefficients for the 5CB liquid crystal were taken according to experimental data [9]. Earlier, the value of coefficient $\alpha = \nu^2 j \pi^2$ was based on the resonant frequency $\nu^* = 350$ MHz obtained experimentally in [10]. In the present work, calculations were carried out for various values of ν . It was studied how the orientation of molecules changes at different time steps in this case. The bulk density of the moment of inertia is determined as $j = \rho (N\delta_0)^2 / 12$, where $\delta_0 = 1.87$ nm, $N = 10$, $\rho = 1022$ kg/m³. A finite difference grid is introduced in the space x_1, x_2 with the space step Δx_1 in the direction x_1 and the space step Δx_2 in the direction x_2 . The time step is defined as Δt . The grid consists of a set of nodes $R_{i_1, i_2}^n = R(t_n, x_{1i_1}, x_{2i_2})$. Loads can be specified on some sections of the boundary.

Figs. 2–4 show the results of calculations for $10 \times 4 \mu\text{m}$ liquid crystal layer under the action of electric field for various initial orientations of molecules and various arrangements of plates.

The horizontal lines show the boundaries of the layer exposed to electric field. The thick lines show the capacitor plates. The capacitor plates are arranged non-symmetrically in Fig. 2 *a*, and they are arranged symmetrically in Fig. 2 *b*. The length of the upper plate is $1 \mu\text{m}$, the length of the lower plate is $2.5 \mu\text{m}$ in both calculations. The finite difference grid in the LC layer contains 640×256 cells, and in the outer parts of the layer it contains 640×128 cells.

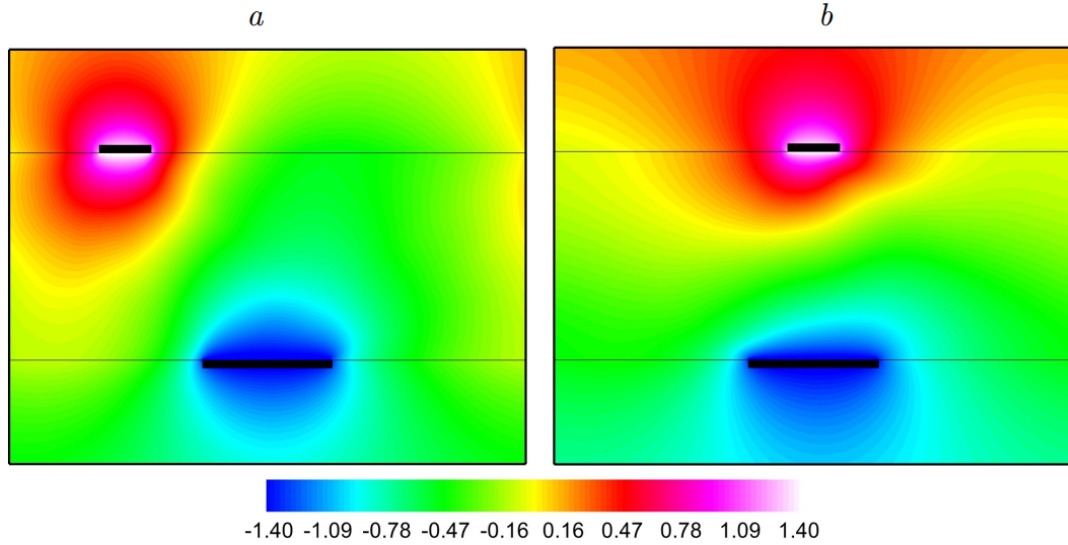


Fig. 2. Disturbance of the LC layer by electric field: level lines of electric potential φ at 10000th time step; rotation angle of molecules $\theta = \pi/4$ (*a*), 0 (*b*)

Fig. 3 shows the level lines for the rotation angle of molecules in the LC layer for the problem in Fig. 2 *a* for different α and ν at various time steps. The results for $\nu = 11$ MHz and $\alpha = 0.36$ Pa are shown on the left side, and results for $\nu = 35$ MHz and $\alpha = 3.6$ Pa are shown on the right side. The potential difference is 1.5 V that exceeds the threshold value of 1 V. Therefore, liquid crystal molecules are reoriented in the direction of the electric field. One can also observe the effect of formation of large domains of identically oriented molecules (so-called swarms), the size of which changes with time.

Fig. 4 shows level lines with similar parameters but for symmetrical capacitor plates for the problem in Fig. 2 *b*.

It is noted that the smaller ν and hence coefficient α the larger swarms are formed which more slowly break up into smaller ones over time. Swarms disintegrate already at 20000–25000 time step for $\nu = 35$ MHz. That is not observed for $\nu = 11$ MHz.

Conclusion

This paper presents mathematical model of the action of electrical field on liquid crystals. Equations of the model are obtained from the previously developed dynamic model within the framework of acoustic approximation. The model allows one to significantly speed up the time of calculations. The algorithm for numerical solution of model equations is implemented as a parallel program in C++ using CUDA technology.

The developed model can be used to study the behaviour of liquid crystals under the action of electric field in dynamics and formation of swarms depending on the intensity of electric field, the

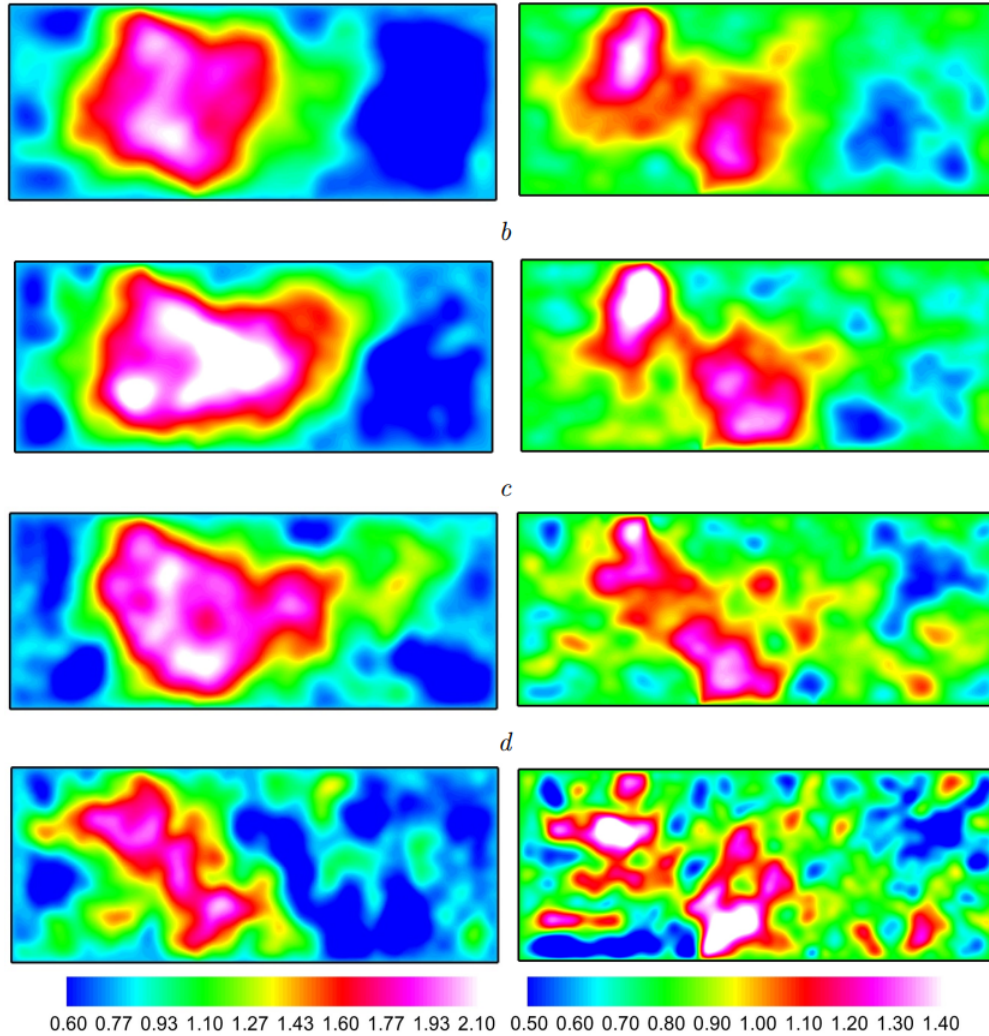


Fig. 3. Distribution of orientation angles of LC molecule domains with symmetrical arrangement of plates: 5000th (a), 10000th (b), 15000th (c), 25000th (d) time steps

initial rotation angle of molecules and location of the capacitor plates. The results showed that as frequency increases smaller swarms are formed which quickly break up into smaller swarms. The results of calculations can be applied to the study of the dynamics of liquid crystals in the problems of propagation of thermoelastic waves caused by weak mechanical and electrical disturbances.

This work is supported by the Krasnoyarsk Mathematical Center and financed by the Ministry of Science and Higher Education of the Russian Federation in the framework of the establishment and development of regional Centers for Mathematics Research and Education (Agreement No. 075-02-2023-912).

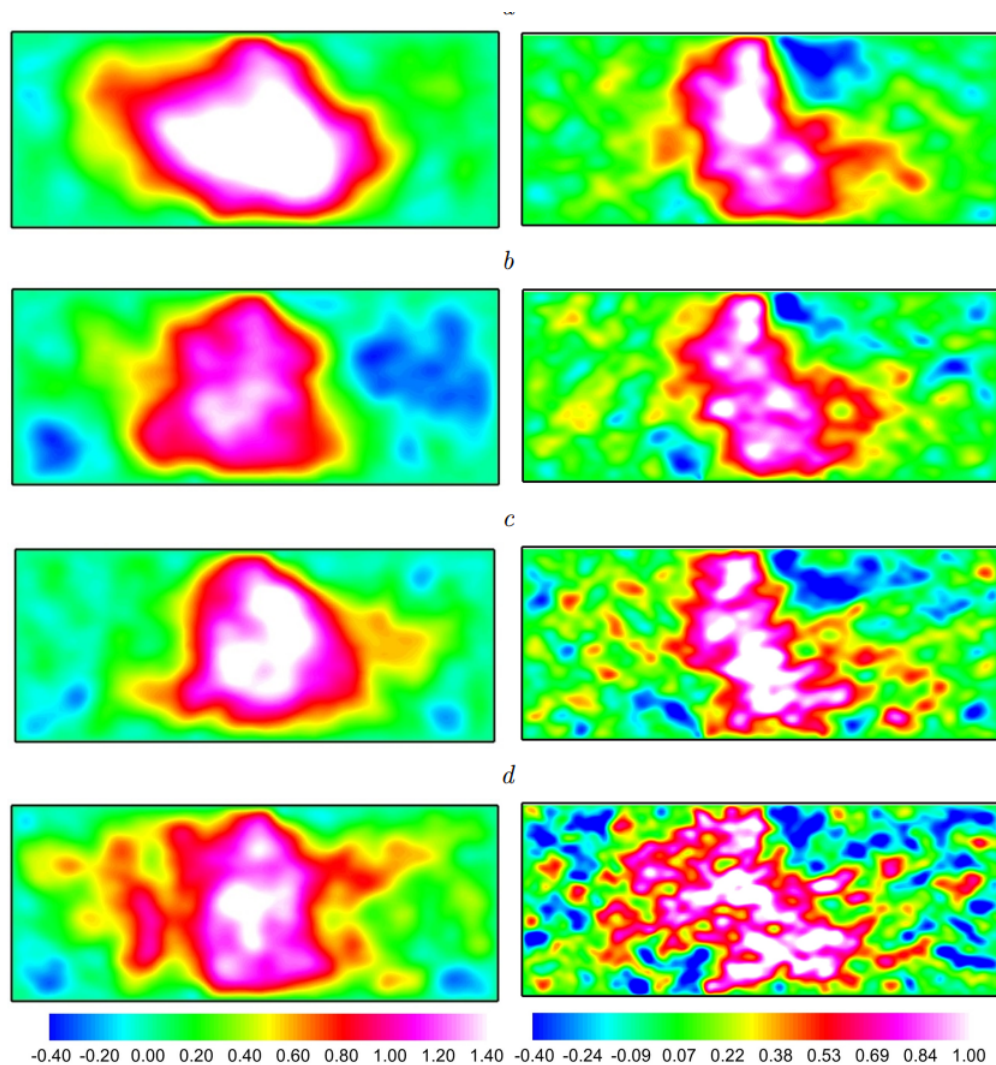


Fig. 4. Distribution of orientation angles of LC molecule domains with symmetrical arrangement of plates: 5000th (a), 10000th (b), 15000th (c), 25000th (d) time steps

References

- [1] V. Fréedericksz, V. Zolina, Forces causing the orientation of an anisotropic liquid, *Trans. Faraday Soc.*, **29**(1933), 919–930. DOI: 10.1039/TF9332900919.
- [2] C.W. Oseen, The theory of liquid crystals, *Trans. Faraday Soc.*, **29**(1933), 883–899. DOI: 10.1039/TF9332900883.
- [3] F.C. Frank, On the theory of liquid crystals, *Disc. Faraday Soc.*, **25**(1958), 19–28. DOI: 10.1039/DF9582500019.
- [4] J.L. Ericksen, Conservation laws for liquid crystals, *Trans. Soc. Rheol.*, **5**(1961), no. 1, 23–34. DOI: 10.1122/1.548883.

- [5] F.M. Leslie, Some constitutive equations for liquid crystals, *Arch. Ration. Mech. Anal.*, **28**(1968), no. 4, 265–283.
- [6] V. Sadovskii, O. Sadovskaya, Acoustic Approximation of the Governing Equations of Liquid Crystals under Weak Thermomechanical and Electrostatic Perturbations, in: *Advances in Mechanics of Microstructured Media and Structures* (eds.: F. dell’Isola, V.A. Eremeyev, A. Porubov), Ser.: *Advanced Structured Materials*, vol. 87, chapt. 17, 297–341, Springer, Cham, 2018. DOI: 10.1007/978-3-319-73694-5_17.
- [7] V.M. Sadovskii, O.V. Sadovskaya, Mathematical modeling of inhomogeneous electric field impact on a liquid crystal layer, *ZAMM*, **103**(2023), art. e202200248. DOI: 10.1002/zamm.202200248.
- [8] V.M. Sadovskii, O.V. Sadovskaya, I.V. Smolekho, Parallel implementation of the algorithm describing the behavior of liquid crystals under the action of electric field, *AIP Conf. Proc.*, **2025**(2018), art. 070005. DOI: 10.1063/1.5064917.
- [9] K. Skarp, S.T. Lagerwall, B. Stebler, Measurements of hydrodynamic parameters for nematic 5CB, *Mol. Cryst. Liq. Cryst.*, **60**(1980), no. 3, 215–236. DOI: 10.1080/00268948008072401.
- [10] B.A. Belyaev, N.A. Drokin, V.F. Shabanov, V.N. Shepov, Dielectric anisotropy of 5CB liquid crystal in a decimeter wavelength range, *Phys. Solid State*, **42**(2000), no. 3, 577–579. DOI: 10.1134/1.1131251.

Анализ неустойчивого состояния нематического жидкого кристалла на основе упрощенной динамической модели

Ирина В. Смолехо

Институт вычислительного моделирования СО РАН
Красноярск, Российская Федерация

Аннотация. В статье моделируется эффект Фредерика, состоящий в переориентации молекул жидкого кристалла в протяженном слое под действием неоднородного электрического поля. Определяющие уравнения для касательного напряжения, угловой скорости и электрического потенциала получены из уравнений упрощенной динамической модели нематического жидкого кристалла 5CB в акустическом приближении. Построен алгоритм численного решения определяющих уравнений с помощью конечно-разностных схем. Программная реализация алгоритма выполнена по технологии CUDA для компьютеров с графическими ускорителями.

Ключевые слова: жидкий кристалл, динамика, электрический потенциал, эффект Фредерика, метод прямых, уравнение Лапласа, параллельное программирование, технология CUDA.

EDN: WNGDYA

УДК 515

Coincidence and Common Fixed Point Theorems for Hybrid Mappings Via C-class Function

Taieb Hamaizia*

Laboratory of Dynamical Systems and Control
Department of Mathematics and Informatics
Larbi Ben M'Hidi University
Algeria

Stojan Radenović†

Faculty of Mechanical Engineering
University of Belgrade
Beograd, Serbia

Arsalan Hojjat Ansari‡

Department of Mathematics and Applied Mathematics
Sefako Makgatho Health Sciences University
Ga-Rankuwa, Pretoria, Medunsa-0204, South Africa

Received 10.08.2023, received in revised form 27.09.2023, accepted 04.02.2024

Abstract. In this paper, we prove common fixed point theorems for two pairs of hybrid mappings in metric spaces using the concept of *C*-class function and *T*-weak commutativity. Our Theorems generalize some well-know results.

Keywords: metric space, hybrid Mappings, C-class function.

Citation: T. Hamaizia, S. Radenović, A.H. Ansari, Coincidence and Common Fixed Point Theorems for Hybrid Mappings Via C-class Function, J. Sib. Fed. Univ. Math. Phys., 2024, 17(2), 282–290. EDN: WNGDYA.



1. Introduction and preliminaries

Recently, many authors have provided new fixed point results for multivalued mappings in the literature by taking into account different conditions on metric spaces (see [4, 7, 8, 11, 17]).

In the present article, we prove a coincidence and common fixed points of multivalued maps via C-class functions with a self map are taken into account with ageneralized form of contraction condition.

Let (X, d) be a metric space. For $x \in X$ and $A \subset X$, we denote

$$D(x, A) = \inf\{d(x, y), y \in A\}.$$

Let $CB(X)$ be the set of all nonempty closed and bounded subsets of X .

*tayebo42000@yahoo.fr

†radens@beotel.net

‡analsisamirmath2@gmail.com

Let H be the Hausdorff-Pompeiu metric with respect to d defined by

$$H(A, B) = \max \left\{ \sup_{a \in A} D(a, B), \sup_{b \in B} D(A, b) \right\},$$

for every $A, B \in CB(X)$.

It is well known that $(CB(X), H)$ is a metric space and if (X, d) is complete, then $(CB(X), H)$ is also complete

Let $f : X \rightarrow X$ be a single-valued mapping and $T : X \rightarrow CB(X)$ be a multi-valued mapping.

- (i) A point $x \in X$ is a fixed point of f (resp. T) if $fx = x$ (resp. $x \in Tx$).
- (ii) A point $x \in X$ is a coincidence point of f and T if $fx \in Tx$.
- (iii) A point $x \in X$ is a common fixed point of f and T if $x = fx \in Tx$.

Lemma 1 ([12]). *If $A, B \in CB(X)$ and $k > 1$, then for each $a \in A$, there exists $b \in B$ such that*

$$d(a, b) \leq kH(A, B). \quad (1)$$

Let $f : X \rightarrow X$ be a single-valued mapping and $T : X \rightarrow CB(X)$ be a multi-valued mapping

Definition 1 ([12]). *1) A point $x \in X$ is said to be a coincidence point of f and T if $fx \in Tx$. We denote by $C(f, T)$ the set of all coincidence points of f and T .*

2) A point $x \in X$ is a fixed point of T if $x \in Tx$.

Definition 2 ([5]). *f and T are said to be commuting in X if for all $x \in X$,*

$$fTx \in Tfx.$$

Definition 3 ([15]). *f and T are said to be weakly commuting on X if for all $x \in X$, $fTx \in CB(X)$ and*

$$H(fTx, Tfx) \leq D(fx, Tx).$$

Definition 4 ([13]). *f and T are said to be R -weakly commuting at $x \in X$, if*

$$fTx \in CB(X)$$

and there exists an $R > 0$ such that

$$H(fTx, Tfx) \leq RD(fx, Tx). \quad (2)$$

Remark 1.1 ([6]). *Commuting implies weakly commuting, but the converse is not true in general.*

We defined that f and T are said to be pointwise R -weakly commuting on X if for all $x \in X$, $fTx \in CB(X)$ and (2) holds for some $R > 0$.

Definition 5 ([16]). *1) f and T are said to be (IT) -commuting at $x \in X$ if*

$$fTx \subset Tfx.$$

- 2) A pointwise R -weakly commuting hybrid pair is not weakly compatible in general.*
- 3) IT -commutativity of f and T at a coincidence point is more general than their weak compatibility at the same point.*
- 4) A pointwise R -weak commutativity at a coincidence point is equivalent to (IT) commutativity at this point.*

Definition 6 ([9]). 1) f is T -weakly commuting at $x \in X$ if $ffx \in Tfx$.

2) For a hybrid pair (f, T) , (IT) commuting at coincidence points implies that f is T -weakly commuting at these points.

Lemma 2. a) If f is T -weakly commuting at $x \in X$, then $fx \in C(f, T)$.

b) If f is T -weakly commuting at $x \in X$ and $fx = ffx$, then fx is a common fixed point of f and T .

In 2014, A. H. Ansari [2] introduced the concept of a C -class functions which covers a large class of contractive conditions.

Definition 7 ([2]). A continuous function $F : [0, +\infty)^2 \rightarrow \mathbb{R}$ is called C -class function if for any $s, t \in [0, +\infty)^2$; the following conditions hold

$$c1 \quad F(s, t) \leq s,$$

$$c2 \quad F(s, t) = s \text{ implies that either } s = 0 \text{ or } t = 0.$$

An extra condition on F that $F(0, 0) = 0$ could be imposed in some cases if required. The letter C will denote the class of all C -functions.

Example 1. The following examples shows that the class C is nonempty:

$$1. \quad F(s, t) = s - t.$$

$$2. \quad F(s, t) = ms, \text{ for some } m \in (0, 1).$$

$$3. \quad F(s, t) = \frac{s}{(1+t)^r}, \text{ for some } r \in (0, 1).$$

$$4. \quad F(s, t) = \frac{\log(t + a^s)}{(1+t)}, \text{ for some } a > 1.$$

Let Φ denote the class of the functions $\varphi : [0, +\infty) \rightarrow [0, +\infty)$ which satisfy the following conditions:

a) φ is continuous ;

b) $\varphi(t) > 0, t > 0$ and $\varphi(0) \geq 0$.

Definition 8 ([10]). A function $\psi : [0, +\infty) \rightarrow [0, +\infty)$ is called an altering distance function if the following properties are satisfied:

i) ψ is non-decreasing and continuous;

ii) $\psi(t) = 0$ if and only if $t = 0$.

Let us suppose that Ψ denote the class of the altering distance functions.

Definition 9. A tripled (ψ, φ, F) where $\psi \in \Psi$; $\varphi \in \Phi_u$ and $F \in C$ is said to be a monotone if for any $x, y \in [0, +\infty)$;

$$x \leq y \text{ implies } F(\psi(x), \varphi(x)) \leq F(\psi(y), \varphi(y)).$$

Example 2. Let $F(s, t) = s - t$, $\varphi(x) = \sqrt{x}$

$$\psi(x) = \begin{cases} \sqrt{x} & \text{if } 0 \leq x \leq 1 \\ x^2 & \text{if } x > 1 \end{cases},$$

then (ψ, φ, F) is monotone.

Lemma 3 ([14]). Let (X, d) be a metric space and let $\{y_n\}$ be a sequence in X such that $d(y_n, y_{n+1}) = 0$ is nonincreasing and

$$\lim_{n \rightarrow +\infty} d(y_n, y_{n+1}) = 0.$$

If $\{y_{2n}\}$ is not a Cauchy sequence, then there exist $\varepsilon > 0$ and sequences $\{m_k\}$ and $\{n_k\}$ of positive integers such that the following sequences tend to ε when $k \rightarrow +\infty$

$$d(x_{2n_k}, x_{2m_k}), d(x_{2n_k+1}, x_{2m_k}), d(x_{2n_k}, x_{2m_k-1}), d(x_{2n_k+1}, x_{2m_k-1}), d(x_{2n_k+1}, x_{2m_k+1}), \dots \quad (3)$$

2. Main results

In the following theorem we obtain the coincidence and common fixed point for a hybrid pair of mappings via C -class function

Theorem 2.1. *Let (X, d) be a metric space, $S, T : X \rightarrow X$ and $K, G : X \rightarrow CB(X)$ satisfying*

$$K(X) \subset T(X) \quad \text{and} \quad G(X) \subset S(X) \quad (4)$$

$$\psi(rH(Kx, Gy)) \leq F(\psi(M(x, y)), \varphi(M(x, y))) \quad (5)$$

where $r \geq 1$, $F : [0, +\infty)^2 \rightarrow \mathbb{R}$ is C -class function, $\psi : [0, +\infty) \rightarrow [0, +\infty)$ is an altering distance function, $\varphi : [0, +\infty) \rightarrow [0, +\infty)$ is an ultra altering distance function and

$$M(x, y) = \max \left\{ d(Sx, Ty), D(Sx, Kx), D(Ty, Gy), \frac{D(Sx, Gy) + D(Kx, Ty)}{2} \right\}$$

for all $x, y \in X$, $D(Sx, Gy) + D(Kx, Ty) \neq 0$ and $H(Kx, Gy) = 0$ whenever $D(Sx, Gy) + D(Kx, Ty) = 0$. Suppose that one of $S(X)$ or $T(X)$ is complete. Then

a) there exists $p, q \in X$ such that $Sp \in Kp$ and $Tq \in Gq$.

Further, if S is K -weakly commuting and T is G -weakly commuting at their coincidence points, therefore

b) There exists $z \in X$ such that $Sz \in Kz$ and $Tz \in Gz$.

c) In the case (b), if $Sz = Tz$, then $Sz = Tz \in Kz \cap Gz$.

d) In the case (c), if $Sz = Tz = z$, then z is a common fixed point of S, T, K and G .

Proof. First, assume that there exists $p, q \in X$ such that

$$D(Sp, Gq) + D(Kp, Tq) = 0.$$

So, $D(Sp, Gq) = 0$ and $D(Kp, Tq) = 0$ which implies that $Sp \in Gq$ and $Tq \in Kp$. Since $H(Kp, Gq) = 0$, it follows that

$$D(Sp, Kp) \leq H(Kp, Gq) = 0.$$

Hence $Sp \in Kp$.

In a similar manner, we get $Tq \in Gq$.

Now, assume that

$$D(Sx, Gy) + D(Kx, Ty) \neq 0 \quad \text{for all } x, y \in X.$$

Let $x_0 \in X$ be an arbitrary point. By (4) and (1), we define a sequence $\{y_n\}$ in X such that

$$y_{2n} = Sx_{2n} \in Gx_{2n-1}, \quad y_{2n+1} = Tx_{2n+1} \in Kx_{2n}$$

$$\begin{aligned} d(y_{2n}, y_{2n+1}) &\leq kH(Kx_{2n}, Gx_{2n-1}), \\ d(y_{2n+1}, y_{2n+2}) &\leq kH(Kx_{2n+1}, Gx_{2n+1}), \quad \text{for } n = 1, 2, \dots \end{aligned}$$

Using (5) we have

$$\begin{aligned}
\psi(rH(Kx_{2n}, Gx_{2n-1})) &\leq F(\psi(M(x_{2n}, x_{2n-1})), \varphi(M(x_{2n}, x_{2n-1}))) \leq \\
&\leq F(\psi(\max\{d(y_{2n}, y_{2n-1}), D(y_{2n}, Kx_{2n}), D(y_{2n-1}, Gx_{2n-1}) \\
&\quad \frac{D(y_{2n}, Gx_{2n-1}) + D(Kx_{2n}, y_{2n-1})}{2}\}), \\
&\quad \varphi(\max\{d(y_{2n}, y_{2n-1}), D(y_{2n}, Kx_{2n}), D(y_{2n-1}, Gx_{2n-1}) \\
&\quad \frac{D(y_{2n}, Gx_{2n-1}) + D(Kx_{2n}, y_{2n-1})}{2}\})) \leq \\
&\leq F(\psi(\max\{d(y_{2n}, y_{2n-1}), D(y_{2n}, y_{2n+1}), D(y_{2n-1}, y_{2n}) \\
&\quad \frac{0 + D(y_{2n+1}, y_{2n-1})}{2}\}), \\
&\quad \varphi(\max\{d(y_{2n}, y_{2n-1}), D(y_{2n}, y_{2n+1}), D(y_{2n-1}, y_{2n}) \\
&\quad \frac{0 + D(y_{2n+1}, y_{2n-1})}{2}\})) \leq \\
&\leq F(\psi(\max\{d(y_{2n}, y_{2n-1}), d(y_{2n}, y_{2n+1}), \frac{d(y_{2n+1}, y_{2n-1})}{2}\}), \\
&\quad \varphi(\max\{d(y_{2n}, y_{2n-1}), d(y_{2n}, y_{2n+1}), \frac{d(y_{2n+1}, y_{2n-1})}{2}\})) \leq \\
&\leq F(\psi(\max\{d(y_{2n}, y_{2n-1}), d(y_{2n}, y_{2n+1}) \\
&\quad \frac{d(y_{2n+1}, y_{2n}) + d(y_{2n}, y_{2n-1})}{2}\}), \\
&\quad \varphi(\max\{d(y_{2n}, y_{2n-1}), d(y_{2n}, y_{2n+1}) \\
&\quad \frac{d(y_{2n+1}, y_{2n}) + d(y_{2n}, y_{2n-1})}{2}\}))) \leq \\
&\leq F(\psi(\max\{d(y_{2n}, y_{2n-1}), d(y_{2n}, y_{2n+1})\}), \\
&\quad \varphi(\max\{d(y_{2n}, y_{2n-1}), d(y_{2n}, y_{2n+1})\})). \tag{6}
\end{aligned}$$

Therefore, we obtain

$$d(y_{2n}, y_{2n+1}) \leq rH(Kx_{2n}, Gx_{2n-1}).$$

By the increasing of ψ , we get

$$\psi(d(y_{2n}, y_{2n+1})) \leq \psi(rH(Kx_{2n}, Gx_{2n-1})). \tag{7}$$

Applying (7) in (6) and the nondecreasing property of ψ that

$$\begin{aligned}
\psi(d(y_{2n}, y_{2n+1})) &\leq F(\psi(\max\{d(y_{2n}, y_{2n-1}), d(y_{2n}, y_{2n+1})\}), \\
&\quad \varphi(\max\{d(y_{2n}, y_{2n-1}), d(y_{2n}, y_{2n+1})\})) \leq \\
&\leq \psi(\max\{d(y_{2n}, y_{2n-1}), d(y_{2n}, y_{2n+1})\}) \leq \\
&\leq \psi(d(y_{2n}, y_{2n-1})).
\end{aligned}$$

Analogously, we can show that

$$\begin{aligned}
\psi(d(y_n, y_{n+1})) &\leq F(\psi(\max\{d(y_n, y_{n-1}), d(y_n, y_{n+1})\}), \varphi(\max\{d(y_n, y_{n-1}), d(y_n, y_{n+1})\})) \leq \\
&\leq \psi(\max\{d(y_n, y_{n-1}), d(y_n, y_{n+1})\}) \leq \\
&\leq \psi(d(y_n, y_{n-1})). \tag{8}
\end{aligned}$$

Then the sequence $[d(y_n, y_{n+1}) \downarrow 0]$ is bounded below and non-increasing, hence there exist $r \geq 0$ such that

$$\lim_{n \rightarrow +\infty} d(y_n, y_{n+1}) = 0.$$

By taking $n \rightarrow +\infty$ in (8) and using continuity of φ and ψ , we deduce that

$$\psi(r) \leq F(\psi(r), \varphi(r)) \leq \psi(r).$$

So, $\varphi(r) = 0$ or $\psi(r) = 0$. It follows that $r = 0$.

Now, we prove that the sequence $\{y_{2n}\}$ is a Cauchy in the metric space (X, d) . Suppose that the sequence $\{y_{2n}\}$ is not a Cauchy sequence in (X, d) , then there exist $\varepsilon > 0$ and two sequences $\{m(k)\}$ and $\{n(k)\}$ as in Lemma 1.10 such that all sequences in (3) are tend to $\varepsilon > 0$, when $k \rightarrow +\infty$. Now, for $x = x_{2n(k)}$ and $y = x_{2m(k)+1}$ in equation (5), we get

$$\begin{aligned} \psi(rH(Kx_{2n(k)}, Gx_{2m(k)+1})) &\leq F(\psi(M(x_{2n(k)}, x_{2m(k)+1})), \varphi M(x_{2n(k)}, x_{2m(k)+1})) \leq \\ &\leq F(\psi(\max\{d(Sx_{2n(k)}, Tx_{2m(k)+1}), D(Sx_{2n(k)}, Kx_{2n(k)}), \\ &\quad D(Tx_{2m(k)+1}, Gx_{2m(k)+1}), \\ &\quad \frac{D(Sx_{2n(k)}, Gx_{2m(k)+1}) + D(Kx_{2n(k)}, Tx_{2m(k)+1})}{2}\}) \\ &\quad \varphi(\max\{d(Sx_{2n(k)}, Tx_{2m(k)+1}), D(Sx_{2n(k)}, Kx_{2n(k)}), \\ &\quad D(Tx_{2m(k)+1}, Gx_{2m(k)+1}), \\ &\quad \frac{D(Sx_{2n(k)}, Gx_{2m(k)+1}) + D(Kx_{2n(k)}, Tx_{2m(k)+1})}{2}\})) \leq \\ &\leq F(\psi(\max\{d(y_{2n(k)-1}, y_{2m(k)}), D(y_{2n(k)-1}, y_{2n(k)}), \\ &\quad D(y_{2m(k)}, y_{2m(k)+1}), \\ &\quad \frac{D(y_{2n(k)-1}, y_{2m(k)+1}) + D(y_{2n(k)}, y_{2m(k)})}{2}\}) \\ &\quad \varphi(\{\max d(y_{2n(k)-1}, y_{2m(k)}), D(y_{2n(k)-1}, y_{2n(k)}), \\ &\quad D(y_{2m(k)}, y_{2m(k)+1}), \\ &\quad \frac{D(y_{2n(k)-1}, y_{2m(k)+1}) + D(y_{2n(k)}, y_{2m(k)})}{2}\})) \end{aligned} \quad (9)$$

Therefore, taking $k \rightarrow +\infty$ in inequality (9) and using the properties of F we get

$$\psi(\varepsilon) \leq F(\psi(\varepsilon), \varphi(\varepsilon)) \leq \psi(\varepsilon).$$

So, $\psi(\varepsilon) = 0$ or $\varphi(\varepsilon) = 0$, hence we get $\varepsilon = 0$ which contradiction with $\varepsilon > 0$. Thus $\{y_{2n}\}$ is a Cauchy sequence in (X, d) , hence by (3) we deduce that the sequence $\{y_n\}$ is Cauchy sequence in X . As $S(X)$ is complete, it converges to $z \in S(X)$ and so there exists $p \in X$ such that $z = Sp$. Using (5)

$$\begin{aligned} \psi(H(Kp, Gx_{2n-1})) &\leq F(\psi(\max\{d(Sp, Tx_{2n-1}), D(Sp, Kp), D(Tx_{2n-1}, Gx_{2n-1}), \\ &\quad \frac{D(Sp, Gx_{2n-1}) + D(Kp, Tx_{2n-1})}{2}\}) \\ &\quad \varphi(\max\{d(Sp, Tx_{2n-1}), D(Sp, Kp), D(Tx_{2n-1}, Gx_{2n-1}), \\ &\quad \frac{D(Sp, Gx_{2n-1}) + D(Kp, Tx_{2n-1})}{2}\})) \end{aligned}$$

So

$$\begin{aligned} \psi (D(Kp, y_{2n})) \leq & F(\psi(\max \{d(Sp, y_{2n-1}), D(Sp, Kp), d(y_{2n-1}, y_{2n}), \\ & \frac{d(Sp, y_{2n}) + D(Kp, y_{2n-1})}{2}\}) \\ & \varphi(\max \{d(Sp, y_{2n-1}), D(Sp, Kp), d(y_{2n-1}, y_{2n}), \\ & \frac{d(Sp, y_{2n}) + D(Kp, y_{2n-1})}{2}\})). \end{aligned}$$

Letting n tend to infinity, we get

$$\begin{aligned} \psi (D(Kp, Sp)) \leq & F(\psi(\max \{0, D(Sp, Kp), 0, \frac{0 + D(Kp, Sp)}{2}\})) \\ & \varphi(\max \{0, D(Sp, Kp), 0, \frac{0 + D(Kp, Sp)}{2}\}) \leq \\ \leq & F(\psi(D(Sp, Kp)); \varphi(D(Sp, Kp)) \leq \psi D(Sp, Kp). \end{aligned}$$

Thus, we hold $\psi(D(Sp, Kp)) = 0$ or $\varphi(D(Sp, Kp)) = 0$, then $D(Sp, Kp) = 0$, with imple $Sp \in Kp$.

Similarly, as $K(X) \subset T(X)$, there exists $q \in X$ such that $z = Sp = Tq$. Applying (5) and letting $n \rightarrow +\infty$, bu the same calculate, we can find $Tq \in Gq$.

Since S is F -weakly commuting at $p \in C(S, T)$ and T is G -weakly commuting at $q \in C(G, T)$ it follows that $z = Sp \in C(K, T)$ and $z = Tq \in C(G, T)$. Hence, $Sz \in Kz$ and $Tz \in Gz$. If $Sz = Tz$, then $Sz = Tz \in Kz \cap Gz$ and if $Sz = Tz = z$, then z is a common fixed point of S, T, K and G .

Corollary 1. *Let (X, d) be a metric space, $S, T : X \rightarrow X$ and $K, G : X \rightarrow CB(X)$ satisfying*

$$\begin{aligned} K(X) \subset T(X) \quad \text{and} \quad G(X) \subset S(X) \\ rH(Kx, Gy) \leq M(x, y) \beta(M(x, y)) \end{aligned}$$

where

$$M(x, y) = \max \left\{ d(Sx, Ty), D(Sx, Kx), D(Ty, Gy), \frac{D(Sx, Gy) + D(Kx, Ty)}{2} \right\}$$

for all $x, y \in X$, $D(Sx, Gy) + D(Kx, Ty) \neq 0$ and $H(Kx, Gy) = 0$ whenever $D(Sx, Gy) + D(Kx, Ty) = 0$. Suppose that one of $S(X)$ or $T(X)$ is complete. Then

a) there exists $p, q \in X$ such that $Sp \in Kp$ and $Tq \in Gq$.

Further, if S is K -weakly commuting and T is G -weakly commuting at their coincidence points, therefore

b) There exists $z \in X$ such that $Sz \in Kz$ and $Tz \in Gz$.

c) In the case (b), if $Sz = Tz$, then $Sz = Tz \in Kz \cap Gz$.

d) In the case (c), if $Sz = Tz = z$, then z is a common fixed point of S, T, K and G .

Proof. Set $\psi(t) = t$, $F(s, t) = s\beta(s)$ in Theorem (2.1), $\beta : [0, 1) \rightarrow [0, +\infty)$. □

Corollary 2. *Let (X, d) be a metric space, $S, T : X \rightarrow X$ and $K, G : X \rightarrow CB(X)$ satisfying*

$$\begin{aligned} K(X) \subset T(X) \quad \text{and} \quad G(X) \subset S(X) \\ rH(Kx, Gy) \leq mM(x, y) \end{aligned}$$

where $r \geq 1$ and

$$M(x, y) = \max \left\{ d(Sx, Ty), D(Sx, Kx), D(Ty, Gy), \frac{D(Sx, Gy) + D(Kx, Ty)}{2} \right\}$$

for all $x, y \in X$, $D(Sx, Gy) + D(Kx, Ty) \neq 0$ and $H(Kx, Gy) = 0$ whenever $D(Sx, Gy) + D(Kx, Ty) = 0$. Suppose that one of $S(X)$ or $T(X)$ is complete. Then

a) there exists $p, q \in X$ such that $Sp \in Kp$ and $Tq \in Gq$.

Further, if S is K -weakly commuting and T is G -weakly commuting at their coincidence points, therefore

b) There exists $z \in X$ such that $Sz \in Kz$ and $Tz \in Gz$.

c) In the case (b), if $Sz = Tz$, then $Sz = Tz \in Kz \cap Gz$.

d) In the case (c), if $Sz = Tz = z$, then z is a common fixed point of S, T, K and G .

Proof. Set $\psi(t) = t$, $F(s, t) = ms$ in Theorem (2.1), $m \in (0, 1)$. □

Now we present some examples to support our Theorem

Example 3. Define $\psi, \varphi : [0, +\infty) \rightarrow [0, +\infty)$ by $\psi(t) = \frac{t}{15}$; $\varphi(t) = 2t$ and $F(s, t) = ks$ for $k \in (0, 1)$.

Let $X = [0, 1]$ be endowed with the Euclidean metric d . Let $Gx = [0, x^2]$, for all $x, y \in X$, we have

$$d(x, y) = |x - y|, D(x, Gx) = \inf \{d(x, b), b \in [0, x^2]\}, D(y, Gy) = \inf \{d(y, c), c \in [0, y^2]\}$$

$$\begin{aligned} H(Gx, Gy) &= H([0, x^2], [0, y^2]) = \\ &= |x^2 - y^2| = (x + y)|x - y| \leq kd(x, y), \quad k \in (0, 1) \quad \text{with } x, y \in [0, 1]. \end{aligned}$$

Consequently, these mappings are satisfy all conditions of theorem, then they have a fixed point in X .

References

- [1] R.P.Agarwal, M.Meehan, D.O'Regan, Fixed Point Theory and Applications, Cambridge University Press, 2001.
- [2] A.H.Ansari, Note on φ - ψ -contractive type mappings and related fixed point, The 2nd regional conference on mathematics and applications, Payame Noor University, 2014, 377–380.
- [3] S.Banach, Sur les operations dans les ensembles abstraits et leur applications aux equations integrals. *Fundamenta Mathematicae*, **3**(1922), 133–181.
- [4] P.Debnath, N.Konwar, S.Radenovic, Metric Fixed Point Theory: Applications in Science, Engineering and Behavioural Science, Springer Nature, Singapore, 2021.
- [5] M.Imdad, T.I.Khan, Results on Nonlinear Hybrid Contractions Satisfying a Rational Inequality, *Southeast Asian Bulletin of Mathematics*, **26**(2002), 421–432.
- [6] G.Jungck, B.E.Rhoades, Fixed points for set-valued functions without continuity, *Indian J. Pure Appl. Math.*, **29**(1998), no. 3, 227–238.
- [7] T.Hamaizia, A.H.Ansari, Related fixed point on two metric spaces via C-class functions, *Palestine Journal of Mathematics*, **10**(2021), no. 2, 537–546.

- [8] T.Hamaizia, P.P.Murthy, Z -contraction condition involving simulation function in b -metric space under fixed points considerations, *Mathematica Moravica*, **25**(2021), no. 2, 43–52.
- [9] T.Kamran, Coincidence and fixed points for hybrid strict contractions, *J. Math. Anal. Appl.*, **299**(2004), no. 1, 235–241.
- [10] M.S.Khan, M.Swaleh, S.Sessa, Fixed point theorems by altering distances between the points, *Bulletin of the Australian Mathematical Society*, **30**(1984), 1–9.
- [11] S.Merdaci, T.Hamaizia, A.Aliouche, Some generalization of non-unique fixed point theorems for multi-valued mappings in b -metric spaces, *U.P.B. Sci. Bull., Series A*, **83**(2021), no. 4.
- [12] S.B.Nadler, Multi-valued contractions mappings, *Pacific J. Math.*, **30**(1969), no. 3, 475–488.
- [13] R.P.Pant, Common fixed points of noncommuting mappings, *J. Math. Anal. Appl.*, **188**(1994), 436–440.
- [14] S.Radenović, Z.Kadelburg, D.Jandrlić, and A.Jandrlić, Some results on weakly contractive maps, *Bull. Iran. Math. Soc.*, **32**(2012), no. 3, 625–645.
- [15] S.Sessa, On a weak commutativity condition of mappings in fixed point considerations, *Publ. Inst. Math. (Beograd)*, **32**(1982), 149–153.
- [16] S.L.Singh, S.N.Mishra, Coincidence and fixed points of non-self hybrid contractions, *J. Math. Anal. Appl.*, **256**(2001), no. 2, 486–497.
- [17] V.Todorčević, *Harmonic Quasiconformal Mappings and Hyperbolic Type Metrics*, Springer Nature Switzerland, 2019. DOI: 10.1007/978-3-030-22591-9

Теоремы о совпадении и общих неподвижных точках для гибридных отображений с помощью функции C -класса

Тайеб Хамайзия

Лаборатория динамических систем и управления
Кафедра математики и информатики
Университет Ларби Бен Мхиди
Алжир

Стоян Раденович

Факультет машиностроения
Белградский университет
Белград, Сербия

Арсалан Ходжат Ансари

Кафедра математики и прикладной математики
Университет медицинских наук Сефако Макгато
Га-Ранкува, Претория, Медунса-0204, Южная Африка

Аннотация. В данной статье мы доказываем общие теоремы о неподвижной точке для двух пар гибридных отображений в метрических пространствах, используя концепцию функции C -класса и T -слабую коммутативность. Наши теоремы обобщают некоторые хорошо известные результаты.

Ключевые слова: метрическое пространство, гибридные отображения, функция C -класса.